DROP BREAKAGE IN AGITATED LEAN LIQUID—LIQUID DISPERSIONS

A The
In Partial Fulfilment o
for the Degree

DOCTOR OF PHILOSOPH

G. NARASIMHAN

to the

DEPARTMENT OF CHEMICAL ENGINEERING

INDIAN INSTITUTE OF TECHNOLOGY KANPUR

MARCH, 1979

CERTIFICATE

This is to certify that the work presented in this thesis entitled, 'DROP BREAKAGE IN AGITATED LEAN LIQUID-LIQUID DISPERSIONS' has been carried out by Mr. Ganesan Narasimhan under our supervision and the same has not been submitted elsewhere for a degree.

D. Ramkrishna
Professor
School of Chemical Engineering
Purdue University
Lafayette, Indiana
U.S.A.

Date:

12 MAR 1979

J. P. Gupta
Assistant Professor
Department of Chemical Engg.
Indian Institute of Technology
Kanpur-208016, India

Date:

12 MAR 1979

ACKNOWLEDGEMENTS

To me this thesis is the embodiment of about half a decade of endeavour marked by the cooperation, enthusiasm and affection of a large number of people who have contributed in various ways to various extents to make this work possible. It is therefore difficult to do full justice to the job of acknowledging all these people in these few paragraphs; however, I wish to mention some of these who have been directly associated with my work.

Professor D. Ramkrishna introduced me to this field and improved my understanding through stimulating discussions and communications. I would like to record my deep gratitude to him for his constant help and guidance during these years without which this work would not have been possible.

I would also like to record my deep gratitude to Dr. J.P. Gupta for his constant help and guidance in the laboratory.

I would like to recall the innumerable hours I had spent in our research group meetings which helped me a great deal in diversifying my knowledge and improving my understanding. I would like to thank the members of our research group, Drs. B.H. Shah, P.N. Singh, R.K. Bajpai and Mr. Mayur Seth for enthusiasm and critical attention in the group discussions.

I would like to record my sincere thanks to Professors K. Sriram, S. Mukherjee and G.K. Mehta for allowing me to make use of the facilities in Central Nuclear Laboratories.

I would also like to thank Drs. C.P.P. Singh, T. Swaminath and S.C.Shenoy for their cooperation, encouragement and constant help during my stay at Kanpur.

I would like to acknowledge with deep gratitude the cooperation and help I have received from Messers Ramesh Chandra, Ayodhya Singh, N.K. Metia and D.N. Mishra in the laboratory.

I would also like to thank Messers Balal, Ramachandran and Krishnan for their help in drawings and proof reading.

I would like to thank Mr. B.S. Pandey for his efficient typing, Mr. D.S. Panesar for his excellent drawings, Mr. Hari Ram for neat cyclostyling and Mr. Jai Ballabh for good ammonia printing.

G. NARASIMHAN
Author

CONTENTS

LIST OF FIGURES

LIST OF TABLES

SYNOPSIS

Drop size distributions in liquid-liquid dispersions evolve due to the dynamics of breakage and coalescence. Evolution of drop size distribution is important for prediction of, interfacial area, heat and/or mass transfer in liquid-liquid dispersions. In lean liquid-liquid dispersions, coalescence is negligible due to negligible interaction between droplets. The present investigation attempts to study the breakage of droplets in agitated lean liquid-liquid dispersions.

Drop breakage in agitated lean liquid-liquid dispersions is random and hence is described by related probabilities, namely, the transitional breakage probability and the daughter droplet size distribution. The present investigation consists of three parts:

(i) A model for transitional breakage probability

(ii) A model for equilibrium drop size distribution from a statistical thermodynamic viewpoint.

and (iii) Experimental measurement of transient as well as equilibrium drop volume distributions in a batch agitated lean liquid-liquid dispersion in order to verify the two models and also to obtain the daughter droplet size distribution.

The model for transitional breakage probability is based on the mechanism of breakage of droplets due to their

oscillations resulting from relative velocity fluctuations. A universal transitional breakage probability in terms of non-dimensionalized drop volume is derived for all dispersed phases whose density and viscosity are almost same as that of the continuous phase. The maximum stable drop diameter derived from this model shows a dependence of $N_{We}^{-0.6}$. It is shown that the proposed transitional breakage probability can be approximated by a series of 'power law' models Kv^n with different exponents for differeat drop volume regions and that the value of the exponent increases as drop volume decreases. A functional relation for the rate constant K in the 'power law' approximation of the transitional breakage probability is derived in terms of the parameters and physical properties of the system. A universal non-dimensionalized equilibrium drop volume distribution for agitated lean liquid-liquid dispersions is derived by analytical solution of the population balance equation simplified by order of magnitude estimates under the assumptions of constant coalescence frequency and uniform binary breakage.

The prediction of equilibrium drop size distribution by solution of population balance equation necessitates the knowledge of breakage and coalescence. Even for lean dispersions, where the interaction between droplets is negligible, it is necessary to take coalescence into account which makes the population balance equation non-linear. Hence

it becomes necessary to make simplifying assumptions for the population balance equation to be amenable to solution. Prediction of equilibrium drop size distribution from a statistical thermodynamic viewpoint overcomes this drawback as it considers only the total energy of the system i.e. the kinetic, potential and interfacial energies of droplets. A statistical thermodynamic model for equilibrium drop size distribution is proposed. As the interaction between droplets is negligible for a lean liquid-liquid dispersion, the system is assumed to consist of independent droplets. A canonical ensemble of droplets is considered for the derivation of equilibrium drop size distribution. The energy of a droplet is split into: (i) Kinetic energy of pulsating convective motion (ii) Kinetic and potential energies of oscillation and (iii) Potential energy of a droplet at its spherical equilibrium shape. A partition function for a droplet is derived. A droplet is found to have 6 degrees of freedom. A universal non-dimensionalized drop volume density in terms of dimensionless drop diameter $d/\bar{d}_{32}$ is derived from the partition function of a droplet.

Drop volume distributions in a batch agitated lean liquid-liquid dispersion eventually approach an asymptotic distribution in the similarity variable $(1+Kt)v^n$ if (i) the transitional breakage probability $\Gamma(v)$ follows a 'power law' Kv^n and (ii) the breakage is 'similar' i.e. the daughter

droplet size distribution depends only on the ratio of the daughter and parent drop volumes. The existence of such a similarity transformation is made use of to verify the 'power law' approximation for transitional breakage probability and also to obtain the exponent n, rate constant K and the daughter droplet distribution from the transients of drop volume distribution in a batch agitated lean liquid-liquid dispersion.

Drop volume distribution measurements were made in a jacketted glass vessel agitated by a 6 blade paddle impeller. Measurements were made at the dispersed phase volume fraction of 0.1 per cent in order to minimise drop coalescence./ Microencapsulation technique was employed to freeze the system at the time of measurement. This technique encapsulates the droplets with a thin nylon film formed as a result of an interfacial polycondensation reaction. The volume distribution of drops was measured by means of electronic size analysis (Coulter Counter). Special probe assemblies consisting of platinum electrodes with apertures of 2 mm and 0.8 mm diameter were used to monitor the droplets. The pulse signals from the probe were processed and fed to a Multichannel analyser to give number count of droplets for different droplet volumes. This yielded volume distribution of droplets.

Transients of drop volume distribution in agitated lean liquid-liquid dispersions were measured for water - CCl_4 + i-Octane (50 - 50 per cent) system at three different agitator speeds of 480, 420 and 300 RPM with 3 inch diameter paddle impeller and at the agitator speed of 480 RPM with 2 inch diameter paddle impeller. Transients of drop volume distribution were also measured at the agitator speed of 300 RPM with 3 inch diameter paddle impeller for water-Anisole + CCl_4 (80-20 per cent) and water-chlorobenzene systems. Experimental results showed that the transitional breakage probability could be approximated by a 'power law' of varying exponents. The value of the exponents obtained from the experimental data agreed fairly well with the values obtained from the approximation of the predicted transitional breakage probability by a series of 'power law' models of varying exponents. The computations of the transitional breakage probability as predicted by the model yielded very large values of maximum stable drop volumes thus necessitating the introduction of a factor in the predicted transitional breakage probability in order to match its variation with experimentally observed variation. It is believed that the introduction of this factor is necessary to account for important inhomogeneities in the flow field of an agitated vessel. As the transitional breakage probability $\Gamma(v)$ could be approximated by a series of 'power law' models with different value of exponent for different

drop volume range and for each of these regions $Kv^n \cdot t$ is the similarity transformation at sufficiently large times, one would expect that a transformation $\Gamma(v) \cdot t$ would collapse all the drop volume distributions into a single curve irrespective of their region if the model for transitional breakage probability is indeed valid. The transformation

$$\text{erfc}\left[\left\{2(2^{1/3}-1)\pi^{1/3}6^{2/3}\frac{\sigma}{\rho}\right\}^{1/2}\left(\frac{\pi}{6}\right)^{1/9} v^{-5/18}/10\ \bar{\varepsilon}^{1/3}\right]\cdot t$$

seems to collapse all the drop volume distributions into a single curve thus vindicating the model for transitional breakage probability.

The modified similarity transformation $\left(\frac{v}{\bar{v}}\right)\cdot t^{1/n}$ collapses all the drop volume densities in a region into a single curve thus vindicating the assumption of 'similar' breakage made in the derivation of the similarity transformation. Hence the moments of daughter droplet distribution were computed from the moments of the modified drop volume density $f\left\{\left(\frac{v}{\bar{v}}\right) t^{1/n}\right\}$ and the daughter droplet distribution was estimated through orthonormal polynomial expansion. The estimated daughter droplet distribution indicated that (i) the breakage mechanism seems to be the same for all systems and experimental conditions (ii) the normalised daughter droplet density is more or less same for all the cases and (iii) the daughter droplet density is broad. The functional dependence of the estimated rate constant K with respect to the agitator speed and interfacial tension agrees well with the model.

The non-dimensionalized equilibrium drop volume density in terms of dimensionless drop diameter ($d/\bar{d}_{32}$) predicted by the kinetic and statistical thermodynamic models agree very well with each other. It is very interesting to note that the equilibrium drop volume density arrived at through two entirely different approaches predict more or less the same density. The experimental drop volume density $f_V(d/\bar{d}_{32})$ agreed fairly well with the gaussian approximation. However, there is a shift in the experimental drop volume density towards smaller dimensionless drop diameter ($d/\bar{d}_{32}$) when compared with the kinetic and statistical thermodynamic models and the agreement with the coalescence-redispersion model seems to be better. Comparison of the three models with the experimental data of Chen and Middleman, Brown and Pit and Shinnar showed that the experimental data agreed fairly well with kinetic and statistical thermodynamic models and that the coalescence-redispersion model did not agree with the experimental data. The discrepancy between the present experimental data of equilibrium drop volume density and the experimental data of Chen and Middleman, Brown and Pit and Shinnar could be due to loss of count of very small voltage pulses corresponding to droplets of very small volumes because of poor signal to noise ratio for these droplets.

NOMENCLATURE

a_{mn} = Constant defined in equation (4.2.8)

A = Work function

b_{mn} = Constant defined in equation (4.2.8)

c_{mn} = Constant defined in equation (4.2.23)

d = Drop diameter

$\bar{d}_{32}$ = Sauter mean drop diameter

d^* = Drop diameter at which the equilibrium drop volume density exhibits a maximum.

df = Area of a surface element

df_s = Area of a spherical surface element

d_{mn} = Constant defined in equation (4.2.23)

d_s = Maximum stable drop diameter

E = Internal energy

$\bar{E}$ = Ensemble average energy of a droplet

E_{min} = Minimum increase in specific interfacial energy of a droplet for fragmentation

f = Non-dimensionalized drop volume density in terms of droplet diameter

f = Cumulative distribution function in terms of similarity variable z

f_n = Normalised f

f_v = Non-dimensionalized drop volume density in terms of droplet volume

f' = Drop volume density function in terms of similarity variable z

F = Cumulative drop volume distribution function

g = Cumulative volume fraction of daughter droplets expressed in terms of the ratio of daughter and parent drop volumes

g' = Volume density of daughter droplets expressed in terms of the ratio of daughter and parent drop volumes.

G = Cumulative distribution function of daughter droplet volume.

H = Liquid depth in agitated vessel

H = Hamiltonian of a droplet

k = Boltzmann's constant

K = Rate constant in 'power law' expression for transitional breakage probability

L = Impeller diameter

M = Mass of a droplet

n = Exponent in 'power law' expression for transitional breakage probability

N = Speed of agitation, rotations/unit time

$\bar{N}$ = Ensemble average of total number of droplets

$N_{We} = \frac{L^3 N^2 \sigma}{\rho}$ = Weber number

p = Density function of daughter droplet volume arising from breakage of a parent droplet in terms of number

p = Momentum of a droplet

p = Induced pressure distribution on the surface of a droplet

p_σ = Capillary pressure

P = Power input

P = Pressure

$(P.E)_{eq}$ = Potential energy of a droplet at its spherical equilibrium shape

P_m^n = Associated Legendre function

P_m = Legendre polynomial of order m

Q = Partition function of a droplet

r = Droplet radius

t = Time

T = Diameter of the mixing vessel

T = Kinetic energy of oscillation

T = Temperature

T_d = Dispersion temperature

u = Relative velocity between two points

u_α = Characteristic velocity of an eddy of scale α

v = Drop volume

v_s = Maximum stable drop volume

v^* = Drop volume at which the equilibrium drop volume density exhibits a maximum

V = Dispersed phase volume fraction

V = Volume of liquid-liquid dispersion

V_{os} = Velocity of oscillation

w = Frequency of fluctuation

w_{nm} = mth natural frequency of oscillation of a droplet

x = Non-dimensionalized drop volume

x = Variable representing the ratio of daughter droplet volume to parent drop volume

X = Droplet diameter

X^* = Parameter defined in equation (4.3.2)

z = Similarity variable $(1 + Kt)V^n$

Greek Symbols:

α = Parameter defined in equation (3.2.12)

α_{mn} = Constant defined in equation (4.2.2)

β = Moment of modified daughter droplet distribution function for 'similar' breakage

β = Parameter defined in equation (4.2.23)

β_{mn} = Constant defined in equation (4.2.2)

γ = Universal transitional breakage probability in terms of non-dimensionalized droplet volume or diameter

γ = Moment of daughter droplet distribution function for 'similar' breakage

Γ = Transitional breakage probability

λ = Average number of eddies arriving on the surface of a droplet/unit time

λ = Moment of drop volume density in terms of modified similarity variable $(v/\bar{v})t^{1/n}$

σ = Interfacial tension

σ = Standard deviation of equilibrium drop volume density

ρ = Density of continuous phase

$\bar{\varepsilon}$ = Average power input/unit mass

ε = Energy dissipation rate/unit mass

μ = Coalescence frequency

μ = Moment of drop volume density in terms of similarity variable

μ = Viscosity of the continuous phase

μ = Chemical potential

ν = Mean number of droplets from breakage of a parent droplet

ϕ = Density function of droplet volume in terms of number

ϕ = Dispersed phase volume fraction

Ψ' = Velocity potential of the flow field inside a droplet

Ψ = Modified velocity potemtial

η = Generalized deformation coordinate

ξ = Non-dimensionalized droplet diameter

ξ = Deformation of a droplet from its spherical shape

Subscripts

x = x component

y = y component

z = z component

η = Momentum conjugate to η

X = Momentum conjugate to X

CHAPTER 1

INTRODUCTION

Dispersed systems are of common occurrence in many industrially important processes. Dispersed phase reaction, liquid-liquid extraction, gas absorption and emulsion polymerization are some such frequently encountered processes. Dispersed systems involve exchange of mass, momentum, energy or their combination between the dispersed and the continuous phases. The primary reason for dispersing one phase into the other in the form of droplets or bubbles is to increase the overall extent of such exchange through the increase of interfacial area.

Agitated liquid-liquid dispersions are encountered mainly in stagewise liquid-liquid extraction and emulsion polymerization. The interfacial area in such systems depends upon the drop size distribution, which is greatly influenced by drop breakage and coalescence. Moreover, the overall performance of an extraction stage or an emulsion polymerization reactor is influenced by such factors as the drop breakage, the repeated coalescence and redispersion of drops in turbulent flow field, local mass transfer and reaction rates between drops and the continuous phase. Although a cohesive model of the whole cannot yet be formulated, it is

necessary for a designer to have some information on each of the factors mentioned above, in order to make an intelligent selection of design or scale-up rules for his apparatus.

The general approach to the calculation of rate processes in liquid-liquid dispersions has been through the definition of an overall transfer coefficient or reaction rate based on the total interfacial area and average properties (concentration and temperature). This approach ignores altogether the fact that the dispersed phase exists as a population of droplets of different sizes and properties. Therefore, it does not take into account two important features of a dispersed system. Firstly, the transfer coefficient from an individual droplet directly depends on the size of the droplet which is influenced by breakage and coalescence; secondly, when the droplets coalesce, the gradients of concentration and temperature existing in the droplet before coalescence are destroyed and the resultant droplet attains the average concentration and temperature [1]. Moreover, the rate of breakage of 'primary droplets' [2] (Droplets formed due to breakage of large globules) will be quite small. The droplet size range of these primary droplets would possess large surface to volume ratio causing concentration and temperature changes at a rate likely to compete with the breakage rate of these drops. Thus, it is necessary to take into account the simultaneity of droplet phenomena

and rate processes for prediction of overall rate and extent of transfer in liquid-liquid dispersions.

The problem of prediction of transfer rates between dispersed and continuous phases in liquid-liquid dispersions, is therefore quite complex and must consider many factors that are not yet very well understood. Among these are the nature of drop breakage in a turbulent flow field with the associated formation of a wide distribution of drop sizes, the interaction between mass transfer and hydrodynamic effects, the repeated coalescence and redispersion of droplets in a dynamic environment. Though it is not possible to study all these factors at a time due to their inherent complexity, it is believed that study of these factors separately will not only lead to a better understanding of the process but also will contribute greatly to the evolution of a rational methodology for the prediction of transfer rates in liquid-liquid dispersions. With this in view, the present study restricts itself to drop breakage in agitated liquid-liquid dispersions. Moreover, in case of lean liquid-liquid dispersion (low dispersed phase fraction) only breakage need be considered as coalescence will be negligible due to negligible interaction between droplets.

Drop breakage in a turbulent flow field is random and hence is described by related probabilities, namely (i) the transitional breakage probability and (ii) daughter droplet

distribution [3]. An attempt is made to relate these probabilities to the characteristics of turbulent flow field and physical properties of the system. A model is proposed for the transitional breakage probability of droplets exposed to a turbulent flow field based on the mechanism of droplet breakage due to their oscillation resulting from relative velocity and pressure fluctuations of the turbulent flow field. Using this model, population balance equation was solved to predict the equilibrium drop size distribution. Transients of drop volume distribution in a batch agitated lean liquid-liquid dispersion was measured using encapsulation and electronic size analysis. Ramkrishna [4] proposed a method of evaluating the transitional breakage probability and daughter droplet distribution from the transients of drop volume distribution in a batch agitated lean liquid-liquid dispersion. This method was employed to calculate these probabilities from the experimental data which are then compared with the model. A model for equilibrium drop size distribution is also proposed from a statistical thermodynamic viewpoint. This model considers the total energy of liquid-liquid dispersion but does not take into account explicitly drop breakage and coalescence. The measured equilibrium drop size distribution was also compared with the model.

Chapter 2 gives a brief review of literature on drop breakage. Chapter 3 discusses the model for transitional

breakage probability and the evaluation of the probability and daughter droplet distribution from transients of drop volume distribution in a batch agitated lean liquid-liquid dispersion. Chapter 4 deals with the model on equilibrium drop size distribution from a statistical thermodynamic viewpoint. Chapter 5 discusses the experimental technique, apparatus and procedure. Experimental results and comparison between experimental data and the above models are presented in Chapter 6. Chapter 7 gives conclusion and recommendations.

CHAPTER 2

LITERATURE REVIEW

Drop breakage in agitated liquid-liquid dispersions is complex due to the complex nature of the turbulent hydrodynamic flow field to which the droplets are exposed. Since it is necessary to understand the droplet phenomena of breakage and coalescence in order to estimate the rate processes in agitated liquid-liquid dispersions, considerable attempts have been made to study drop breakage in agitated liquid-liquid dispersions. A brief review of the work accomplished in this direction is presented below.

2.1 DROP BREAKAGE MECHANISMS:

In liquid-liquid dispersions most of the ordinary dimunitive processes function either by injection of one phase into the other or by inducement of turbulence in the continuous phase. In case of injection, the potential energy of the phase to be dispersed is converted into kinetic energy, and at the same time usually interaction takes place with the continuous phase. This interaction generates forces in the phase to be dispersed which may result in its breaking up. In case of turbulence, it is the kinetic energy of the turbulent motion in the continuous phase that brings about the breakup of the other phase.

In general, the disintegration process takes place in stages. When one fluid is just squirted into another or when agitation has just started, the phase to be dispersed is at first present in bulk. The deformation of this bulk of fluid and its initial breakup into chunks of fluid, which may breakup further into smaller parts, has been much studied [5,6]. The mechanism of breakup of the bulk of fluid into globules seems to be the penetration of lamellae and ligaments of one fluid into another [6]. These ligaments then breakup into globules, which may further split into smaller parts. Important contributions have been made by theoretical and experimental studies of the instability of liquid films and cylindrical liquid ligaments [6,7]. These should give insight into the rupture of the lamellae into globules. These theories can be applied to some simple types of atomisation. But, in most cases, the breakup of bulk of the dispersed phase into globules is only the first stage of disintegration. This is usually followed by further breakup of these globules into smaller drops. When the viscosity and interfacial tension of the dispersed phase are not very high, this first stage of disintegration, viz. disintegration of bulk of liquid into globules, is extremely rapid and chaotic [8]. Since this first stage of disintegration is extremely rapid, it generally does not control the size distribution of droplets formed after further disintegration of globules.

The second stage of breakage is the further disintegration of the globules into smaller droplets as stated earlier. The study of this stage of disintegration is very important as it seems that this will control the sizes of droplets eventually formed in a breakage process. Fundamental work on the splitting of drops in viscous flow was done by Taylor [9] and Tomotika [10]. Taylor [9] developed a theory based on a few obvious assumptions, such as, small deformations, no slip at the interface and continuous shear stress across the interface. He considered two types of flow, namely, the couette flow and the plane hyperbolic flow. According to Taylor's theory, the deformation of drops is predominantly determined by the generalised Weber group $N_{We} = \frac{\mu_c S D}{\sigma}$, where S is the maximum velocity gradient in the flow field of the continuous phase. He determined the value of S at which breakup of a drop occurs, that is $(N_{We})_{Cri}$. He observed that the droplet exposed to the shear field elongated into a threadlike form. The disintegration of this thread led to formation of drops which are of the order of 1/100th of the size of the original drop. Ramscheidt and Mason [11] studied the deformation and burst of fluid drops in a liquid subjected to both hyperbolic and shear flow for a wide range of viscosity ratio. At low deformation, excellent agreement with the theoretical equations of Taylor was found. The critical conditions of burst were also found to be in reasonable agreement with the theory.

Hinze [8] studied the breakup of globules in viscous flow, breakup of drops exposed to airstream and emulsification in turbulent flow. He proposed that the deformation of a globule can be due to viscous stress or dynamic pressure and that the interfacial tension will give rise to a surface force that will in general counteract the deformation. He identified two dimensionless groups which would control the deformation and breakup: a Weber group N_{We} and a viscosity group N_{Vi}. He also proposed that breakup occurs when N_{We} exceeds a critical value $(N_{We})_{Crit.}$. Experimental observations showed that the mechanism of breakup was found to be quite simple when N_{We} is equal to or slightly higher than $(N_{We})_{Crit.}$. The more N_{We} exceeds its critical value, the more complicated this mechanism becomes. For $N_{We} \gg (N_{We})_{Crit}$ the mechanism is very complex and the disintegration process is more or less chaotic [8]. This is probably the reason why the second stage of breakage is simple and amenable to study compared to the first stage of disintegration. Hinze [8] also showed that in case of droplets exposed to an airstream and emulsification in turbulent flow, dynamic pressure forces rather than viscous forces were responsible for deformation and breakup. In case of emulsification in turbulent flow, the dynamic pressure forces were caused by changes in velocity at most equal to the diameter of the drop [8].

2.2 HYDRODYNAMIC CHARACTERISTICS OF THE FLOW FIELD IN AN AGITATED VESSEL:

In order to study the drop breakage in agitated liquid-liquid dispersions, it is necessary to have knowledge about the hydrodynamic characteristics of the flow field in an agitated vessel since the interacting forces responsible for deformation and eventual breakup of a droplet will depend on the nature of the flow field. Considerable amount of work has been done regarding the flow pattern, power consumption and the use of dimensional analysis in agitated vessels. Excellent reviews of the voluminous literature on flow fields in agitated vessels have been made [12, 13].

The flow regions of a stirred tank may be classified into impeller stream flowing radially towards the wall, the recirculation regions and the region surrounding the impeller where the recirculation loops meet. An extensive study of the flow pattern in a 60 cm tank has been reported by Nagata et al. [14]. They divided the recirculation flow pattern into roughly four zones: (i) the horizontal discharge jet, running from the impeller to the tank wall (ii) the vertical flow along the wall, (iii) the horizontal flow returning the fluid to the vicinity of the tank axis and (iv) the vertical flow along the axis towards the impeller. Power consumption in stirred vessels has been measured extensively and reported in the form of correlation for dimensionless power number as

a function of Reynolds number for different types of impellers [15, 16]. Measurement of the discharge rate of impellers has also been reported as a function of agitator speed and diameter [17].

Considerable attempts have recently been made to understand the nature of turbulence in agitated vessels. Cutter [18] studied turbulence in a batch baffled stirred tank with a disc turbine by means of a photographic technique. Most of the results presented were about the impeller stream. The important turbulence parameters obtained were intensities of turbulence, macroscales in the radial and tangential directions and estimates of energy dissipation rates in various parts of the tank from the energy equation. This work indicated that half of the total energy dissipation in the tank occurred in the impeller stream, a fifth in the impeller region itself and the remaining in the rest of the tank exhibiting important inhomogeneities in the flow regime. An important conjecture of Cutter [18] was the presence of intermittancy in the impeller stream. Schwartzberg and Treybal [19] used a photographic technique to determine the mean and fluctuating velocities in a baffled agitated vessel with a disc turbine. The measurements were made outside the impeller stream. Kim and Manning [20] presented radial intensity spectra as measured with a transducer probe. A region of slope -5/3 was observed in their spectra.

Muzumdar et al. [21] measured the turbulence parameters in a turbine stirred baffled tank with air as the medium using hot wire anemometer in the impeller stream. They observed large periodic components in the velocity near the impeller. They could not detect the region of -5/3 slope in the energy spectrum due to superimposition of periodic non-random velocities on the random velocity fluctuations. They also measured the probability density of velocity fluctuation which was found to be far from gaussian. I. Komasawa, R. Kuboi et al. [22] studied the turbulence in turbine stirred baffled vessel using tracer particles with the help of photography. Energy spectrum obtained by fourier analysis of autocorrelation showed a region of -5/3 slope. M. Ananda Rao and Broadkey [23] measured the mean velocities, RMS value of velocity fluctuation, one-dimensional energy spectra, normalised autocorrelation and probability density of velocity fluctuation in a continuous turbine stirred vessel with water as the medium using hot wire anemometer. They also observed periodic velocity components near the impeller. One dimensional energy spectrum exhibited a region of -5/3 slope over a decade of wave number range. The probability density of velocity fluctuation was found to be skewed negatively and far from gaussian due to intermittancy and non-isotropic conditions. A.A. Günkel and M.E.Weber [24] measured the turbulence parameters in a baffled stirred tank agitated by a six blade

disk turbine with air as the medium both in the impeller stream as well as in the bulk of the tank using hot wire probe. They also observed periodic velocity components in the impeller stream near the impeller. Their one dimensional energy spectrum in the impeller stream consisted of three regions, namely, the region of zero slope followed by the regions of -5/3 and -7 slopes. The nature of the energy spectrum was very much similar to the spectrum obtained by others [20, 21, 22, 23]. They calculated the rate of energy dissipation within the impeller stream by using the energy balance equation. The calculations showed that very little energy is dissipated within the impeller stream indicating that most of the energy dissipation took place in the bulk of the tank. This was in contradiction with the findings of Cutter [18]. A.A. Günkel and M.E. Weber [24] claimed that the inhomogenities observed by Cutter [18] were due to experimental errors in the measurement of velocity fluctuation. The measurements of A.A. Günkel and M.E.Weber [24] in the bulk of the tank showed that the turbulence in the bulk of the tank is isotropic and the velocity fluctuations did not change appreciably with position. One - dimensional energy spectrum obtained in the bulk of the tank also showed regions of zero, -5/3 and -7 slopes. The calculations of energy dissipation rates from the one-dimensional energy spectrum seem to confirm the view that most of the energy was dissipated in the bulk of the tank.

They compared their value of macroscale with the values obtained by Cutter [18], Rao and Broadkey [23] and Chao et al. [25] and showed that the turbulence in the bulk of the tank in the -5/3 slope region of the energy spectrum was independent of the viscosity of the medium and depends only on ε, thus vindicating Kolmogorov's theory of local isotropy.

2.3 EXPERIMENTAL INVESTIGATIONS ON DROP BREAKAGE IN AGITATED LIQUID-LIQUID DISPERSIONS:

The study of agitated liquid-liquid dispersions has been the subject of numerous investigations [26, 27]. In such systems, the drops of the dispersed phase are continuously broken and coalesced at a rate depending on the local hydrodynamic characteristics of the turbulent flow field and the physical properties of the system. Earlier experimental investigations on agitated liquid-liquid dispersions focussed on measurements of average droplet diameter by the use of light transmission, photographic techniques or chemical methods. Such experimental measurements resulted in correlations for average drop diameter in agitated liquid-liquid dispersions. Drop size distribution measurements were also made with photography, encapsulation, sedimentation and electronic size analysis. A number of investigators reported experimental data on interfacial area and drop size distribution in flow systems. Drop breakage in agitated liquid-liquid dispersions

has been analysed by many using Kolmogorov's theory of local isotropy. The applicability of the above theory in case of agitated liquid-liquid dispersions was illustrated with experimental evidence by Shinnar and Church [28]. They characterized breakage in turbulent flow field by a maximum stable drop diameter and derived an equation for the same as a function of impeller diameter, agitator speed, density and interfacial tension. Similar equations were derived by Hinze[8], Levich [29] and Chen and Middleman [30]. For drops much larger than the microscale of turbulence η, consideration of the balance between inertial and interfacial forces leads to a maximum stable drop diameter $d_{max} \alpha \quad \varepsilon^{-0.4}$. This has been confirmed experimentally for a variety of dispersed phase systems,covering a wide range of physical properties and experimental techniques [28, 30, 31, 32, 33, 34]. For drops smaller than η, viscous effects predominate, and Taylor's analysis [9] predicts $d_{max} \alpha \quad \varepsilon^{-0.5}$[33]. Experimental evidence of this dependence has been reported for gas-liquid systems [31], and for low interfacial tension systems [34], although in both cases the drop size was greater than the microscale of turbulence.

Vermuellen et al. [31] measured the interfacial area and mean drop diameter for agitated liquid-liquid dispersions using light transmission technique and arrived at a correlation for mean drop diameter which showed a dependence of $(N_{We})^{-0.6}$. The form of this correlation was found to be identical to the

theoretical equation derived by Shinnar and Church [28]. However, the correlation showed a dependence of mean drop diameter on dispersed phase fraction $\emptyset$ which indicated that coalescence was also important in their experiments. They also studied the effect of μ_c, μ_d and $\Delta \rho$ on mean drop diameter and found that they were relatively unimportant. Their Weber number was based on the mean density of the dispersion. Their experimental data exhibited deviation of as much as $\pm$ 60 per cent from the correlation. Only limited geometries, two tanks of different sizes and one impeller were employed in their experiments. Calderbank [32] measured the interfacial area in agitated liquid-liquid dispersions with concentration of the dispersed phase ranging from 0-20 per cent. The variation in the physical properties of the systems studied was limited. Their correlation for the sauter mean drop diameter $\bar{d}_{32}$ showed a dependence of $(N_{We})^{-0.6}$. The maximum deviation was found to be $\pm$ 10 per cent. Rodger et al. [35] measured average drop size in agitated liquid-liquid dispersions using equal volumes of both liquids. Their correlation for $\bar{d}_{32}$ showed a dependence of $(N_{We})^{-0.36}$. This agreed quite well with the relation for minimum stable drop diameter for coalescence of drops derived by Shinnar [33], using the concepts of local isotropy. This is understandable, as in Rodger et al.'s [35] experiments coalescence may be dominant due to high dispersed phase fraction. Chen and Middleman [30] measured

the equilibrium drop size distribution for agitated lean liquid-liquid dispersions. Their experimental sauter mean drop diameter $\bar{d}_{32}$ agreed well with the correlation of Vermuellen et al. [31]. Chen and Middleman [30] established the normality of the equilibrium drop volume distribution and showed that the equilibrium drop volume distributions for different experimental conditions and systems can be represented by a single distribution when reduced in terms of dimensionless drop diameter $d/\bar{d}_{32}$. Shinnar [33] measured drop size distributions of molten wax dispersed in hot water using photomicrography. He showed that it is possible to obtain turbulence stabilized dispersions under certain conditions if the maximum stable drop diameter for drop breakage is above the minimum stable drop diameter for coalescence. His experimental data on equilibrium drop volume distributions when reduced to dimensionless drop diameter $d/\bar{d}_{32}$ seem to agree fairly well with the correlation of Chen and Middleman [30]. Brown and Pit [36] measured equilibrium drop size distribution in kerosene-water system using photography for low dispersed phase fractions. The experimental data suggested that coalescence was absent. The equilibrium drop volume density in terms of dimensionless drop diameter $d/\bar{d}_{32}$ agreed fairly well with the correlation of Chen and Middleman [30]. Observation of an equilibrium drop size distribution in batch lean liquid-liquid dispersions [30, 33, 36] are indicative of restricted form of breakage

that lends credibility to the concept of maximum stable drop diameter. Since coalescence rates are expected to be negligible for a lean liquid-liquid dispersion due to negligible interaction between droplets, equilibrium drop size distribution in a batch agitated lean liquid-liquid dispersion does in fact correspond to a sluggish dynamic equilibrium between breakage and coalescence with the equilibrium density centred more or less around the maximum stable drop diameter [2]. Sprow [34] measured drop size distributions in the vicinity of a turbine impeller for lean iso-octane dispersion in salt water using electronic size analysis (coulter counter). The experimental results of d_{max} agreed well with the correlation of Vermuellen et al. [31]. Sprow [37] also measured drop size distributions in a strongly coalescing agitated liquid-liquid system. The drop size was found to vary considerably with position and drop sizes were found to be much smaller near the impeller and bigger outside the impeller stream. Such strong variation of drop size with position was also observed by Vanderveen [38] and Calderbank [32]. The experimental results of Sprow [37] indicated that drop breakup predominated near the impeller, whereas coalescence of drops was controlling in other locations. However, the experimental measurement of drop sizes in water-CCl_4 + i-octane system at low dispersed phase fractions using microencapsulation by Mylnek and Resnick [39] showed that there is almost no dependence of drop size on location. This

was due to the fact that coalescence rate was low compared to the circulation time. Comparison of mean drop diameters obtained using different impellers showed that the criterion of equal power per unit volume could be used for estimating drop size when going from one geometry to another, not too different, geometry at moderate impeller speeds. Park and Blair [40] studied the droplet interaction phenomena in lean agitated liquid-liquid dispersions using cine photography and light transmission technique. They observed coalescence and breakup events and measured the rate of coalescence at various positions in the tank. They found that drop breakup occurred near the impeller and the droplet coalescence predominated at other locations and that beyond distances from the impeller region of order of only 1/6th the impeller diameter, breakup was virtually non-existent.

Various investigators have reported average drop size and drop size distribution measurements for continuous flow agitated liquid-liquid dispersions. In continuous flow systems, drop size will be determined by the residence time of the dispersed phase in addition to the hydrodynamic conditions and physical properties. No correlation has been developed to account for this. Schindler and Treybal [41] and Coulaloglou and Tavlarides [42] observed that drop size varied with position in a continuous flow system. Coulaloglou and Tavlarides [42] measured the drop size distributions in the

circulation and impeller regions. They also measured coalescence frequencies. Differences observed in the size distributions between the regions were found to be smaller than would be expected considering the largely different hydrodynamic characteristics of the flow field. They attributed the relative spatial homogeneity of the dispersion to the low coalescence frequency amongst the droplets relative to the average internal circulation frequency of the fluid elements from the impeller tip and back and suggested that the ratio of the coalescence frequency to the circulation frequency can serve as a measure to determine whether or not one should treat a dispersion as being spatially homogeneous. It was observed that the dispersion was homogeneous as this ratio approached zero.

2.4 MODELLING OF DROP BREAKAGE IN AGITATED LIQUID-LIQUID DISPERSIONS:

The general mathematical formulation for the description of particulate systems was put forward by Hulbert and Katz [43] in which they describe the particulate system by a set of phase coordinates viz. the spatial coordinates of the particle and the properties of the particle. They developed a partial differential equation for the number density of particles in the phase space. Curl [44] employed population balance approach to describe dispersed phase mixing in agitated liquid-liquid dispersions. A simplified model was employed in which only uniform drop sizes were considered. The model assumed

two drop coalescences, the probability of coalescence being the same for every droplet. According to the model, the coalesced drops redisperse immediately to form new drops of equal size and coalescence and redispersion phenomena have no effect on mass transfer. The model is unrealistic as it does not include effects due to a distribution of drop sizes, uneven breakup of drops or a distribution of probabilities of coalescence with drop size or concentration. Baynes and Laurence [45] employed a trivariate distribution of droplet mass, amount of solute and age and population balance equation to describe mass transfer in agitated liquid-liquid dispersions. They considered homogeneous batch stirred tanks with equal rates of coalescence and breakage and with only binary coalescences followed by instantaneous breakup to form two drops of equal volume. They considered the simultaneity of droplet phenomena and mass transfer by introducing the concept of 'age' of a droplet and by employing a multivariate density for the calculation of mass transfer rates. Valentes, Bilous and Amundson [3] developed a comprehensive mathematical model for drop breakage in agitated liquid-liquid dispersion and predicted the drop size distribution evolved due to breakage by solving the population balance equation. They represented drop breakage by related probabilities, namely, the transitional breakage probability, daughter droplet size distribution and average number of daughter droplets formed upon breakage. They

considered limited and unlimited breakage of drops. They assumed a 'power law' model for transitional breakage probability. The model for limited breakage included the effects of agitator speed and physical properties of the system by taking into account the maximum stable drop diameter. Their calculations showed that the drop size distribution was sensitive to the average breakage time and the average number of daughter droplets formed upon breakage. Non-ideality in mixing vessels was also found to affect the drop size distribution in a continuous system. Valentes and Amundson [46] predicted the drop size distribution for a coalescing agitated liquid-liquid dispersion by proposing a model for coalescence frequency. The calculation of transients of drop size distribution in a batch agitated liquid-liquid dispersion with limited breakage indicated the existence of a dynamic equilibrium between breakage and coalescence for large times with the equilibrium drop size density independent of initial size distribution. Bajpai, Ramkrishna and Prokop [47] proposed a coalescence-redispersion model for equilibrium drop size distribution for an agitated liquid-liquid dispersion. They assumed that drop coalescence is followed by immediate redispersion into two drops whose sizes are distributed according to a uniform distribution in the ratio of the daughter drop volume to parent drop volume. They solved the population balance equation

under the assumption of constant coalescence frequency and obtained an exponential distribution for equilibrium drop volume distribution. It was found that the prediction was good for flat blade turbine agitated systems. For circulation stirring systems, the model predictions were substantially improved by assuming that the coalescence frequency is proportional to the diameters of the interacting drops. Steidl [48] proposed a statistical thermodynamic model for equilibrium drop size distribution in agitated liquid-liquid dispersion. The equilibrium drop size distribution was expressed in terms of a new temperature scale. However, the coordinates and the corresponding momentum coordinates of the defined phase space for liquid-liquid dispersions were not conjugate to each other. Although not directly applicable to agitated liquid-liquid dispersions, the work of Collins and Knudson [49] is of interest. They measured photographically the drop size distributions produced by turbulent pipe flow of two immiscible fluids and developed a stochastic model to describe the breakage of drops. They assumed that coalescence is absent. They incorporated maximum stable drop diameter d_{max} in their stochastic model. They also introduced a parameter $d_{1.0}$ which referred to the drop size above which drop breakup occurred instantaneously. One of the many postulated stochastic models was found to represent the experimental data fairly well. The introduction of the parameter $d_{1.0}$ corroborates the view

that drop breakage occurs in two stages and that the first stage of breakage, viz. breakage of large lumps of fluid, is instantaneous. Shah and Ramkrishna [1] proposed a population balance model for mass transfer in lean liquid-liquid dispersions. They accounted for the simultaneity of drop breakage phenomena and mass transfer by using a trivariate density in terms of drop size, concentration and age. They used a 'power law' model for transitional breakage probability similar to the one proposed by Valentes, Bilous and Amundson[3]. They assumed breakage to be limited and introduced a parameter akin to $d_{1.0}$ introduced by Collins and Knudson [49], in their model for transitional breakage probability. Zeitlin and Tavlarides [50] developed a model which accounts for complex fluid-fluid interactions and hydrodynamic effects in an agitated liquid-liquid dispersion. The mixing vessel was divided into different regions to account for the hydrodynamic inhomogeneities. Based on the model, the system was simulated using Monte-Carlo simulation technique. Both micromixing and macromixing effects on particle size distribution were taken into account by simulating the particle movement in the vessel and interaction between the droplets. The dispersed phase was assumed to consist of spherical drops with non-uniform size distribution and only biparticle coalescences were assumed to occur. Drop breakage was assumed to be limited and binary. Maximum stable drop diameter d_{max} and a parameter d_{min} analogous to $d_{1.0}$ introduced by Collins and Knudson [49] were incorporated

in the breakage model. Probability of breakage of a droplet was assumed to follow a 'power law'. The parameters of the model were estimated by comparing the calculated and experimental distributions.

Swift and Freidlander [51] in their study of coagulation of hydrosols have introduced the concept of self-preserving distributions which depends upon the existence of a similarity transformation between particle size variable and time. Kapur [52] has provided an application of this concept to problems in size reduction. Fillipov [53] in an interesting study of batch particle splitting processes has shown the existence of explicit similarity transformation under the conditions of 'power law' model for transitional breakage probability and 'similar' breakage. Ramkrishna [4] has shown the method of estimation of the 'power law' constants of transitional breakage probability and daughter droplet distribution from the transients of drop volume distribution in a batch agitated lean liquid-liquid dispersion. A preliminary analysis of the experimental data of transients of drop size distribution in batch agitated lean liquid-liquid dispersion obtained by Madden and McCoy [54] showed that 'power law' model for transitional breakage probability is indeed valid. Coulaloglou and Tavlarides [55] proposed phenemenological models for drop breakage and coalescence in a turbulently agitated liquid-liquid dispersion. Population

balance equation with the proposed models for breakage and coalescence was solved using iterative technique to predict the evolved drop size distribution. Drop breakage was described by a transitional breakage probability. A model for transitional breakage probability was proposed using Kolmogorov's theory of local isotropy. It was assumed that the fraction of drops breaking due to dynamic velocity and pressure fluctuations is proportional to the fraction of turbulent eddies colliding with the droplets that have a turbulent kinetic energy greater than the interfacial energy of the droplet. This was estimated under the assumption that the probability distribution of kinetic energy of eddies is exponential. Concept of breakage time was introduced in the definition of transitional breakage probability. Breakage time was estimated by assuming that the motion of the centres of mass of the daughter droplets to be formed is similar to the relative motion of two lumps of fluid in a turbulent flow field. The model was found to predict correctly the effect of impeller speed on maximum stable drop diameter.

CHAPTER 3

A MODEL FOR TRANSITIONAL BREAKAGE PROBABILITY OF DROPLETS IN AGITATED LEAN LIQUID-LIQUID DISPERSIONS

Drop size distributions in liquid-liquid dispersions evolve due to the dynamics of breakage and coalescence. Evolution of drop size distribution is important for prediction of, interfacial area, heat and/or mass transfer in liquid-liquid dispersions. Attempts have been made [1,3,46] to predict the drop size distribution in liquid-liquid dispersions using population balance equation. If considerations are restricted to lean dispersions (i.e. with low dispersed phase fractions) only breakage need be considered as coalescence is negligible due to very little interaction of droplets. Drop breakage in an agitated liquid-liquid dispersion is random due to random velocity and pressure fluctuations responsible for deformation and breakup of drops. Dynamics of drop breakage in agitated liquid-liquid dispersions has been characterised by transitional breakage probability $\Gamma(v)$ and daughter droplet size distribution $G(v,v')$ [3,4] defined as,

$\Gamma(v)dt$ = Probability that a drop of volume v will break in time interval t and t+dt.

and $G(v,v')$ = Volume fraction of daughter droplets with volume less than v formed from breakage of a droplet of volume v'.

Quantitative prediction of droplet dynamics in lean dispersions requires information regarding transitional breakage probability $\Gamma(v)$ and daughter droplet distribution $G(v,v')$. A model for transitional breakage probability of droplets in agitated lean liquid-liquid dispersions is proposed based on the mechanism of breakage of droplets due to their oscillations resulting from relative velocity fluctuations. A universal non-dimensionalized equilibrium drop volume distribution for batch agitated lean liquid-liquid dispersions is derived by analytical solution of population balance equation simplified by order of magnitude estimates. Since it is not possible to make a direct experimental measurement of transitional breakage probability $\Gamma(v)$, one has to devise an indirect method of estimation of $\Gamma(v)$ in order to verify the model. Ramkrishna [4] has shown the method of estimating 'power law' constants of transitional breakage probability and daughter droplet size distribution from the transients of drop volume distribution in a batch agitated lean liquid-liquid dispersion. The details of the method are also presented.

3.1 MODEL FOR TRANSITIONAL BREAKAGE PROBABILITY:

A droplet exposed to a turbulent flow field will be subject to both inertial as well as viscous forces [33]. If the droplet is much larger than the microscale of turbulence,

the viscous forces can be neglected. In agitated vessels, the Reynolds numbers are so high that the microscale of turbulence is found to be much smaller than the size range of droplets encountered [28]. In such a case, the droplet will oscillate about its spherical equilibrium. The oscillations are brought about by the kinetic energy of the turbulent motion in the continuous phase [28, 33], or equivalently, by the relative velocity fluctuations between points near the vicinity of the droplet surface. In other words, the kinetic energy of the turbulent motion brings about the increase in the interfacial energy of the droplet through deformations. Fragmentation of the droplet occurs, if the turbulent motion provides the minimum increase in the interfacial energy for breakup.

In a turbulent flow field, velocity fluctuations at a point can be thought of as due to arrival of eddies of different scales (frequencies). Similarly, the relative velocity fluctuations around the surface of a droplet exposed to a turbulent flow field can be viewed as due to arrival of either an eddy or eddies of different scale (frequency) on the surface of the droplet.

At this point, we compare the time scales of (1) arrival of an eddy on the surface of a droplet and (2) oscillation of the droplet. The time scale of oscillation of a droplet should correspond to the frequency of the eddy causing these

oscillations. Since oscillations can be caused only by eddies of scale smaller than the diameter of the droplet, for sufficiently small droplets the time scales of oscillation should be very small. Moreover, oscillation of a droplet around its spherical equilibrium position necessitates the time scale of arrival of an eddy to be much larger than the time scale of oscillations, for otherwise, the effect of an eddy will not persist long enough for the oscillations of a droplet around its spherical equilibrium position to occur. If the time scales of arrival of an eddy is comparable to or less than the time scale of oscillation of the droplet, the effect of eddies will be to cause an irregular or bulgy deformation of the droplet. Hinze [8] considered bulgy deformation as one of the possible mechanisms of deformation of a globule exposed to a turbulent flow field.

At sufficiently high Reynolds numbers, the flow field in an agitated lean liquid-liquid dispersion is locally isotropic [20, 21, 23, 24, 28]. Hence we need to consider only the relative velocity fluctuations between any two diametrically opposite points on the surface of the droplet [33] i.e. the oscillating droplet can be considered as a one-dimensional simple harmonic oscillator. The points A and B represent any two diametrically opposite points on the droplet

surface. The restoring action of the drop due to interfacial tension can be represented by the spring connecting the points A and B. Since the size range of droplets is much above the microscale (unless the agitation speeds are very high), viscosity effects are negligible. Therefore, the simple harmonic oscillator can be considered undamped. For an undamped oscillator, the sum of potential and kinetic energy is constant, the potential energy signifying the interfacial energy of the droplet. Taking the datum of interfacial energy to be that at the spherical equilibrium position,

Maximum interfacial energy = Maximum kinetic energy of oscillation

Thus,

Maximum specific interfacial energy	= Energy of the arriving eddy
Maximum increase in the specific interfacial energy above the equilibrium value	= Energy of the arriving eddy

Here we make a postulate that the number of eddies arriving on the surface of a droplet is a poisson process i.e.

(i) The numbers of eddies arriving on the surface of a droplet in disjoint time intervals are independent.

(ii) Pr [one eddy arrives on the surface in time interval $t, t+dt] = \lambda\, dt + 0(dt^2)$

(iii) Pr [more than one eddy arrives on the surface in time interval t, t+dt] = 0 (dt^2)

where λ = average number of eddies arriving on the surface of a droplet/unit time.

Since we need to consider only the inertial subrange of Kolmogorov's universal spectrum and the effect of eddies of scale less than or of the order of microscale of turbulence is negligible, we can neglect the effect of μ on λ. However, we can expect , the parameter of the Poisson process, to depend both on the diameter of the droplet and power input per unit mass $\bar{\varepsilon}$. In the absence of a priori information about the dependence of λ on the droplet diameter and $\bar{\varepsilon}$, we assume it to be independent of droplet diameter and $\bar{\varepsilon}$ i.e. λ can be regarded as a constant.

We consider a small time interval τ, and define two events A and B as

A : An eddy arrives on the surface of a droplet in the time interval τ.

B : The arriving eddy has energy greater than or equal to the minimum increase in the interfacial energy required to break a droplet of volume V, $E_{min}(v)$.

Clearly we have $P(A) = \lambda\tau$.

$$\Pr[\text{Droplet of volume } v \text{ breaks in time interval } \tau]$$
$$= P(A) \cdot P(B \mid A)$$
$$= \lambda\tau \cdot P(B \mid A)$$

Therefore,

$$\lim_{\tau \to 0} = \frac{\Pr[\text{Droplet of volume } v \text{ breaks in time interval } \tau]}{\tau}$$

$$= \Gamma(v) = \lambda \cdot P(B \mid A) \qquad (3.1.1)$$

The interfacial energy of a droplet of volume v

$$= \sigma\, \pi^{1/3}\, 6^{2/3}\, v^{2/3}$$

It can easily be shown that the increase in the interfacial energy required for fragmentation is minimum if binary equal breakage occurs.

Therefore, minimum increase in the interfacial energy for fragmentation

$$= (2^{1/3} - 1)\, \sigma\, \pi^{1/3}\, 6^{2/3}\, v^{2/3}$$

This energy is provided by the kinetic energy of oscillation of the droplet.

Therefore, minimum relative velocity of oscillation required for fragmentation is given by,

$$\frac{1}{2} (\rho v)\, u_{min}^2 = (2^{1/3} - 1)\, \sigma\, \pi^{1/3}\, 6^{2/3}\, v^{2/3} \qquad (3.1.2)$$

$$\frac{1}{2}\, u_{min}^2 = (2^{1/3} - 1)\, \frac{\sigma}{\rho}\, \pi^{1/3}\, 6^{2/3}\, v^{-1/3} \qquad (3.1.3)$$

If the characteristic velocity of an eddy of scale α is u_α, then its kinetic energy is $\frac{1}{2} u_\alpha^2$ and for breakage to occur, we must have $\frac{1}{2} u_\alpha^2 \geq \frac{1}{2} u_{min}^2$.

In order to evaluate $\Gamma(v)$, we need to know the probability distribution of the relative velocity between two points separated by a distance r. Experimental measurements of probability distribution of velocity fluctuation at a point in the impeller stream in an agitated vessel [21,23] have shown that this probability distribution may not be far from Gaussian. The gaussian approximation may be better at higher impeller speed (or higher Reynolds number) as intermittant flow conditions and non-isotropic conditions tend to become less pronounced. Given that the probability distribution of velocity at a point in an agitated vessel is normal, the most natural assumption about the joint probability distributions of velocities at two points is that it is normal. This, according to Batchelor [56] follows from the central limit theorem, since the turbulent velocities are subject to the influence of a large number of random eddies or local flow. On the other hand, such an assumption cannot be exactly true especially for very small values of r, because it amounts to neglecting non-linear terms in the dynamical equations, or, equivalently, the non-linear modulations of the energy spectrum [56]. Due to lack of adequate information regarding the joint probability distribution of 2-point velocities in agitated vessels, we make the assumption that the joint probability distribution is normal. From this assumption, it follows that the probability

distribution of relative velocity between two points is also normal.

If u is the relative velocity between two points separated by a distance d at any time t, from Kolmogorov's theory of local isotropy

$$\overline{u^2(d)} = 2(\bar{\varepsilon}\, d)^{2/3} \qquad (3.1.4)$$

By integration of the universal inertial subrange of the energy spectrum, it can be seen that only the effect of eddies whose scale is less than d is taken into account in the evaluation of $\overline{u^2(d)}$ as given by (3.1.4).

Hence the probability density of the relative velocity u between two points separated by distance d is given by,

$$P(x) = \frac{1}{\sqrt{2\pi}\,\sigma} \exp\left[-\frac{x^2}{2\,\sigma^2}\right] \qquad (3.1.5)$$

where $\sigma^2 = \overline{u^2(d)}$. Hence the transitional breakage probability $\Gamma(v)$ is obtained as

$$\Gamma(v) = \lambda \Pr[u^2 \geqslant u_{min}^2] = \lambda \operatorname{erfc}\,(u_{min}/\sqrt{2}\sigma)$$

$$= \lambda \operatorname{erfc}\left(\sqrt{a}\left(\frac{\pi}{6}\right)^{1/9} v^{-5/18}/2\, \bar{\varepsilon}^{\,1/3}\right) \qquad (3.1.6)$$

where $a = 2(2^{1/3}-1)\,\pi^{1/3}\,6^{2/3}\,\frac{\sigma}{\rho}$

Similarly

$$\Gamma(d) = \lambda \operatorname{erfc}\left(\sqrt{a}\,\left(\frac{\pi}{6}\right)^{-1/6} d^{-5/6}/2\, \bar{\varepsilon}^{\,1/3}\right) \qquad (3.1.7)$$

We define a maximum stable drop diameter d_s such that

$$\frac{\sqrt{a}\,(\frac{\pi}{6})^{-1/6}\,d_s^{-5/6}}{2\,\bar{\varepsilon}^{1/3}} = 3.5 \qquad (3.1.8)$$

as $\operatorname{erfc}(\beta) \simeq 0$, if $\beta \geqslant 3.5$. From squaring equation (3.1.8) we have

$$2(2^{1/3}-1)\,\pi^{1/3}\,6^{2/3}\,\frac{\sigma}{\rho}\,\frac{(\frac{\pi}{6})^{-1/3}\,d_s^{-5/3}}{4\,\bar{\varepsilon}^{2/3}} = 12.25$$

Thus, $$d_s^{-5/3} = C_1\,\frac{\bar{\varepsilon}^{2/3}\,\rho}{\sigma}$$

where $$C_1 = \frac{24.5}{(2^{1/3}-1)6}$$

For a baffled agitated vessel [33],

$$\bar{\varepsilon} = C_2\,N^3L^2; \quad \bar{\varepsilon}^{2/3} = C_3\,N^2\,L^{4/3} \qquad (3.1.9)$$

Substituting,

$$d_s^{-5/3} = C_1C_3\,\frac{N^2L^{4/3}}{\sigma}$$

$$(\frac{d_s}{L}) = C_4(\frac{N^2L^3}{\sigma})^{-0.6} = C_4\,N_{We}^{-0.6} \qquad (3.1.10)$$

where $C_4 = (C_1C_3)^{-0.6}$

The functional form of this expression is identical to the empirical relations obtained for average drop diameter of equilibrium distribution in batch agitated liquid-liquid dispersions [31, 32, 39].

Redefining the transitional probability in terms of dimensionless drop volume and drop diameter we get,

$$\gamma\left(\frac{v}{v_s}\right) = \lambda \operatorname{erfc}\left\{3.5 \left(\frac{v}{v_s}\right)^{-5/18}\right\} \qquad (3.1.11a)$$

$$\gamma\left(\frac{d}{d_s}\right) = \lambda \operatorname{erfc}\left\{3.5 \left(\frac{d}{d_s}\right)^{-5/6}\right\} \qquad (3.1.11b)$$

We recognise that this is a universal relation for all liquid dispersions whose viscosity and density are not very different from those of the continuous phase. The behaviour of γ with $\frac{v}{v_s}$ is shown in Figure 3.1.

From Figure 3.2, we see that the transitional breakage probability $\gamma\left(\frac{v}{v_s}\right)$ can be approximated by a series of 'power law' approximations of varying exponents for different volume regions. Figure 3.2 gives the region of dimensionless droplet volume $\frac{v}{v_s}$ and the corresponding exponent of 'power law' approximation of transitional breakage probability. From the experimental data of Madden and McCoy [54] on cumulative volume distribution of dispersed phase in a batch agitated vessel, Ramkrishna [4] has found that a 'power law' approximation for the transitional breakage probability holds good. The exponent obtained with respect to droplet volume v, by a preliminary analysis, was 2.0. This value agrees fairly well with the exponent 2.12 for the dimensionless droplet volume $\frac{v}{v_s}$ range of 2 to 4.5 as can be seen from Figure 3.2.

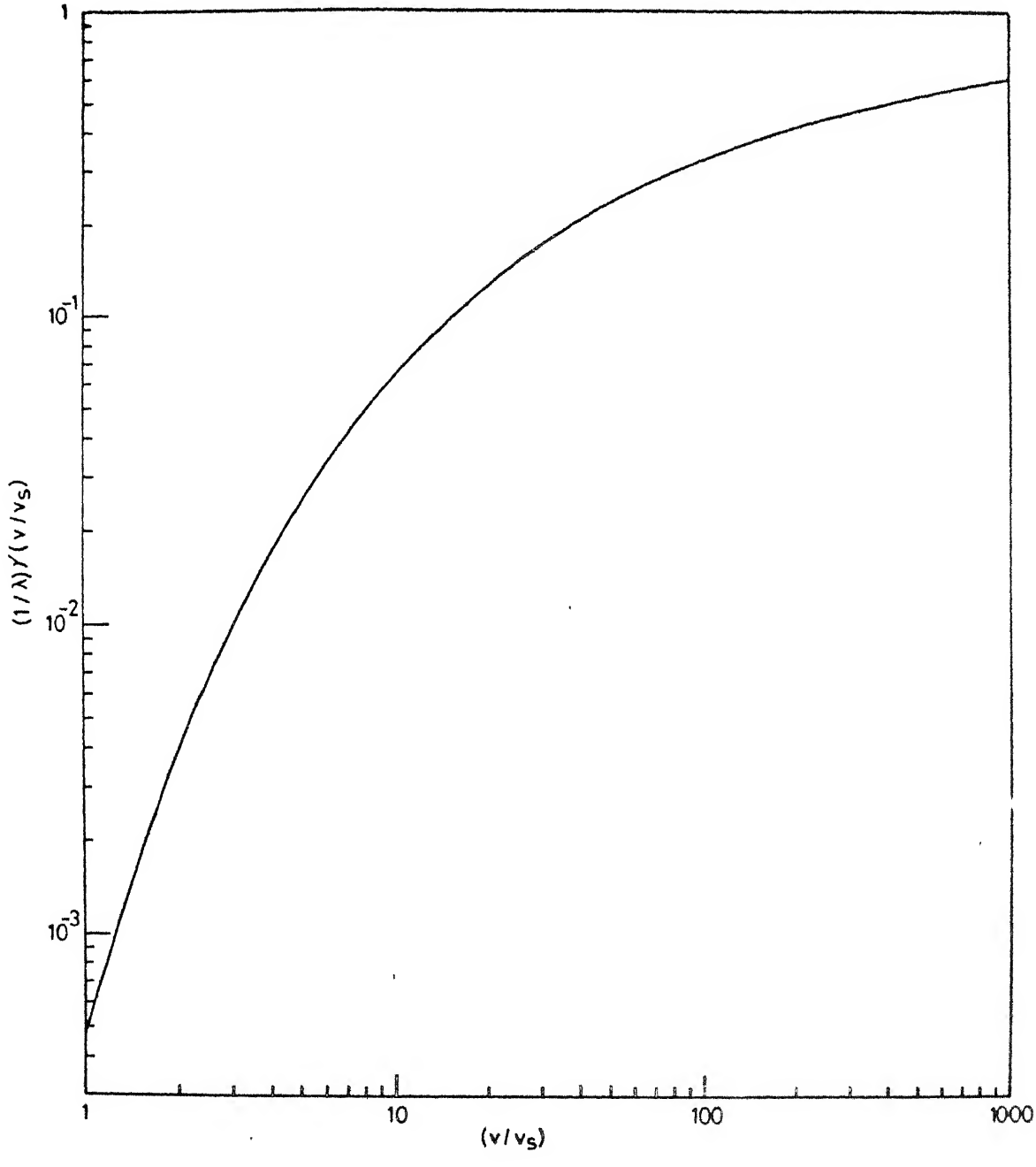

Fig. 3.1 -Transitional breakage probability γ as a function of (v/v_s)

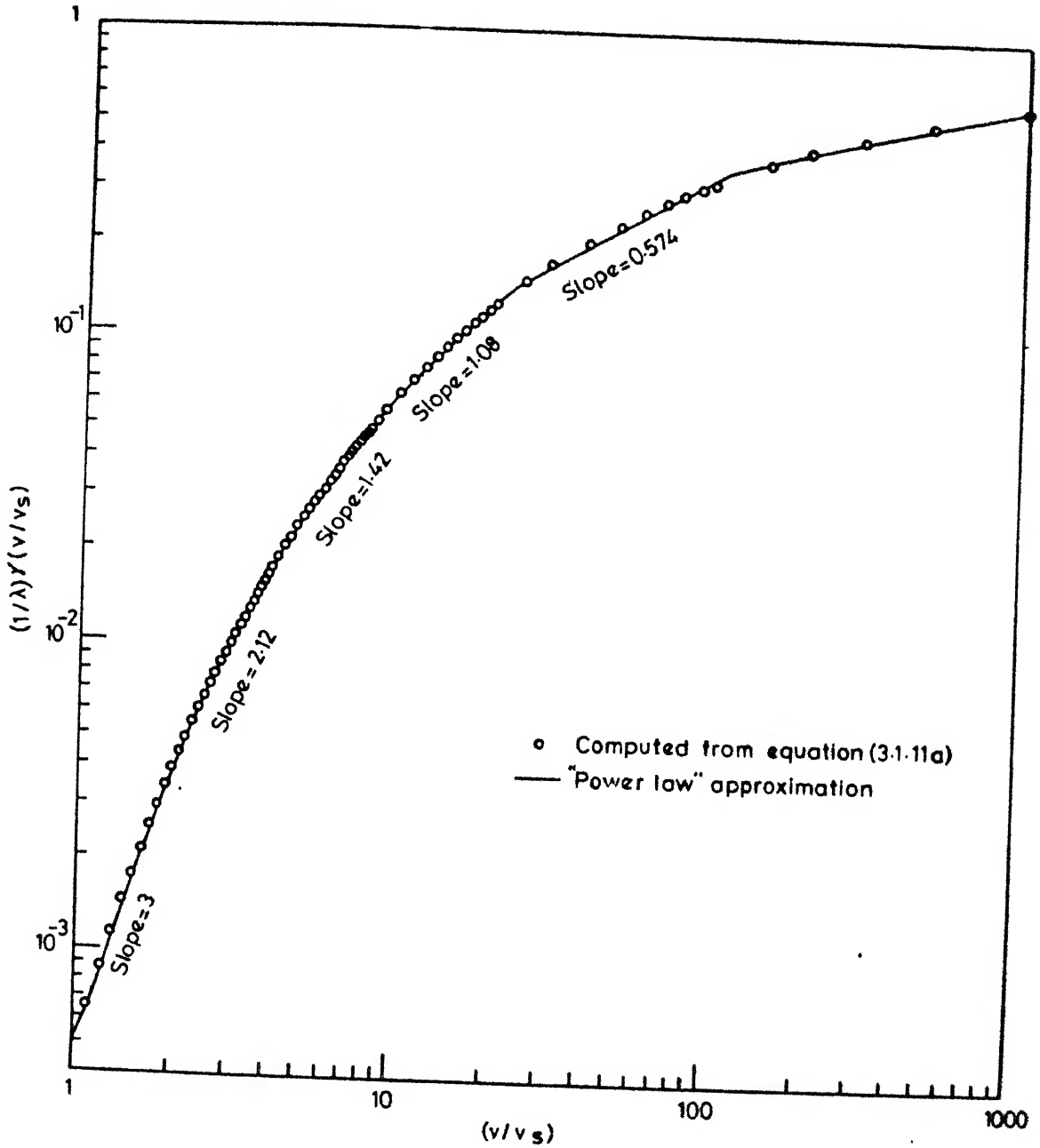

Fig.3.2 -"Power law" approximation for transitional breakage probability.

For the 'power law' approximation of the transitional breakage probability, we have,

$$\Gamma(v) = K\, v^{n}$$

where K is the rate constant.

Expressing the transitional breakage probability in terms of dimensionless droplet volume ($\frac{v}{v_s}$), we have,

$$\gamma\left(\frac{v}{v_s}\right) = \Gamma(v) = b\left(\frac{v}{v_s}\right)^{n}$$

where b is a universal constant for the region of dimensionless droplet volumes for which n is the value of the exponent.

$$K = b\, v_s^{-n}$$

i.e. $K \alpha v_s^{-n} \alpha d_s^{-3n}$

From the expression for maximum stable drop diameter d_s, we see that,

$$K \alpha (\bar{\varepsilon})^{\frac{6n}{5}} (\rho)^{\frac{9n}{5}} (\sigma)^{-\frac{9n}{5}} \qquad (3.1.12)$$

From the above expression for functional dependence of the rate constant K on ρ, $\bar{\varepsilon}$ and σ, we see that K increases as $\bar{\varepsilon}$ increases, and decreases as σ increases. This behaviour is of course as it should be.

Substituting for power input per unit mass $\bar{\varepsilon}$ in terms of agitator speed and impeller diameter in equation (3.1.12), we get,

$$K \alpha N^{\frac{18n}{5}} L^{\frac{12n}{5}} \rho^{\frac{9n}{5}} \sigma^{-\frac{9n}{5}} \qquad (3.1.13)$$

Near d_s, the asymptotic expansion of the complimentary error function yields an approximate expression for γ as

$$\gamma\left(\frac{d}{d_s}\right) = \frac{\lambda}{\sqrt{\pi}} \frac{1}{3.5} \left(\frac{d}{d_s}\right)^{5/6} \exp\left[-12.25 \left(\frac{d}{d_s}\right)^{-5/3}\right] \tag{3.1.14}$$

For $\frac{d}{d_s} \simeq 1$

$$\gamma\left(\frac{d}{d_s}\right) \simeq \frac{\lambda}{\sqrt{\pi}} \frac{1}{3.5} \left(\frac{\bar{d}}{d_s}\right)^{5/6} \exp\left[-12.25\left(\frac{d}{d_s}\right)^{-5/3}\right] \tag{3.1.15}$$

$\bar{d}$ denoting an average diameter.

From Figure 3.3, it can be seen that this approximation is quite good upto $\frac{d}{d_s} = 1.5$. We shall later use this expression of γ as given by equation (3.1.15) in the derivation of equilibrium drop volume distribution in a batch agitated lean liquid-liquid dispersion.

Substituting for d_s in equation (3.1.14) from equation (3.1.10), the approximate expression for the transitional breakage probability near d_s can be written as,

$$\Gamma(v) \simeq C_I \, N \, L^{2/3} \, \rho^{1/2} \, v^{5/18} \exp\left[-C_{II} \frac{\sigma}{v^{5/9} N^2 L^{4/3} \rho}\right] \tag{3.1.16}$$

C_I and C_{II} being constants.

At this point, we compare the present model for the transitional breakage probability with the model proposed by Coulaloglou and Tavlarides [55]. Their final expression for the transitional breakage probability is given by,

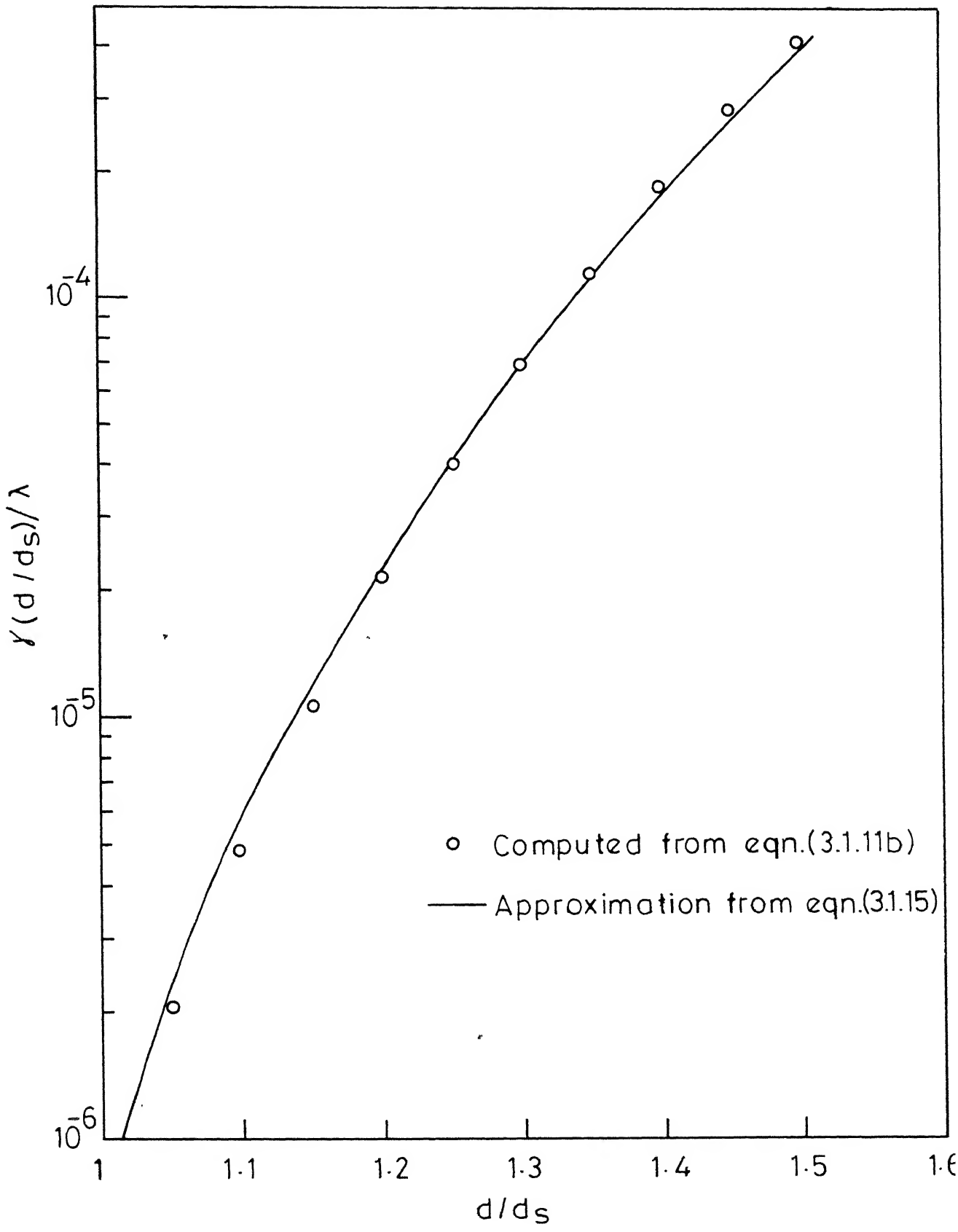

Fig. 3·3 -Approximation for transitional breakage probabil
γ near d_s.

$$\Gamma(v) = C_I \, v^{-2/9} \, L^{2/3} \, N \quad \exp\left[- \frac{C_{II} \, \sigma}{\rho \, v^{5/9} L^{4/3} N^2} \right].$$

The functional form of this expression does not agree with the present model. However, comparing the above expression with the asymptotic expansion of transitional breakage probability near v_s as given by equation (3.1.16), we find that the functional forms are similar and that the arguements of the exponential function in both the cases are identical. Coulaloglou and Tavlarides [55] have not defined a maximum stable drop diameter. However, their functional dependence of maximum stable drop diameter on agitation speed N, viz. $d_s \propto N^{-6/5}$, agrees with equation (3.1.10). They assumed that the fraction of drops breaking is proportional to the fraction of turbulent eddies colliding with the droplet that have a turbulent kinetic energy greater than the droplet interfacial energy. They also assumed that the probability distribution of kinetic energy of eddies is exponential. Such an assumption is not supported by the experimental measurement of probability density of velocity at a point in agitated vessels [21, 23]. They introduced the concept of 'breakage time' in their derivation of transitional breakage probability. The breakage time was estimated by assuming that the motion of the centres of mass of the daughter droplets to be formed by binary breakage is similar to the relative motion of two lumps of fluid in

a turbulent flow field. In their estimation of breakage time, they did not take into account the resistance to deformation and breakage of droplets because of the restoring force due to the interfacial tension.

3.2 EQUILIBRIUM DROP VOLUME DISTRIBUTION FOR BATCH AGITATED LEAN LIQUID-LIQUID DISPERSIONS:

In an agitated batch liquid-liquid dispersion, continuous breakup and coalescence of drops occur. Eventually, a dynamic equilibrium between breakup and coalescence is established and a spectrum of drop sizes results. For a lean liquid-liquid dispersion, the rate of coalescence, though small, becomes important near equilibrium as the equilibrium is dynamic. Hence at equilibrium the rate of breakage, in order to compensate for the rate of coalescence, has to be small. So, we can expect the equilibrium distribution to be narrow around the maximum stable drop diameter d_s. Experimental observations of equilibrium distribution do show that they are narrow [30].

A population balance equation for a batch liquid-liquid dispersion is given by,

$$\frac{\partial \phi(v,t)}{\partial t} = \int_v^\infty \nu(v')\ \Gamma(v')\ p(v,v')\ \phi(v',t)\ dv' - \Gamma(v)\ \phi(v,t) + \frac{1}{2}\int_0^v \mu\ \phi(v',t)\ \phi(v-v',t)\ dv' - \int_0^\infty \mu\ \phi(v,t)\ \phi(v',t)\ dv' \qquad (3.2.1)$$

where $\phi(v,t)$ = Number density of drop population,

$\nu(v')$ = Mean number of daughter droplets obtained by breakage of a parent droplet of volume v'

$p(v, v')dv$ = Probability that a daughter droplet arising from a parent of volume v' has its volume between v and $v+dv$

and μ = Coalescence frequency.

At equilibrium,

$$0 = \int_v^\infty \nu(v')\ \Gamma(v')\ p(v,v')\ \phi(v')\ dv' - \Gamma(v)\ \phi(v) + \frac{1}{2}\int_0^v \mu\ \phi(v')\ \phi(v-v')\ dv' - \int_0^\infty \mu\ \phi(v)\ \phi(v')\ dv' \qquad (3.2.2)$$

We assume that the coalescence frequency μ is a constant as the equilibrium distribution is narrow. Moreover, at equilibrium, the rate of breakage is small i.e. the energy of oscillation available from the turbulence of the continuous phase is only slightly higher than the minimum increase in the interfacial energy for breakage. Hence we can expect the breakage to be mostly binary. We also assume that the daughter droplet size distribution is uniform (i.e. perfectly random).

i.e. $\nu(v) = 2$; $p(v,v') = \frac{1}{v'}$

Hence the population balance equation is,

$$0 = 2 \int_{v}^{\infty} \Gamma(v') \frac{\phi(v')}{v'} dv' - \Gamma(v)\, \phi(v) + \frac{\mu}{2} \int_{0}^{v} \phi(v')\, \phi(v-v')\, dv' - \mu\, \phi(v) \int_{0}^{\infty} \phi(v')dv' \qquad (3.2.3)$$

Bajpai, Ramkrishna and Prokop [47] have proposed an equilibrium drop size model based on viewing the coalescence-redispersion process as a single step process based on a constant coalescence frequency and a perfectly random redispersion. This model, which showed good agreement with experimental drop size distributions, is not applicable for very low dispersed phase fractions in which both breakage and coalescence rates are very small. This is the situation, which the present model is aimed at.

As $\phi(v) = \frac{f_v(v)}{v}$, the population balance equation can be written in terms of volume density $f_v(v)$ as,

$$0 = 2 \int_{v}^{\infty} \Gamma(v') \frac{f_v(v')}{v'^2} dv' - \frac{\Gamma(v)\, f_v(v)}{v} + \frac{\mu}{2} \int_{0}^{v} \frac{f_v(v')}{v'} \frac{f_v(v-v')}{(v-v')} dv' - \mu \frac{f_v(v)}{v} \int_{0}^{\infty} \frac{f_v(v')}{v'} dv' \qquad (3.2.4)$$

Let v^* be the volume at which the equilibrium density $f_v(v)$ exhibits a maximum. We define a non-dimensional drop volume $x = \frac{v}{v^*}$. In terms of non-dimensional volume x equation (3.2.4) is

For a narrow equilibrium distribution, it can be shown that (see Appendix I) the coalescence term

$$\frac{\mu}{2} \xi^5 \int_0^{\xi} \frac{f(\xi')}{\xi'^3} \frac{d}{d\xi} \left[\frac{f(\xi - \xi')}{(\xi - \xi')^5} \right] d\xi'$$

is of a much smaller order of magnitude than the other terms in the above equation. Hence equation (3.2.7) becomes,

$$0 = -\frac{\gamma(\xi) f(\xi)}{\xi} - \gamma'(\xi) f(\xi) - \gamma(\xi) f'(\xi) - \mu f'(\xi) \kappa + \mu \frac{5 f(\xi)}{\xi} \kappa \qquad (3.2.8)$$

where $\kappa = \int_0^{\infty} \frac{f(\xi)}{\xi^3} d\xi$ is a constant.

Thus

$$\frac{f'(\xi)}{f(\xi)} = \frac{5\mu\kappa - \gamma(\xi) - \xi\gamma'(\xi)}{\xi[\mu\kappa + \gamma(\xi)]} \qquad (3.2.9)$$

In Appendix I, it is shown that $\mu\kappa \gg \gamma(\xi)$ so that equation (3.2.9) becomes,

$$\frac{f'(\xi)}{f(\xi)} = \frac{5\mu\kappa - \gamma(\xi) - \xi\gamma'(\xi)}{\xi\mu\kappa} \qquad (3.2.10)$$

Since we expect the distribution to be narrow around d_s, we use the approximate expression for γ near d_s given by equation (3.1.15)

$$\gamma'(\xi) = A \exp\left[-\alpha B \xi^{-5/3}\right] \qquad (3.2.11)$$

where $A = \frac{\lambda}{3.5\sqrt{\pi}} \left(\frac{\bar{d}}{d_s}\right)^{5/6}$; $B = 12.25$; $\alpha = \left(\frac{d^*}{d_s}\right)^{-5/3}$ (3.2.12)

Substituting for γ in equation (3.2.10),

$$\frac{f'(\xi)}{f(\xi)} = \frac{\frac{5\mu\kappa}{\xi} - \frac{A}{\xi}\exp\left[-\alpha B \xi^{-5/3}\right] - A \alpha B \frac{5}{3} \xi^{-8/3}\exp\left[-\alpha B \xi^{-5/3}\right.}{\mu \kappa} \tag{3.2.13}$$

Since $f'(1) = 0$

$$5 \mu \kappa - A \exp[-\alpha B] - A \alpha B \frac{5}{3} \exp[-\alpha B] = 0 \tag{3.2.14}$$

The elimination of A from equation (3.2.13) using (3.2.14) yields,

$$\frac{f'(\xi)}{f(\xi)} = 5\left[\xi^{-1} - \exp\left[-\alpha B(\xi^{-5/3} - 1)\right] \frac{(\frac{5}{3}\alpha B \xi^{-8/3} + \xi^{-1})}{(\frac{5}{3}\alpha B + 1)}\right] \tag{3.2.15}$$

Now $\frac{5 \alpha B}{3} \simeq 18$ and for $\xi \simeq 1$ we have

$$\frac{\frac{5}{3}\alpha B \xi^{-8/3} + \xi^{-1}}{\frac{5}{3}\alpha B + 1} \simeq \xi^{-8/3}$$

Hence

$$\frac{f'(\xi)}{f(\xi)} = 5\left[\xi^{-1} - \xi^{-8/3} \exp\{-\alpha B(\xi^{-5/3} - 1)\}\right] \tag{3.2.16}$$

Integrating,

$$\ln f(\xi) = 5\left[\ln \xi - \frac{3}{5\alpha B} \exp\{-\alpha B(\xi^{-5/3} - 1)\}\right] + C \tag{3.2.17}$$

where C is the constant of integration. Expanding $\ln \xi$ and $\exp\{-\alpha B(\xi^{-5/3} - 1)\}$ in a Taylor series around $\xi = 1$ and retaining terms up to second order, we obtain

$$\ln f(\xi) = 5\left[\frac{-3}{5 \alpha B} - \frac{5}{6}(\alpha B - 1)(\xi - 1)^2\right] + C \tag{3.2.18}$$

Normalizing the non-dimensionalized volume density and denoting it by $f_n(\xi)$, we have,

$$f_n(\xi) = \frac{1}{\sqrt{2\pi}\,\sigma} \exp\left[-\frac{(\xi - 1)^2}{2\sigma^2}\right] \qquad (3.2.19)$$

where $\sigma^2 = \frac{3}{25(\alpha B - 1)}$

From equation (3.2.19), we find that the non-dimensional equilibrium volume distribution is normal. Interestingly enough the empirical equilibrium drop volume density in terms of non-dimensionalized drop diameter $d/\bar{d}_{32}$ obtained by Chen and Middleman [30] is also normal. Quantitative comparison of the derived distribution with the experimental data is possible only if the value of α is known.

3.3 EVALUATION OF 'POWER LAW' CONSTANTS OF TRANSITIONAL BREAKAGE PROBABILITY AND DAUGHTER DROPLET DISTRIBUTION FROM THE TRANSIENTS OF DROP VOLUME DISTRIBUTION IN BATCH AGITATED LEAN LIQUID-LIQUID DISPERSION:

3.3.1 Equation for the Transients of Drop Volume Distribution in Batch Agitated Lean Liquid-Liquid Dispersions:

We characterize the droplet population in a batch agitated lean liquid-liquid dispersion by the cumulative distribution function of drop volume F(v,t) defined as,

F(v,t) = volume fraction of droplets whose volume is $\leqslant$ v at time t.

For a batch agitated lean liquid-liquid dispersion, it can be seen [4] that,

$$\frac{\partial F(v,t)}{\partial t} = \int_v^\infty \Gamma(v')\, G(v,v')\, dF(v',t) \qquad (3.3.1)$$

In equation (3.3.1), the right hand side is a stieljes integral which may also be written as,

$$\int_{v}^{\infty} \Gamma(v') \quad G(v,v') \frac{\partial F(v',t)}{\partial v'} dv' \qquad (3.3.2)$$

where $\frac{\partial F}{\partial v}$ is the density function.

Equation (3.3.1) may be solved for $F(v,t)$ if $\Gamma(v)$ and $G(v,v')$ are known. However, our present interest is one of determining $\Gamma(v)$ and $G(v,v')$ when $F(v,t)$ is experimentally measured.

If the 'power law' approximation for the transitional breakage probability is valid, then

$$\Gamma(v) = K v^{n} \qquad (3.3.3)$$

For the range of drop sizes encountered in agitated liquid-liquid dispersions, breakage is not chaotic [8] and is caused by oscillations of droplets due to random velocity and pressure fluctuations [8]. It is believed that the mechanism of breakage is the same for all droplets in which case one would expect the daughter droplet distribution $G(v,v')$ to be a function only of the ratio of daughter and parent droplet volumes $\frac{v}{v'}$; i.e. once a droplet is broken the daughter droplet distribution is independent of parent droplet volume. We call this 'similar breakage'. If the breakage is 'similar', then

$$G(v,v') = g\left(\frac{v}{v'}\right) \qquad (3.3.4)$$

Then equation (3.3.1) becomes,

$$\frac{\partial F(v,t)}{\partial t} = \int_{v}^{\infty} K v'^{n} g\left(\frac{v}{v'}\right) dF(v't) \qquad (3.3.5)$$

3.3.2 Estimation of 'Power Law' Constant n:

Fillipov [53] has shown that the solution of equation (3.3.5) under the assumptions (3.3.3) and (3.3.4) eventually approaches an asymptotic distribution in the similarity variable $z = (1+Kt)v^n$. That the grouping $(1+Kt)v^n$ is indeed a similarity variable is easily verified by letting $f(z) = F(v,t)$ and substituting into equation (3.3.5) which yields,

$$z f'(z) = \int_{z}^{\infty} \zeta f'(\zeta)\, g_1\left(\frac{z}{\zeta}\right) d\zeta \qquad (3.3.6)$$

where f' is the derivative of f and

$$\zeta = (1+Kt)\, v'^{n} \; ; \quad g_1\left(\frac{z}{\zeta}\right) = g\left[\left(\frac{z}{\zeta}\right)^{1/n}\right].$$

Equation (3.3.6) can be rewritten as,

$$\phi(z) = \int_{z}^{\infty} \phi(\zeta)\, g_1\left(\frac{z}{\zeta}\right) d\zeta \qquad (3.3.7)$$

where $\phi(z) = z f'(z)$

For times sufficiently large, the similarity variable z is nearly equal to Ktv^n which suggests an interesting possibility of evaluating the 'power law' constants K and n from the measurements of cumulative volume distribution F(v,t) in batch systems [4]. If for large times, Ktv^n

is indeed the similarity transformation, the cumulative drop volume distribution F(v,t) for different times when plotted in terms of the similarity variable should collapse into a single distribution. Therefore, for a fixed F(v,t), the corresponding values of v and t should be such that

$$Ktv^n = \text{constant; i.e. } v^n t = \text{constant.}$$

Thus a log-log plot of v versus t for a fixed F(v,t) should yield a straight line with a slope of $-\frac{1}{n}$. Further, similar plots for different fixed values of F(v,t) should yield a set of parallel lines if the assumptions (3.3.3) and (3.3.4) are tenable. A preliminary analysis of the transients of drop volume distribution obtained by Madden and McCoy [54] by Ramkrishna [4] does yield such parallel straight lines thus vindicating the assumptions.

3.3.3 Evaluation of K and g(x):

For sufficiently large times, one may use the similarity variable $y=v^n t$ which gives,

$$y\, f'(y) = K\int_y^\infty \xi f'(\xi)\; g_1\left(\frac{y}{\xi}\right) d\xi \qquad (3.3.6a)$$

Multiplying (3.3.6a) by y^{r-1} and integrating from 0 to ∞ one gets,

$$\int_0^\infty y^r f'(y)\, dy = K\int_0^\infty y^{r-1} \int_y^\infty \xi f'(\xi)\, g_1\left(\frac{y}{\xi}\right) d\xi\, dy$$

$$= K \int_0^\infty \xi f'(\xi) \int_0^\xi y^{r-1}\, g_1\left(\frac{y}{\xi}\right) dy\, d\xi \qquad (3.3.8)$$

i.e. $\mu_r = K\, \mu_{r+1}\, \beta_{r-1}$ (3.3.9)

where $\mu_r = \int_0^\infty y^r f'(y)\, dy$ (3.3.10)

and $\beta_r = \int_0^1 x^r g_1(x)\, dx$ (3.3.11)

If we define a function in terms of a new similarity variable $y^{1/n} = v\, t^{1/n}$ such that

$$\Psi(y^{1/n}) = f(y) \tag{3.3.12}$$

with moments

$$\lambda_r = \int_0^\infty y^{r/n}\, d\Psi\,(y^{1/n}) \tag{3.3.13}$$

then it follows that

$$\mu_{r/n} = \lambda_r \tag{3.3.14}$$

If we define

$$\gamma_r = \int_0^1 x^r g(x)\, dx \tag{3.3.15}$$

where $\{\gamma_r\}$ are the moments of the daughter droplet distribution $g(x)$,

then, it is easily seen that

$$\beta_r = n\, \gamma_{(r+1)n-1} \tag{3.3.16}$$

Now, equation (3.3.9) may be transformed to yield,

$$\lambda_r = K\, \lambda_{r+n}\, \beta_{(\frac{r}{n}-1)} \tag{3.3.17}$$

which in combination with (3.3.16) gives,

$$\lambda_r = K\, n\, \lambda_{r+n}\, \gamma_{r-1} \tag{3.3.18}$$

Measurements of the transients of the cumulative volume distribution $F(v,t)$ in a batch system should in principle give the moments $\{ \lambda_r \}$ after transformation of the distribution using the similarity transformation $y^{1/n} = v\, t^{1/n}$. Thus, from a plot of $\Psi(y^{1/n})$ versus $y^{1/n}$ the moments $\{ \mu_r \}$ can be obtained.

Equation (3.3.18) then provides the values of $\{K\, \gamma_r\}$. From the values of $\{K\, \gamma_r\}$ it is possible to estimate the function $K\, g(x)$ by means of a suitable orthonormal expansion [43]. Since $g(1) = 1$, K can be evaluated from the value of $K\, g(x)$ at $x=1$. However, from equation (3.3.18) it can be seen that the evaluation of moments $\{ \gamma_r \}$ involves knowledge of moments of $d\Psi / dy^{1/n}$ of higher order. Due to inaccuracies involved in the evaluation of higher moments of experimentally measured distribution $F(v,t)$, it may not be possible to evaluate the higher moments of $g(x)$ accurately. However, since $g(x)$ ranges between 0 and 1, the moments of $g(x)$ progressively decrease. Hence, it may be sufficient to evaluate only the leading moments of $g(x)$ in order to evaluate $g(x)$ satisfactorily through polynomial expansion. Furthermore, zeroth moment of $g(x)$ represents the average volume of the daughter droplet and the first moment the standard deviation around the mean. This in itself constitutes useful information about the daughter droplet distribution.

The function K g(x) can be expressed as a sum of orthonormal polynomials, the coefficients of which are related to the moments $\{K\ \gamma_r\}$. The orthonormal polynomials can be generated with respect to a weighting function w(x) which is a good approximation of g(x) i.e. orthonormal polynomials $\phi_n(x)$ can be generated by orthonormalising $1, x, x^2, \ldots$ with respect to the weighting function w(x) such that,

$$\int_0^1 w(x)\ \phi_n(x)\ \phi_m(x)\ dx = 0 \qquad n \neq m$$
$$= 1 \qquad n = m$$

Expanding K g(x) in terms of $\{\phi_n(x)\}$, we have,

$$K\ g(x) = \sum_{n=0}^{\infty} C_n\ w(x)\ \phi_n(x) \tag{3.3.19}$$

then,

$$C_n = \int_0^{\infty} K\ g(x)\ \phi_n(x)\ dx$$
$$= C_n \{K\ \gamma_0,\ K\ \gamma_1, \ldots . K\ \gamma_n\} \tag{3.3.20}$$

Thus, the polynomial expansion introduces a series of perturbations around the weighting function w(x) the coefficients of the perturbations being determined by the moments $\{K\ \gamma_r\}$ [43]. If the weighting function is a good approximation of g(x), it may be sufficient to consider only a few terms in the expansion i.e. the expansion will converge after the inclusion of a few terms.

CHAPTER 4

A STATISTICAL THERMODYNAMIC MODEL FOR EQUILIBRIUM DROP SIZE DISTRIBUTION IN AGITATED LEAN LIQUID-LIQUID DISPERSIONS

Dispersed phase systems are of common occurrence in many industrially important processes. The study of agitated liquid-liquid dispersions has been the subject of numerous investigations. Due to droplet phenomena of breakage and coalescence, dispersed systems reach a dynamic equilibrium wherein the drop size distribution is invariant with time. Knowledge of the equilibrium drop size distribution is important for characterisation of such systems.

A statistical mechanical formulation for such systems was proposed by Hulbert and Katz [43] where the system was described by a population balance equation. Population balance equations were used by Valentes et al. [3, 46] to describe the behaviour of agitated liquid-liquid dispersions. Breakage and coalescence, being random due to random velocity and pressure fluctuations in the turbulent flow field, were represented by related probabilities, namely, the transitional breakage probability, coalescence frequency and size distributions for newly formed droplets by breakage. The prediction of equilibrium drop size distribution using such a kinetic approach necessitates knowledge of breakage and coalescence. Even for lean dispersions, where the interaction between droplets is negligible, it is necessary to take coalescence

into account for predicring the equilibrium drop size distribution from a kinetic approach. This makes the population balance equation non-linear due to which it becomes necessary to make simplifying assumptions for the equation to be amenable to solution. Curl [44] and Erickson [57] assumed that the droplets redisperse immediately after coalescence without change in size. Bajpai, Ramkrishna and Prokop [47] proposed a coalescence-redispersion model for drop size distribution in agitated vessels by assuming that droplets coalesce in pairs and redisperse instantly into new pairs arbitarily. In Chapter 3, the equilibrium drop size distribution in an agitated lean liquid-liquid dispersion was predicted using population balance equation under the assumptions of binary breakage, perfectly random sizes for daughter droplets from breakage and a constant coalescence frequency. Although, justifications for these assumptions can be given, the prediction of equilibrium drop size distribution hinges critically on them.

In this chapter we investigate the problem of predicting equilibrium drop size distributions from a statistical thermodynamic viewpoint which considers only the total energy of the system i.e. the kinetic, potential and interfacial energies of the droplets. Since the thermodynamic approach does not explicitly take breakage and coalescence into account, it is not necessary to make simplifying assumptions in regard to them.

Moreover, in case of dilute dispersions the thermodynamic approach neglects the effect of interaction between droplets as it is negligible. This is justified as the phase average of the energy of the system is a very weak function of interactions [58], though droplet interaction is, in principle, very important without which the system would never attain a dynamic equilibrium.

4.1 THE SYSTEM:

The system consists of the dispersed phase in the form of droplets of various sizes exposed to a turbulent flow field in a well-stirred vessel. The flow field is stationary i.e. the droplets are exposed to a turbulent flow field whose characteristics are time invariant. The flow field can also be considered as homogeneous[1] and locally isotropic [20, 21, 23, 24, 28]. Eventhough the droplets continually interact with their environment i.e. the continuous phase, we would consider the system to be consisting of only the dispersed phase in the form of droplets. This is justified as we will see later that the interaction of droplets with the continuous phase is accounted for by considering (i) the convective motion of the droplets (ii) the oscillations of the droplets and (iii) the potential energy of the droplet

[1] Eventhough inhomogeneity is observed in a well-stirred vessel due to most of the energy dissipation taking place in the impeller stream [18], the flow field is fairly homogeneous outside the impeller stream.

at its equilibrium spherical shape. The power input into the system per unit mass $\bar{\varepsilon}$, total volume of the system V(volume of the dispersion) and dispersed phase fraction ϕ are fixed. Since the total number of droplets is determined by breakage and coalescence, one would expect the total number of droplets for fixed $\bar{\varepsilon}$, V and ϕ to be random as breakage and coalescence are random. Since the microscopic system consists of a very large number of droplets, one would also expect the fluctuation in the total number of droplets around the average (ensemble average) number $\bar{N}$ to be extremely small. In other words, one can, for all practical purposes, consider the total number of droplets in the system at equilibrium to be constant. As the interaction between droplets is negligible for a lean liquid-liquid dispersion, the system can be assumed to consist of $\bar{N}$ independent droplets. This is justified as the phase average of the energy of the system is a very weak function of interaction [58]. In order to derive the equilibrium drop size distribution, we consider a canonical ensemble of subsystems, each subsystem being a droplet i.e. each droplet is exposed to a constant 'temperature'. 'Temperature' here refers to the characteristi of the turbulent flow field. Therefore, we need only to evaluate the partition function of a droplet in order to evaluate the equilibrium drop size distribution.

4.2 PARTITION FUNCTION OF A DROPLET:

A droplet exposed to a turbulent flow field will be acted upon by turbulent eddies of different scales or frequencies. Eddies of scale greater than the drop diameter will impart a pulsating convective motion to the droplet. There will be relative velocity and pressure fluctuations on the surface of the droplet due to eddies of scale less than the diameter of the droplet which will result in oscillatio of the droplet around its spherical equilibrium shape. Because of the interface, the droplet will also have potential energy which will be a function of the interfacial tension and the interfacial area.

Therefore, the energy of a droplet can be split up into:

(i) Kinetic energy of pulsating convective motion

(ii) Kinetic and potential energies of oscillation

and (iii) Potential energy at its spherical equilibrium shape.

4.2.1 Kinetic Energy of Convective Motion:

The convective pulsating motion of a droplet of size X is caused by eddies of scale larger than X. Since the drop sizes lie mainly in the inertial subrange of the universal energy spectrum [28], the total turbulent energy available for pulsating motion exhibits very small variations in the prevailing size range. Therefore, the convective

pulsating motion can be assumed to be independent of drop size [48]. Therefore,

$$\text{Kinetic Energy} = \frac{1}{2M}(p_x^2 + p_y^2 + p_z^2) \qquad (4.2.1)$$

where p_x, p_y, p_z are the momenta corresponding to the cartesian coordinates x, y and z and M is the mass of the droplet.

4.2.2 Energy of Oscillation:

A spherical droplet is acted upon by turbulent velocity and pressure fluctuations on its surface. The turbulent velocity and pressure fluctuations can be considered to be due to eddies 'striking' the surface of the droplet. The eddies (or velocity and pressure fluctuations) create oscillations of the droplet and hence their deformation. Near equilibrium, the rate of breakage is small i.e. the deformation of the droplets is small. This is because the energy of eddies of scale smaller than the droplet diameter is of the same order of magnitude as the minimum energy required for breakage. Moreover, small size droplets more or less behave as rigid spheres i.e. the tangential momentum transfer across the interface resulting in internal circulation is small. Therefore, the droplets can be assumed to undergo pure deformation without rotation.[2] Hence the induced flow field inside the

[2] This assumption is only approximate as there will be some internal circulation.

droplet due to its oscillation can be considered to be irrotational. For small pure deformation, a sphere will be deformed into an ellipsoid. It is evident that for oscillations of a droplet, the velocity and pressure fluctuation can occur only at a point on the surface of a droplet at a time, as otherwise, the effect of velocity and pressure fluctuations would be to create bulgy deformation of the droplet [8]. Hence, the oscillations of a droplet are to be viewed as forced oscillations of a sphere due to a random periodic disturbing pressure acting at two diametrically opposite points on the surface. Since the equilibrium drop size distribution is narrow and the drop sizes lie in the inertial subrange of the universal energy spectrum, we can assume the turbulent energy available for oscillation to be independent of drop sizes.

Consider a droplet of size X. At any time, the droplet will be acted upon by a random periodic pressure of random frequency at any two diametrically opposite points A and B. Since the droplet is incompressible, the effect of this pressure will be to induce a pressure distribution $p(\theta, \phi)$ along the surface of the droplet. Because of local isotropy, the droplet will oscillate between oblate and prolate spheroidal shapes. Therefore, it

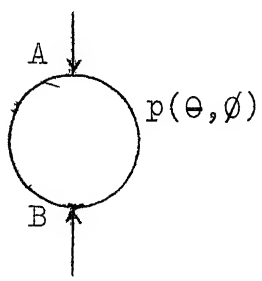

should be possible to find out the pressure distribution $p(\theta, \phi)$.

The periodic pressure fluctuation $p(\theta, \phi)$ can be written as,

$$p(\theta, \phi) = p_a(\theta, \phi)\, e^{-i w t},$$

w being the frequency of the fluctuation.
Here both $p_a(\theta, \phi)$ and w are random variables. Since the deformation of the droplet is small, the function $p_a(\theta, \phi)$ can be represented in terms of surface harmonic functions as,

$$p_a(\theta, \phi) = \sum_m \sum_n (\alpha_{mn} \cos n\phi + \beta_{mn} \sin n\phi)\, P_m^n(\cos\theta) \tag{4.2.2}$$

where $P_m^n(\cos\theta) = \sin^n\theta \dfrac{d^n P_m(\cos\theta)}{d(\cos\theta)^n}$, is what is called an associated Legendre function, $P_m(\cos\theta)$ being the Legendre polynomial of order m. As is well known, m takes all positive integer values from zero, while n takes the values 0, ± 1, ± 2,... $\pm$ m.

The constants α_{mn} and β_{mn} are given by,

$$\alpha_{mo} = \frac{2m+1}{4\pi} \int_0^{2\pi}\int_0^{\pi} p_a(\theta,\phi) \sin\theta\, d\theta\, d\phi \tag{4.2.3}$$

$$\alpha_{mn} = \frac{2m+1}{2\pi} \frac{(m-n)!}{(m+n)!} \int_0^{2\pi}\int_0^{\pi} p_a(\theta,\phi)\, P_m^n(\cos\theta) \cos n\phi \sin\theta\, d\theta\, d$$

(4.2.4)

and

$$\beta_{mn} = \frac{2m+1}{2\pi} \frac{(m-n)!}{(m+n)!} \int_0^{2\pi}\int_0^{\pi} p_a(\theta,\phi)\, P_m^n(\cos\theta) \sin n\phi \sin\theta\, d\theta\, d\phi$$

(4.2.5)

Once $p_a(\theta, \phi)$ is known, it is possible to evaluate the constants α_{mn} and β_{mn}.

The equilibrium spherical surface of the droplet is given by r=R (droplet radius). We can describe the deformed surface of the droplet by the equation $r=R + \xi(\theta,\phi)$, where $\xi(\theta,\phi)$ is the deformation of the droplet from its spherical shape. As stated earlier, the induced flow field due to the oscillation of the droplet is assumed to be irrotational and hence can be described by a velocity potential $\Psi'(r, \theta, \phi)$.

The velocity potential $\Psi'(r, \theta, \phi)$ satisfies the Laplace equation

$$\nabla^2 \Psi' = 0 \tag{4.2.6}$$

with the boundary condition [59],

$$\rho\frac{\partial\Psi'}{\partial t} + \sigma\left\{\frac{2}{R} - \frac{2\xi}{R^2} - \frac{1}{R^2}\left[\frac{1}{\sin\theta}\frac{\partial}{\partial\theta}\left(\sin\theta\frac{\partial\xi}{\partial\theta}\right) + \frac{1}{\sin^2\theta}\frac{\partial^2\xi}{\partial\phi^2}\right]\right\} = + p_o + p(\theta,\phi) = 0 \tag{4.2.7}$$

$$\text{at } r = R$$

where p_o is the average pressure in the continuous phase.

Defining a new velocity potential $\Psi = \Psi' + (\frac{2\sigma}{R} + p_o)t$, we get,

$$\nabla^2 \Psi = 0 \tag{4.2.6a}$$

with the boundary condition,

$$\rho\frac{\partial\Psi}{\partial t} - \frac{\sigma}{R^2}\left[2\xi + \left\{\frac{1}{\sin\theta}\frac{\partial}{\partial\theta}\left(\sin\theta\frac{\partial\xi}{\partial\theta}\right) + \frac{1}{\sin^2\theta}\frac{\partial^2\xi}{\partial\phi^2}\right\}\right] + p(\theta, \phi) = 0 \qquad \text{at } r=R \tag{4.2.7a}$$

Differentiating (4.2.7a) with respect to time and putting $\frac{\partial \Psi}{\partial t} = v_r = \frac{\partial \Psi}{\partial r}$, we have the modified boundary condition,

$$\rho \frac{\partial^2 \Psi}{\partial t^2} - \frac{\sigma}{R^2}\left[2 \frac{\partial \Psi}{\partial r} + \frac{\partial}{\partial r}\left\{ \frac{1}{\sin\theta} \frac{\partial}{\partial \theta}(\sin\theta \frac{\partial \Psi}{\partial \theta}) + \frac{1}{\sin^2\theta} \frac{\partial^2 \Psi}{\partial \phi^2} \right\}\right]$$

$$+ \frac{\partial}{\partial t} p(\theta, \phi) = 0 \quad \text{at } r=R \qquad (4.2.7b)$$

Now,

$$\frac{\partial}{\partial t} p(\theta, \phi) = w\, p_a(\theta, \phi)\, e^{-i(wt + \pi/2)}.$$

Since Ψ satisfies Laplace equation, Ψ can be represented as a linear combination of volume spherical harmonic functions $r^m \begin{matrix}\cos n\phi \\ \sin n\phi\end{matrix} P_m^n(\cos\theta)$. Therefore we seek a solution of the form,

$$\Psi = \sum_m \sum_n r^m (a_{mn} \cos n\phi + b_{mn} \sin n\phi) P_m^n(\cos\theta)\, e^{-i(wt+\pi/2)} \qquad (4.2.8)$$

Substituting for Ψ in equation (4.2.7b), we get,

$$\rho w^2 e^{-i(wt + \pi/2)} \{ \sum_m \sum_n R^m (a_{mn} \cos n\phi + b_{mn} \sin n\phi) P_m^n(\cos\theta)$$

$$+ \frac{\sigma}{R^2}\left[\sum_m \sum_n R^{m-1} (a_{mn} \cos n\phi + b_{mn} \sin n\phi) P_m^n(\cos\theta) \times \right.$$

$$\left. m(m-1)(m+2)\right] e^{-i(wt + \pi/2)}$$

$$+ w e^{-i(wt + \pi/2)}\left[\sum_m \sum_n (\alpha_{mn} \cos n\phi + \beta_{mn} \sin n\phi) P_m^n(\cos\theta)\right] = 0 \qquad (4.2.9)$$

after using the relation [59] satisfied by the surface harmonic functions

$$\frac{1}{\sin\theta}\frac{\partial}{\partial\theta}\left(\sin\theta\frac{\partial Y_{mn}}{\partial\theta}\right)+\frac{1}{\sin^2\theta}\frac{\partial^2 Y_{mn}}{\partial\phi^2}+n(m+1)\,Y_{mn}=0$$

where $Y_{mn}=\begin{matrix}\cos n\phi\\ \sin n\phi\end{matrix} P_m^n(\cos\theta)$. (4.2.10)

Therefore, equation (4.2.9) reduces to

$$\sum_m\sum_n P_m^n(\cos\theta)\left[\cos n\phi\left\{-\rho w^2 R^m a_{mn}+\frac{\sigma}{R^3}R^m m(m-1)(m+2)a_{mn}+w\alpha_{mn}\right\}+\sin n\phi\left\{-\rho w^2 R^m b_{mn}+\frac{\sigma}{R^3}R^m m(m-1)(m+2)b_{mn}+w\beta_{mn}\right\}\right]=0 \quad (4.2.11)$$

Therefore,

$$a_{mn}=\frac{w}{R^m\left[\rho w^2-\frac{\sigma}{R^3}m(m-1)(m+2)\right]}\alpha_{mn}$$

$$=\frac{w}{\rho R^m[w^2-w_{nm}^2]}\alpha_{mn} \quad (4.2.12)$$

where $w_{nm}^2=\frac{\sigma}{\rho R^3}m(m-1)(m+2)$, w_{nm} being the mth natural frequency of oscillation of the droplet [59].

Similarly,

$$b_{mn}=\frac{w}{\rho R^m[w^2-w_{nm}^2]}\beta_{mn} \quad (4.2.13)$$

Obviously, the relations (4.2.12) and (4.2.13) hold good only

if $w \neq w_{nm}$ $\forall$ m. Measurement of equilibrium drop size distribution for water - CCl_4 + i-octane (50-50 per cent) system has shown that typical droplet volume $\simeq 10^{-6}$ cc. As $\sigma \simeq 40$ dynes/cm, the smallest natural frequency of oscillation $w_{n2} \simeq 4 \times 10^4$. Measurement of the energy spectrum in stirred vessels [23] shows that the inertial sub-range of the universal energy spectrum (-5/3 slope) corresponds to eddies whose frequency is of the order of 500 Hertz. Therefore, the natural frequency of oscillation of droplets is much higher than the forcing frequency of the random pressure fluctuation.

Therefore, the velocity potential Ψ can be expressed as

$$\Psi = \sum_m \sum_n (a_{mn} \cos n\phi + b_{mn} \sin n\phi) P_m^n (\cos\theta) e^{-i(wt + \pi/2)}$$

From equation (4.2.3), we get,

$$\alpha_{oo} = \frac{1}{4\pi} \int_0^{2\pi} \int_0^{\pi} p_a(\theta, \phi) \sin\theta \, d\theta \, d\phi \qquad (4.2.14)$$

The integral is the total radial force acting on the droplet due to the induced pressure distribution $p_a(\theta, \phi)$. The total radial force would result in radial oscillations of the liquid droplet. Since the droplet is incompressible, radial oscillations are not possible and hence the total radial force has to be zero. i.e. $\alpha_{oo} = 0$.

From equations (4.2.4) and (4.2.5), we get,

$$\alpha_{11} = \frac{3}{2\pi}\,\frac{1}{2!}\int_0^{2\pi}\int_0^{\pi} p_a(\theta,\phi)\, P_1^1(\cos\theta)\cos\phi\sin\theta\, d\theta\, d\phi$$

$$\beta_{11} = \frac{3}{2\pi}\,\frac{1}{2!}\int_0^{2\pi}\int_0^{\pi} p_a(\theta,\phi)\, P_1^1(\cos\theta)\sin\phi\sin\theta\, d\theta\, d\phi$$

$$\alpha_{10} = \frac{3}{2\pi}\int_0^{2\pi}\int_0^{\pi} p_a(\theta,\phi)\, P_1^0(\cos\theta)\sin\theta\, d\theta\, d\phi$$

and

$$\beta_{10} = 0.$$

Since $P_1^1(\cos\theta) = i\sin\theta$ and $P_1^0(\cos\theta) = \cos\theta$,

$$\alpha_{11} = \frac{3i}{4\pi}\int_0^{2\pi}\int_0^{\pi} p_a(\theta,\phi)\sin\theta\cos\phi\sin\theta\, d\theta\, d\phi \qquad (4.2.15)$$

$$\alpha_{10} = \frac{3}{2\pi}\int_0^{2\pi}\int_0^{\pi} p_a(\theta,\phi)\cos\theta\sin\theta\, d\theta\, d\phi \qquad (4.2.16)$$

and

$$\beta_{11} = \frac{3i}{4\pi}\int_0^{2\pi}\int_0^{\pi} p_a(\theta,\phi)\sin\theta\sin\phi\sin\theta\, d\theta\, d\phi \qquad (4.2.17)$$

It can be seen that the three integrals are the components of the total force acting on the droplet along x, z and y coordinates respectively. These components would result in the translation of the droplet. Since the induced pressure distribution $p(\theta,\phi)$ results only in the oscillations of the droplet, the three components of the force are zero, i.e. $\alpha_{11} = \alpha_{10} = \beta_{11} = \beta_{10} = 0$.

Therefore, the summation in the expression for Ψ starts only from m=2 i.e. m=2 corresponds to the smallest frequency of oscillation.

The kinetic energy of oscillation T is given by,

$$T = \frac{1}{2} \rho \iiint_V (\nabla \Psi \cdot \nabla \Psi) \, dv$$

By applying Green's formula, we get,

$$T = \frac{1}{2} \rho \iint_S \Psi \frac{\partial \Psi}{\partial n} \, dS$$

where n denotes the outward normal to the surface.

Therefore,

$$T = \frac{1}{2} \rho \int_0^{2\pi} \int_0^{\pi} \Psi \left. \frac{\partial \Psi}{\partial r} \right|_{r=R} R^2 \sin\theta \, d\theta \, d\phi \qquad (4.2.18)$$

substituting for Ψ from equation (4.2.8) and using the following relations,

$$\int_0^{2\pi} \int_0^{\pi} T^e_{mn}(\theta,\phi) \, T^o_{pq}(\theta,\phi) \sin\theta \, d\theta \, d\phi = 0$$

$$\int_0^{2\pi} \int_0^{\pi} T^i_{mn}(\theta,\phi) \, T^i_{pq}(\theta,\phi) \sin\theta \, d\theta \, d\phi = 0 \quad m,n \neq p,q.$$

and

$$\int_0^{2\pi} \int_0^{\pi} [T^i_{mn}(\theta,\phi)]^2 \sin\theta \, d\theta \, d\phi = \begin{cases} \frac{4\pi}{2n+1}, & m=0, \; i=e \\ \frac{2\pi}{2n+1} \frac{(n+m)!}{(n-m)!}, & m \neq 0 \end{cases}$$

where $T^{e}_{mn}(\theta,\phi) = P^{m}_{n}(\cos\theta)\cos m\phi$

$T^{o}_{mn}(\theta,\phi) = P^{m}_{n}(\cos\theta)\sin m\phi$

and i=e or o , we get,

$$T = \frac{1}{2}\rho \sum_{m=2} \bar{[}m R^{2m+1} \{ \frac{4\pi}{2m+1} a^2_{mo} + \sum_{n=\pm 1\ldots} (\frac{2\pi}{2m+1} \frac{(m+n)!}{(m-n)!} (a^2_{mn} + b^2_{mn})) \}] e^{-2i(wt + \pi/2)} \quad (4.2.19)$$

We can define the momentum of oscillation p_η by the relation,

$$\frac{1}{2M} p^2_\eta = T. \quad (4.2.20)$$

Therefore,

$$p_\eta = \bar{[}M\rho \sum_{m=2} \bar{[}m R^{2m+1} \{ \frac{4\pi}{2m+1} a^2_{mo} + \sum_{n=\pm 1\ldots} (\frac{2\pi}{2m+1} \frac{(m+n)!}{(m-n)!} (a^2_{mn} + b^2_{mn}))]]^{1/2} e^{-i(wt + \pi/2)} \quad (4.2.21)$$

The velocity of oscillation V_{os} is given by,

$$V_{os} = \frac{p_\eta}{M} \quad (4.2.22)$$

Since a_{mn}, b_{mn} and w are random variables, p_η and V_{os} are also random variables.

Substituting for Ψ from equation (4.2.8) in equation (4.2.7a), we get,

$$\rho w \sum_m \sum_n R^m (a_{mn} \cos n\phi + b_{mn} \sin n\phi) P_m^n (\cos\theta) e^{-i wt}$$

$$- \frac{\sigma}{R^2} \left[2\xi + \frac{1}{\sin\theta} \frac{\partial}{\partial \theta} \left(\sin\theta \frac{\partial \xi}{\partial \theta} \right) + \frac{1}{\sin^2\theta} \frac{\partial^2 \xi}{\partial \phi^2} \right]$$

$$+ \sum_m \sum_n (\alpha_{mn} \cos n\phi + \beta_{mn} \sin n\phi) P_m^n (\cos\theta) e^{-i wt} = 0$$

(4.2.23)

We seek a solution for ξ of the form,

$$\xi = \sum_m \sum_n (c_{mn} \cos n\phi + d_{mn} \sin n\phi) P_m^n (\cos\theta) e^{-iwt}$$

(4.2.24)

Substituting for ξ in equation (4.2.23) and using the relation (4.2.10), we get,

$$\sum_m \sum_n \left[\left\{ \rho w R^m a_{mn} + \frac{\sigma}{R^2} (m+2)(m-1) c_{mn} + \alpha_{mn} \right\} \cos n\phi \right.$$

$$\left. + \left\{ \rho w R^m b_{mn} + \frac{\sigma}{R^2} (m+2)(m-1) d_{mn} + \beta_{mn} \right\} \sin n\phi \right] P_m^n (\cos\theta)$$

$$= 0$$

i.e. $$c_{mn} = \frac{-\alpha_{mn}}{R} \frac{m}{w_{nm}^2} \left[1 + \frac{w^2}{(w^2 - w_{nm}^2)} \right] \qquad (4.2.25)$$

and

$$d_{mn} = \frac{-\beta_{mn}}{R} \frac{m}{w_{nm}^2} \left[1 + \frac{w^2}{(w^2 - w_{nm}^2)} \right] \qquad (4.2.26)$$

Take a surface element between θ, $\theta + d\theta$ and ϕ and $\phi + d\phi$. The area of the surface element df is given by,

$$df = \left[(R+\xi)^2 + \frac{1}{2} \left[\left(\frac{\partial \xi}{\partial \theta} \right)^2 + \frac{1}{\sin^2\theta} \left(\frac{\partial \xi}{\partial \phi} \right)^2 \right] \right] \sin\theta \, d\theta \, d\phi.$$

The area of the spherical surface element df_s is given by, $df_s = R^2 \sin\theta \, d\theta \, d\phi$. Therefore, the increase in the area of the surface element due to deformation is given by,

$$\Delta df = df - df_s = \left[2R\xi + \xi^2 + \frac{1}{2} \left\{ \left(\frac{\partial \xi}{\partial \theta}\right)^2 + \frac{1}{\sin^2\theta} \left(\frac{\partial \xi}{\partial \phi}\right)^2 \right] \right.$$

$$\sin\theta \, d\theta \, d\phi.$$

Since $\frac{\partial \xi}{\partial \theta}$ and $\frac{\partial \xi}{\partial \phi}$ are small compared to ξ , neglecting the terms within the braces on the right hand side, we get,

$$\Delta df = (2R\xi + \xi^2) \sin\theta \, d\theta \, d\phi.$$

For small deformation, we can take the increase in the potential energy or equivalently, the potential energy of oscillation, as the increase in the interfacial energy due to deformation. Therefore, the potential energy of oscillation P_{os} is given by,

$$P_{os} = \sigma \int_0^{2\pi} \int_0^{\pi} (2R\xi + \xi^2) \sin\theta \, d\theta \, d\phi.$$

Now,

$$\int_0^{2\pi} \int_0^{\pi} \xi \sin\theta \, d\theta \, d\phi$$

$$= \int_0^{2\pi} \int_0^{\pi} \sum_m \sum_n (c_{mn} \cos n\phi + d_{mn} \sin n\phi)$$

$$P_m^n(\cos\theta) \, e^{-iwt} \sin\theta \, d\theta \, d\phi$$

$$= 4\pi c_{oo} e^{-iwt} = \frac{4\pi R^2}{\sigma} \alpha_{oo} e^{-iwt} = 0.$$

Therefore,

$$P_{os} = \sigma \int_0^{2\pi} \int_0^{\pi} \xi^2 \sin\theta \, d\theta \, d\phi \qquad (4.2.27)$$

Substituting for ξ from (4.2.24),

$$P_{os} = \sigma \sum_m \left[\frac{4\pi}{2m+1} c_{mo}^2 + \sum_{n=\pm 1 \ldots} \left\{ \frac{2\pi}{(2m+1)} \frac{(m+n)!}{(m-n)!} (c_{mn}^2 + d_{mn}^2) \right\} \right] e^{-2iwt} \qquad (4.2.28)$$

Defining the generalised deformation coordinate η by the relation,

$$P_{os} = \frac{1}{2} \sigma \eta^2 \qquad (4.2.29)$$

$$\eta = \left[\sum_m \frac{8\pi}{(2r+1)} c_{mo}^2 + \sum_{n=\pm 1 \ldots} \left\{ \frac{4\pi}{(2m+1)} \frac{(m+n)!}{(m-n)!} (c_{mn}^2 + d_{mn}^2) \right\} \right]^{1/2} e^{-iwt} \qquad (4.2.30)$$

Therefore the kinetic and potential energies of oscillation are given by,

$$T = \frac{1}{2M} p_\eta^2 \; ; \qquad P_{os} = \frac{1}{2} \sigma \eta^2$$

where η is the generalised deformation coordinate and p_η is the momentum conjugate to η and both η and p_η are random.

4.2.3 Potential Energy of a Spherical Droplet:

The potential energy of a droplet at its equilibrium spherical shape is only due to the interface. It is assumed that the density and viscosity of the dispersed phase are the

same as that of the continuous phase. At equilibrium, the temperature and chemical potential in the droplet will be equal to the temperature and chemical potential in the continuous phase. Since the potential energy of a spherical droplet is only due to the interface, it should be equal to the work done in transferring a volume $v(= \frac{\pi}{6} X^3)$ of the dispersed phase reversibly from a bath of dispersed phase liquid at the same temperature, pressure and chemical potential as that of the continuous phase into the continuous phase in the form of a spherical droplet of diameter X replacing an equal volume of continuous phase.

The internal energy E_1 and work function A_1 of the dispersed phase liquid of volume v in the dispersed phase liquid bath are given by,

$$E_1 = T.S - P_1 v + \mu n \qquad (4.2.31)$$

$$A_1 = -P_1 v + \mu n \qquad (4.2.32)$$

where P_1 = continuous phase pressure

n = number of molecules.

Now, the internal energy E_2 and work function A_2 of the droplet of volume v are given by,

$$E_2 = T.S - P_2 v + \sigma A + \mu n \qquad (4.2.33)$$

$$A_2 = -P_2 v + \sigma A + \mu n \qquad (4.2.34)$$

where P_2 = Pressure inside the droplet

A = Interfacial area.

Therefore, $A_2 - A_1 = \Delta A = -(P_2 - P_1)\, v + \sigma A$ (4.2.35)

$-\Delta A$ = Maximum work obtainable from the system in an isothermal reversible change from state 1 to 2.

Therefore, the potential energy of a spherical droplet of X is given by,

$$(\bar{P} \cdot \bar{E})_{eq} = \Delta A = -(P_2 - P_1)\, v + \sigma A$$

$$= -\Delta P \frac{\pi}{6} X^3 + \sigma \pi X^2 \qquad (4.2.36)$$

Since a droplet at its equilibrium spherical shape does not have any kinetic energy, the total energy of the droplet is its potential energy. Therefore, the Hamiltonian for a spherical droplet of size X can be written as,

$$H = -(\Delta P) \frac{\pi}{6} X^3 + \sigma \pi X^2 \qquad (4.2.37)$$

where X is the generalized coordinate, the drop diameter. If p_X is the momentum conjugate to the generalized coordinate X, we know that,

$$-\frac{\partial H}{\partial X} = \dot{p}_X \quad ; \quad \frac{\partial H}{\partial p_X} = \dot{X}.$$

Substituting for H,

$$\frac{\partial H}{\partial X} = -(\Delta P) \frac{\pi}{2} X^2 + 2 \pi \sigma X.$$

At equilibrium, the pressure difference between the droplet and the continuous phase is the capillary pressure p_σ. Therefore,

$$\Delta P = p_\sigma = \frac{4 \sigma}{X} \qquad (4.2.38)$$

Substituting,

$$\frac{\partial H}{\partial X} = \frac{-4\sigma}{X} \frac{\pi}{2} X^2 + 2\pi\sigma X = 0.$$

Therefore $\dot{p}_X = 0$ i.e. p_X = constant.

And $\frac{\partial H}{\partial p_X} = 0$ i.e. $\dot{X} = 0$ or $p_X = 0$.

i.e. the generalized momenta p_X conjugate to the generalized coordinate X is identically zero for all values of X. This is understandable as a droplet at its spherical equilibrium shape does not have any kinetic energy. Substituting for P from (4.2.38) into (4.2.37), we get,

$$(P.E)_{eq} = \frac{1}{3} \sigma \pi X^2 \qquad (4.2.39)$$

4.2.4 Derivation of Partition Function of a Droplet:

The coordinates of the phase space are x, y, z, η, X, p_x, p_y, p_z, p_η and p_X. A droplet has 6 degrees of freedom. The total energy of a droplet of diameter X can be written as

$$E = \frac{1}{2M} (p_x^2 + p_y^2 + p_z^2) + \frac{1}{2M} p_\eta^2 + \frac{\sigma}{2} \eta^2 + \frac{\sigma}{3} \pi X^2 \qquad (4.2.40)$$

Therefore, the Hamiltonian H of a droplet can be written as,

$$H(\vec{X}, \vec{p}) = \frac{1}{2M} (p_x^2 + p_y^2 + p_z^2) + \frac{1}{2M} p_\eta^2 + \frac{\sigma}{2} \eta^2 + \frac{\sigma}{3} \pi X^2 \qquad (4.2.41)$$

Hence, the partition function of a droplet can be written as,

$$Q(V, \beta) = \int \int \ldots \int \exp\left[-\beta \left\{\frac{1}{2M} (p_x^2 + p_y^2 + p_z^2) + \frac{1}{2M} p_\eta^2 + \frac{\sigma}{2} \eta^2 + \frac{\sigma}{3} \pi X^2 \right\}\right] dx\, dy\, dz\, dp_x\, dp_y\, dp_z\, d\eta\, dp_\eta\, dX$$

where $-\infty < p_x, p_y, p_z < \infty$, $-\infty \quad \eta < \infty$, $-\infty < p_\eta < \infty$, $0 < X < \infty$.

Here the integration is not performed with respect to p_X as $p_X = 0 \quad \forall\, X$.

Integrating with respect to x, y and z,

$$Q(V, \beta) = V \int \int \dots \int \exp\left[-\beta \left\{ \frac{1}{2M} (p_x^2 + p_y^2 + p_z^2) + \frac{1}{2M} p_\eta^2 + \frac{\sigma}{2} \eta^2 + \frac{\sigma}{3} \pi X^2 \right\}\right] dp_x\, dp_y\, dp_z\, d\eta\, dp_\eta\, dX.$$

Now, $M = \alpha X^3$ where $\alpha = \frac{\pi}{6}$.

and $$\int_{-\infty}^{\infty} \exp\left[-\frac{\beta}{2\alpha X^3} p_x^2\right] dp_x = \left(\frac{2\pi \alpha X^3}{\beta}\right)^{1/2}$$

$$\int_{-\infty}^{\infty} \exp\left[-\frac{\beta}{2} \sigma \eta^2\right] d\eta = \left(\frac{2\pi}{\beta \sigma}\right)^{1/2}.$$

therefore,

$$Q(V,\beta) = V \int_0^{\infty} \left(\frac{2\pi \alpha X^3}{\beta}\right)^2 \left(\frac{2\pi}{\beta \sigma}\right)^{1/2} \exp\left[-\beta \frac{\pi}{3} \sigma X^2\right] dX$$

$$= V \frac{15}{16} \frac{\alpha^2 2^{5/2} 3^{7/2}}{\pi^{1/2} \sigma^4} \frac{1}{\beta^6} \qquad (4.2.42)$$

Now,

$$-\frac{\partial \ln Q}{\partial \beta} = \frac{6}{\beta} = \bar{E}$$

where $\bar{E}$ = Average energy of a droplet.

Therefore, $\beta = \frac{6}{\bar{E}}$ (4.2.43)

If we define a 'Dispersion Temperature' T_d such that,

$$k T_d = \frac{1}{\beta} = \frac{\bar{E}}{6}$$

i.e. $$T_d = \frac{\bar{E}}{6k} \qquad (4.2.44)$$

where k is the Boltzmann's constant.

It is interesting to note that the average energy of a droplet $\bar{E} = 6k\ T_d$. If the 6 degrees of freedom of a droplet could be further partitioned i.e. independent, then one would have expected the average energy of a droplet $\bar{E}$ to be $3\ kT_d$ according to the law of equipartition of energy. From equation (4.2.44) it is clear that the total energy of the droplet is not equally partitioned into different degrees of freedom. This is understandardable as the kinetic energies of convective motion and oscillation of a droplet are not only functions of the corresponding momenta but also functions of droplet diameter, a generalized coordinate i.e. the different forms of energy of a droplet are not independent.

4.3 DERIVATION OF EQUILIBRIUM DROP VOLUME DISTRIBUTION:

The probability density of drop size f(X) is given by,

$$f(X) = \frac{\int\int \ldots \int \exp[-\beta\ H]\ dx\ dy\ dz\ dp_x\ dp_y\ dp_z\ d\eta\ dp_\eta}{Q\ (V,\ \beta)}$$

Evaluating the numerator and substituting for $Q(V, \beta)$, we get,

$$f(X) = \frac{X^6\ \exp\left[-\beta\ \frac{\pi\ \sigma}{3}\ X^2\right]}{\frac{15}{16}\ \left(\frac{3}{\pi\ \beta\ \sigma}\right)^{7/2}\ (\pi)^{1/2}}$$

$$= \frac{16}{15}\ \frac{\pi^3}{3^{7/2}}\ \left(\frac{6}{\bar{E}}\right)^{7/2}\ \sigma^{7/2}\ X^6\ \exp\left[-\frac{2\ \pi\ \sigma}{\bar{E}}\ X^2\right] \qquad (4.3.1)$$

Let $X^* = \left(\frac{\bar{E}}{2\pi\sigma}\right)^{1/2}$ (4.3.2)

Non-dimensionalizing f(X) with respect to X^* and taking into account the relation $f\left(\frac{X}{X}\right) = X^* f(X)$, we get,

$$f\left(\frac{X}{X^*}\right) = \frac{16}{15} \frac{1}{\pi^{1/2}} \left(\frac{X}{X^*}\right)^6 \exp\left[-\left(\frac{X}{X^*}\right)^2\right] \quad (4.3.3)$$

The equilibrium drop volume density in terms of drop diameter $f_v(X)$ is given by,

$$f_v(X) = \frac{X^3 f(X)}{\int X^3 f(X)}$$

Non-dimensionalizing $f_v(X)$ with respect to X^*,

$$f_v\left(\frac{X}{X^*}\right) = \frac{1}{12} \left(\frac{X}{X^*}\right)^9 \exp\left[-\left(\frac{X}{X^*}\right)^2\right] \quad (4.3.4)$$

Now,

$$\bar{d}_{32} = \frac{\int_0^\infty X^3 f(X)\,dX}{\int_0^\infty X^2 f(X)\,dX}$$

$$= \frac{X^* \int_0^\infty \left(\frac{X}{X^*}\right)^3 f\left(\frac{X}{X^*}\right) d\left(\frac{X}{X^*}\right)}{\int_0^\infty \left(\frac{X}{X^*}\right)^2 f\left(\frac{X}{X^*}\right) d\left(\frac{X}{X^*}\right)}$$

$$= \frac{X^* \frac{16}{15} \frac{1}{\pi^{1/2}} \frac{1}{2} 4!}{\frac{16}{15} \frac{1}{2} \frac{35.3}{16}}$$

$$= X^* \frac{16.24}{35.3} \frac{1}{\pi^{1/2}}$$

i.e. $\bar{d}_{32} = A\,X^*$ where $A = \frac{16.24}{35.3} \frac{1}{\pi^{1/2}}$ (4.3.5)

Therefore,

$$f_v\left(\frac{X}{\bar{d}_{32}}\right) = \frac{\bar{d}_{32}}{X^*} f_v\left(\frac{X}{X}\right) = A\, f_v\left(\frac{X}{X^*}\right)$$

i.e. $$f_v\left(\frac{X}{\bar{d}_{32}}\right) = \frac{A^{10}}{12}\left(\frac{X}{\bar{d}_{32}}\right)^9 \exp\left[-A^2\left(\frac{X}{\bar{d}_{32}}\right)^2\right] \qquad (4.3.6)$$

Figure 4.1 shows a plot of non-dimensionalized drop volume density $f_v\left(\frac{X}{\bar{d}_{32}}\right)$ versus non-dimensionalized drop diameter $\left(\frac{X}{\bar{d}_{32}}\right)$.

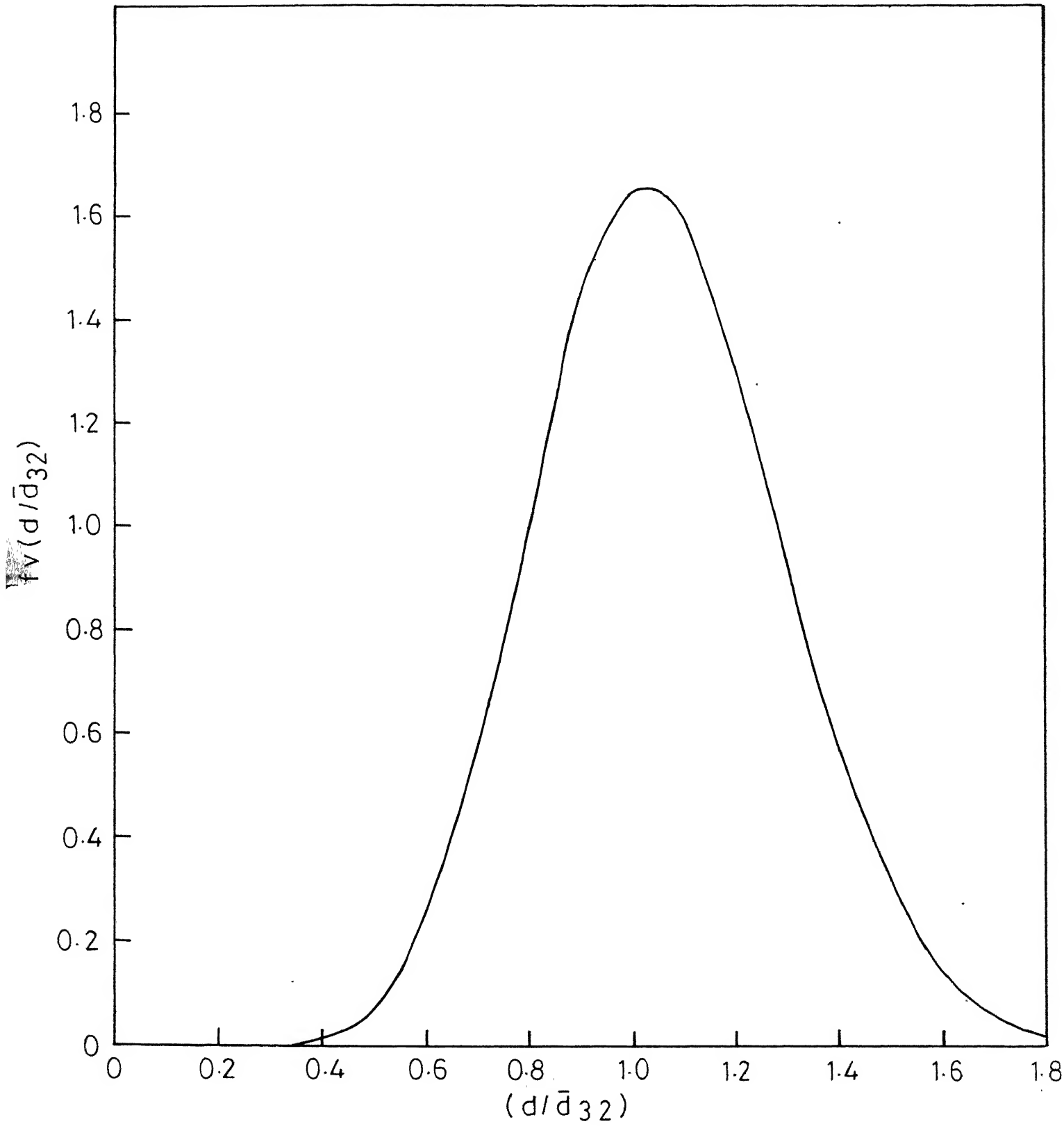

Fig. 4·1 - Plot of equilibrium drop volume density predicted by statistical thermodynamic model.

CHAPTER 5

EXPERIMENTAL TECHNIQUES, APPARATUS AND PROCEDURE

5.1 EXPERIMENTAL TECHNIQUE:

The droplets in an agitated lean liquid-liquid dispersion were encapsulated with a thin nylon film at the time of measurement through an interfacial polycondensation reaction. The encapsulation stops further breakage and coalescence of droplets thus freezing the population at the time of measurement. The encapsulated drops behave more or less like solid particles thus enabling their size distribution measurement by a standard size measurement technique. Electronic size analysis (Coulter Counter) was employed to measure the volume distribution of droplets as it was found to be superior to other standard techniques like sieving, sedimentation, microscopy and photography.

5.1.1 Comparison of Electronic Size Analysis with Other Techniques:

Though there are a large number of techniques available for particle size measurement, for the size range of droplets encountered (50-800μ), only a few of the techniques would be effective. They are: (i) Sieving (ii) Sedimentation (iii) Microscopy (iv) Photography and (v) Electronic Size analysis. Figure 5.1 shows the size range of the above methods of measurement [60].

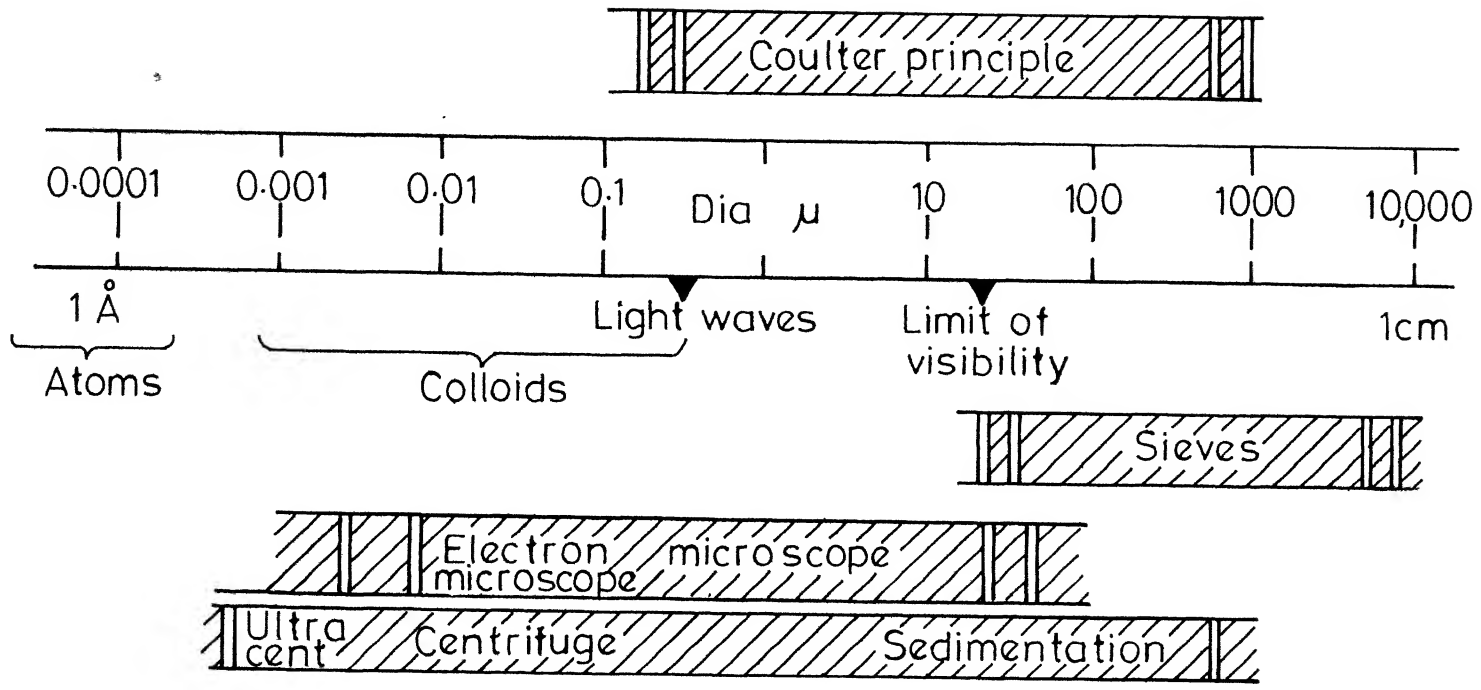

Fig. 5·1 - Size range of coulter method compared with coverage of sieve, sedimentation and microscope methods and overlap of electron microscope and centrifuge ranges.

Madden and McCoy [54] employed wet screening for size measurement of the encapsulated drops. They found that nylon coating alone is not sufficient for successful sieving as the drops tend to become sticky and do not possess enough strength to withstand the impact. So, they further coated the drops with silver thus increasing the strength of the coating. This method was tried and was found to be unsuccessful due to breakage of encapsulated drops during sieving.

Sedimentation was tried to obtain the cumulative weight fraction for different drop volumes. Water glycerine mixture was used as the settling medium in order to increase the settling times. The sample was thoroughly mixed by passing air from the bottom of the settling column before allowing the droplets to settle. This had to be done as it was found to be very difficult to introduce a monolayer of sample at the surface of the settling column without agglomeration of encapsulated droplets. Two difficulties were encountered. (i) Due to high viscosity of the medium, air bubbles continued to exist in the column for a long time (ii) Agglomeration of encapsulated droplets during settling could not be avoided inspite of very low (0.~ per cent) volume fraction of sample. Observation of settling droplets through cathetometer revealed existence of big agglomerates which affected the results considerably. Mechanical mixing could not be employed as the drops were fragile and broke easily.

Microscopic counting was also tried for the measurement of drop size distribution. Sample was withdrawn from the system, diluted and a microscopic slide was prepared. Random sites were chosen in the slide and the size and the number of droplets were recorded. This was very tedious and time consuming procedure involving a lot of personal errors. Moreover, only the droplet diameters could be measured. Though the drops are spherical, a small error in the counts of large sized drops gets magnified when the data of number counts vs drop diameter is converted to drop volume density as this involves evaluation of the third moment of number density with respect to drop diameter.

Until recently, photography was the main technique by which drop size distribution measurements were made. Though this technique can measure droplet sizes in situ, it has many drawbacks. It renders only a one dimensional view of the droplet population at one particular plane. Possibilities of overlapping of droplets and blurring of images of droplets not in focus make an accurate drop size measurement very difficult. This technique also suffers from the same drawback as microscopy in that this also measures only the droplet diameter.

Electronic size analysis measures the volume of droplet thus making this technique ideal for the measurement of drop volume distribution. Moreover, in situ sampling is possible

by placing the probe in the agitated vessel and withdrawing the sample soon after encapsulation. This technique is very fast and accurate as it is possible to count around 10,000 droplets for one distribution measurement within minutes.

5.1.2 Principle of Electronic Size Analysis:

The number and size of particle in an electrically conducting liquid are determined by the application of Coulter principle [60, 61]. The suspension of particles is forced to flow through a small aperture having an immersed electrode on each side as shown in Figure 5.2. As each particle passes through the aperture, it replaces its own volume of electrolyte momentarily changing the resistance value between the electrode Since a constant current is maintained between the electrodes through a current source, the momentary change in the resistanc value between the electrodes produces a voltage pulse of short duration having a magnitude proportional to the particle volume

Expressing the particle in electrical effect as a right cylinder aligned with the aperture axis and shorter than the aperture, it can be shown [60, 61] that the change in aperture resistance caused by a particle is

$$\Delta R = \frac{\rho_o \, v}{A^2} \left(\frac{1}{1 - \rho_o/\rho} - \frac{a}{A} \right)^{-1} \qquad (5.2.1)$$

where ρ_o = Resistivity of the medium

A = Aperture area normal to axis

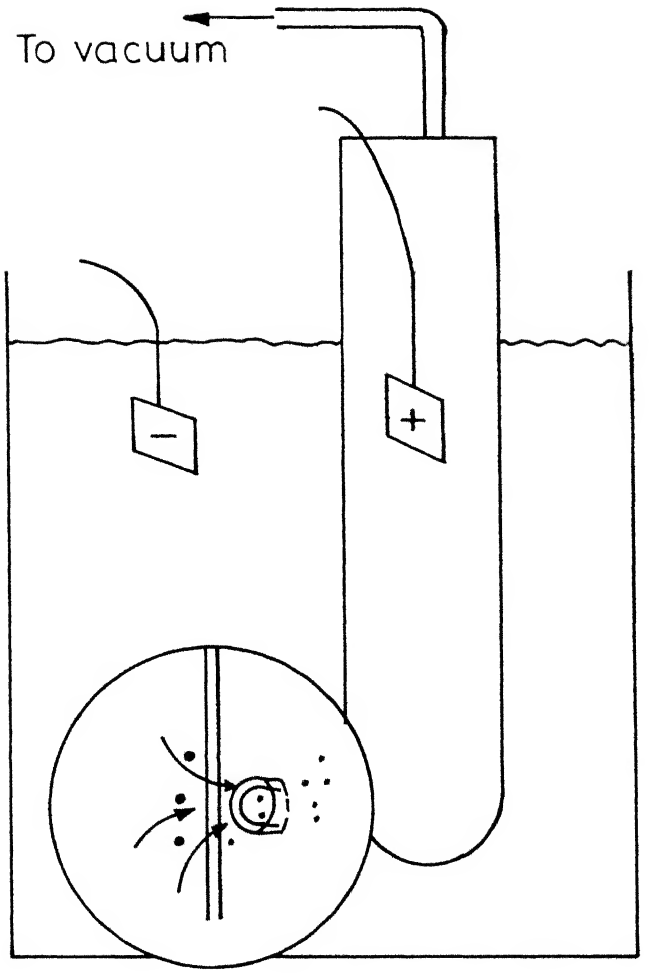

Fig. 5·2 - Basic mechanism of coulter principle.

v = Particle volume

ρ = Effective particle resistivity

a = Area normal to aperture axis of equivalent right cylinder for particle as oriented in passage.

Usually, particle resistivity has been found to be many orders of magnitude greater than that of the electrolyte. Metal powders and other apparently good conductors behave like non-conductors [60]. This is hypothesised as being due to oxide surface films and ionic inertia of the Helmholtz electric double layer and associated solvent molecules at the surface of each particle [60]. In case of drops encapsulated with nylon film, one can expect the resistivity of droplets to be much higher than the medium, nylon being a good insulator.

As indicated in equation (5.2.1), deviation from linear volumetric response becomes appreciable for nearly spherical particles above 30 per cent of aperture diameter ($a/A \simeq 0.09$) [60]. This effect is correctable, if need be. It is markedly reduced for elongated particles, such as fibres, rods and flakes, as the prevailing streamline in the aperture causes predominant alignment of such particles with the aperture axis.

The distortion of the electrical field in the aperture by a particle will conform to the essential surface of the particle rather than follow each crevice and wrinkle, thus sensing the 'envelope volume' of the particle.

The voltage pulse from the electrode is amplified, scaled and counted to yield the volume distribution of particles.

5.1.3 Probe Assembly:

Two glass probes of aperture diameters 2 mm and 0.8 mm were used. The schematic diagram of the probe assembly is shown in Figure 5.3. Probe consisted of a glass tube 1.5 cm diameter fitted with a B-24 female joint, the flattened bottom portion of the tube having an aperture of required diameter. Platinum electrodes were used. Electrodes were made by embedding 1/1000th inch thick platinum foil on a glass plate. The inner electrode ran all along the length of the tube. The outer electrode faced the aperture with a gap of 7.5 mm. Both the electrodes were kept rigid by connecting the glass plates carrying the electrodes to the tube. The dimensions of the inner and outer electrodes were 11.5 cm x 1 cm and 1 cm x 1 cm respectively. Here, the distance between the electrodes remained fixed since both the electrodes were embedded on glass plates. This is an improvement on the probe supplied by Coulter Electronics Inc. for their Coulter Counter Model B where both the electrodes were platinum foils hanging into the medium. There, there is a definite possibility of vibration of outer electrode due to the turbulence of the medium created by agitation. This changes the distance between the electrodes and gives spurious voltage pulses due to the

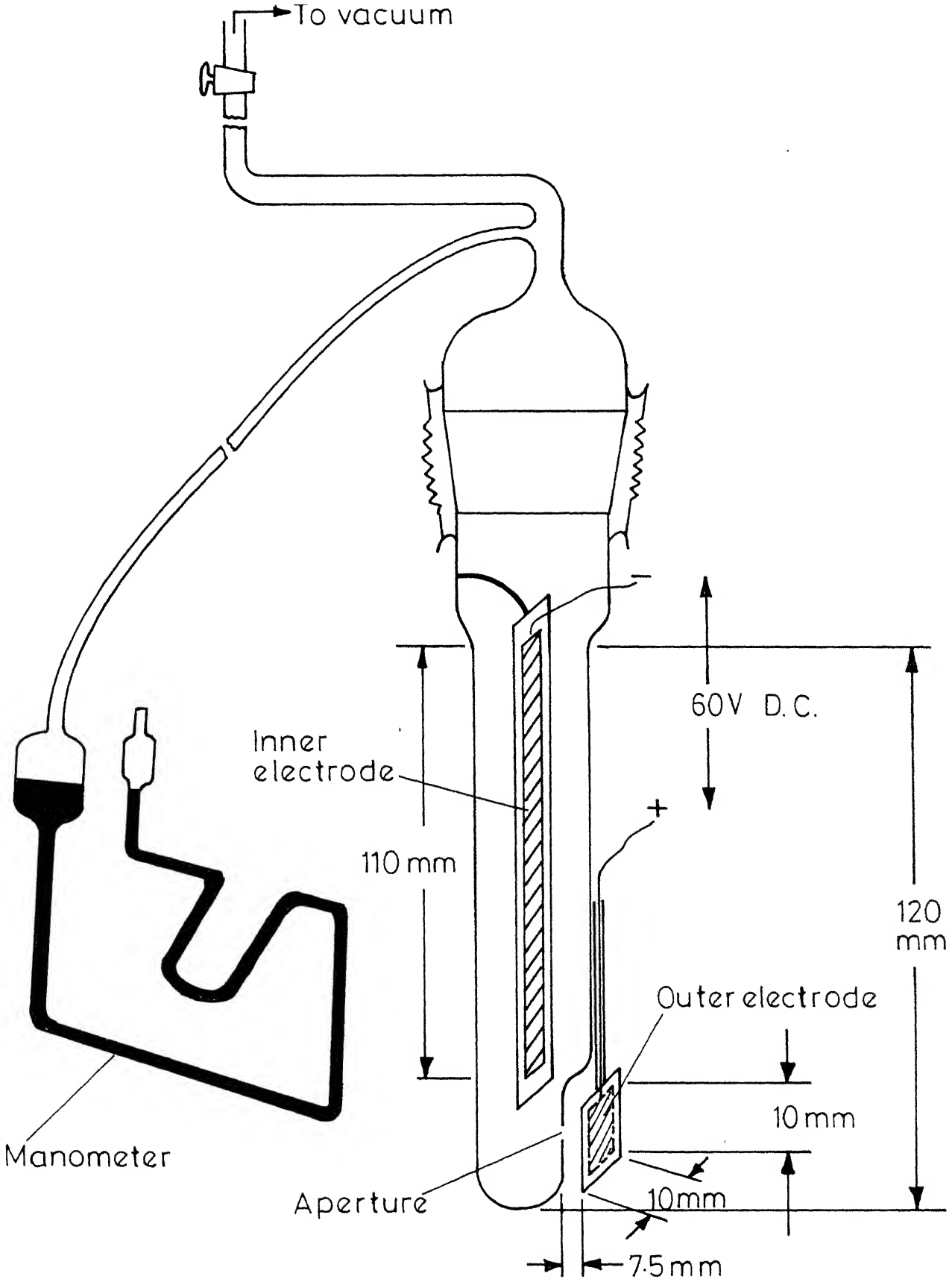

Fig. 5.3 - A schematic diagram of the probe assembly.

vibration of the outer electrode. Moreover, if the distance between the electrodes is not kept fixed then the signal strength for a particle of given volume will not be constant and hence the results will not be reproducible.

The probe tube was connected to a vacuum pump supplied by Coulter Electronics Inc. through a stopcock. The probe assembly was immersed in the suspending electrolytic medium and the inner tube was filled with the medium. At the time of measurement, suction was applied to the tube by means of the vacuum pump and the sample was withdrawn through the small aperture by opening the stopcock. The manometer connected to the probe gave the pressure drop across the aperture during suction.

5.1.4 Electronic Circuitory for Measurement:

The block diagram of the electronic circuitory is shown in Figure 5.4. The inner platinum electrode of the probe was grounded. A positive 60 volts DC was applied between the two electrodes through a constant current source and a series variable resistor. The current source used was a standard current mirror. The current source had provision for setting four different currents, namely, (i) 0.5mA (ii) 1.0 mA (iii) 1.5 mA and (iv) 2 mA. The variable resistor was adjusted so as to minimize the voltage drop across the transistor in constant current source circuit. The output from the probe consisted of a constant D.C. voltage V(=IR,R

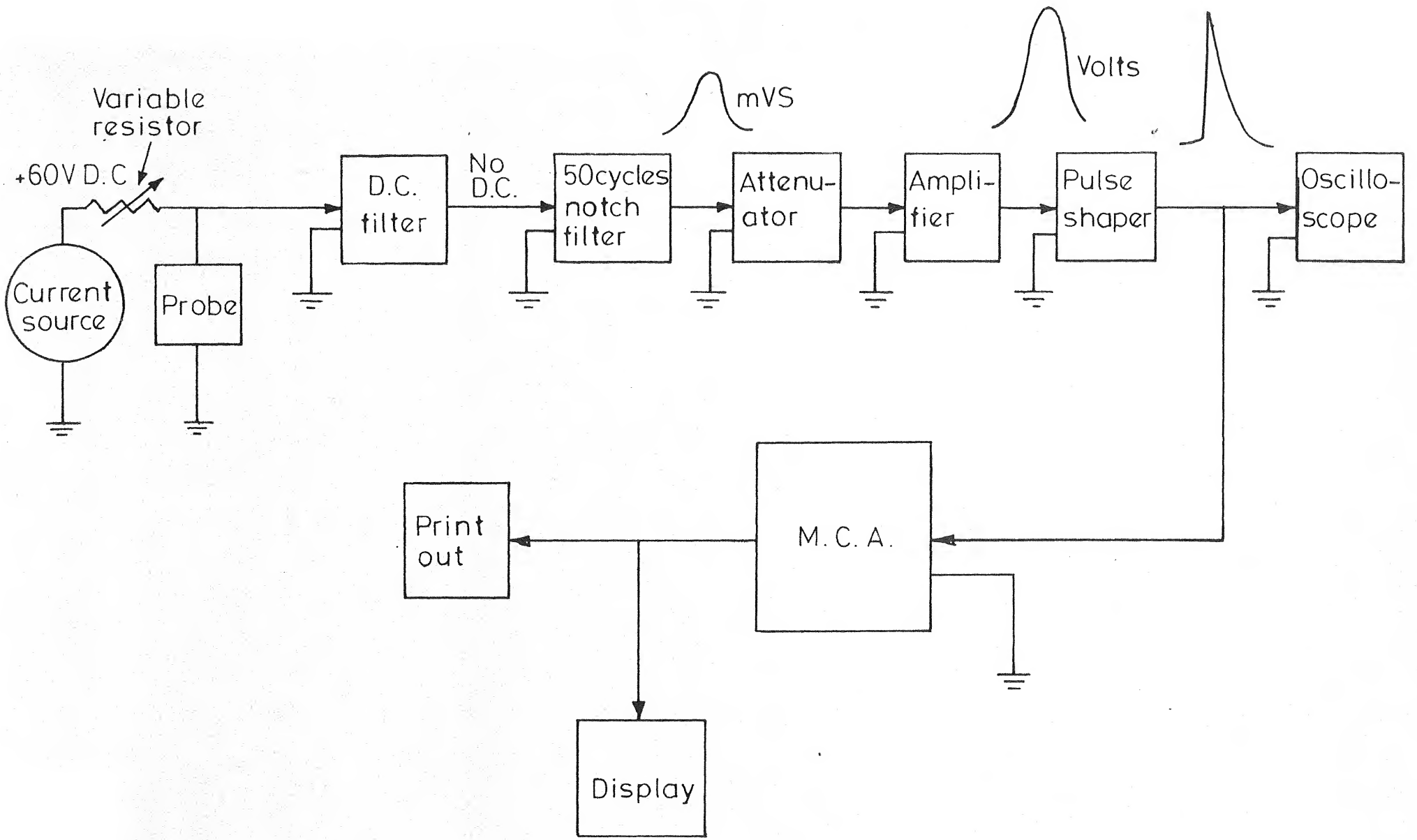

Fig. 5.4 - Block diagram of the electronic circuitory.

being the resistance between the two electrodes) riding over which were the voltage pulse signals given by the encapsu droplets when they pass through the aperture. The output was fed to a passive D.C. filter which filtered the D.C. signal thus permitting only the overriding pulse signals to pass through. Though shielded cables were used to carry the signal and the motors were grounded, there was considerable 50 cycles pick-up especially from the vacuum pump. Hence it was found necessary to use a 50 cycles notch filter to filter off any 50 cycles noise picked up by the probe from its surroundings. The output from the notch filter consisted only of the pulse signals whose amplitude was of the order of milli These pulses had to be amplified prior to analysis. ECIL pre-amplifier was used for this purpose. Since the amplifier had only four discrete gain settings (100, 250, 500 and 1000), it was necessary to use an attenuator with attenuations 1, 1/2 1/5 and 1/10 so that a combination of attenuation and gain settings gave the required amplification. Moreover, large voltage pulse signals had to be attenuated before they were fed to the amplifier as the output of the amplifier saturated at 6 volts. The amplitude of the amplified voltage pulse signal was of the order of volts. These signals were very broad with a large rise time (of the order of msecs). They had to be shaped before they could be fed to the Multi-Channel Analyser (MCA) for analysis. The pulse shaper converted these

broad voltage pulses into sharp voltage pulses with a very small rise time (of the order of microseconds). The amplitude of the voltage pulses were preserved during pulse shaping. The shaped voltage pulse signals were fed to 128 channel ND-110 Multichannel Analyser for analysis. The signals were also fed to a Philips Oscilloscope for visual observation. The MCA could accept pulses in the range of 0-6.8 volts. The current gain and attenuator settings were adjusted so that all the amplified and shaped signals fell in this range. The MCA was operated in Pulse Height Analysis (PHA) mode. The MCA sensed the pulse amplitude (height) and stored the count of number of pulses in the appropriate channel number. The MCA was calibrated with standard pulses from a precision pulse generator. The details of the calibration is given in Appendix II. The calibration gave the relationship between the pulse amplitude (height) and the channel number. The MCA gave a display of number count versus channel number. It was also possible to get a print out of the number count versus channel number.

5.1.5 Size Range of Measurement:

Response correction is unnecessary for most particulate systems if the few largest particles do not exceed 40-50 per cent of the aperture diameter [60, 61]. This is also a practical maximum to avoid excessive aperture blockage due to coincidence of large particles. The noise limitations of

electronic amplification prevent measurement below 1-2 per cent of aperture diameter. Thus, a single aperture size provides a diametric measurement range of 20:1, with the corresponding volume range upwards of 8000:1 [60]. The range of droplet sizes encountered in agitated lean liquid-liquid dispersions was from 50μ to 800μ. Though it is possible to cover the whole size range with one probe, in order to increase the resolution of volume distribution measurements, it was decided to use two probes of aperture diameters 0.8 mm and 2 mm. The smaller probe was used for the measurement of drop population of small sizes - drop population at large stirring time and the bigger probe was used for the measurement of drop population of large sizes - drop population at small stirring time.

5.1.6 Calibration of the Probes:

The amplitude of the voltage pulse given by a particle of certain volume will depend on many factors such as aperture diameter, current, gain and attenuator settings and the resistance between the two electrodes. The relationship between the pulse amplitude and particle volume should be known in order to infer the droplet volume distribution from the output of MCA.

A narrow distribution of spherical standard sized glass particles were suspended in a conducting medium of NaCl solution. A sample of the suspended particles was withdrawn

through the probe and the spectrum measured by the MCA. The average volume of the narrow sized standard sample was measured by microscopic counting. Since the sample is a narrow distribution of particles, the average particle volume should correspond to the average channel number of the spectrum. The same procedure was repeated for different NaCl concentrations electronic settings and sample size to obtain the relationship between particle volume and channel number for different conditions. The details of the calibration is given in Appendix II.

5.1.7 Coincidence Effect:

Sometimes, more than one droplet may pass through the aperture simultaneously. This will give rise to the superimposition of the voltage pulses of these droplets, resulting in loss of count. A typical voltage signal from the probe when two particles pass through the aperture simultaneously is shown in Figure 5.5. As mentioned earlier, the primary effect of coincidence is loss of count as some of the superimposing voltage pulses will be ignored by the electronic circuits. Corrections can be applied to this. These corrections are known functions of aperture size and particle concentration and may be checked experimentally by counting a given suspension at successive dilutions. As a secondary effect, coincidence passages may give rise to voltage pulses of amplitude greater than the amplitudes of pulses corresponding

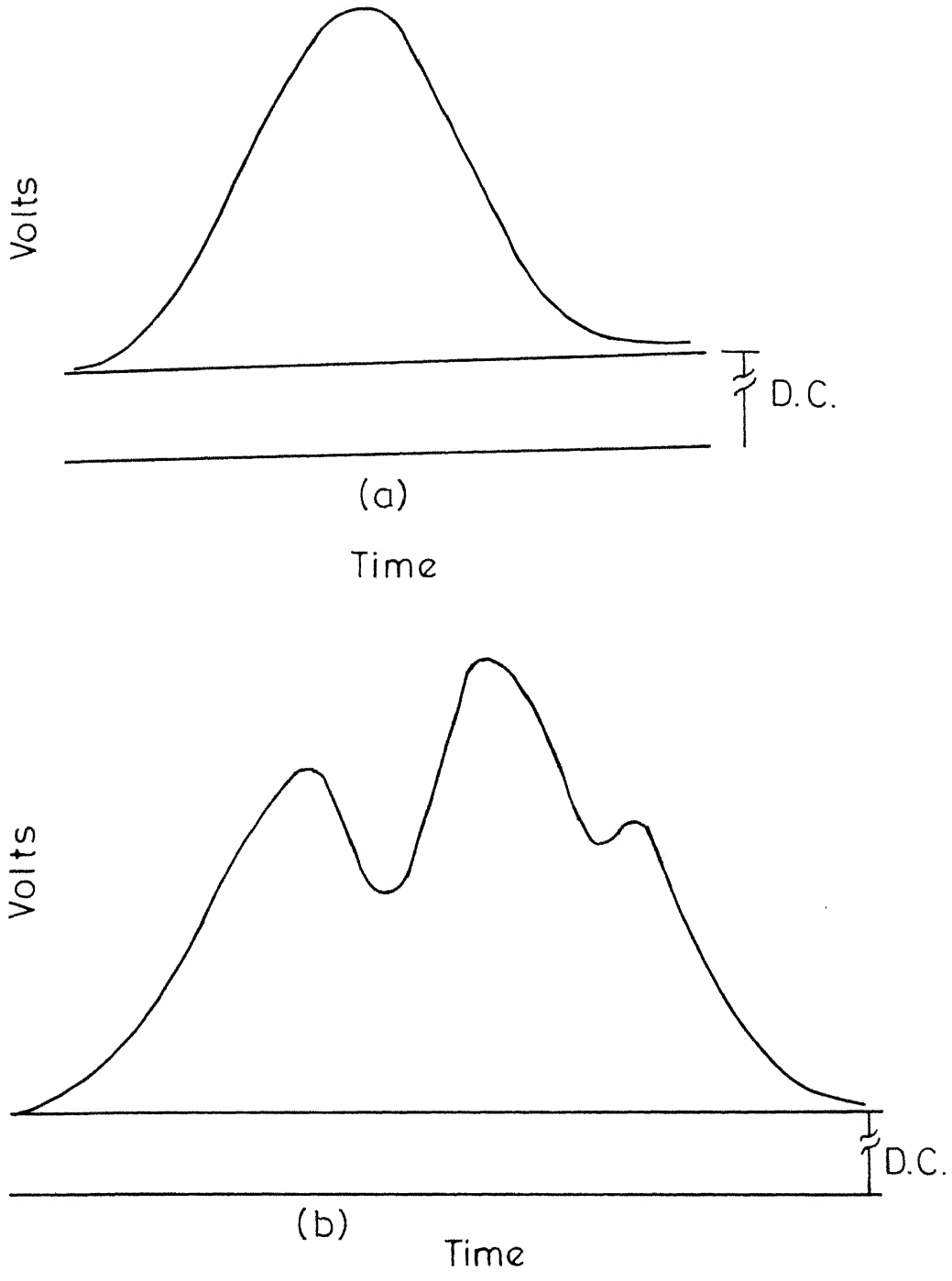

Fig. 5.5 - A typical voltage signal from the probe when
(a) One droplet passes through the aperture
(b) Many droplets pass through the aperture simultaneously.

to either particle thus registering a false particle of large volume. This effect will thus vary with the size range of the system being analysed. If coincidence loss corrections are kept low, this secondary effect will usually be negligible, but may be quite predominent in narrowly distributed systems near the frequency peak [60].

Coincidence corrections were checked experimentally by measuring the spectrum of standard sized spherical glass particles of narrow distribution at different concentrations in the size range of 50-800μ. Since drop volume distribution measurements were made at dispersed phase volume fraction of 0.1 per cent, coincidence effects were verified in the concentration range of 0.05 to 0.5 per cent. It was found that the average channel number corresponding to the standard sample did not vary appreciably with concentration indicating that the coincidence effects are negligible.

5.1.8 Encapsulation Technique:

Sprow [34] has employed electronic size analysis for the measurement of drop size distribution of emulsions by withdrawing a sample of emulsion. In case of emulsions, the droplet sizes are very small and hence their rate of breakage small. Therefore, the drop breakage in the system during sampling is very small. The dilution and stabilization of the emulsion with glycerine retarded drop coalescence in the

system as well as in the aperture tube during sampling. However, in case of liquid-liquid dispersions, the droplet sizes are fairly large. Therefore, it is necessary to avoid breakage and coalescence of droplets during sampling. This was achieved by capturing all the droplets in a liquid-liquid dispersion in their dynamic state by encapsulating them with a thin nylon film. Encapsulation preserved the identity of the droplet by preventing breakage and coalescence during sampling. Encapsulation was achieved through an interfacial polycondensation reaction. This reaction was almost instantaneous and resulted in the formation of very thin (0.1 - 1 micron thick) nylon coating which helped to preserve the identity of the droplets at the time of encapsulation thus making a direct size measurement possible. Madden and McCoy [54] were the first to illustrate the use of this technique for the measurement of drop size distribution. Encapsulation was employed by Mylnek and Resnick [39] for the measurement of drop size distribution in liquid-liquid dispersions.

The dispersed phases used for this study were CCl_4-i-Octane mixture (50-50 per cent), Anisole-CCl_4 mixture (80-20 per cent) and chlorobenzene. The reactants for the interfacial polycondensation reaction were terephthalic acid chloride and piperazine [39]. Terephthalic acid chloride was present in the dispersed phase at a concentration of 1 per cent by weight. At the time of encapsulation, mixture of piperazine and NaOH

solutions was added to the continuous phase for the reaction to occur. The reaction was found to be instantaneous resulting in a coating of Nylon over all the droplets. The nylon film, being very thin (0.1 - 1.0μ), did not affect the drop volume measurement. The details of the reaction and the composition of the reactants are given in Appendix III.

5.2 EXPERIMENTAL SET-UP:

The details of the mixing vessel assembly are given in Figure 5.6. The mixing vessel was a 3 litre jacketted glass vessel, 14 cms in diameter and 20 cms high. It was filled with the liquid-liquid mixture to a height of 16.25 cms. The vessel did not have any sharp corners at the bottom to avoid dead zones. The L/D ratio was very nearly one as per the recommendations of Shinnar and Church [28]. Outer jacket was provided for water circulation from a constant temperature water bath in order to maintain a constant temperature. All experiments were conducted at 30 ± 0.1°C.

The mixing vessel was placed on a bottom aluminium plate fixed to the work bench. Rubber gasket was provided between the vessel flange and the stainless steel baffle assembly. The baffle assembly consisted of a top stainless steel plate and four baffles. The baffles were 19 cms long, 1.4 cm wide and 0.625 cms thick. The baffle assembly was connected to the bottom plate through three brass rods and was kept rigidly in position by tightening the brass flynuts. A teflon bush was connected to the top stainless steel plate.

LEGENDS FOR FIGURE 5.6

1 OUTER JACKET

2 VESSEL

3 STAINLESS STEEL PLATE OF THE BAFFLE ASSEMBLY

4 RUBBER GASKET

5 BAFFLE

6 PADDLE IMPELLER

7 AGITATOR SHAFT

8 BRASS ROD

9 BRASS FLYNUT

10 BOTTOM ALUMINIUM PLATE

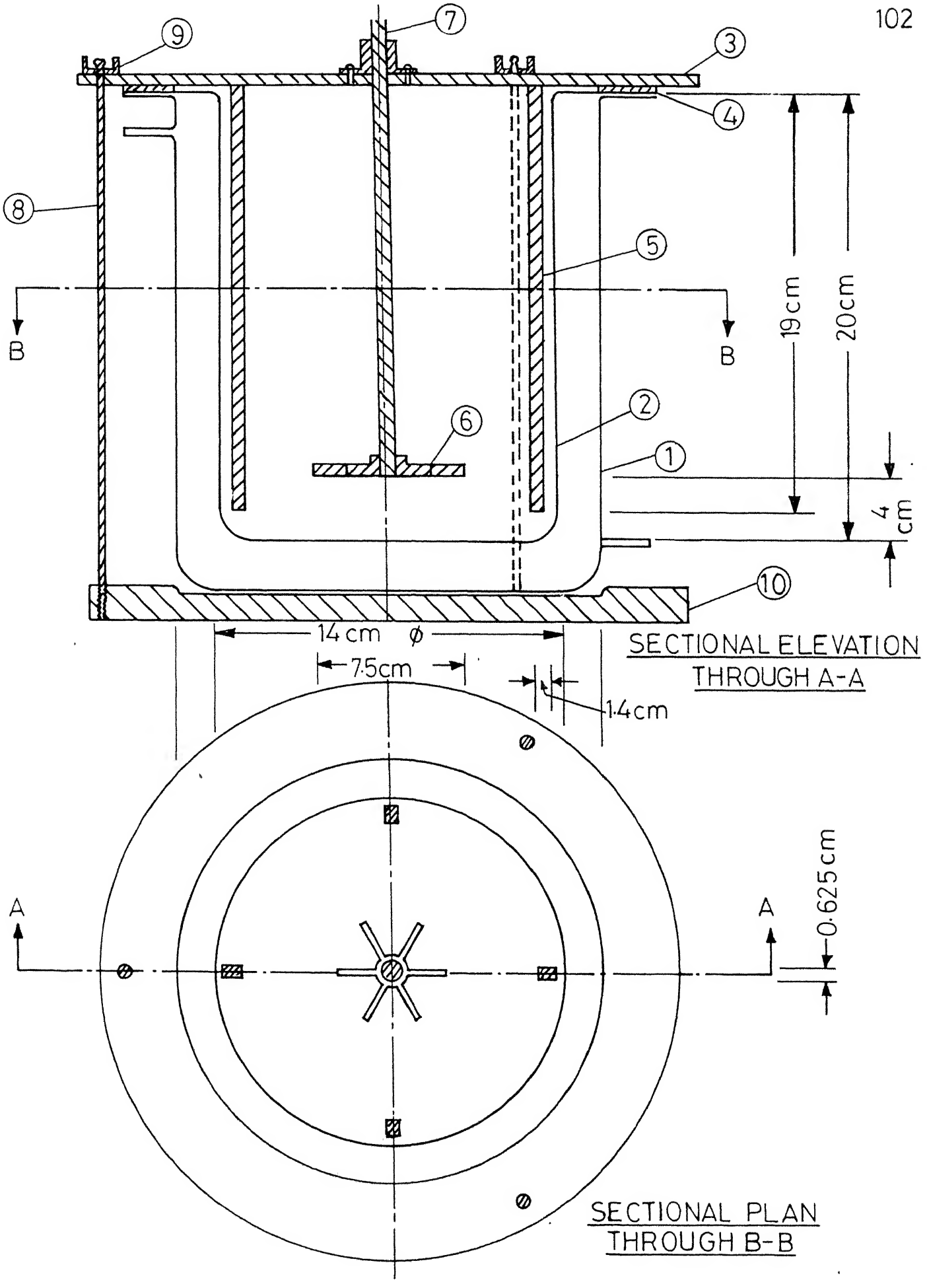

Fig. 5.6 - Plan and elevation of mixing vessel assembly.

This acted as a guide to the agitator shaft and avoided wobbling of the agitator. The number and dimensions of the baffles were fixed based on 'Standard baffling'. Fernandes and Sharma [62] used four vertical baffles, each 1/10th of the vessel diameter, mounted against the vessel wall at right angles to it, spaced at 90° intervals around the vessel. Mack and Kroll [63] and Rushton, Costich and Everett [15] have shown that four baffles are satisfactory for 'standard baffling'. According to Mack and Kroll [63], baffles slightly away from the wall would give more power consumption and hence better mixing than when the baffles are attached to the wall. On the basis of these considerations, four baffles each 1/10th of the vessel diameter were used. The baffles were equally spaced at 90°, right angles to the vessel and 1/4th inch away from the wall.

Two ordinary 6-blade paddle impellers of 2 inch and 3 inch diameters were used. Most of the experiments were conduc with 3 inch diameter impeller to ensure good mixing. The impellers were 3/8th inch wide and 1/16th inch thick. The impelle was placed at 4 cm from the bottom of the vessel.

The agitator was driven by a 1/4 H.P. induction motor with a variable speed drive. The variable speed drive consisted of a combination of step pulleys and gears as the speed reduction ratio required was high. Experiments were conducted at three speeds - 300 RPM, 420 RPM and 480 RPM.

It was not possible to conduct the experiments at higher speeds as the drop volume distribution changed rapidly due to rapid drop breakage.

5.3 EXPERIMENTAL PROCEDURE:

The mixing vessel, the stainless steel baffle assembly and the agitator were cleaned with chromic acid and rinsed thoroughly with distilled water. The mixing vessel was placed on the bottom aluminium plate. The baffle assembly was centred in the vessel and rigidly fixed by tightening the brass flynuts. The agitator was connected to the variable speed drive. The height of the impeller above the vessel bottom was checked. The probe assembly was lowered into the vessel through a hole provided in the top stainless steel plate so that the aperture of the probe was placed between two baffles and at half the depth of the vessel. The vessel was then charged with 2500 cc of distilled water presaturated with the dispersed phase. Presaturation was done to avoid mass transfer of the dispersed phase into continuous phase during agitation. Water was circulated in the outer jacket of the vessel from a thermostat. The system was allowed to equilibrate for about half an hour, after which it was found that the continuous phase temperature reached the set point in the thermostat. The continuous phase temperature was measured with a thermistor probe using a telethermometer. All experimental measurements were made at $30 \pm 0.1^{\circ}C$.

One per cent by weight of terephthalic acid chloride was dissolved in the dispersed phase. 2.5 cc of this was added to the continuous phase maintaining a dispersed phase volume fraction of 0.1 per cent. The induction motor was started and the time of agitation was measured with a stopwatch. The speed of agitation was checked for every observation with General Radio Strobotac. At the time of measurement, 50 cc of mixture of piperazine and NaOH was added to the continuous phase and stirring continued for 10 seconds after which the speed of agitation was reduced. The dispersion was agitated at lower speed for a few minutes for the interfacial polycondensation reaction to be completed in order to increase the strength of nylon coating. Because of the presence of NaOH and formation of NaCl in polycondensation reaction, the continuous phase became a conducting medium. Vacuum was applied to the probe assembly through the vacuum pump. The stopcock in the outlet of the probe tube was then slowly opened to fill the probe with the dispersion. The resistance between the electrodes was then measured with a multimeter. The current, gain and attenuator settings were adjusted. Accordingly, the resistance of the series variable resitor was also adjusted. Electrophoresis power supply was put on to apply 60 volts DC between the electrodes through the constant current source. The output from the amplifier was observed in the Philips oscilloscope. Now, a sample of the dispersion

was withdrawn through the aperture by slowly opening the stopcock at the outlet of the probe. The pressure drop across the aperture was checked with the mercury manometer connected to the probe. The pressure drop was adjusted by adjusting the opening of the stopcock. Same pressure drop was maintained during sampling for all observations. This was done to ensure that enough vacuum was applied to withdraw large size droplets. The amplified voltage pulse signals could be observed in the oscilloscope. The voltage range of the pulses was noted. If the pulses were not in the proper range (either too small or too big) then the current, attenuator and gain settings were adjusted accordingly so as to get the pulses in the proper range. The output from the pulse shaper was observed in the oscilloscope. If found satisfactory, it was fed to the MCA and the pulses were logged in the MCA in PHA mode. Usually, a sample of 200 cc was withdrawn at a time. Then the spectrum was observed in the visual display of the MCA. If the total number count of the droplets was not sufficient, then the withdrawn sample was recycled to the vessel and another sample of 200 cc was withdrawn, pulses logged in MCA. Around 10,000 droplets were counted to obtain a volume distribution. The printout of the spectrum was then taken. The same procedure was repeated to get another reading of the volume distribution. This was done to check the consistency of the measured distribution. The voltage drop between the electrodes was then measured with the multimeter.

CHAPTER 6

RESULTS AND DISCUSSION

This chapter presents the experimental results of transient and equilibrium drop volume distributions in batch agitated lean liquid-liquid dispersions. The experimental results are also compared with the models for transitional breakage probability and equilibrium drop size distribution.

6.1 SYSTEMS AND EXPERIMENTAL CONDITIONS:

In all the experiments the continuous phase was distilled water presaturated with the dispersed phase liquid. Drop volume distribution measurements were made for three different dispersed phases and three agitator speeds. Three inch diameter paddle impeller was used in most of the experiments. Measurements were also made with two inch diameter paddle impeller in order to study the effect of impeller diameter. In all the experiments, the density and viscosity of both the continuous and dispersed phases were more or less equal. In fact, this dictated the choice of the dispersed phases. All the experiments were conducted at $30 \pm 0.1^{\circ}C$ and dispersed phase volume fraction $\emptyset$ was maintained at 0.1 per cent in most of the experiments. Measurements were also made at three more dispersed phase volume fractions, namely 0.25 per cent, 0.375 per cent and 0.5 per cent, to study the effect of $\emptyset$ on drop

volume distribution. The different systems and the experimental conditions are given in Table 6.1. The interfacial tension of the three systems were measured at 30 ± 0.1°C by drop weight method. The physical properties of the dispersed phases are given in Table 6.2. At least 10,000 droplets were counted for each drop volume distribution measurement. In all the measurements, the sample was withdrawn from the same position in the vessel. The sampling probe was positioned to keep the aperture exactly at half the liquid depth midway between two baffles. No attempt was made to study the effect of position on drop volume distribution as it was found that the variation of drop size distribution with position is negligible in systems where the buoyancy effects are negligible [39].

6.2 REPRODUCIBILITY OF MEASUREMENT:

Since drop breakage and coalescence are random in agitated liquid-liquid dispersions, it is necessary to count large number of droplets to get a meaningful distribution data. Therefore, at least 10,000 droplets were counted for each drop volume distribution measurement. A typical plot of number count of droplets versus channel number is shown in Figure 6.1. In each experiment, at least two samples were withdrawn from the drop population in order to ascertain that the samples were representative of the population. Kolmogorov-Smirnov

TABLE 6.1: SYSTEMS AND EXPERIMENTAL CONDITIONS

System	Agitated Speed RPM	Impeller Dia. inches
Water-CCl_4+i-Octane (50-50 per cent)	480	3 and 2
Water-CCl_4+i-Octane (50-50 per cent)	420	3
Water-CCl_4+i-Octane (50-50 per cent)	300	3
Water-Anisole+CCl_4(80-20 per cent)	300	3
Water-Chlorobenzene	300	3

TABLE 6.2: PHYSICAL PROPERTIES OF THE DISPERSED PHASE

Dispersed Phase	Density, gms/cc	Interfacial tension, dynes/c
CCl_4+i-Octane (50-50 per cent)	1.149	46
Anisole+CCl_4(80-20 per cent)	1.113	29
Chlorobenzene	1.101	37.7

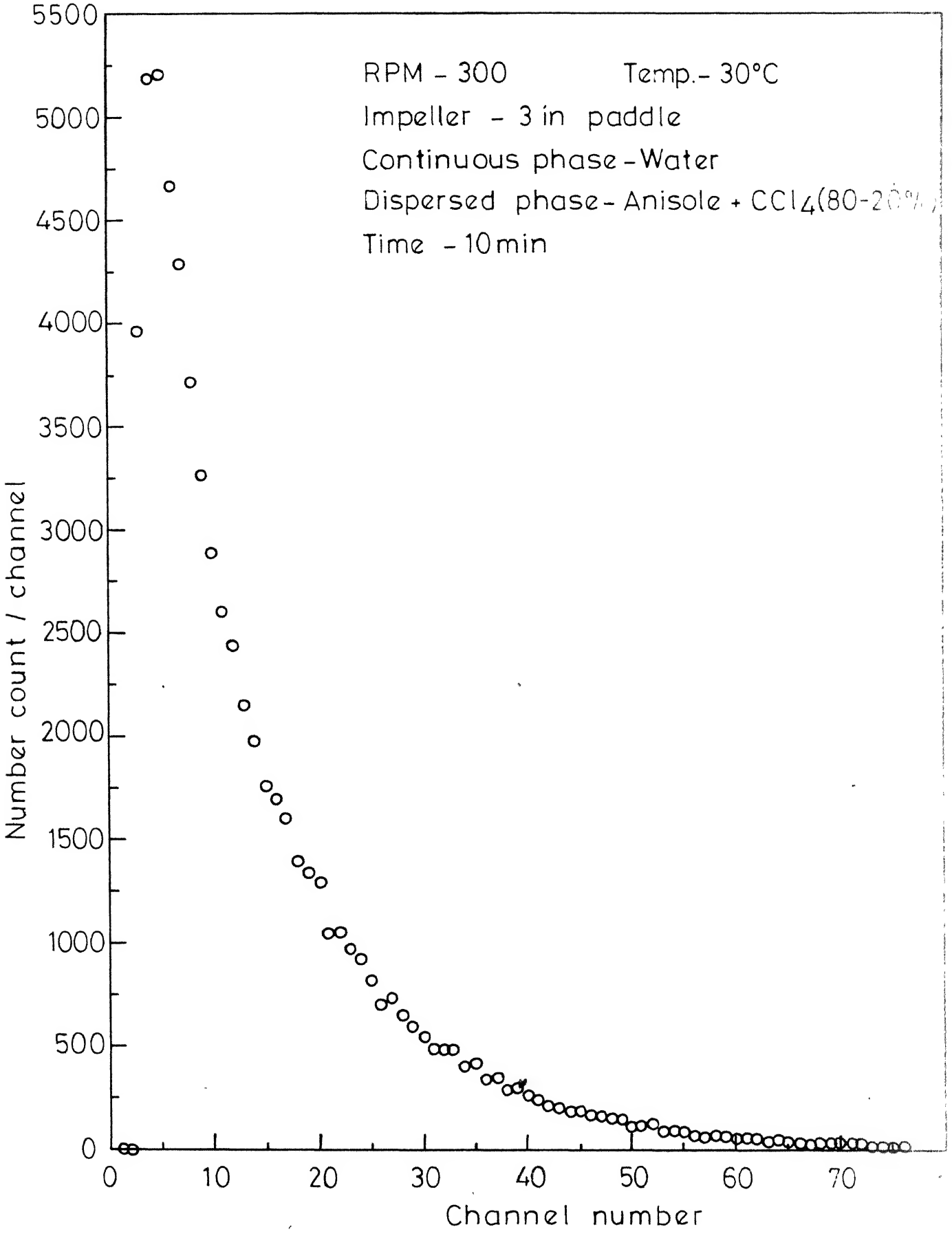

Fig. 6.1 - Plot of number count of droplets versus channel number.

two sample test was employed to verify that the two samples represented the same population. A typical comparison of the cumulative number per cent of two samples from the same population is shown in Figure 6.2. The result of the Kolmogorov-Smirnov two sample test is given in Table 6.3. Kolmogorov-Smirnov two sample test was found to be very stringent as the total number count of droplets for each measurement was very large. The test showed that the probability that the two samples are from the same population is finite though very small. Experiments were also repeated under identical conditions to verify the reproducibility of the experiment. The reproducibility was verified by means of Kolmogorov-Smirnov two sample test. A typical comparison of the cumulative number per cent of two experimental observations is made in Figure 6.3. The result of Kolmogorov-Smirnov two sample test is given in Table 6.3. Though the experimental cumulative number per cents are not very different, Kolmogorov-Smirnov test, being very stringent, gave a very small probability that the two samples are from the same population.

6.3 EFFECT OF DISPERSED PHASE FRACTION:

At low dispersed phase fraction coalescence should be negligible due to negligible interaction between droplets. Therefore, one would expect the effect of dispersed phase fraction $\emptyset$ on drop volume distribution for lean agitated

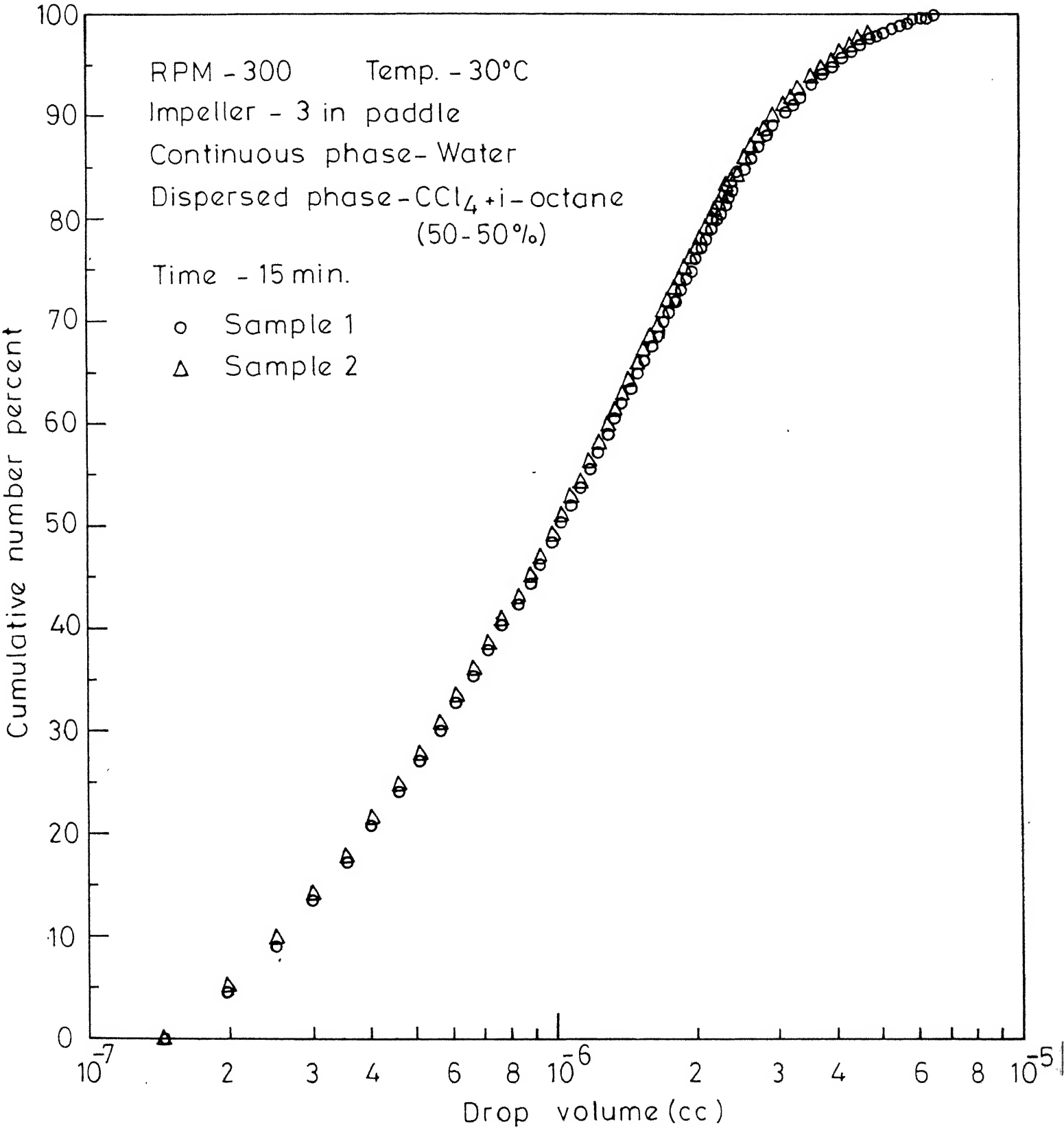

Fig. 6.2 - Comparison of cumulative number percents of two samples.

TABLE 6.3: RESULTS OF KOLMOGOROV-SMIRNOV TWO SAMPLE TEST

	Probability that both the samples are from th same population (per ce
RPM-300 Water-CCl_4+i-Octane (50-50 per cent)	
Time-15 min. 3 in paddle Temp., 30°C	
Sample 1	1.325
Sample 2	
RPM-300 Water-Anisole+CCl_4(80-20 per cent)	
Time-1 min 3 in. paddle Temp., 30°C	
Experiment 1	0.1138
Experiment 2	

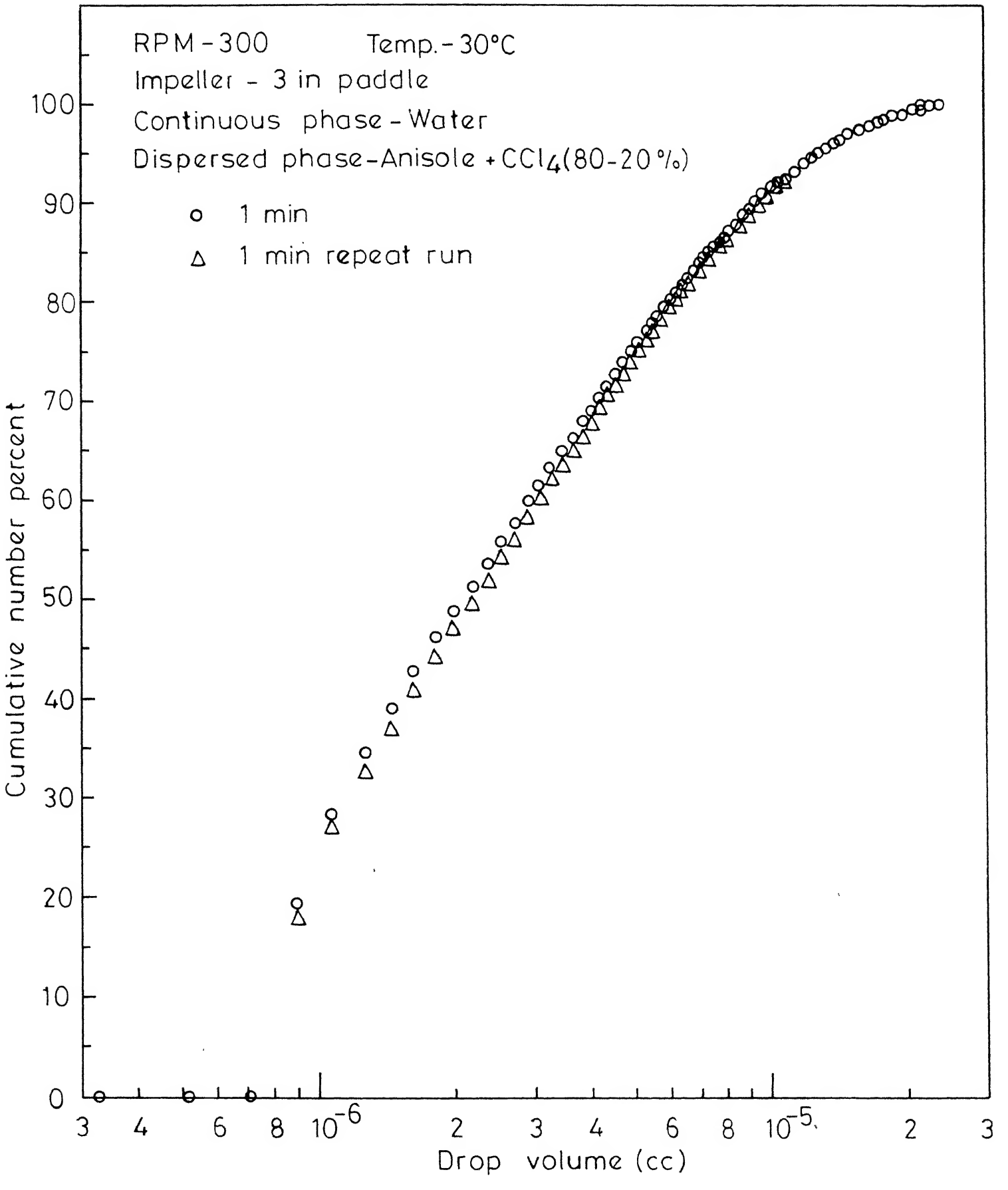

Fig. 6·3 - Comparison of cumulative number percents of repeated experiments.

liquid-liquid dispersions to be negligible. Drop volume distributions were measured at three more dispersed phase volume fractions 0.25 per cent, 0.375 per cent and 0.5 per cent at the agitator speed of 480 RPM for water - CCl_4 + i-octane (50-50 per cent) system. Figure 6.4 compares the cumulative number per cents at different dispersed phase volume fractions. Kolmogorov-Smirnov two sample test showed that the distributions represent different populations. From Figure 6.4, it can be seen that the cumulative number per cent shifts to larger drop volume as the dispersed phase volume fraction increases, though the shift is very small. This shows that there is a definite but negligible effect of dispersed phase volume fraction on drop volume distribution. Hence, in all the experiments it can be assumed that coalescence is negligible.

6.4 TRANSIENTS OF DROP VOLUME DISTRIBUTION:

Transients of drop volume distribution were measured for water-CCl_4+i-octane (50-50 per cent) system at three different agitator speeds of 480 RPM, 420 RPM and 300 RPM with three inch diameter paddle impeller and at the agitator speed of 480 RPM with two inch diameter paddle impeller. Transients of drop volume distribution were also measured at the agitator speed of 300 RPM with three inch diameter paddle impeller for water-Anisole + CCl_4 (80-20 per cent) and water-chlorobenzene systems. Figures 6.5 through 6.10 show the

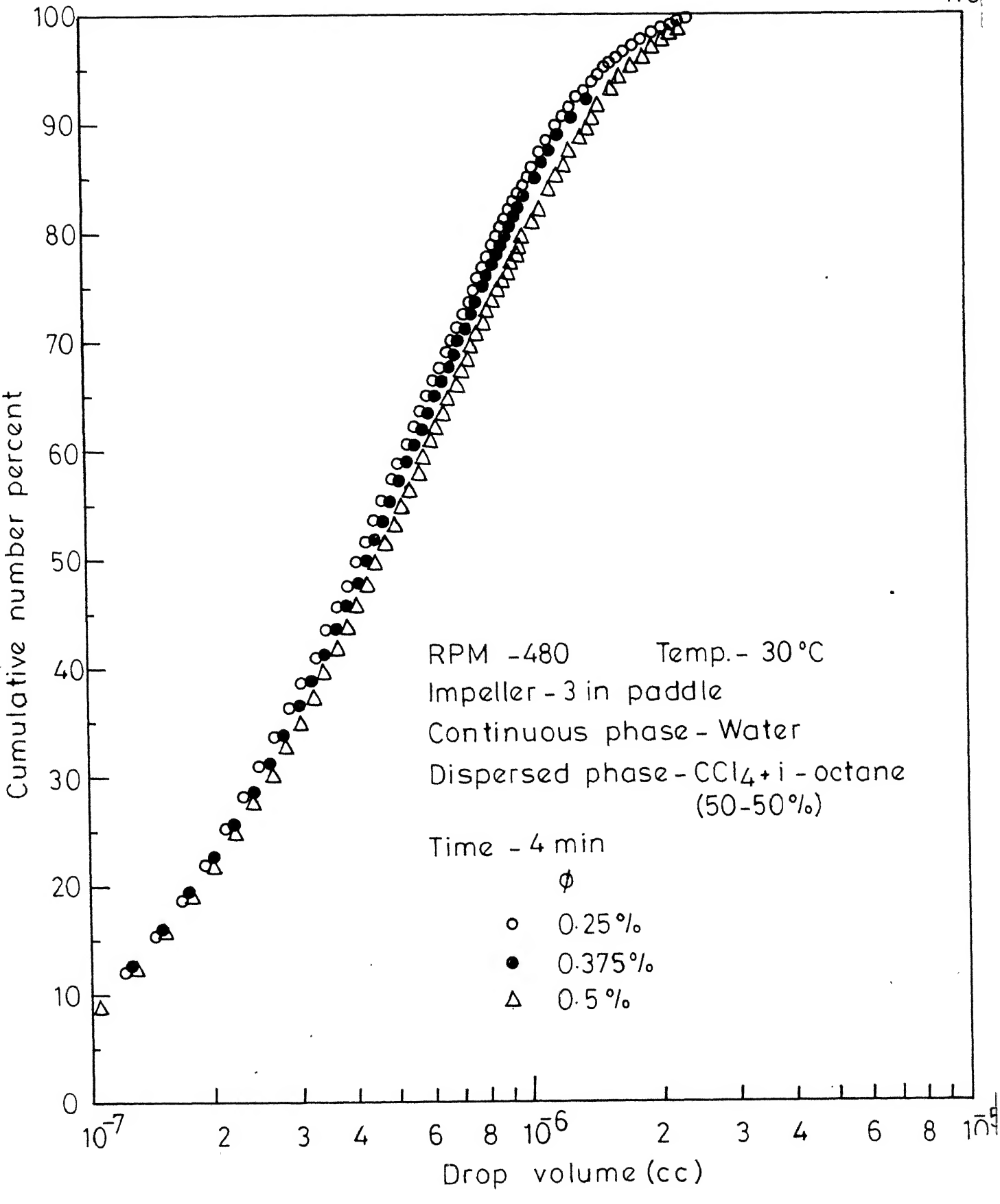

Fig. 6·4 - Effect of dispersed phase fraction on cumulative number percent.

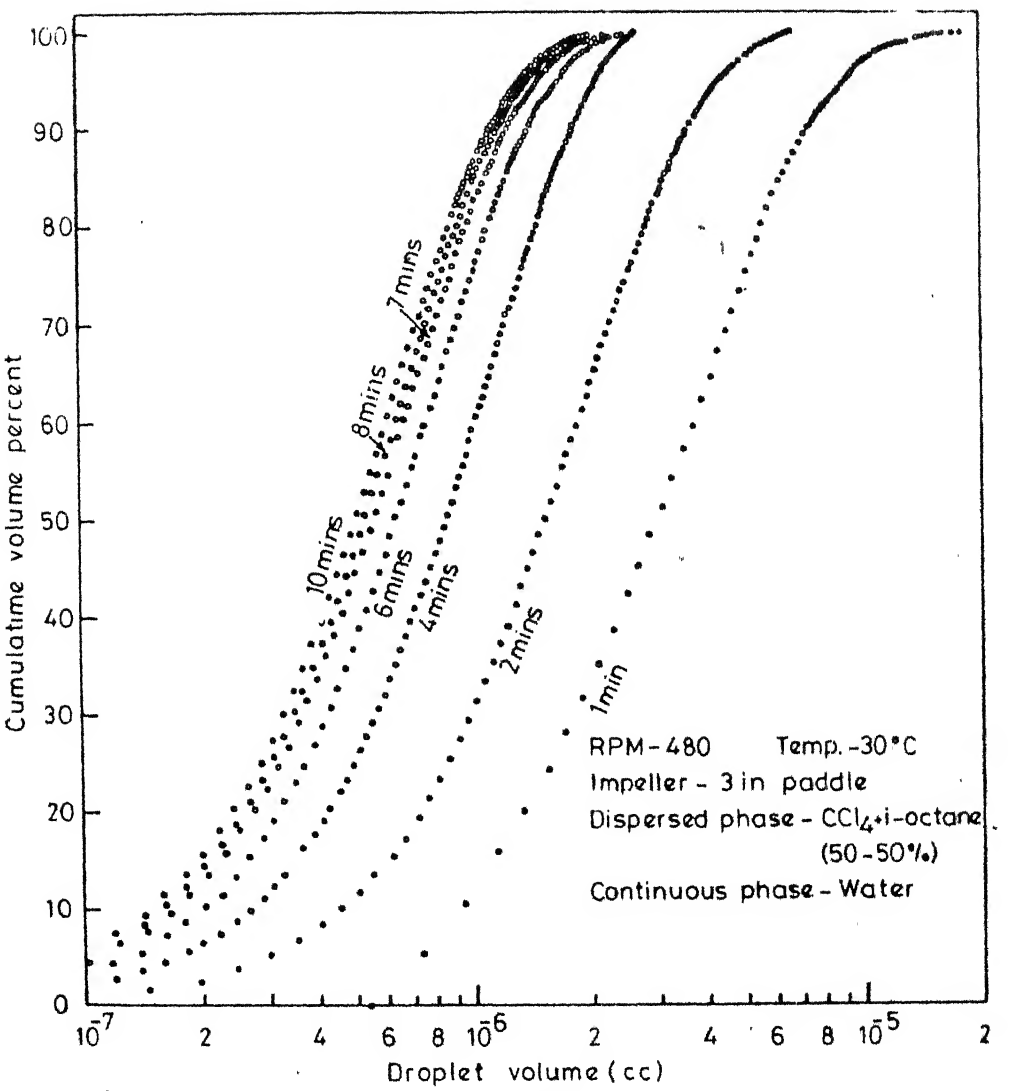

Fig. 6.5 : Effect of stirring time on drop volume distribution

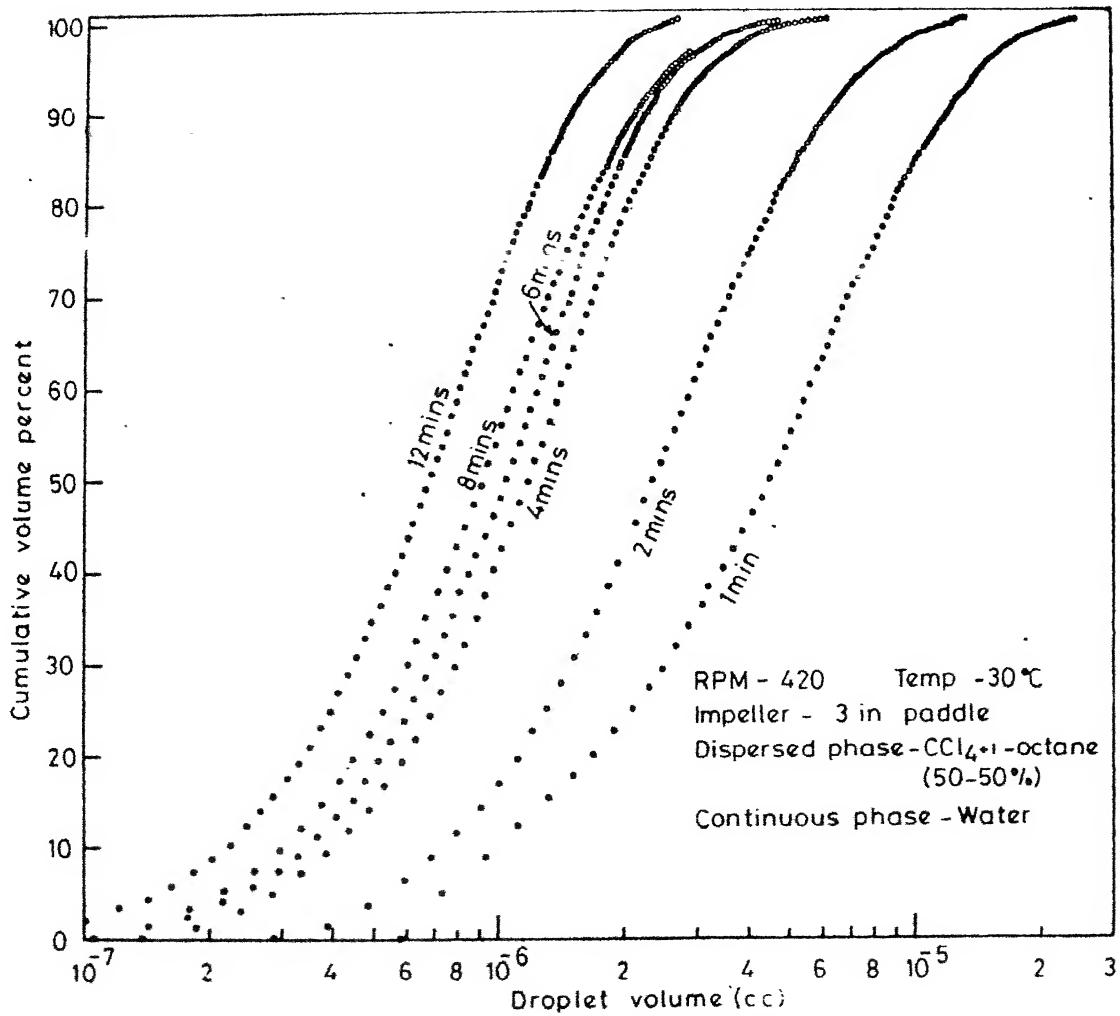

Fig 5.8 Effect of stirring time on drop volume distribution

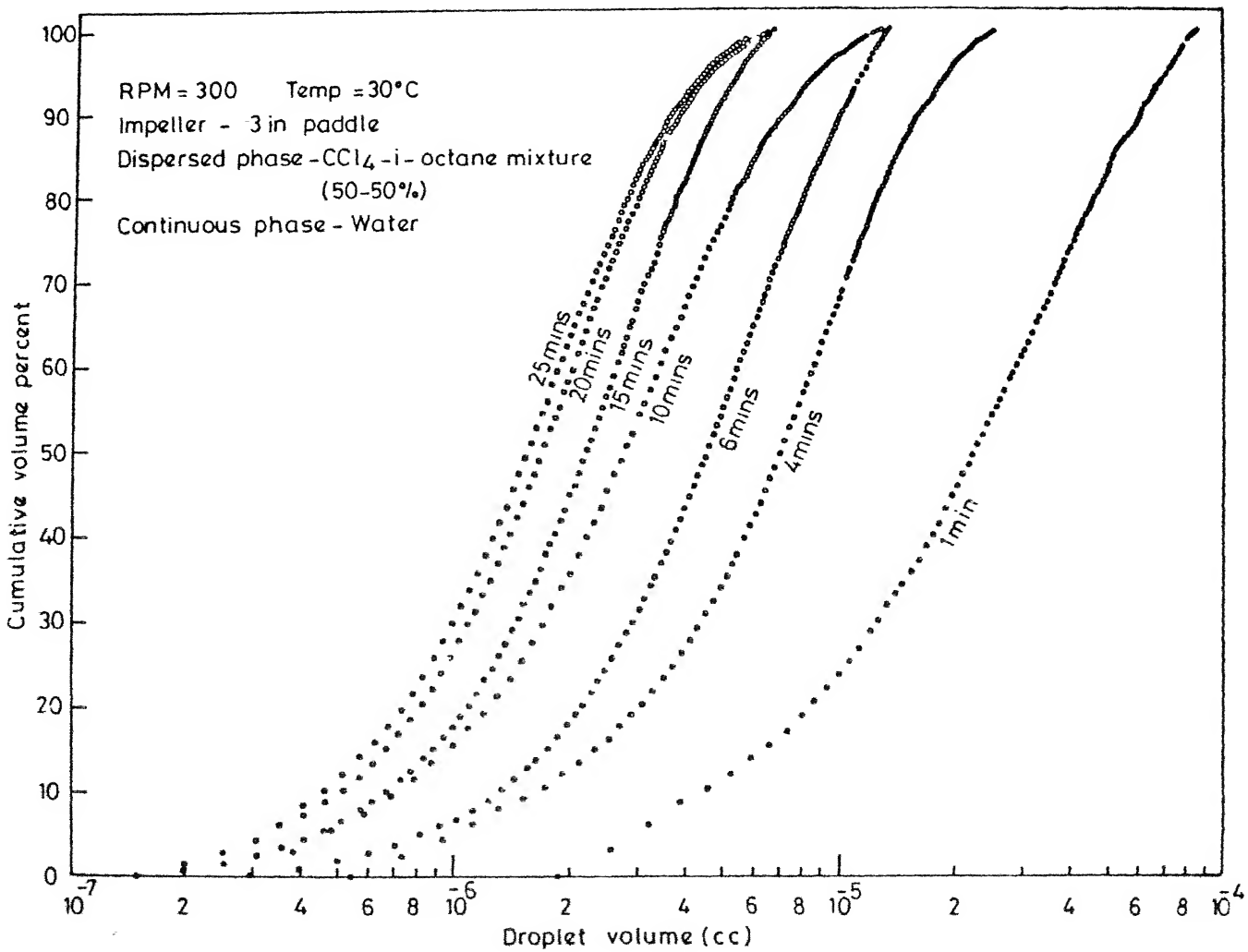

Fig. 6·7 - Effect of stirring time on drop volume distribution

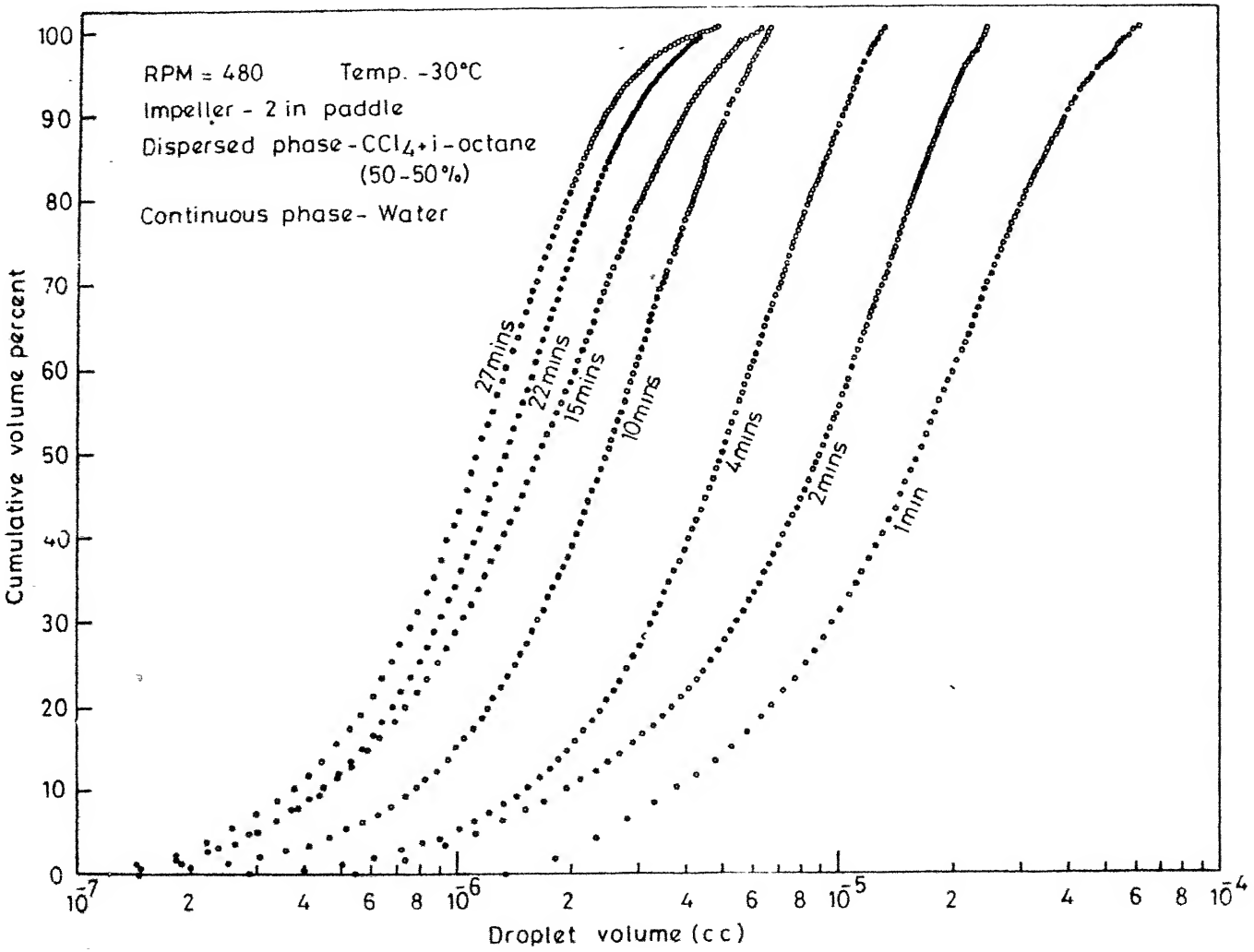

Fig 6-8 - Effect of stirring time on drop volume distribution.

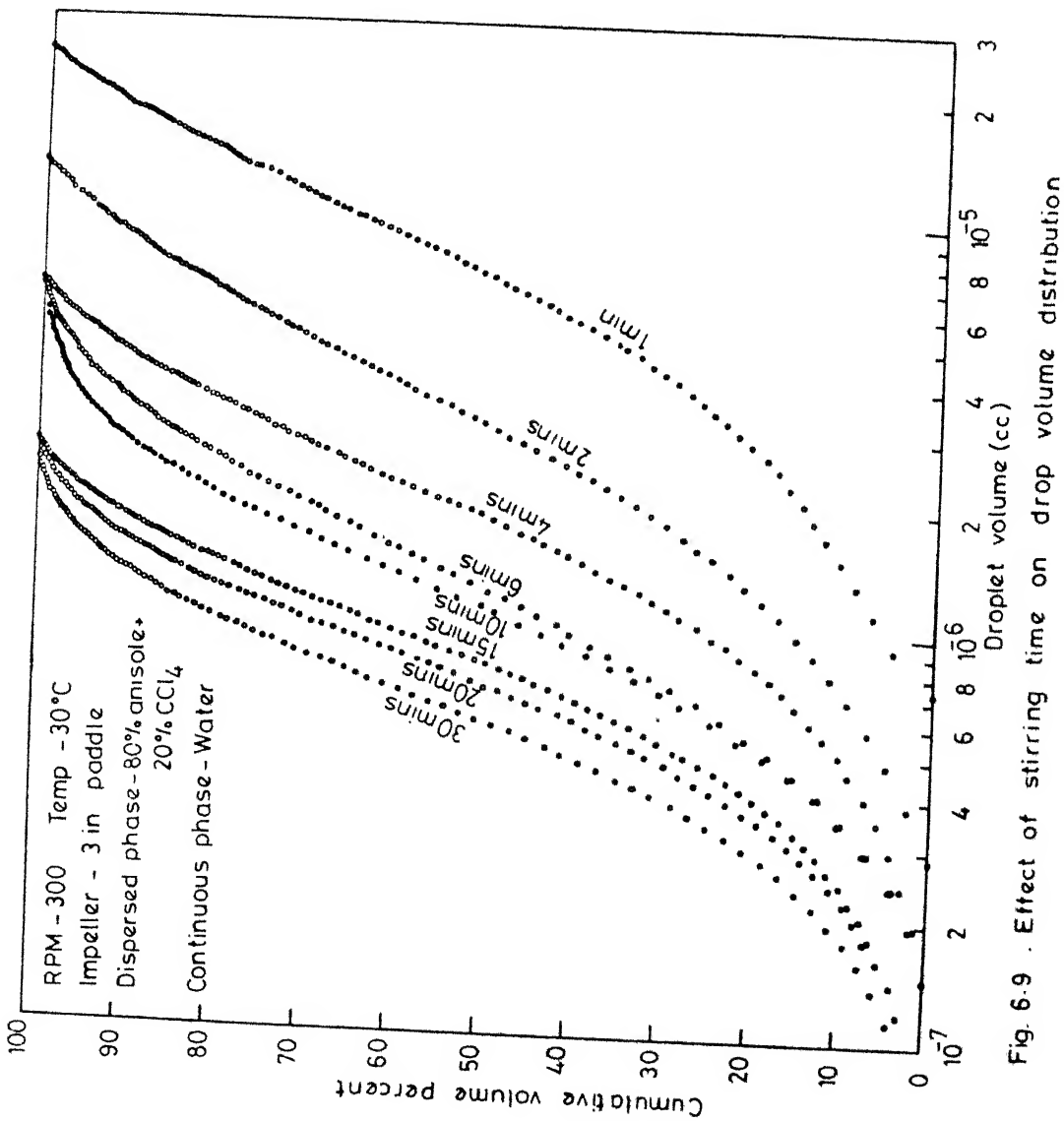

Fig. 6.9 . Effect of stirring time on drop volume distribution

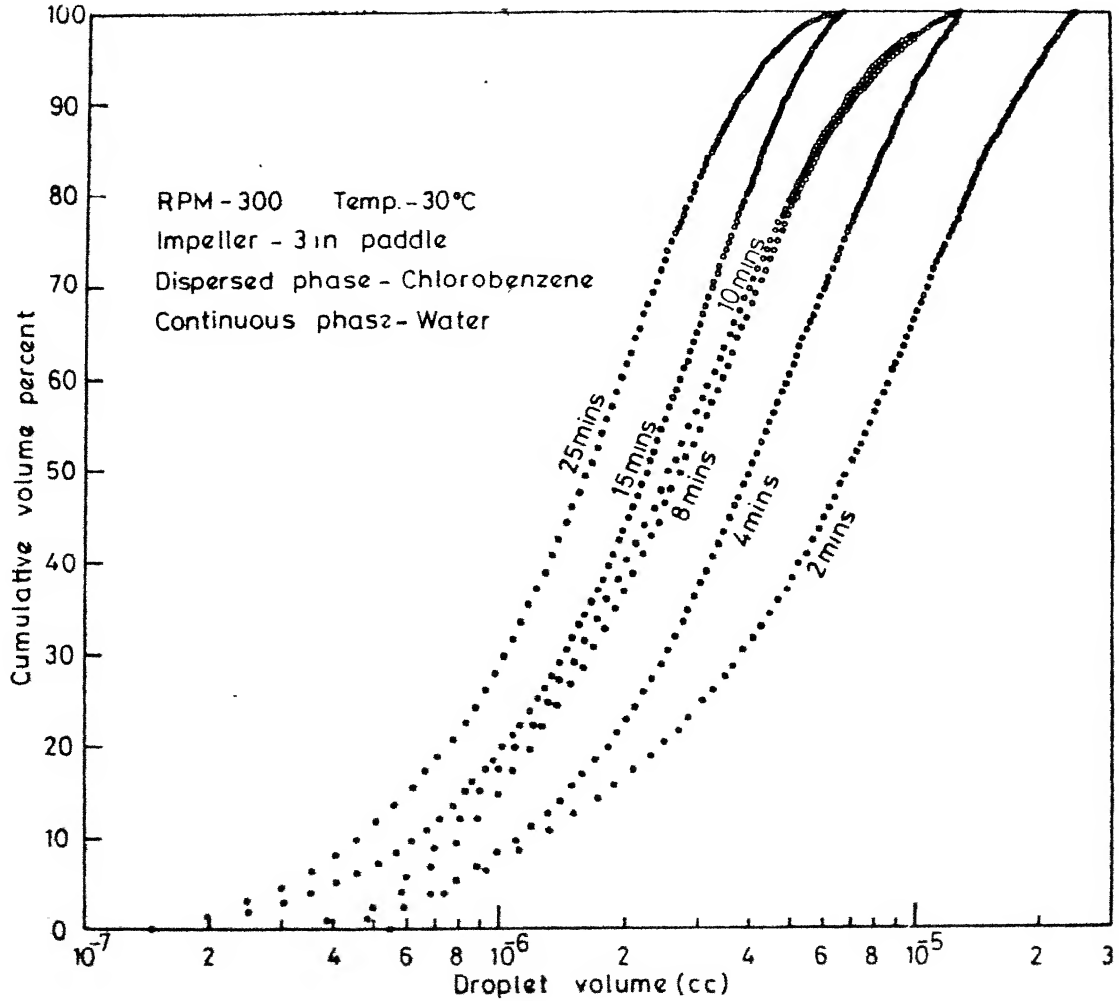

Fig. 6 10 Effect of stirring time on drop volume distribution

effect of stirring time on drop volume distribution for the above measurements.

6.4.1 Verification of 'Power Law' Approximation of Transitional Breakage Probability:

If the 'power law' approximation Kv^n for the transitional breakage probability $\Gamma(v)$ is valid, it should be possible to collapse the drop volume distributions at different times into a single curve under the similarity transformation $v^n t$ for sufficiently large time [4]. Moreover, log-log plots of droplet volume v versus time t for different fixed values of cumulative volume per cents should yield a set of parallel straight lines of slope $-\frac{1}{n}$ [4]. Figures 6.11 through 6.16 show plots of droplet volume v versus time t for different fixed values of cumulative volume per cents. In Figures 6.11 through 6.16, it was found that the data could be represented by two sets of parallel straight lines of different slopes i.e. the transitional breakage probability $\Gamma(v)$ could be approximated by a 'power law' of varying exponents. The sets of data in Figures 6.11 through 6.16 could be divided into two regions of different exponents. The region corresponding to large droplet volumes or small times will be referred to hereafter as region I and the other as region II. Earlier, it was shown from Figure 3.2 that the transitional breakage probability predicted by the model could be approximated by a series of 'power law' models with different exponents for

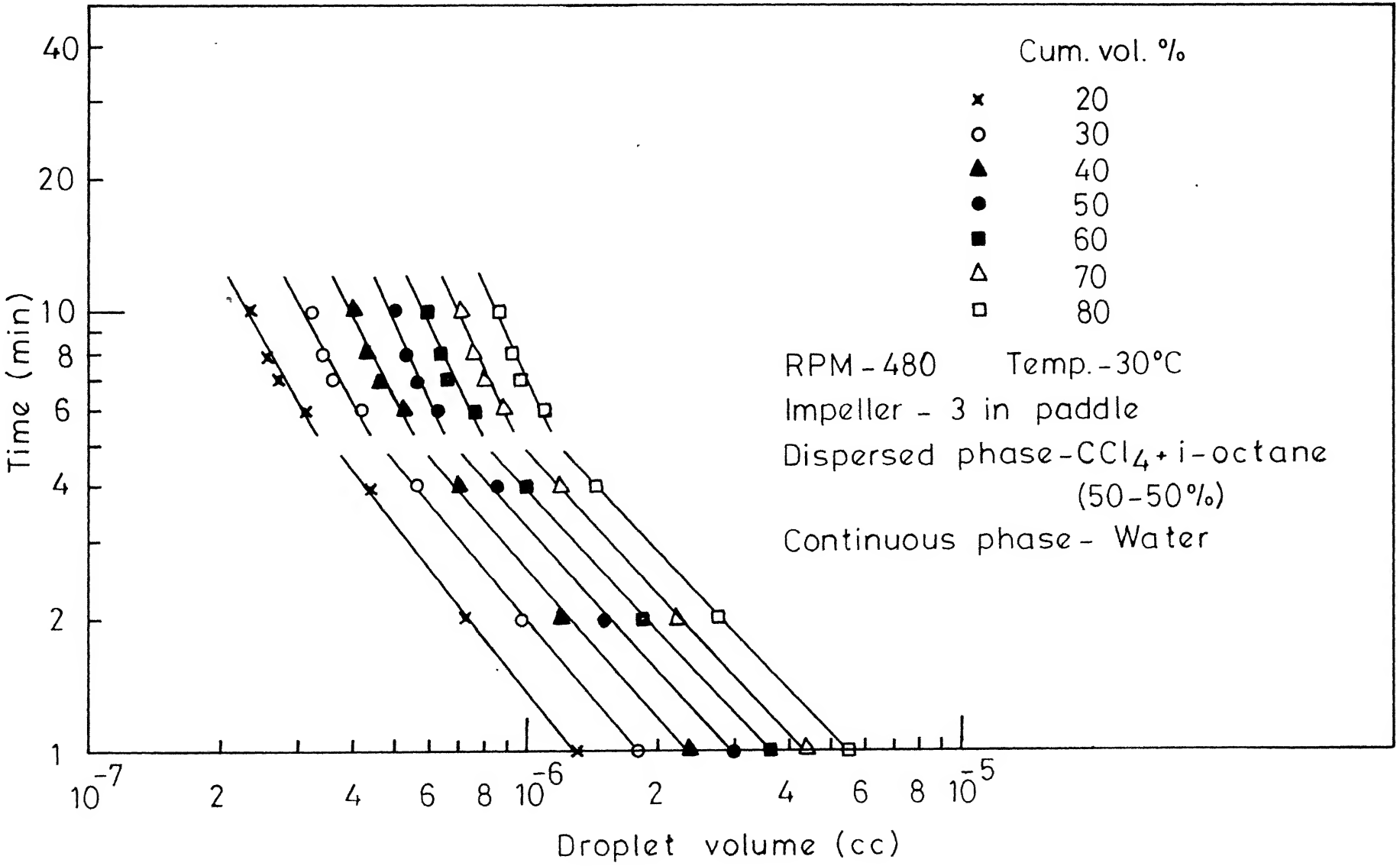

Fig 6·11 : Plot of stirring time vs. droplet volume for a fixed cumulative volume percent.

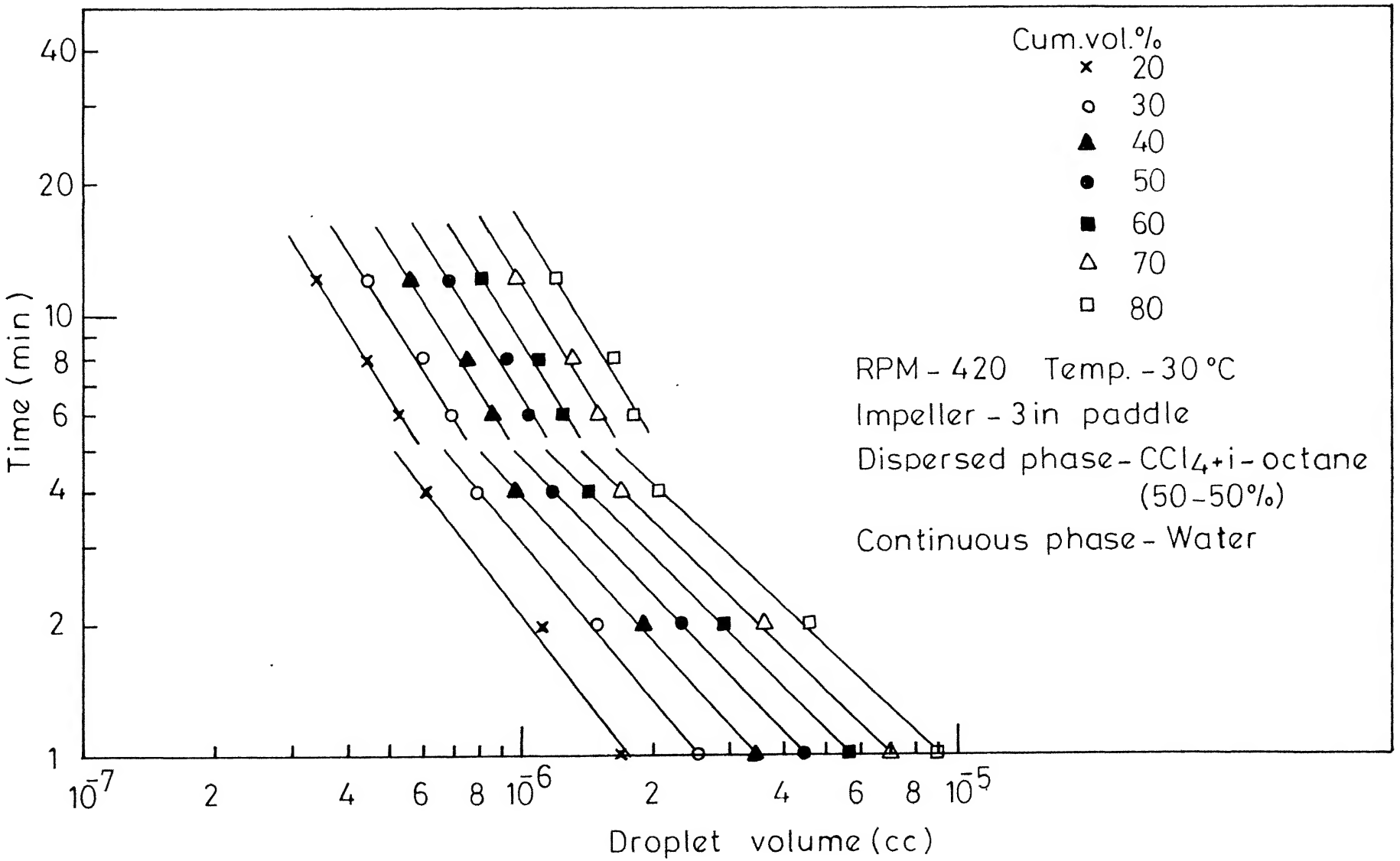

Fig. 6-12 - Plot of stirring time vs. droplet volume for a fixed cumulative volume percent.

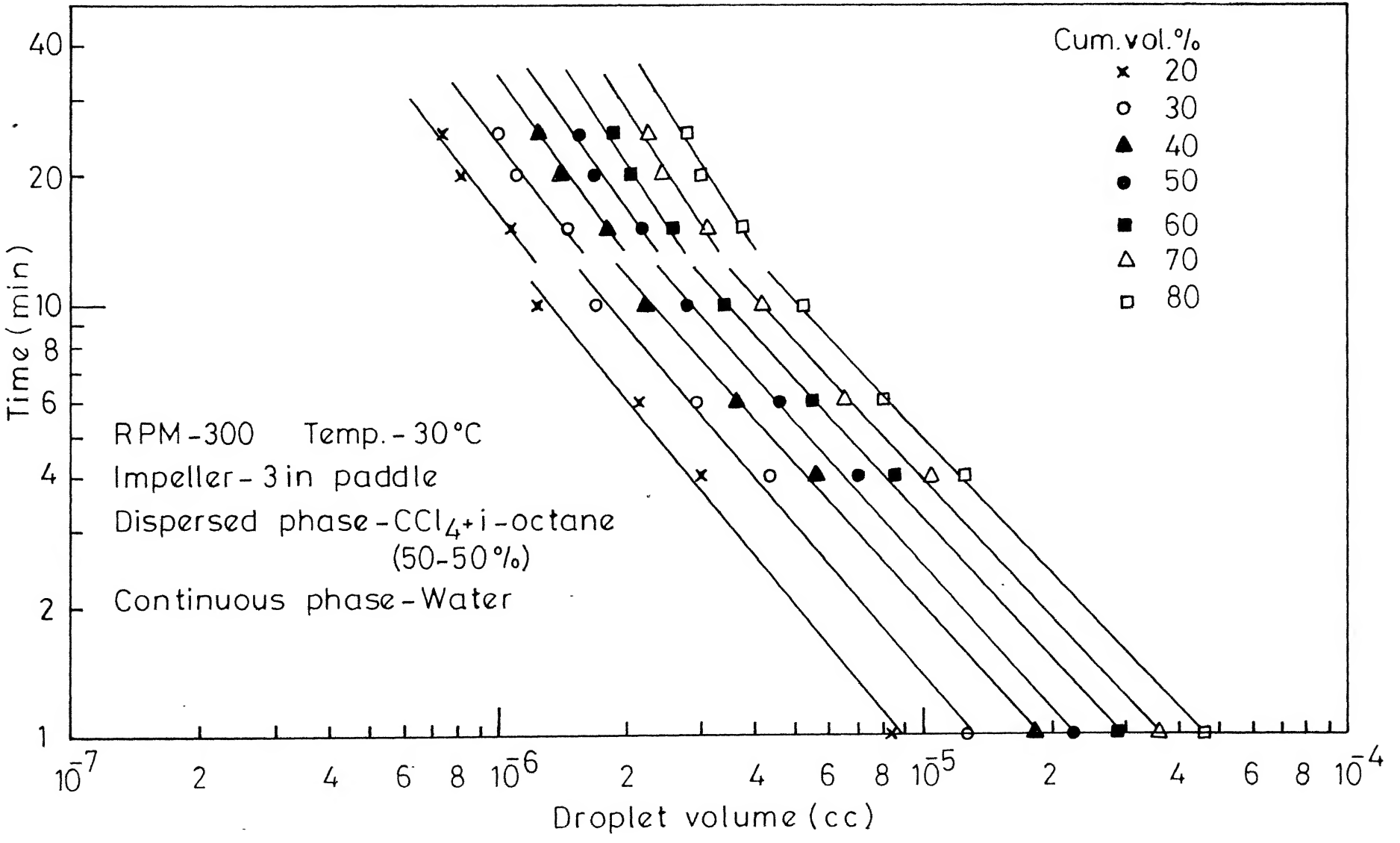

Fig. 6·13 - Plot of stirring time vs. droplet volume for a fixed cumulative volume percent.

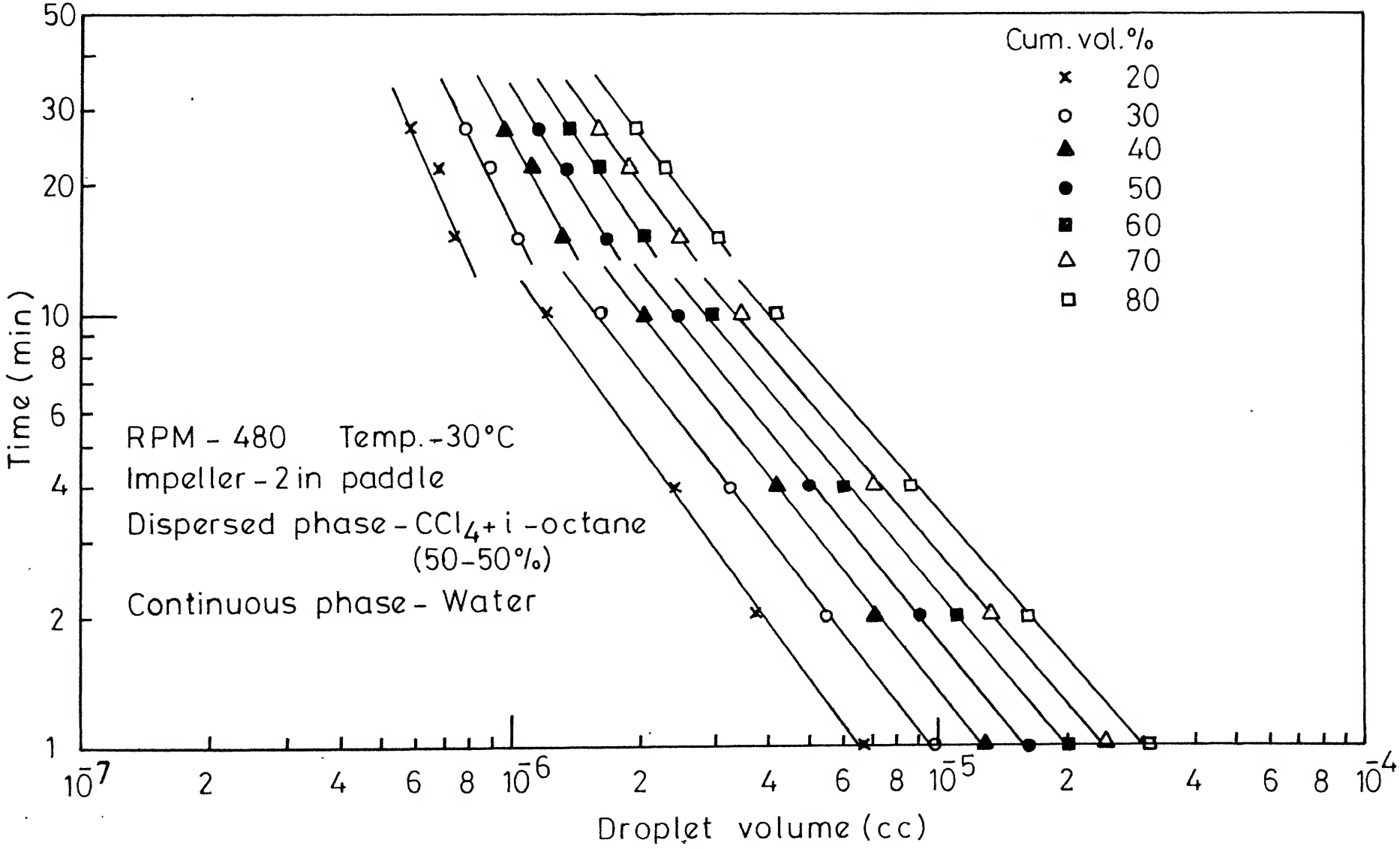

Fig. 6.14 - Plot of stirring time vs. droplet volume for a fixed cumulative volume percent.

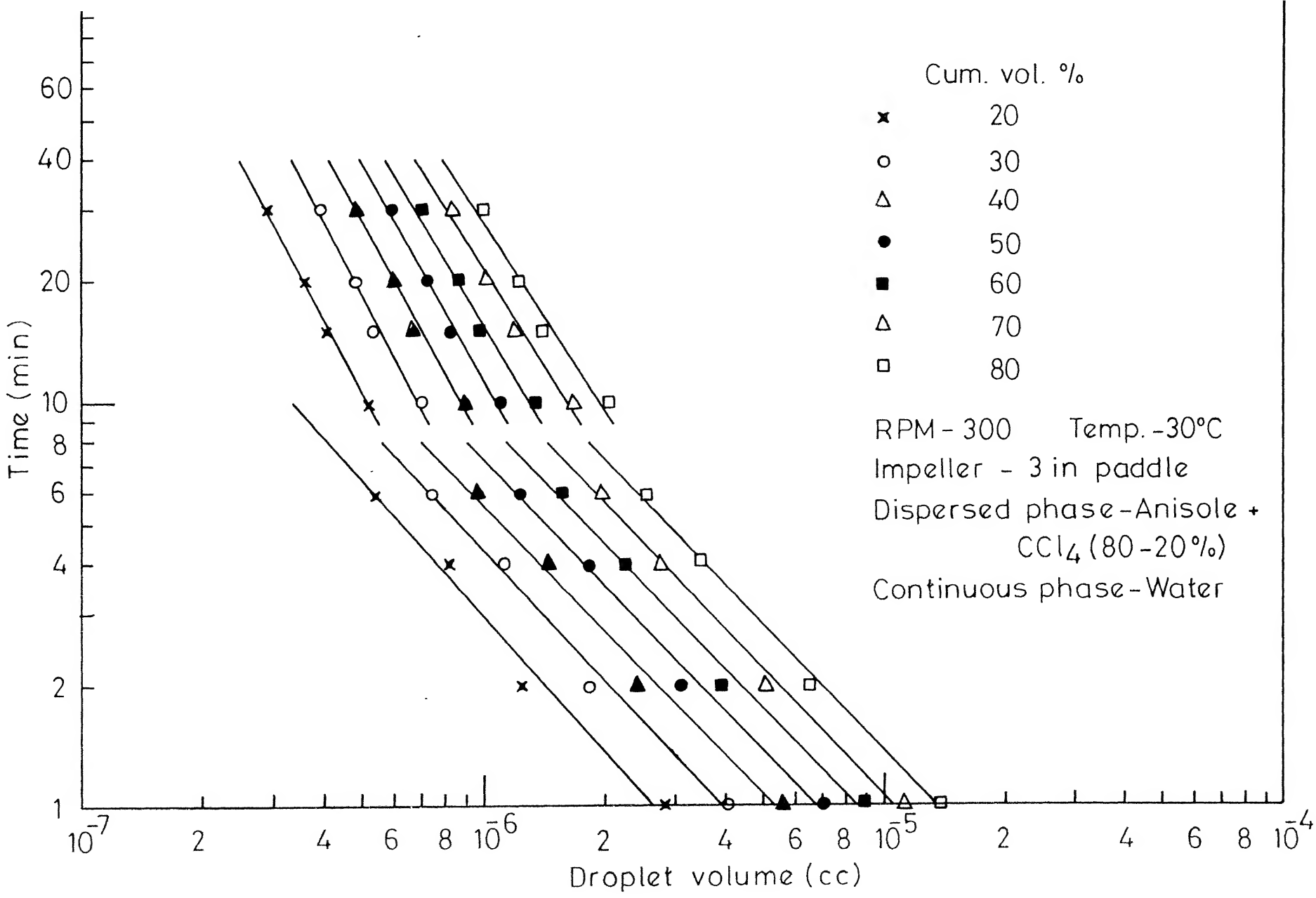

Fig. 6·15: Plot of stirring time vs. droplet volume for a fixed cumulative

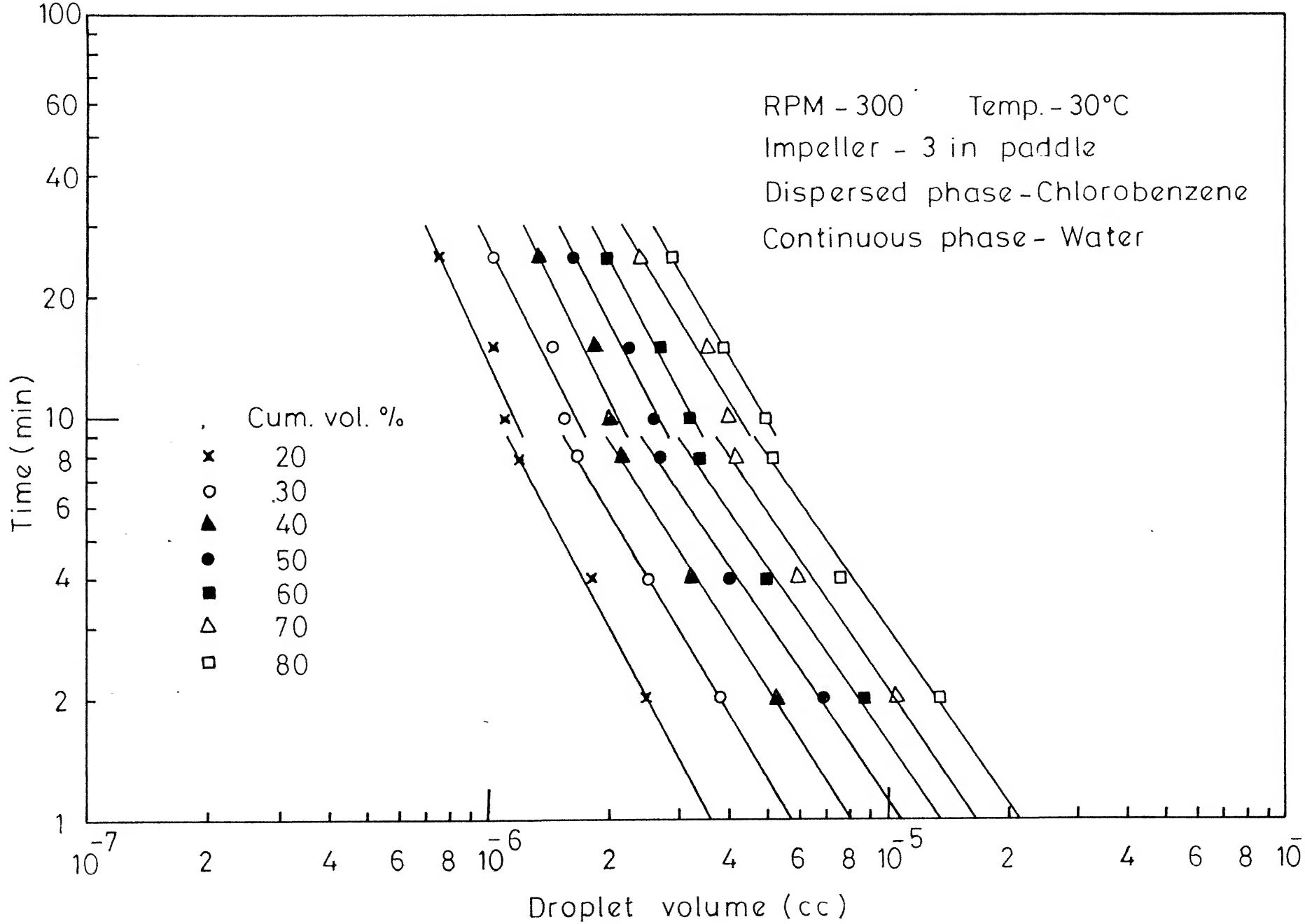

Fig. 6·16 : Plot of stirring time vs. droplet volume for a fixed

different regions of droplet volume with the value of the exponent increasing with the decrease in droplet volume. Figure 3.2 gives the value of the exponents for different regions of droplet volumes. Though all the regions could not be identified in one set of data, in all the cases two distinct regions of different value of the exponent could be detected. Moreover, the value of the exponent n obtained from the slope of the set of parallel straight lines was found to increase at large times, or equivalently, for small droplet volumes. Tables 6.4 through 6.9 present the values of the exponent 'n' obtained through least square fits for different cumulative volume per cents for both the regions. Sets of more or less parallel straight lines were obtained in all the cases especially in the cumulative volume per cent range of 40-70 per cent. However, there is deviation for small and large values of cumulative volume per cents. This could be attributed to the experimental error. All the drop volume distributions should exhibit zero slope at 100 cumulative volume per cent. But, some drop volume distributions do not exhibit zero slope at 100 cumulative volume per cent as can be seen from Figures 6.5 through 6.10. This was due to loss of count of some large voltage pulses corresponding to large volume droplets. With the available combinations of discrete gain and current settings, it was sometimes not possible to choose the required amplification without losing either the

TABLE 6.4: VALUES OF THE 'POWER LAW' EXPONENT FOR DIFFERENT CUMULATIVE VOLUME PER CENTS

RPM - 480 Water-CCl_4+i-Octane (50-50 per cent) Temp.30°C
Impeller: 3 in. paddle

Cum.Vol. Per cent	Exponent 'n'	
	Region I	Region II
20	1.276	1.766
30	1.186	1.783
40	1.006	1.920
50	1.096	2.226
60	1.058	2.048
70	1.066	2.189
80	1.039	2.135

TABLE 6.5: VALUES OF THE 'POWER LAW' EXPONENT FOR DIFFERENT CUMULATIVE VOLUME PER CENTS

RPM 420 Water-CCl_4+i-Octane (50-50 per cent) Temp. 30°C
Impeller.3 in. paddle

Cum.Vol. per cent	Exponent 'n'	
	Region I	Region II
20	1.314	1.577
30	1.191	1.569
40	1.091	1.580
50	1.044	1.559
60	1.004	1.568
70	0.978	1.581
80	0.944	1.592

TABLE 6.6: VALUES OF 'POWER LAW' EXPONENT FOR DIFFERENT CUMULATIVE VOLUME PER CENTS

RPM - 300 Water-CCl_4+i-Octane (50-50 per cent) Temp. 30°C
Impeller - 3 in. paddle

Cum.Vol. per cent	Exponent 'n'	
	Region I	Region II
20	1.213	1.288
30	1.160	1.274
40	1.096	1.362
50	1.107	1.365
60	1.081	1.486
70	1.068	1.483
80	1.050	1.556

TABLE 6.7: VALUES OF 'POWER LAW' EXPONENT FOR DIFFERENT CUMULATIVE VOLUME PER CENTS

RPM - 300 Water-Anisole+CCl_4 (80-20 per cent) Temp. 30°C
Impeller - 3 in. paddle

Cum.Vol. per cent	Exponent 'n'	
	Region I	Region II
20	1.113	1.894
30	1.060	1.888
40	1.039	1.789
50	1.030	1.737
60	1.028	1.667
70	1.036	1.578
80	1.046	1.539

TABLE 6.8: VALUES OF THE 'POWER LAW' EXPONENT FOR DIFFERENT CUMULATIVE VOLUME PER CENTS

RPM 300 Water-Chlorobenzene Temp.: 30°C
Impeller: 3 in. paddle

Cum. Vol. per cent	Exponent 'n' Region I	Region II
20	1.900	2.190
30	1.674	1.946
40	1.551	2.003
50	1.465	1.893
60	1.452	1.877
70	1.455	1.615
80	1.433	1.683

TABLE 6.9: VALUES OF THE 'POWER LAW' EXPONENT FOR DIFFERENT CUMULATIVE VOLUME PER CENTS

Cum. Vol. per cent	Exponent 'n' Region I	Region II
20	1.370	2.267
30	1.285	2.044
40	1.253	1.811
50	1.224	1.588
60	1.199	1.467
70	1.169	1.359
80	1.148	1.332

sensitivity or some pulses of large amplitude.

Excepting for water-chlorobenzene system, the value of the exponent n for region I was around 1.0. For water-chlorobenzene system, the value of n for region I was around 1.5. The value of n for region II for water-CCl_4+i-Octane (50-50 per cent) system at the agitator speed of 480 RPM was around 2.0. For water-chlorobenzene and water-Anisole + CC (80-20 per cent) systems at the agitator speed of 300 RPM the value of n for region II was around 1.8. In all the other cases, the value of n for region II was around 1.5. Hence, three distinct regions of exponents 1.0, 1.5 and 2.0 could be identified. The intermediate value of 1.8 obtained for the exponent n in two cases is believed to be due to overlapping of two regions. It would be interesting to note that in case of low energy input i.e. at the agitator speeds of 300 RPM and 420 RPM and at the agitator speed of 480 RPM with two inch diameter paddle impeller, the region with the exponent of 1.5 could be identified. The value of the exponents obtained from the data agree fairly well with the values of 1.08, 1.42, and 2.12 obtained from the approximation of the predicted transitional breakage probability by a series of 'power law' models of varying exponents. The regions with exponent 0.574 and 3.0 could not be identified in any of the experimental data. This is understandable as drop volume distribution

measurements were not made either at very small times or very near equilibrium.

6.4.2 Verification of the Model for Transitional Breakage Probability:

As the transitional breakage probability $\Gamma(v)$ predicte by the model can be approximated by a series of 'power law' models Kv^n with different values of the exponent n for different droplet volume regions and for each of these regions Kv^n, $\bar{t}$ is the similarity transformation [4] which would collaps all the drop volume distributions in that region into a single curve, one would expect that a transformation $\Gamma(v)\cdot t$ would collapse all the drop volume distributions at all times into a single curve irrespective of their regions if the model for the transitional breakage probability is indeed valid. However, the computation of transitional breakage probability as predicted by the model,

$$\Gamma(v) = \lambda \operatorname{erfc} \left[\left\{ 2(2^{1/3}-1)\, \pi^{1/3}\, 6^{2/3}\, \frac{\sigma}{\rho} \right\}^{1/2} \left(\frac{\pi}{6}\right)^{1/9} v^{-5/18}/2\, \bar{\varepsilon}^{\,1/3} \right]$$

yielded a very large value of the maximum stable drop volume v_s. In other words, for most of the drop volume range encountered in the experiments, the computed transitional breakage probability turned out to be zero. For the computation of transitional breakage probability, power input per unit mass $\bar{\varepsilon}$ was calculated from the empirical relation,

$$\bar{\varepsilon} = 5.1\ N^3 L^2 \qquad (6.4.1)$$

based on the experimental correlation [15, 16] for 2 blade paddle impeller $\bar{\varepsilon} = 1.7\ N^3 L^2$ under the assumption that the power input is proportional to the number of blades. A factor was therefore introduced into the argument of the complimentary error function in order to match the variation of $\Gamma(v)$ with droplet volume v in the drop volume range encountered with the experimentally observed variation. This had to be done by trial and error. A factor of 0.2 was found to represent the variation of transitional breakage probability $\Gamma(v)$ with droplet volume v satisfactorily.

From the observations of Cutter [18], we find that about 20 per cent of the energy is dissipated in the impeller itself, about 50 per cent in the impeller stream, about 30 per cent in the other parts of the stirred vessel. Measurements of $\varepsilon/\bar{\varepsilon}$ in the impeller stream showed an almost exponential variation from 70 near the impeller tip to about 3.5 near the wall. However, Günkel and Weber [24] calculated the energy dissipation rate ε in the impeller stream through energy balance and showed that most of the energy is dissipated in the bulk of the vessel. They also claimed that the observations of Cutter were due to experimental errors. If such important inhomogenities do exist in an agitated vessel as claimed by Cutter [18], it is felt that some statistical

mean ε should be used instead of $\bar{\varepsilon}$ in the probability distribution of relative velocity. Therefore, a statistical mean ε should be used instead of $\bar{\varepsilon}$ in the expression for $\Gamma(v)$. It may be reasonable to use ε averaged over the residence time of the drops in different regions of the stirred vessel i.e. in effect, the mean ε may be the average energy dissipation rate a drop 'experiences' in the stirred vessel. This will depend on the flow pattern in the agitated vessel. If the inhomogenities in the stirred vessel are considerable, one would expect most of the breakage to occur in the impeller stream. In such a case, the dissipation rate per unit mass a droplet 'experiences' will be much larger than $\bar{\varepsilon}$. This may be the reason for the prediction of large maximum stable drop volume v_s from the model for $\Gamma(v)$ using $\bar{\varepsilon}$, thus necessitating the introduction of the factor 0.2. It may also be possible that the energy barrier for breakage of a droplet of volume v, i.e. the minimum increase in the interfacial energy of a droplet of volume v for fragmentation, is much less than the increase in the interfacial energy for binary equal breakage.

Hence, the experimental drop volume distributions were transformed using the transformation $\text{erfc}[\{ 2(2^{1/3}-1)\pi^{1/3}6^{2/3} \frac{\sigma}{\rho} (\frac{\pi}{6})^{1/9} v^{-5/18}/10 \bar{\varepsilon}^{1/3}]\cdot t$. Since the factor 0.2 introduced in the arguement of the complimentary error function was obtained by matching the variation of computed $\Gamma(v)$ with the experimental variation for three inch diameter paddle

impeller and the value of the factor for two inch diameter paddle impeller is believed to be different due to the difference in the flow pattern in the stirred vessel, the transformation was performed only for the experimental drop volume distributions for three inch diameter paddle impeller. Figure 6.17 shows the plot of transformed drop volume distributions. Most of the transformed drop volume distributions seem to fall on a single curve though there is considerable scatter especially in case of drop volume distributions at the agitator speed of 300 RPM.

The transients of the drop volume distribution were found to agree fairly well with the 'power law' model for transitional breakage probability with varying exponents. The values of the exponents 1.0, 1.5 and 2.0 obtained for the three regions identified experimentally also agree fairly well with the values of 1.08, 1.42 and 2.12 obtained from the approximation of the predicted transitional breakage probability by a series of 'power law' models. The transformation

$$\text{erfc}\left[\left\{2(2^{1/3}-1)\,\pi^{1/3}6^{2/3}\,\frac{\sigma}{\rho}\right\}^{1/2}\left(\frac{\pi}{6}\right)^{1/9}\nu^{-5/18}/10\;\bar{\varepsilon}^{\,1/3}\right]\cdot t$$

seems to collapse all the drop volume distributions into a single curve. These findings validate the model for transitional breakage probability.

LEGENDS FOR FIGURE 6.17

CONTINUOUS PHASE - WATER TEMP - 30°C

SYMBOL	RPM	REGION	IMPELLER	DISPERSED PHASE
○	480	I	3 IN.PADDLE	CCl_4+i-OCTANE (50-50 PER CENT)
●	480	II	3 IN.PADDLE	CCl_4+i-OCTANE (50-50 PER CENT)
△	420	I	3 IN.PADDLE	CCl_4+i-OCTANE (50-50 PER CENT)
▲	420	II	3 IN.PADDLE	CCl_4+i-OCTANE (50-50 PER CENT)
▽	300	I	3 IN.PADDLE	CCl_4+i-OCTANE (50-50 PER CENT)
▼	300	II	3 IN.PADDLE	CCl_4+i-OCTANE (50-50 PER CENT)
□	300	I	3 IN.PADDLE	ANISOLE+CCl_4 (80-20 PER CENT)
▩	300	II	3 IN.PADDLE	ANISOLE+CCl_4 (80-20 PER CENT)
×	300	I	3 IN.PADDLE	CHLOROBENZENE
⊗	300	II	3 IN.PADDLE	CHLOROBENZENE

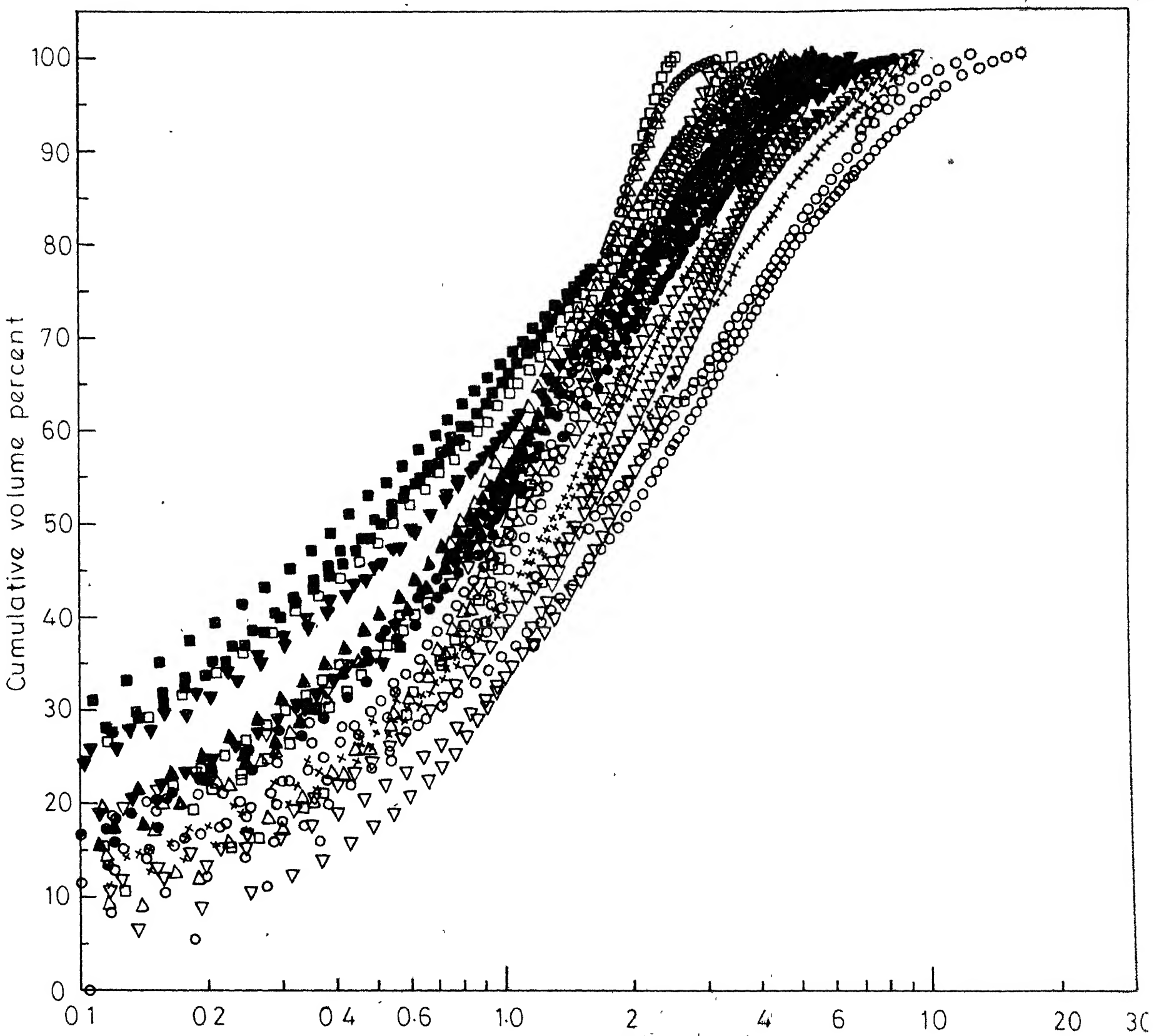

Fig 6 17 - Plot of cumulative volume percent versus

$$\text{Erfc}\left\{\left(\frac{2(2^{1/3}-1)(\pi)^{1/3}6^{2/3}\sigma}{\rho}\right)^{1/2}\left(\frac{\pi}{6}\right)^{1/9}v^{-5/18}/10(\bar{\varepsilon})^{1/3}\right\}t.$$

6.4.3 Estimation of Daughter Droplet Distribution:

The drop volume distributions in a region were transformed using a modified similarity transformation $(\frac{v}{\bar{v}})\cdot t^{1/n}$, $\bar{v}$ and n being an average droplet volume and the exponent of 'power law' approximation of $\Gamma(v)$ for that region respectively Figures 6.18 through 6.29 show the plot of the modified drop volume density $f\{(\frac{v}{\bar{v}})\cdot t^{1/n}\}$ versus $(\frac{v}{\bar{v}})\cdot t^{1/n}$ for regions I and II. It can be seen from Figures 6.18 through 6.29 that the modified drop volume densities do collapse into a single curve. There is considerable scatter at very low droplet volumes especially at low energy input. This can be attributed to the experimental errors. The solid curves in Figures 6.18 through 6.29 are the modified drop volume densities obtained through least-square fit of the data using polynomial expansions. The error sum of squares χ^2 for that fit are given in Figures 6.18 through 6.29. χ^2 was found to be much larger for region I indicating more scatter. This was due to more experimental error in the measurement of drop volume distributions at small stirring times.

Since the similarity transformation $(\frac{v}{\bar{v}})\cdot t^{1/n}$ collapses all the drop volume densities in a region into a single curve, the assumption of 'similar breakage' made for the derivation of the similarity transformation [53] seems to be valid. Therefore, the moments γ_r' of the function Kg(x) could be computed from the relation [4].

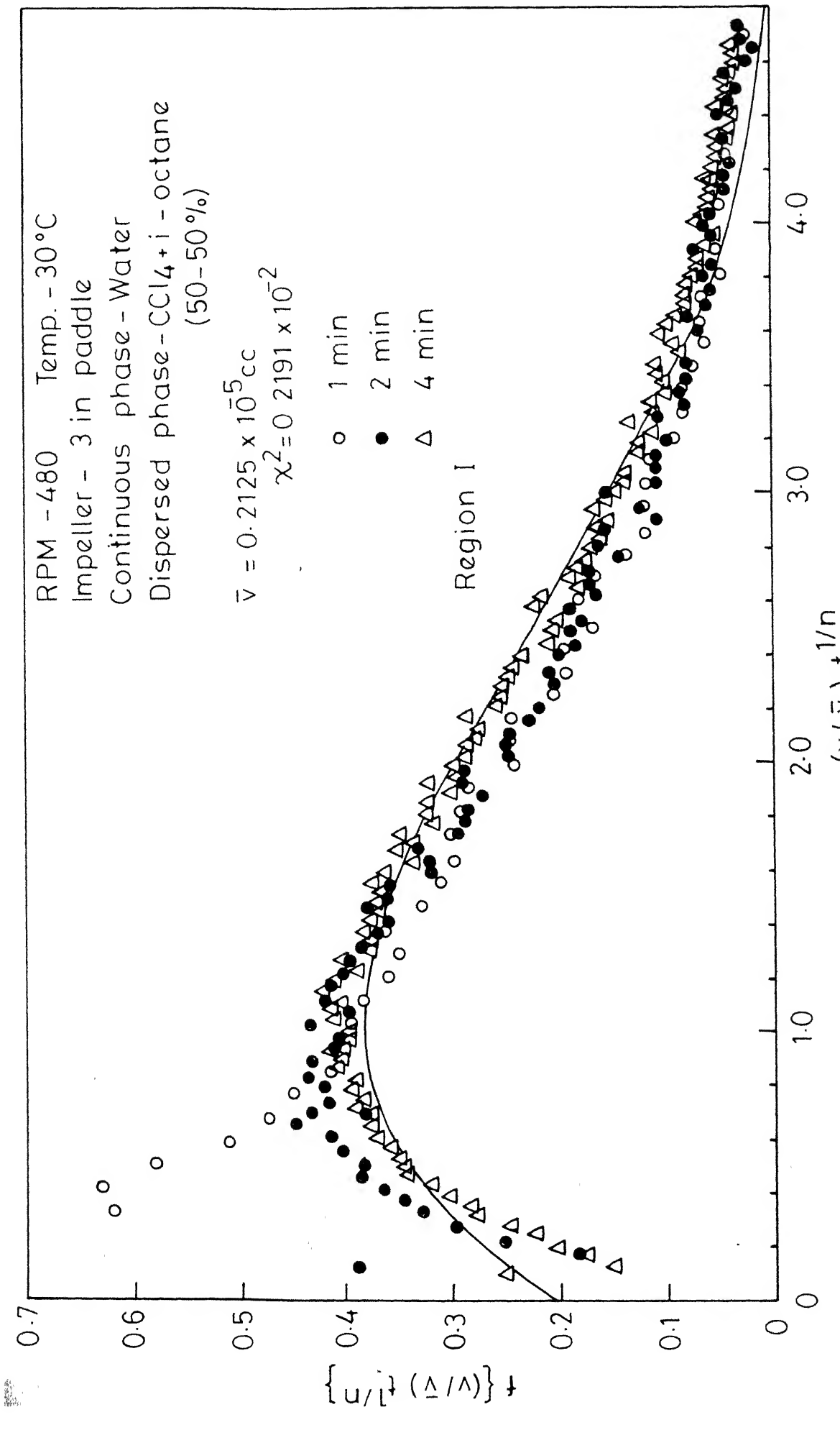

Fig 6.18 - Plot of modified drop volume density $f\{(v/\bar{v})\, t^{1/n}\}$ versus similarity variable $(v/\bar{v})\, t^{1/n}$

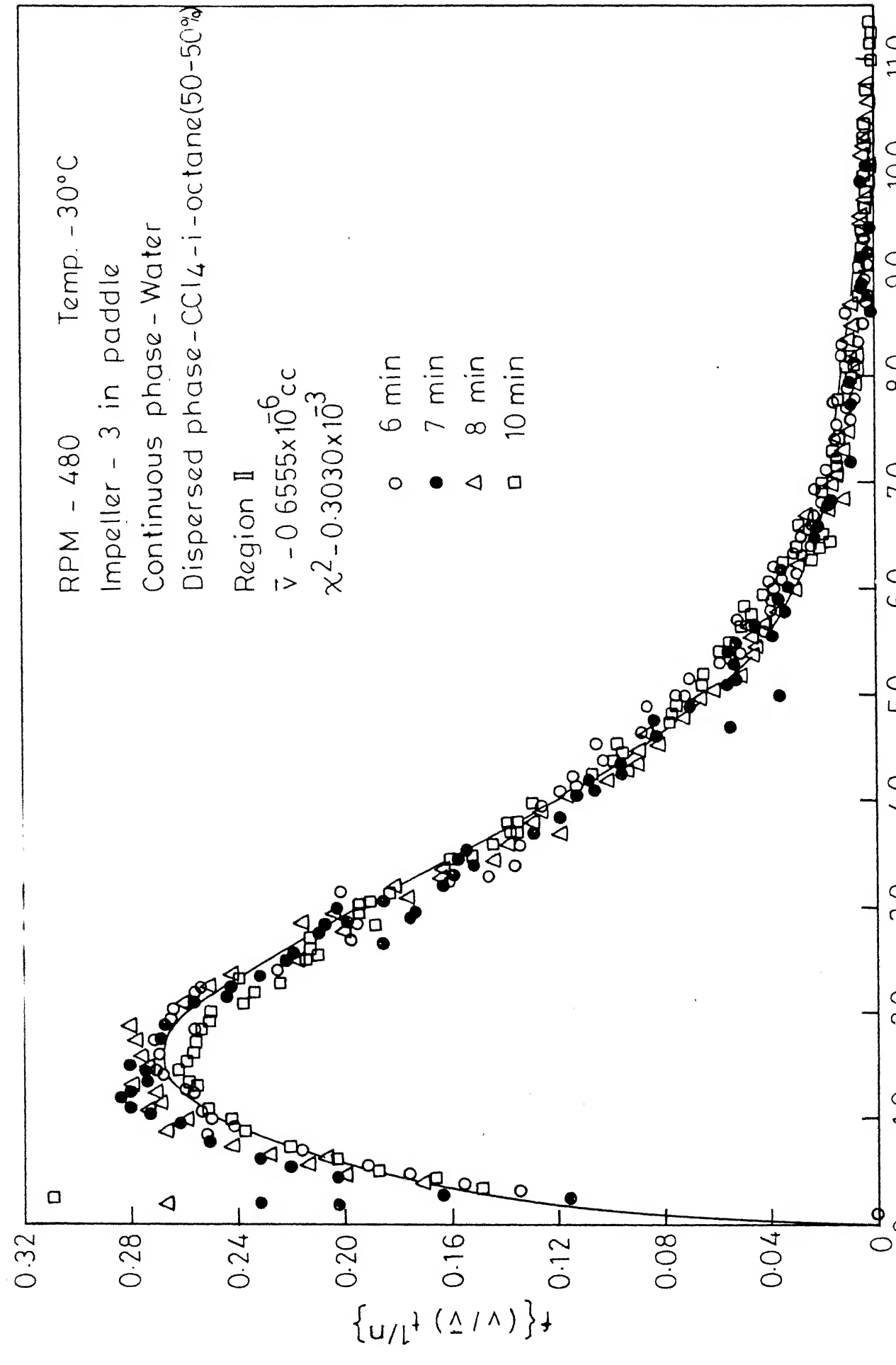

Fig. 6.19 - Plot of modified drop volume density $f\{(v/\bar{v})\, t^{1/n}\}$ versus similarity variable $(v/\bar{v})\, t^{1/n}$

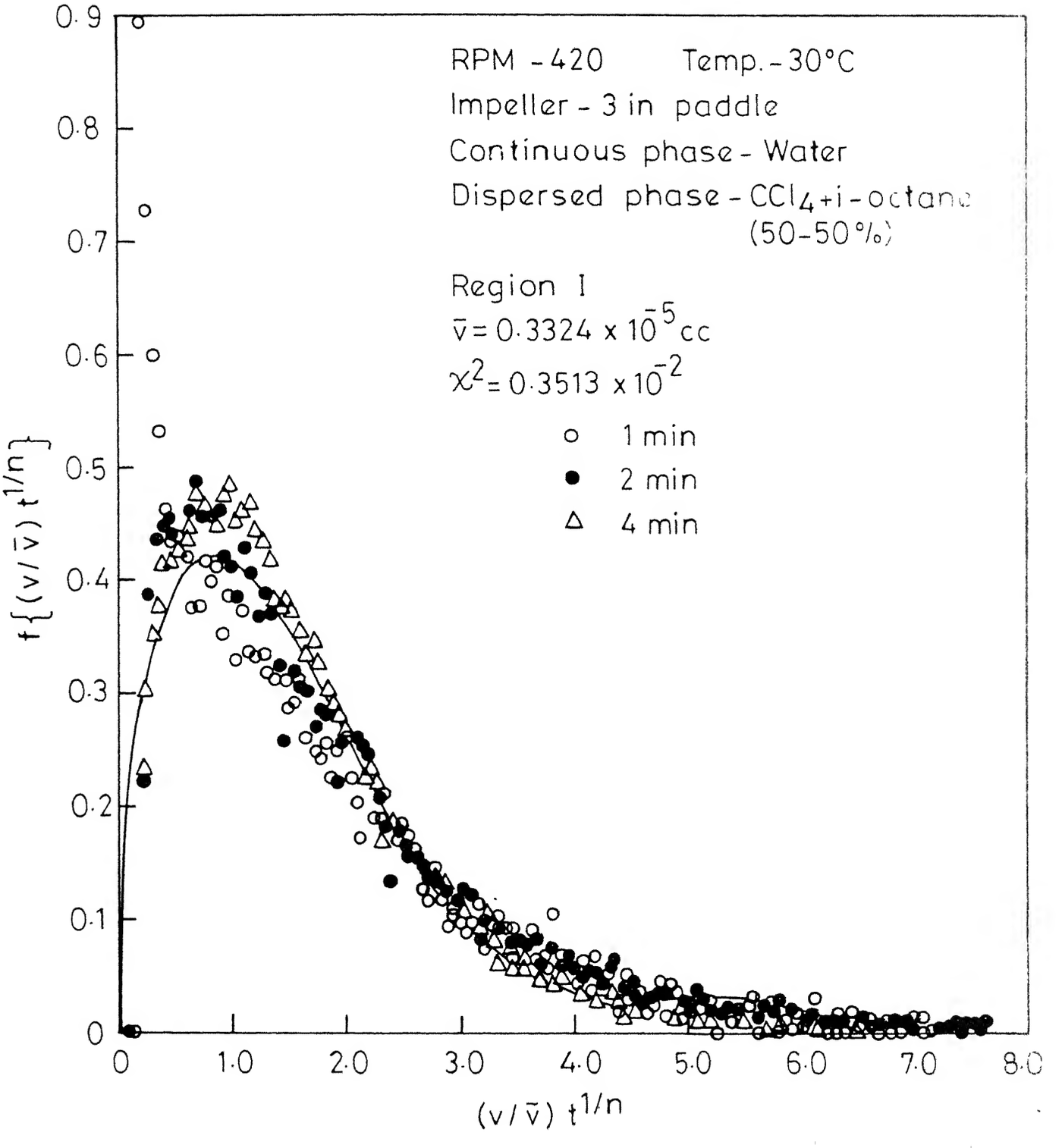

Fig.6-20 - Plot of modified drop volume density $t\{(v/\bar{v})t^{1/n}\}$ versus similarity variable $(v/\bar{v})\,t^{1/n}$

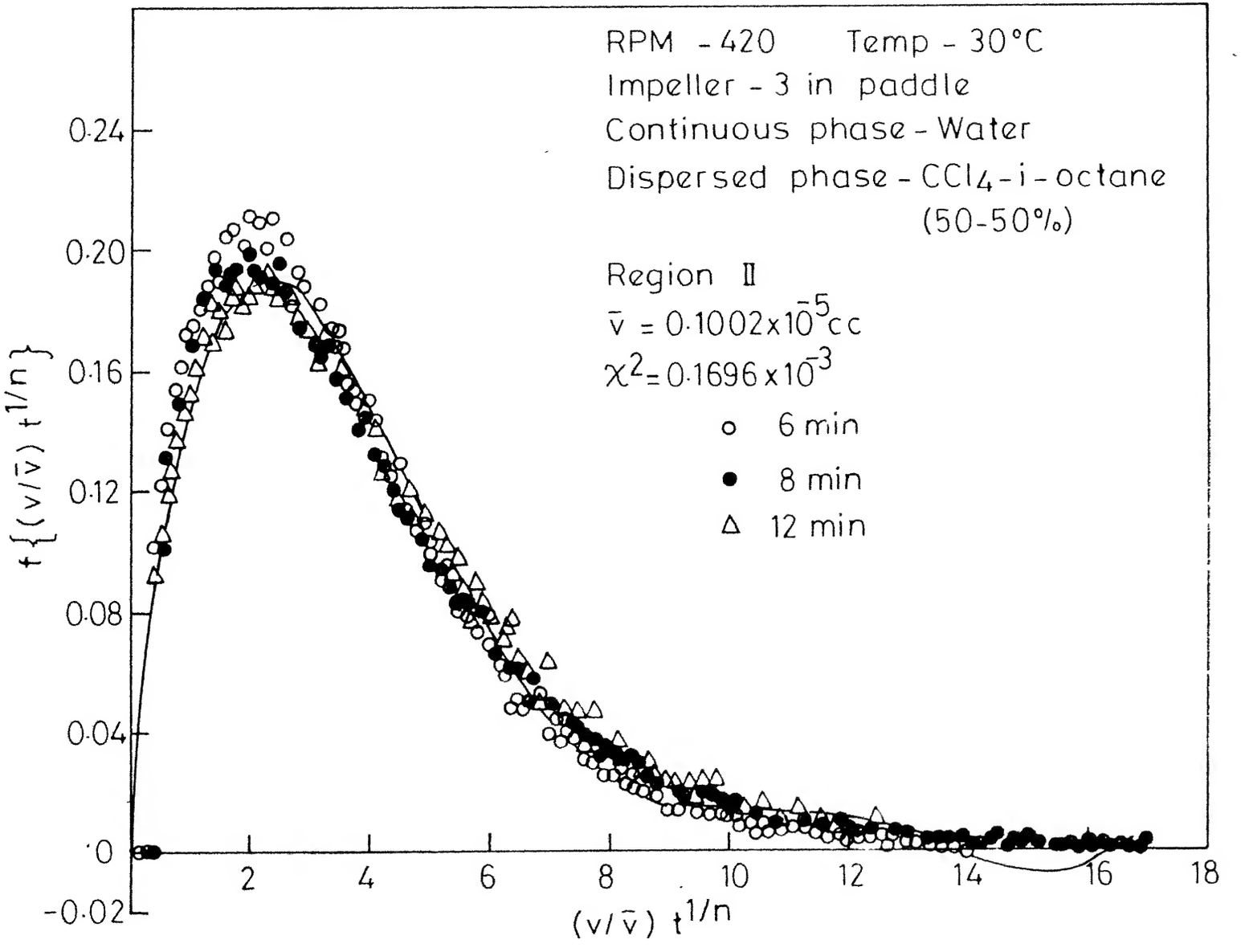

Fig 6·21 - Plot of modified drop volume density $t\{(v/\bar{v})t^{1/n}\}$ vs. similarity variable $(v/\bar{v})\, t^{1/n}$.

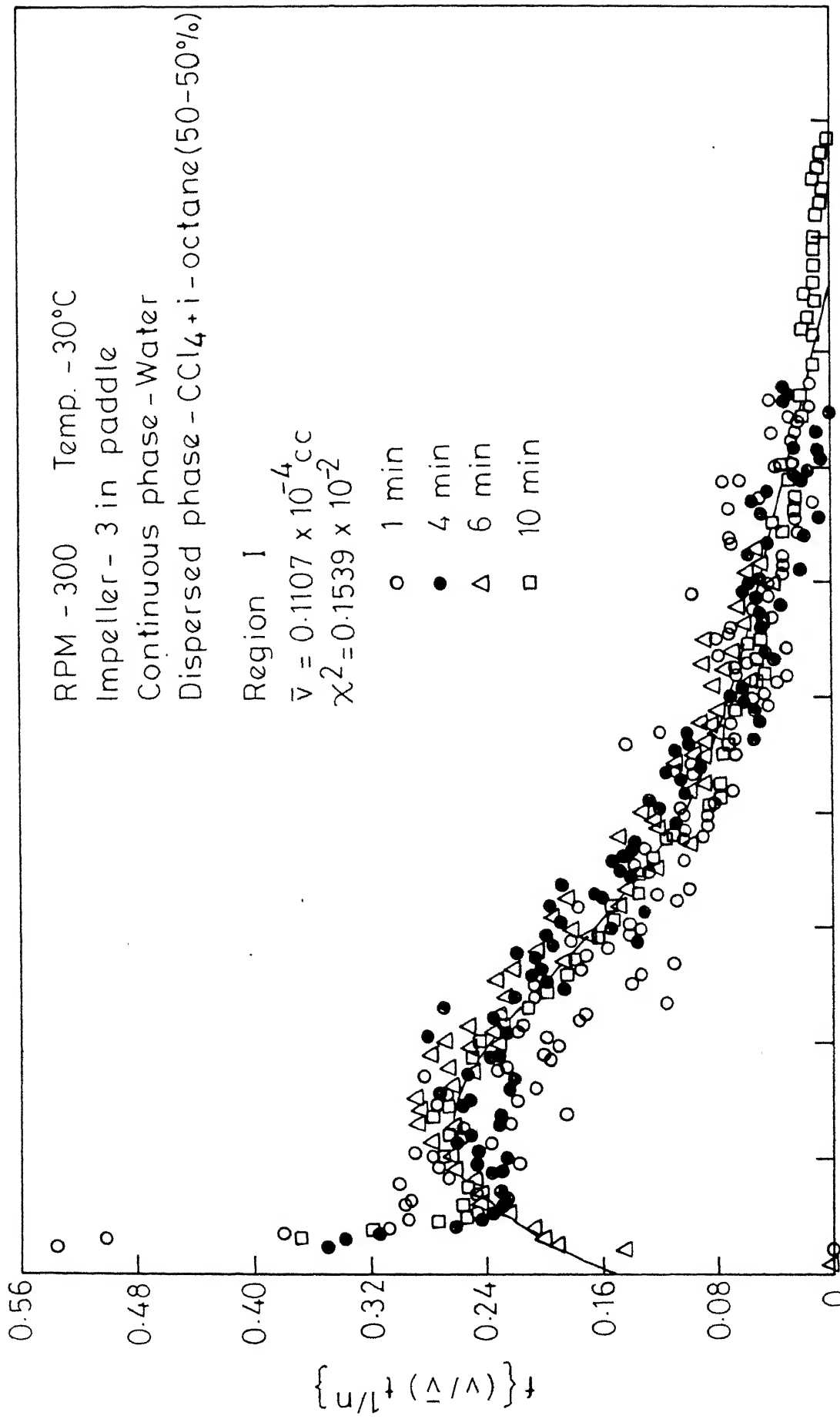

Fig. 6.22 - Plot of modified drop volume density $t\{(v/\bar{v})\,t^{1/n}\}$ versus similarity variable $(v/\bar{v})\,t^{1/n}$

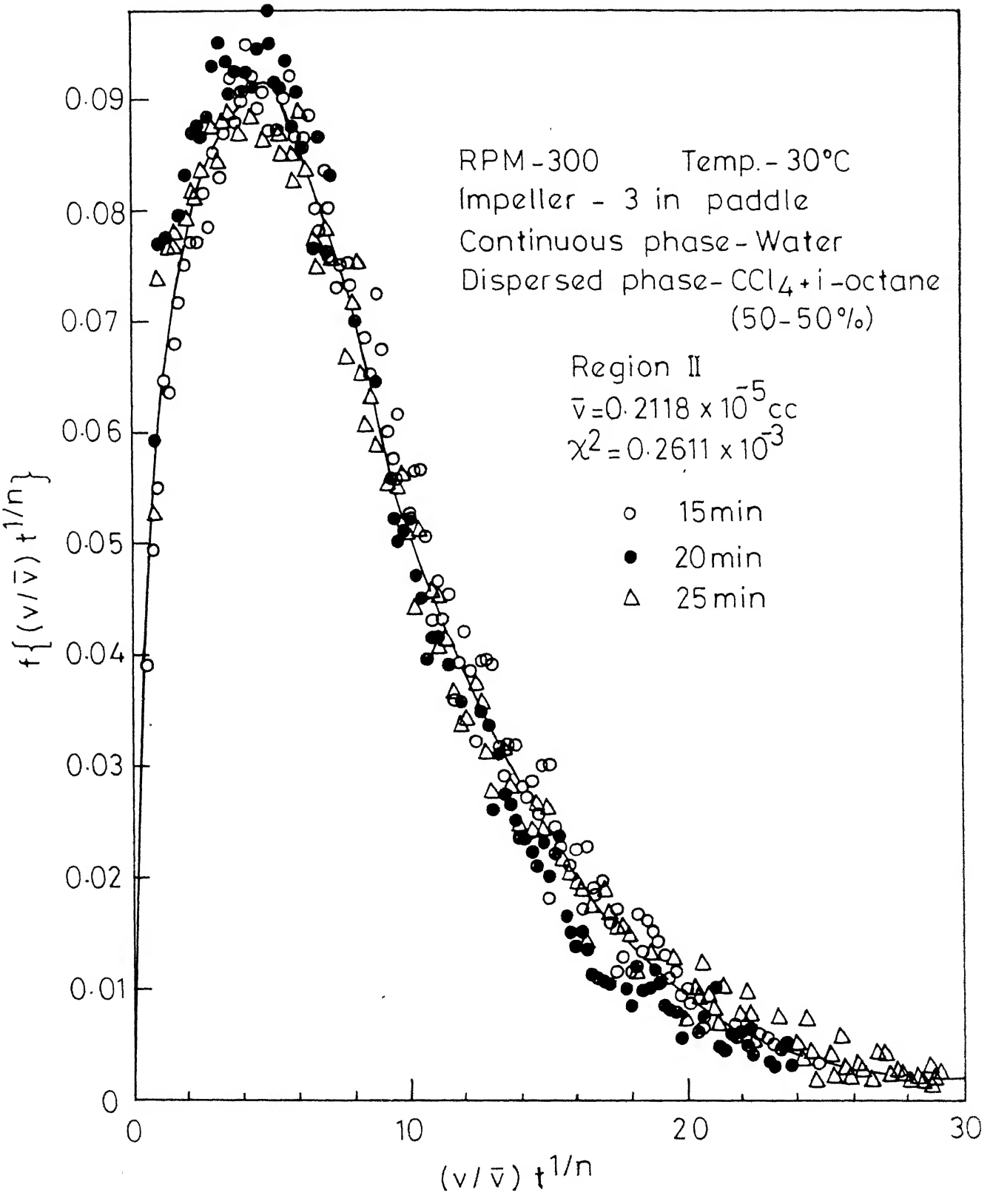

Fig 6.23-Plot of modified drop volume density $t\{(v/\bar{v})t^{1/n}$ versus similarity variable $(v/\bar{v})\,t^{1/n}$.

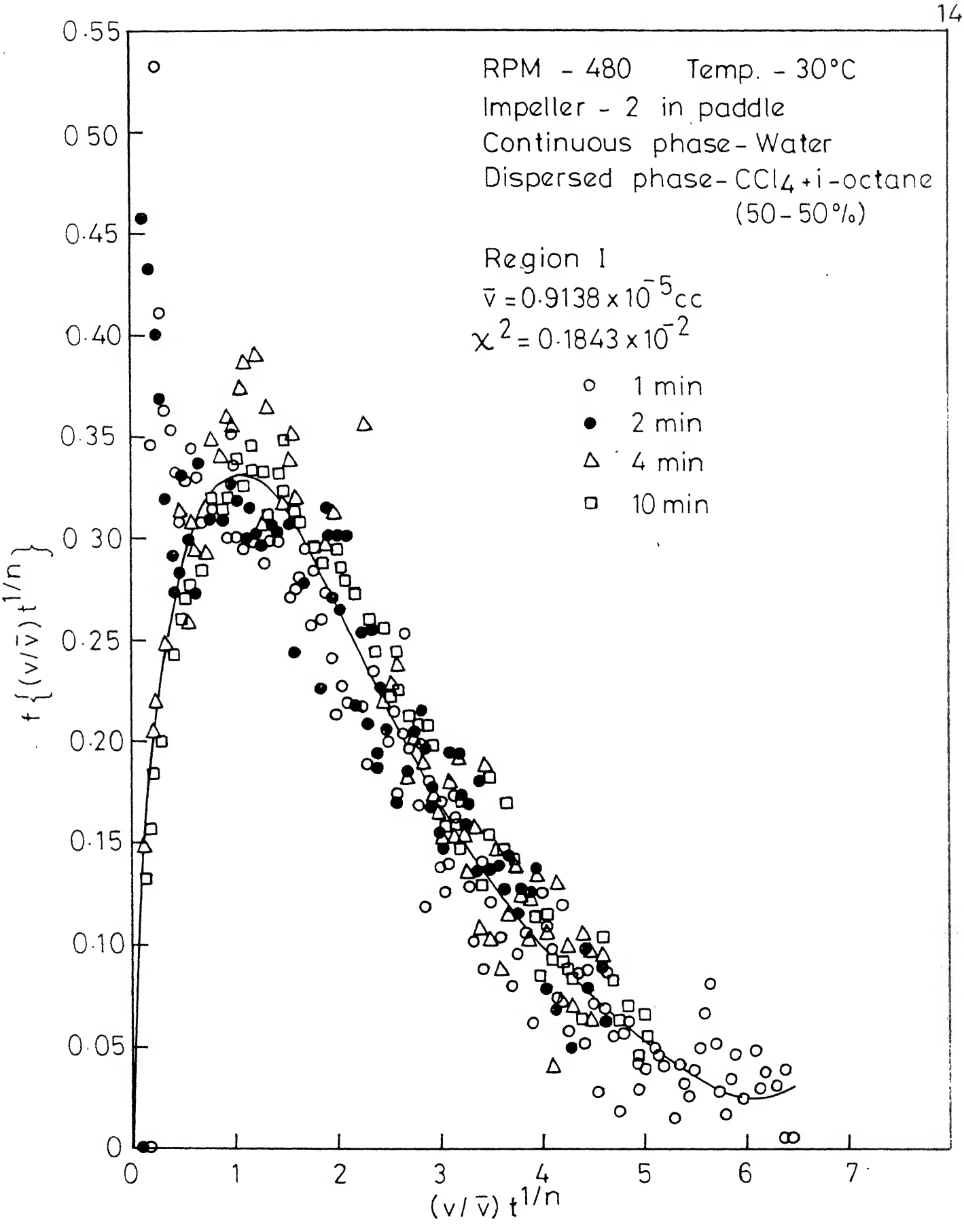

Fig. 6·24 - Plot of modified drop volume density $t\{(v/\bar{v})t^{1/n}\}$ versus similarity variable $(v/\bar{v})t^{1/n}$.

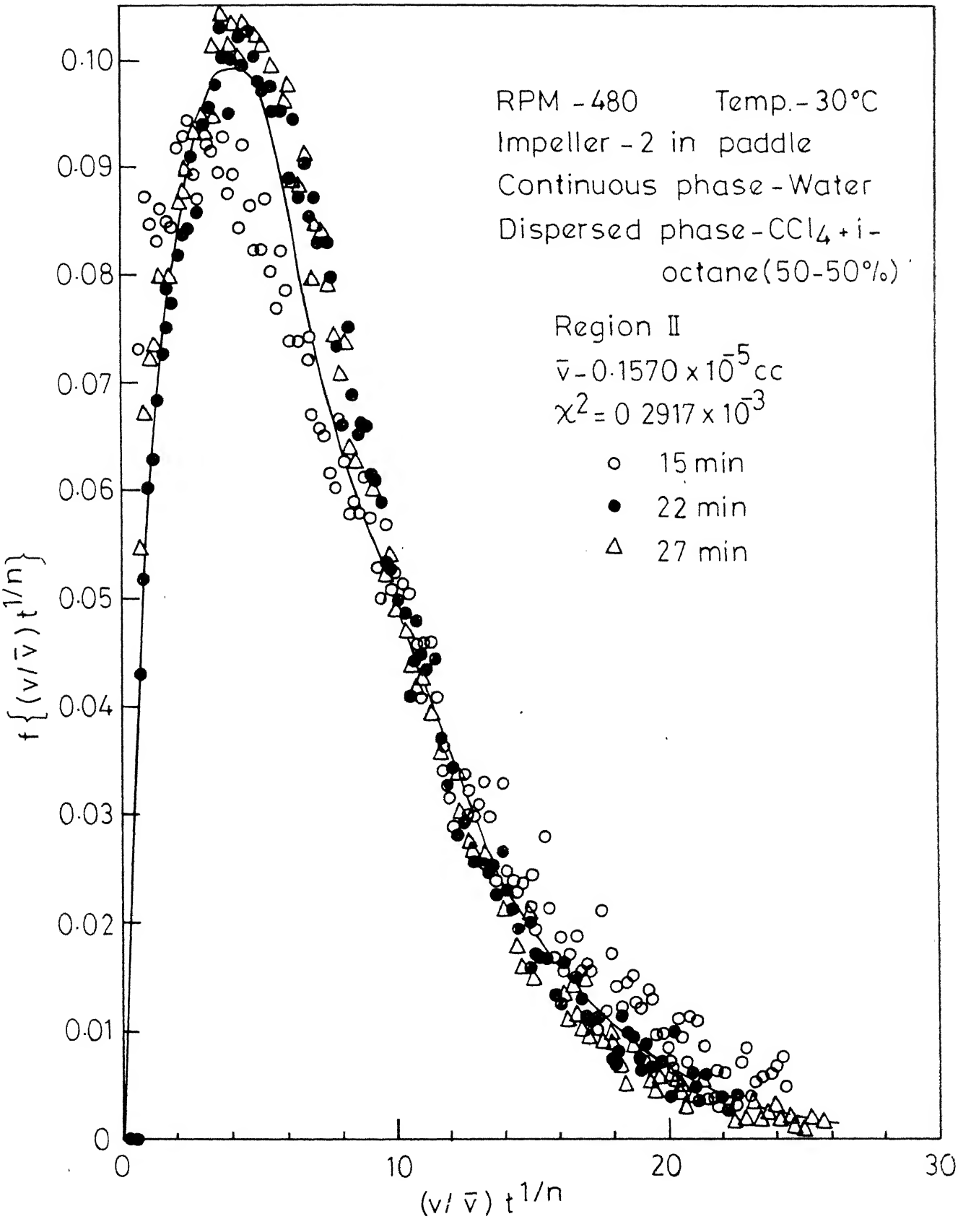

Fig. 6·25 - Plot of modified drop volume density $f\{(v/\bar{v})\, t^{1/n}\}$ versus similarity variable $(v/\bar{v})\, t^{1/n}$.

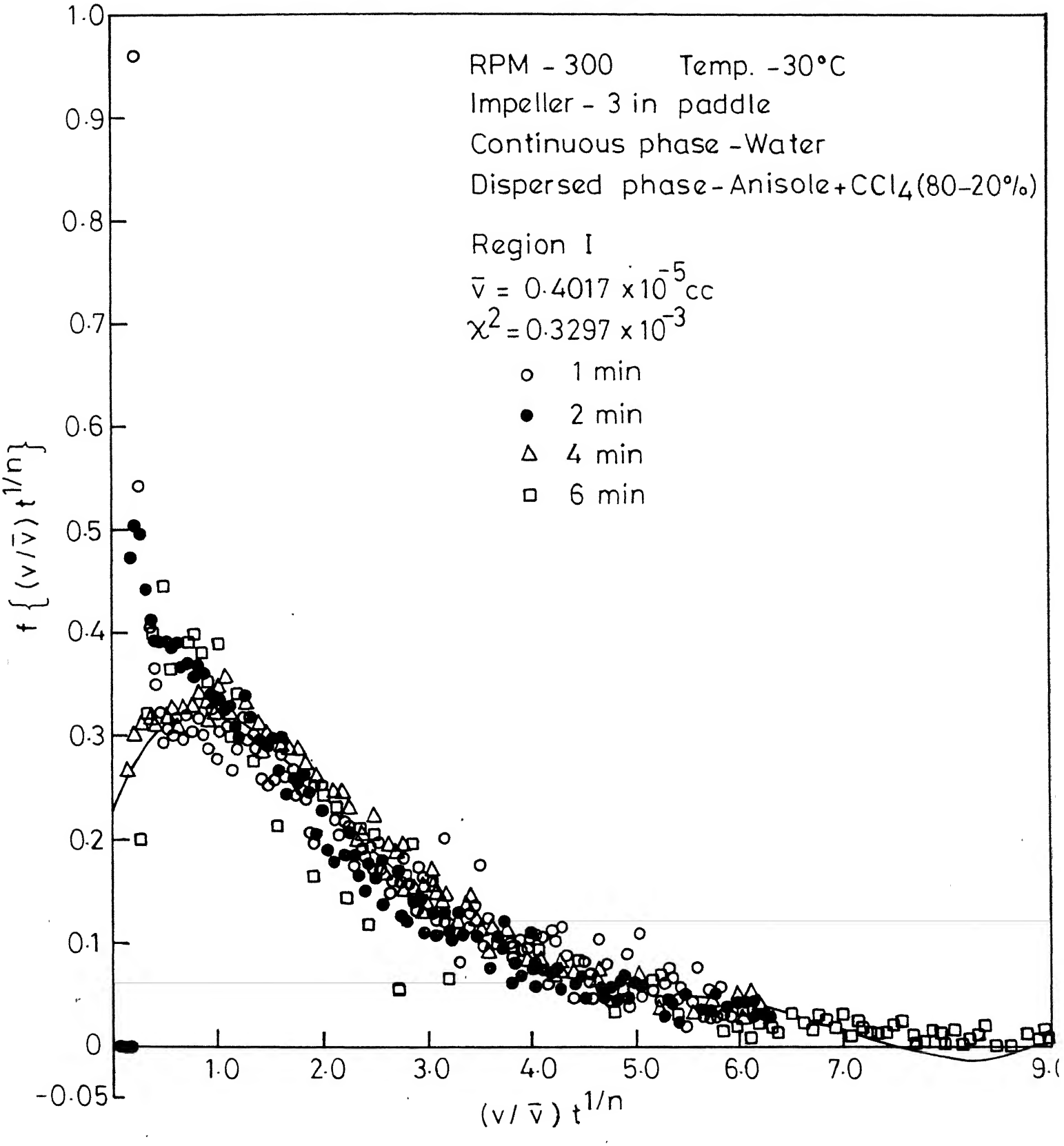

Fig. 6.26 - Plot of modified drop volume density $f\{(v/\bar{v})\, t^{1/n}\}$ versus similarity variable $(v/\bar{v})\, t^{1/n}$.

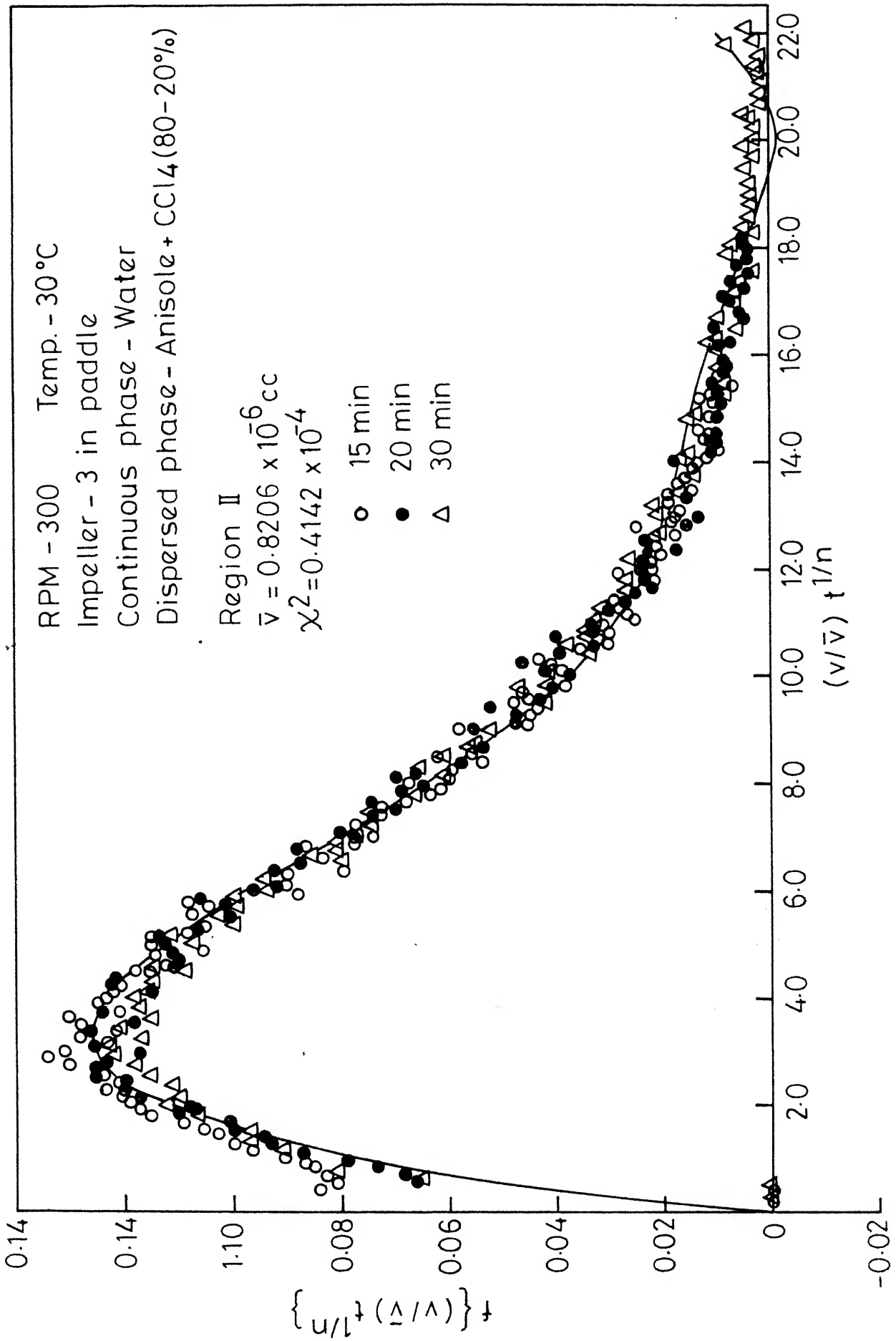

Fig. 6.27 - Plot of modified drop volume density $f\{(v/\bar{v})\, t^{1/n}\}$ versus similarity variable $(v/\bar{v})\, t^{1/n}$

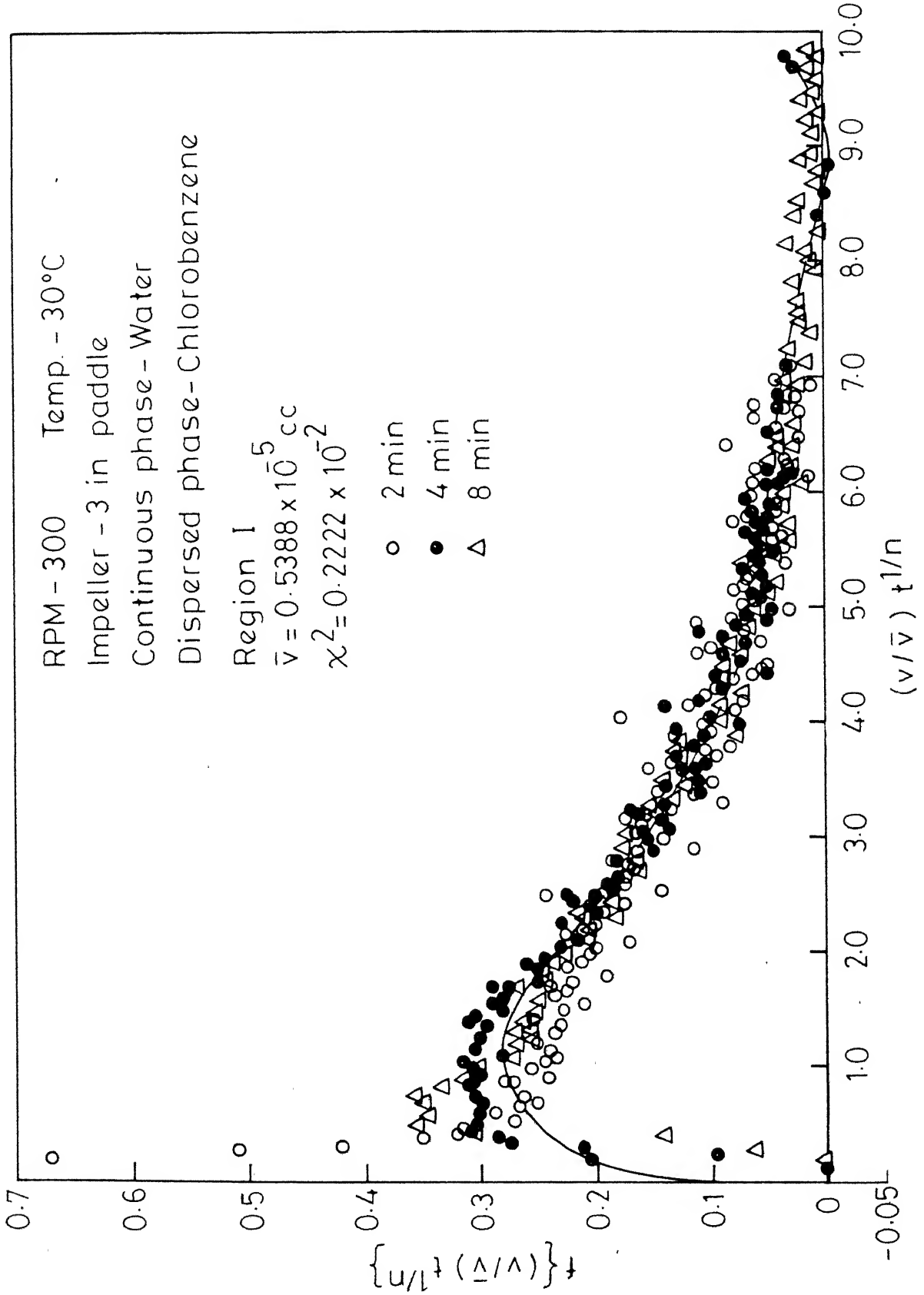

Fig. 6.28 - Plot of modified drop volume density $t\{(v/\bar{v})\, t^{1/n}\}$ versus similarity variable $(v/\bar{v})\, t^{1/n}$.

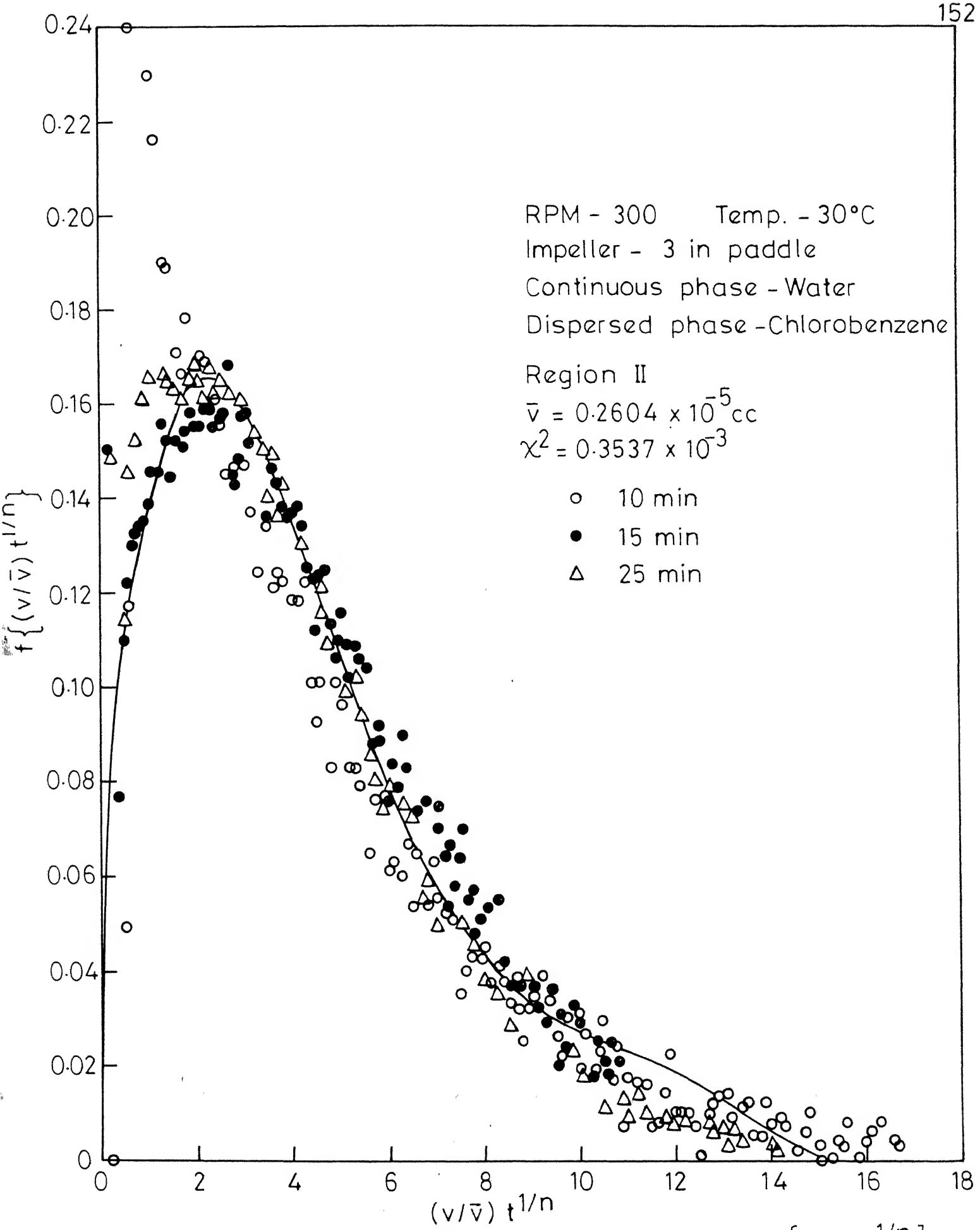

Fig. 6·29 - Plot of modified drop volume density $f\{(v/\bar{v})t^{1/n}\}$ versus similarity variable $(v/\bar{v})t^{1/n}$.

$$\lambda_r = \lambda_{r+n} \; {}^{n}\gamma'_{r-1}$$

where g(x) is the normalised daughter droplet distribution function for 'similar breakage' and

$\lambda_r = \int_0^\infty Z^{r/n} \, d\Psi \, (Z^{1/n})$, Z being the similarity transformation $v \, t^{1/n}$.

The moments $\{\lambda_r\}$ were computed from the moments $\{\lambda_r^m\}$ of the modified drop volume density $f\{(\frac{v}{\bar{v}}) \cdot t^{1/n}\}$ from the relation,

$$\lambda_r = \lambda_r^m \, (\bar{v})^r$$

The modified drop volume density obtained through least square fit of the data was used for the calculation of the moments $\{\lambda_r^m\}$.

The function Kg(x) was then estimated from its moments $\{\gamma'_r\}$ by expressing the function in terms of orthogonal polynomials generated from a suitable weighting function. The coefficients of orthogonal polynomial expansion were estimated from the moments $\{\gamma'_r\}$. Three weighting functions were used for the estimation of the function Kg(x) in order to ascertain the consistency of estimation. They were:(i) 1 (ii) x and (iii) $3x^2-2x^3$, an approximation of gaussian distribution. In case of the first two weighting functions, the convergence was found to be poor even after inclusion of four terms in the expansion. Inclusion of more number of terms in the orthogonal expansion was desisted as the evaluation of higher coefficients would require the knowledge of higher moments of the modified drop volume density $f\{(\frac{v}{\bar{v}}) \cdot t^{1/n}\}$ and the errors involved in the estimation of higher moments λ_r^m are considerable. Hence,

the function Kg(x) could not be estimated with the first two weighting functions. Figure 6.30 shows the estimated function Kg(x) through orthogonal polynomial expansion with the weighting function $3x^2-2x^3$ for 2,3 and 4 terms in the expansion. From Figure 6.30 it can be seen that the convergence is satisfactory. Four terms were included in the orthogonal polynomial expansion for the estimation of the function Kg(x). The rate constant K for the 'power law' approximation Kv^n of the transitional breakage probability was then estimated from the function Kg(x) by making use of the constraint g(1) = 1. Table 6.10 gives the values of the computed rate constants. Table 6.11 gives the computed moments $\{\gamma_r\}$ of the normalised cumulative daughter drop distribution function g(x). It can be seen from Table 6.11 that the moments of g(x) decrease progressively with the increase in the order of the moments. This is understandable as g(x) is non-zero only in the unit interval. In case of water-Anisole + CCl_4(80-20 per cent) and water-chlorobenzene systems the computed moments of g(x) for region II were found to be high. In all the other cases the value of the moments compare fairly well with a variation of around 20 per cent. From the computed values of the moments of g(x) it seems that the normalised cumulative daughter droplet distribution function is more or less same for different systems and experimental conditions. This is further indicated by the plots of estimated cumulative daughter droplet distribution function g(x)

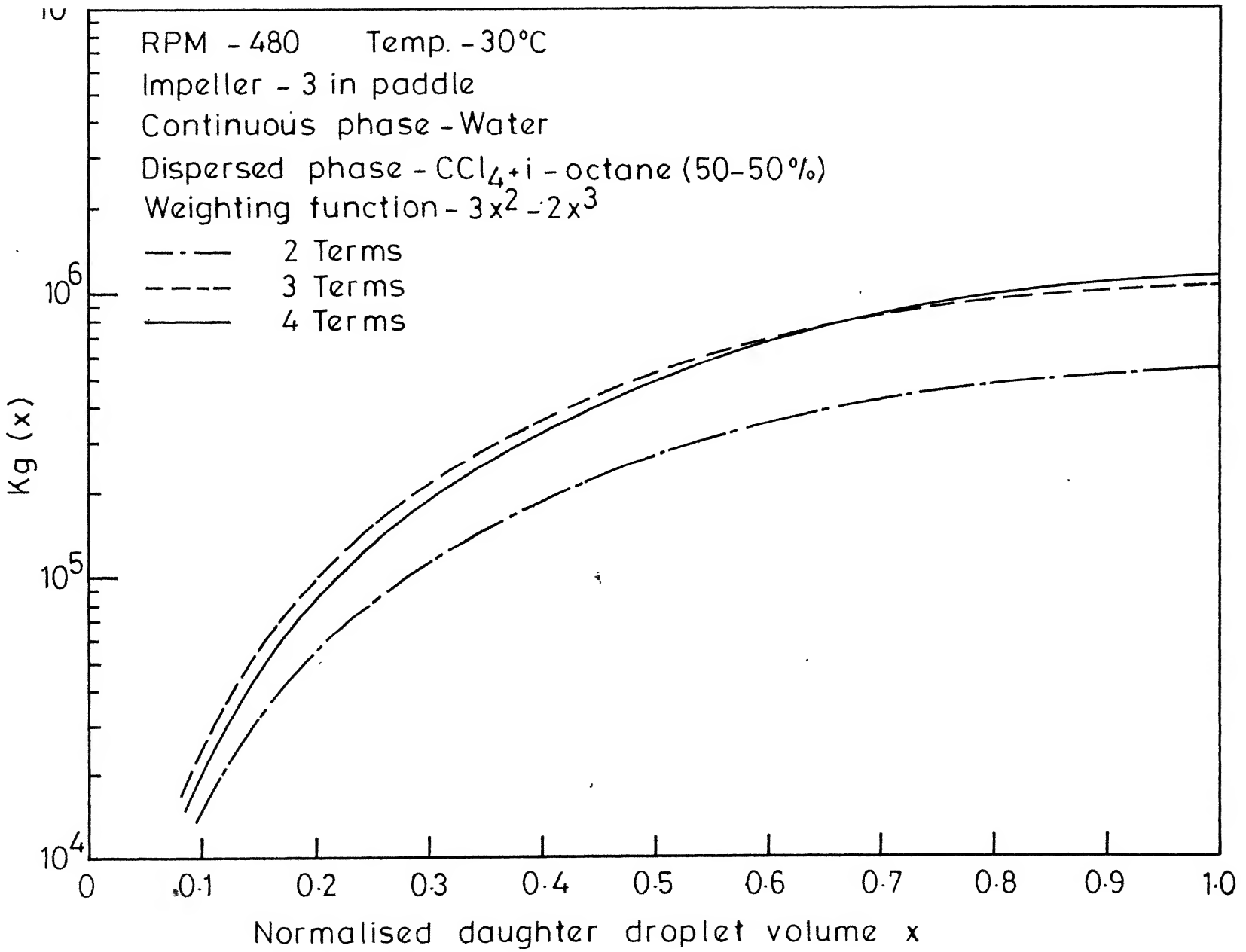

Fig. 6·30 - Plot of estimated function Kg (x).

TABLE 6.10: VALUES OF RATE CONSTANTS

System	Agitated Speed, RPM	Impeller dia., in.	Region I	Region II
Water-CCl_4+i-Octane (50-50 per cent)	480	3	1.086×10^{6}	1.484×10^{12}
Water-CCl_4+i-Octane (50-50 per cent)	420	3	6.833×10^{5}	4.149×10^{8}
Water-CCl_4+i-Octane (50-50 per cent)	300	3	2.255×10^{5}	1.574×10^{7}
Water-Anisole+CCl_4 (80-20 per cent)	300	3	5.143×10^{5}	1.272×10^{9}
Water-Chlorobenzene	300	3	1.701×10^{7}	1.088×10^{9}
Water-CCl_4+i-Octane (50-50 per cent)	480	2	1.183×10^{6}	4.943×10^{7}

TABLE 6.11: MOMENTS OF DAUGHTER DROPLET DISTRIBUTION $g(x)$

System	Agitator speed, RPM	Impeller dia. in.	Region	μ_o	μ_1	μ_2	μ_3
Water-CCl_4+i-Octane (50-50 per cent)	480	3	I	0.23433	0.1700	0.1427	0.1295
			II	0.2355	0.1692	0.1374	0.1163
Water-CCl_4+i-Octane (50-50 per cent)	420	3	I	0.2483	0.1764	0.1395	0.1195
			II	0.2660	0.1830	0.1369	0.1076
Water-CCl_4+-Octane (50-50 per cent)	300	3	I	0.2034	0.1565	0.1324	0.1181
			II	0.1915	0.1513	0.1316	0.1199
Water-Anisole+CCl_4 (80-20 per cent)	300	3	I	0.2093	0.1587	0.1325	0.1160
			II	0.2857	0.1921	0.1460	0.1205
Water-Chlorobenzene	300	3	I	0.2504	0.1766	0.1420	0.1228
			II	0.3225	0.2079	0.1564	0.1298
Water-CCl_4+i-Octane (50-50 per cent)	480	2	I	0.1942	0.1526	0.1312	0.1187
			II	0.1941	0.1525	0.1320	0.1199

and the density g'(x) shown in Figures 6.31 through 6.42, from which it is evident that the nature of the daughter droplet distribution function is the same in all the cases. The above results indicate that the mechanism of drop breakage is the same for different experimental conditions and systems.

Since g(x) is the cumulative daughter droplet distribution function, its zeroth moment would determine the average daughter droplet volume and its first moment would yield the standard deviation about the mean. Table 6.12 gives the average non-dimensionalized daughter droplet volume and the standard deviation for all sets of experimental data. The values of average daughter droplet volume obtained for different sets of experimental data compare fairly well whereas there is appreciable variation in the values of standard deviation. The standard deviation was found to be fairly high which indicates that the daughter droplet density is quite broad. Table 6.13 gives the mean and standard deviation of the daughter droplet distribution g(x) estimated through orthonormal polynomial expansion. From Tables 6.12 and 6.13, we find that the mean daughter droplet volume computed from the moments of g(x) does not compare well with the mean daughter droplet volume of the estimated g(x) whereas the standard deviation in both the cases compare fairly well excepting for water-chlorobenzene and water-Anisole $+CCl_4$ (80-20 per cent) systems for region II. The mean daughter

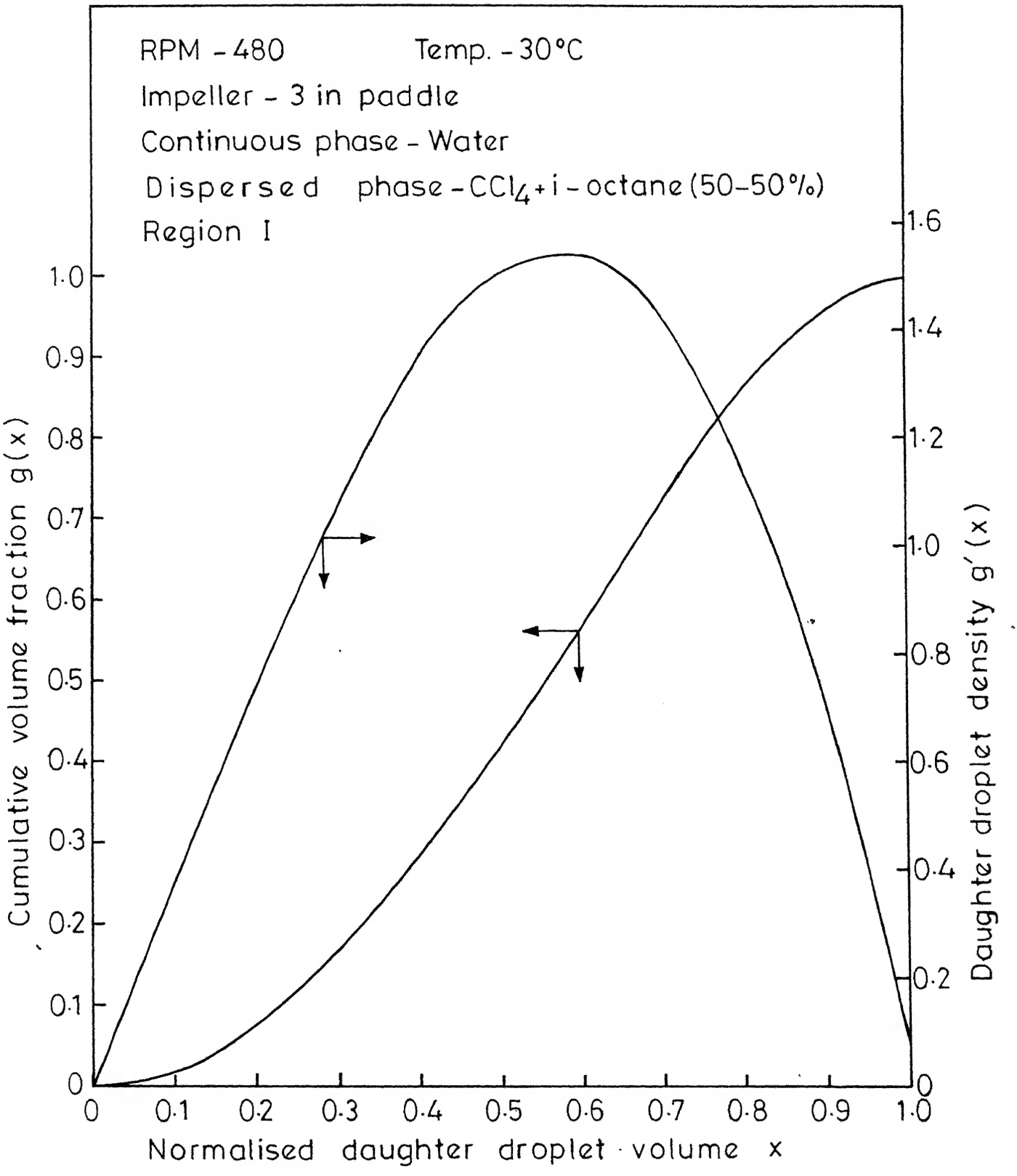

Fig. 6.31 - Plots of estimated daughter droplet distribution and density.

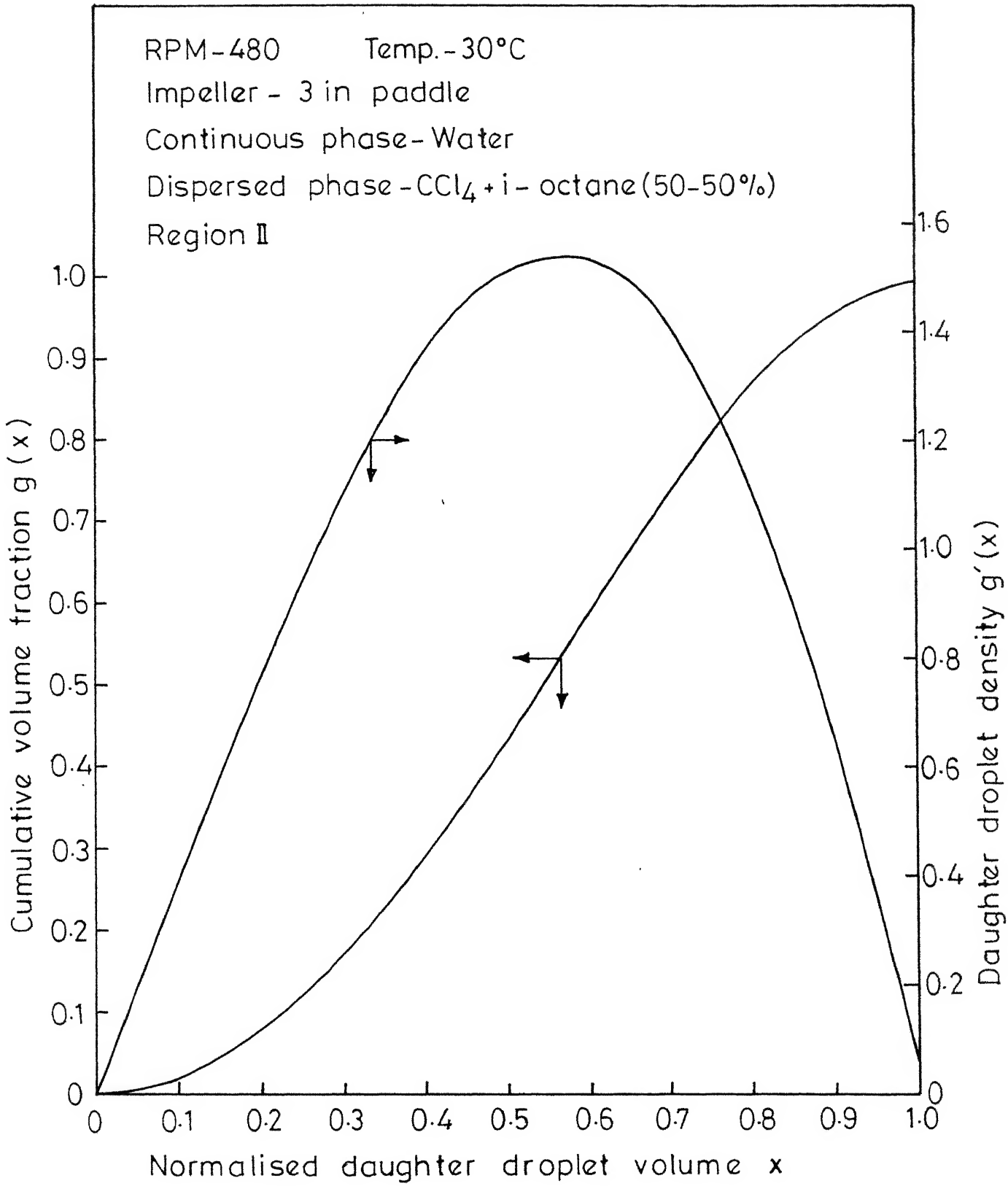

Fig.6.32-Plots of estimated daugher droplet distribution and density.

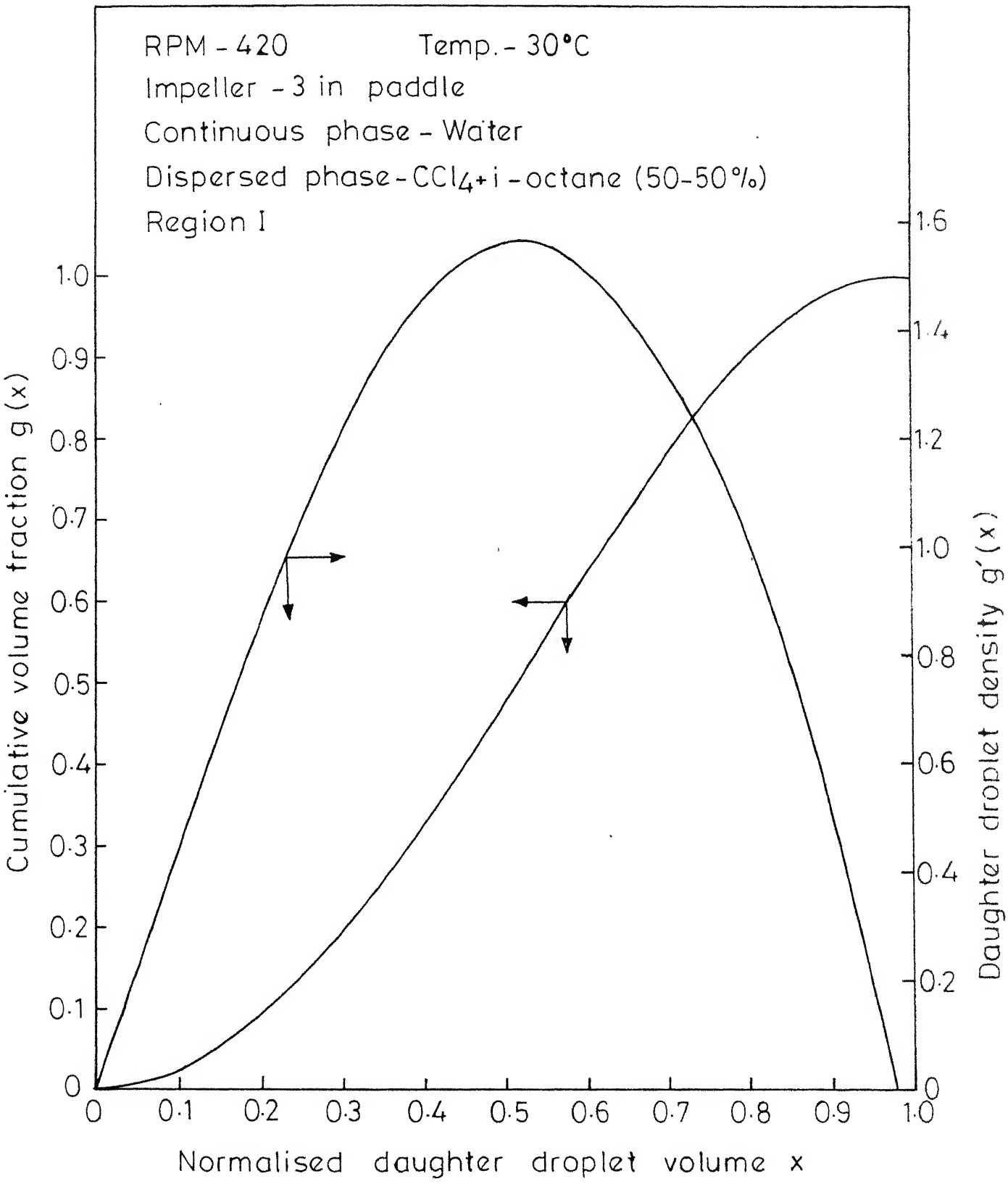

Fig. 6·33 - Plots of estimated daughter droplet distribution and density.

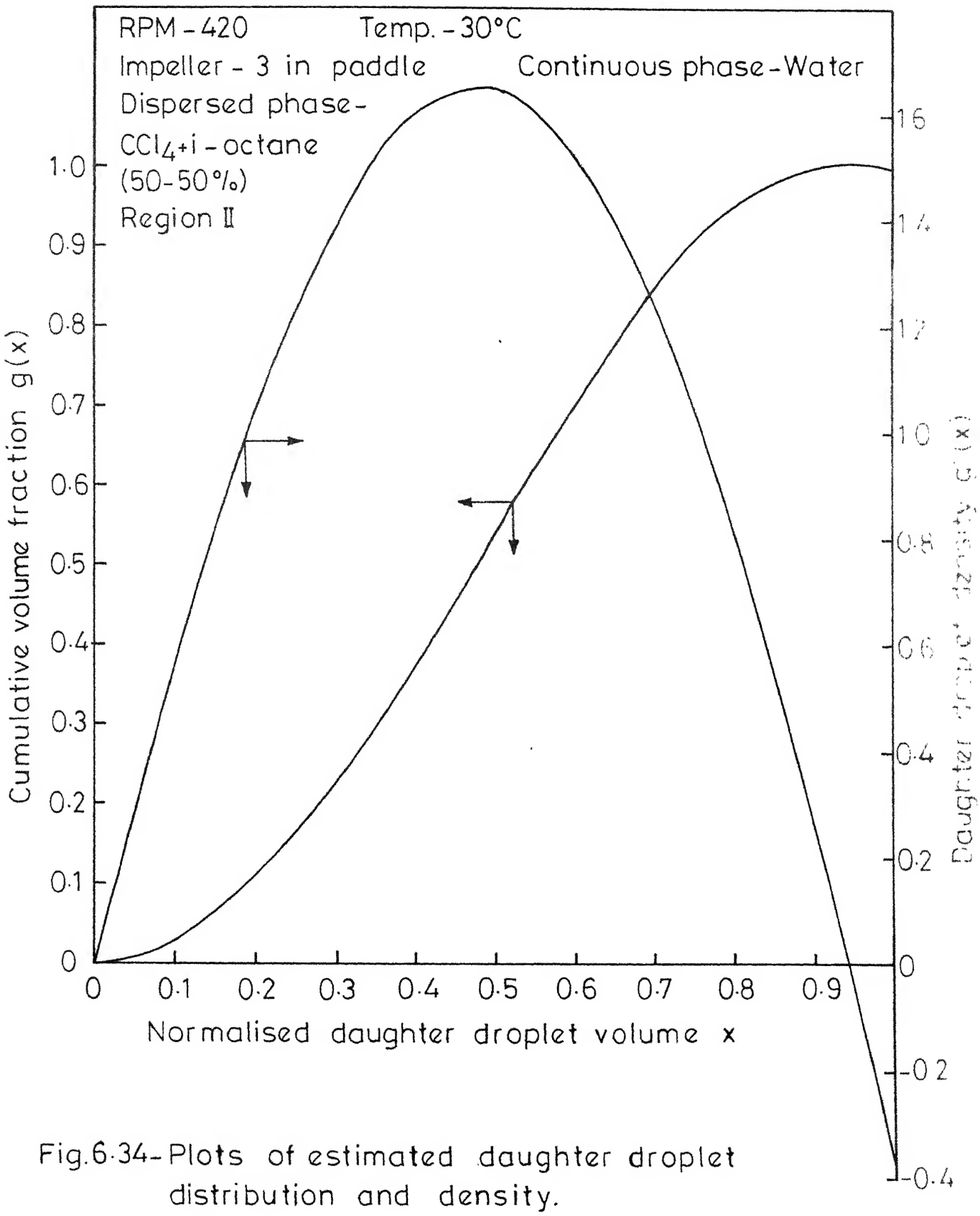

Fig.6.34- Plots of estimated daughter droplet distribution and density.

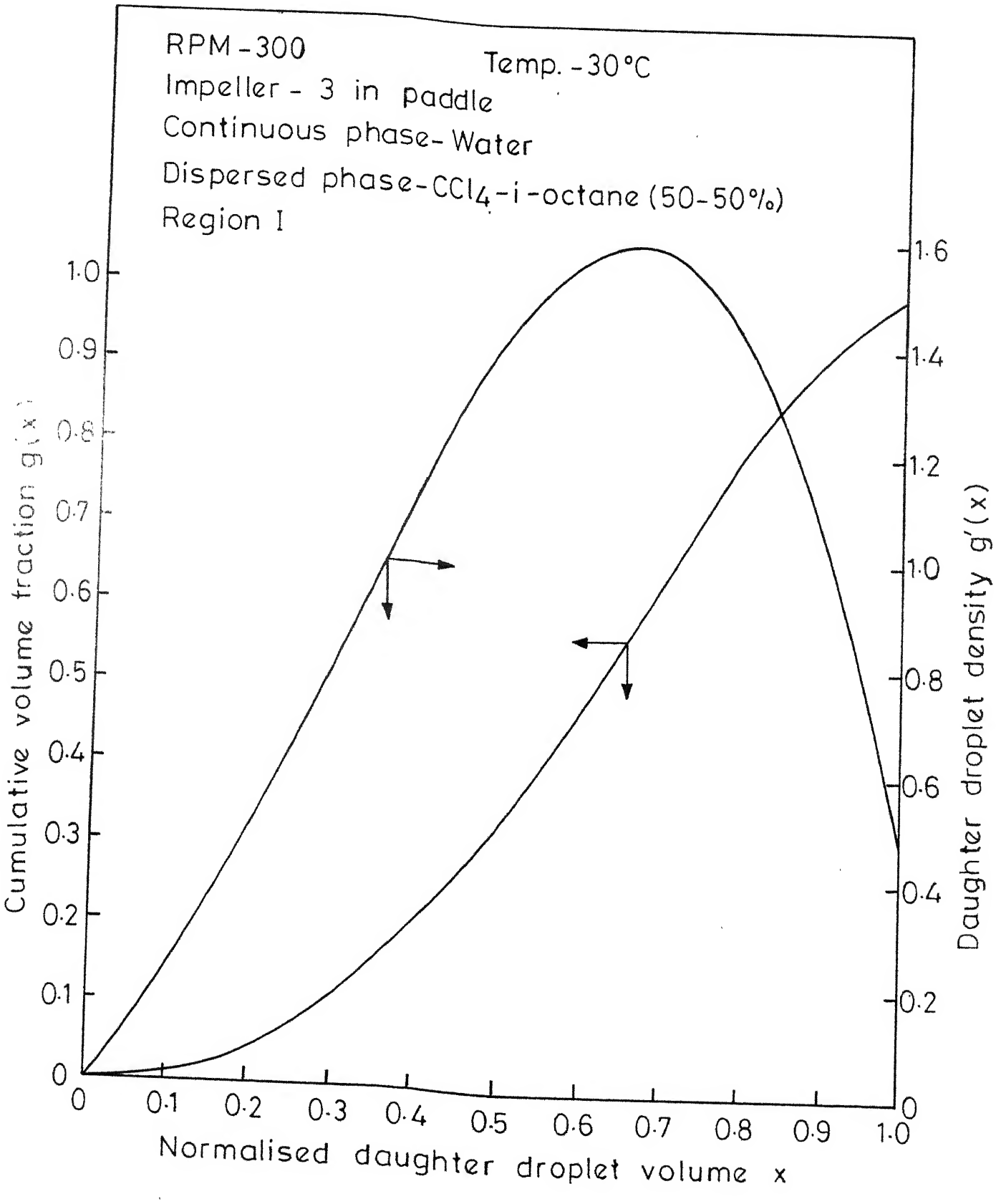

Fig.6.35 - Plots of estimated daughter droplet distribution and density.

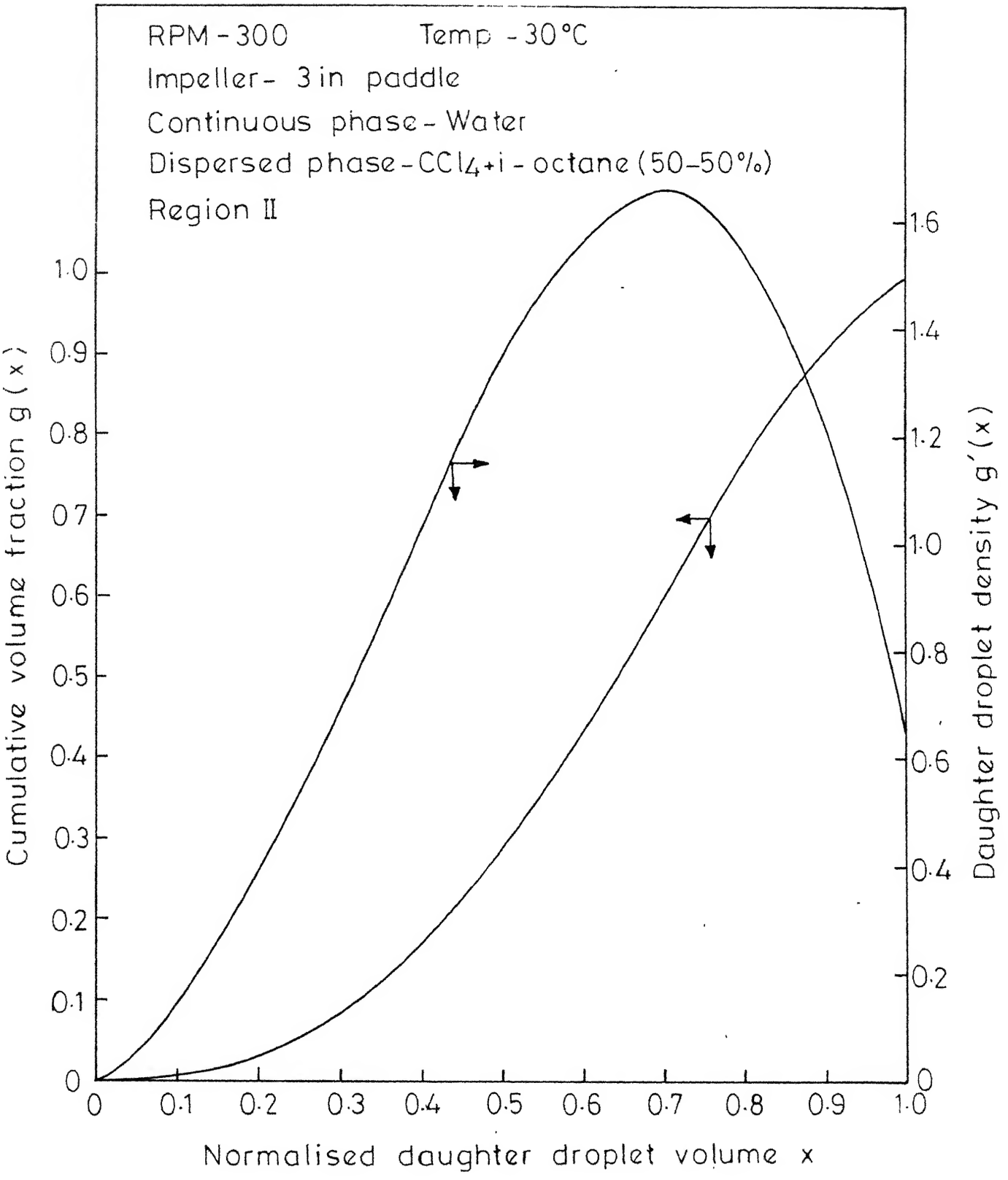

Fig. 6.36 - Plots of estimated daughter droplet distribution and density.

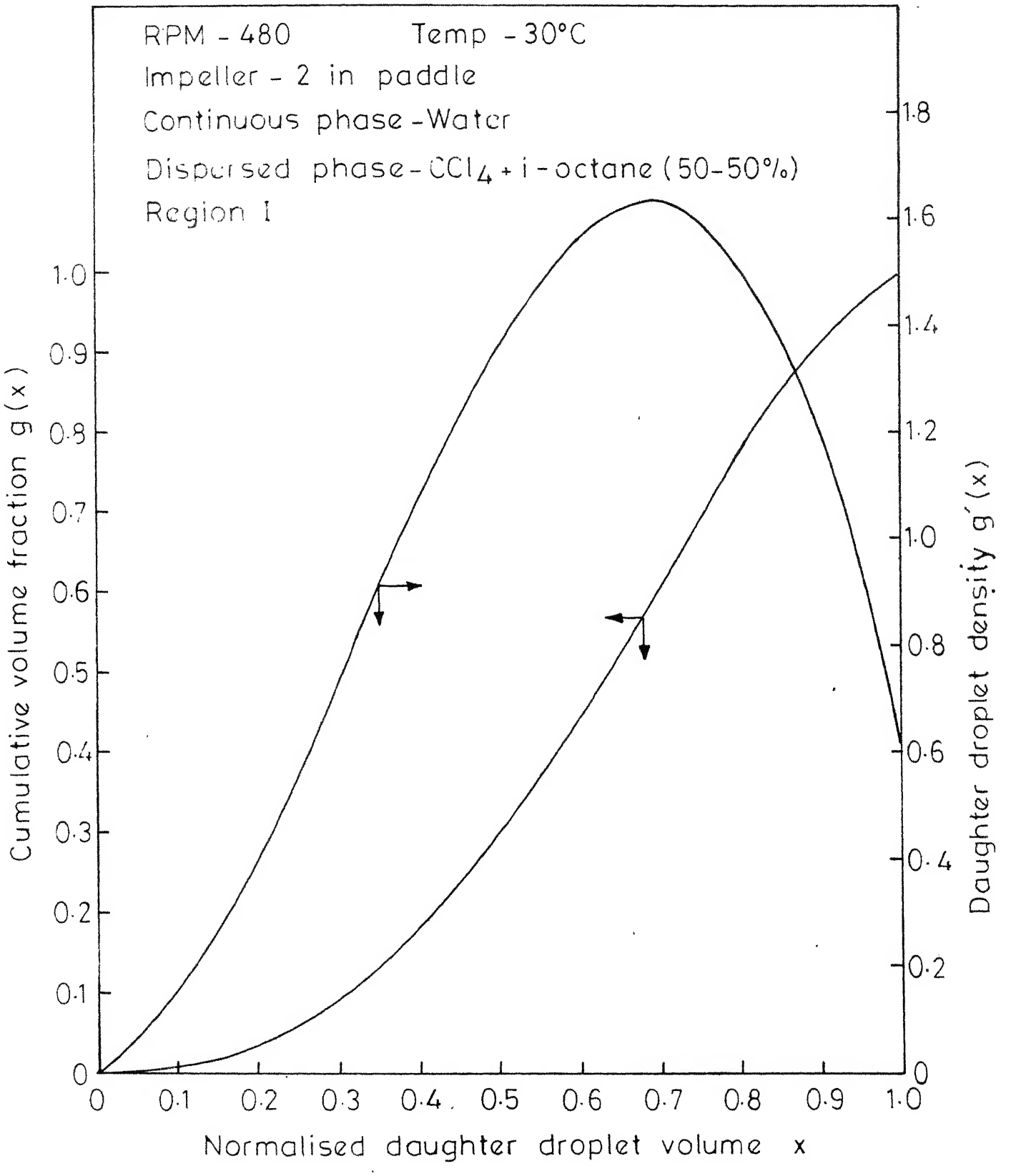

Fig. 6·37 - Plots, of estimated daughter droplet distribution and density .

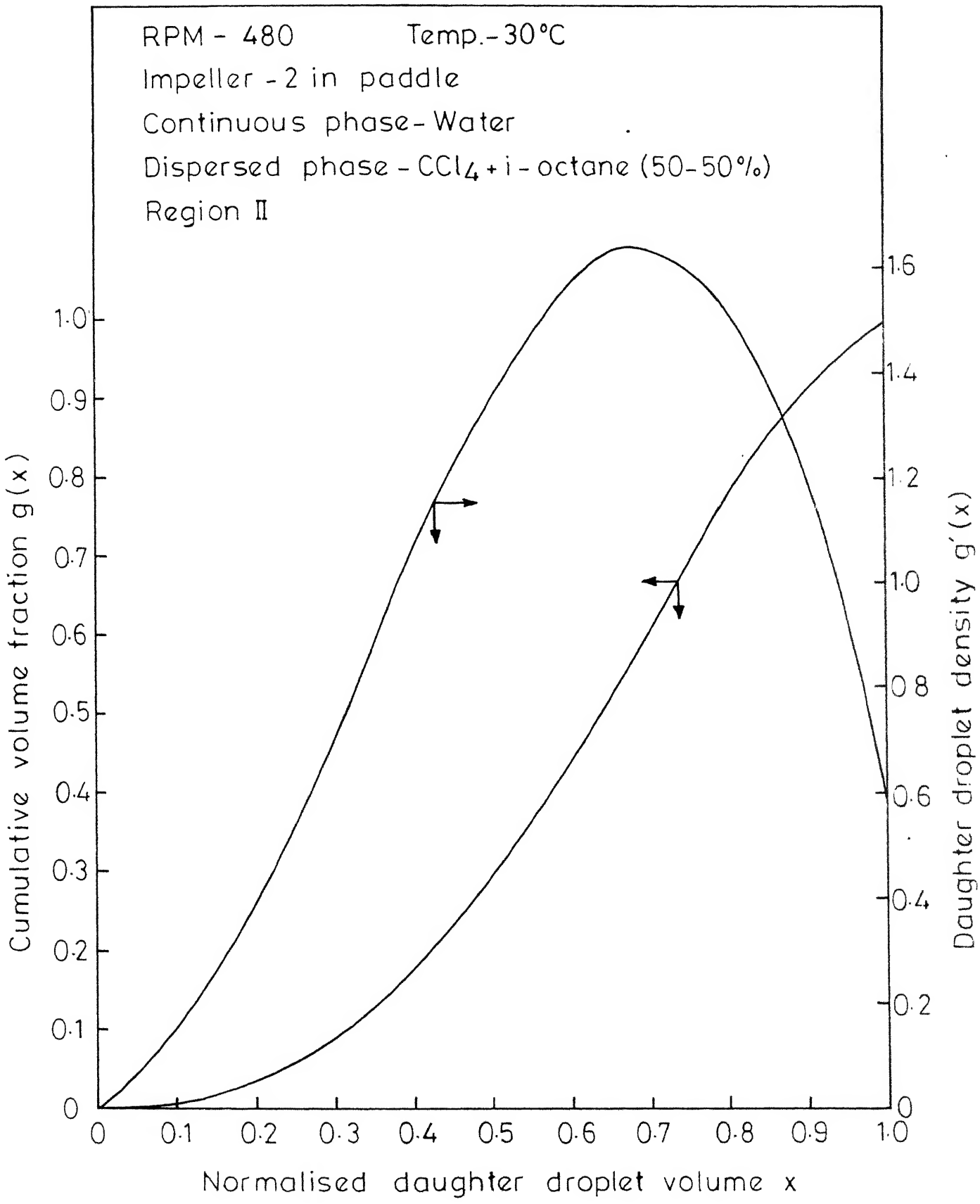

Fig. 6.38 - Plots of estimated daughter droplet distribution and density.

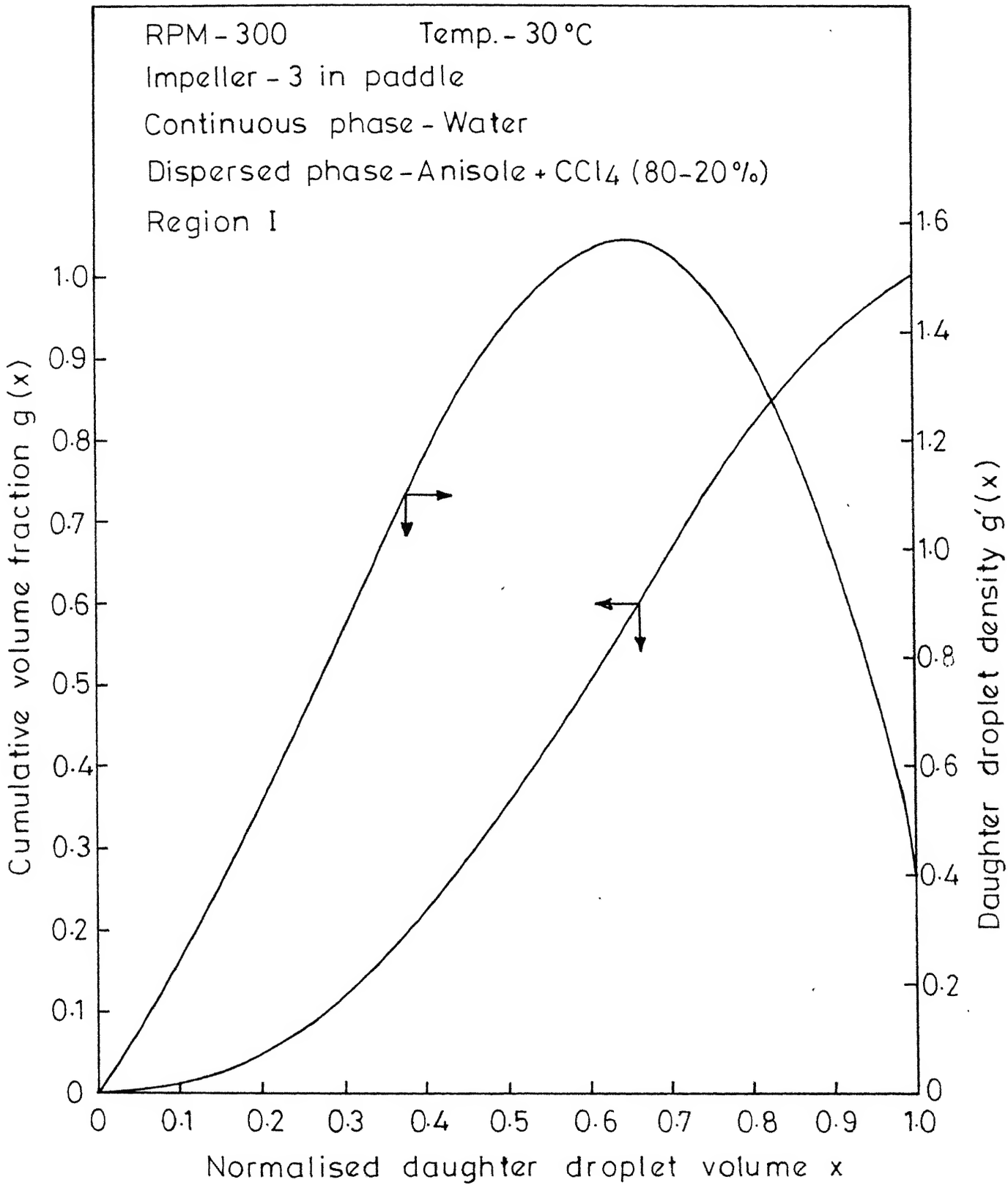

Fig. 6.39 - Plots of estimated daughter droplet distribution and density.

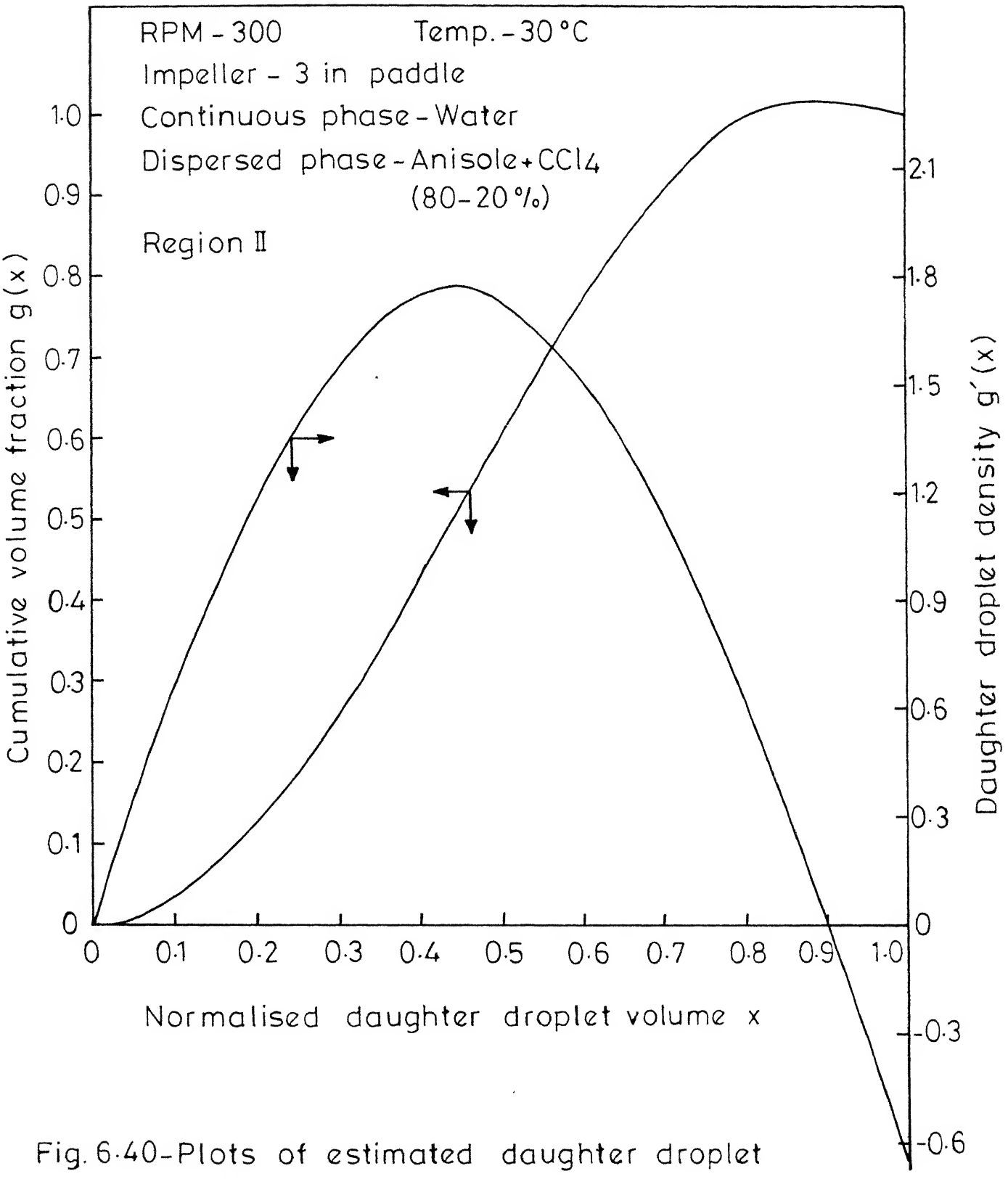

Fig. 6·40-Plots of estimated daughter droplet distribution and density.

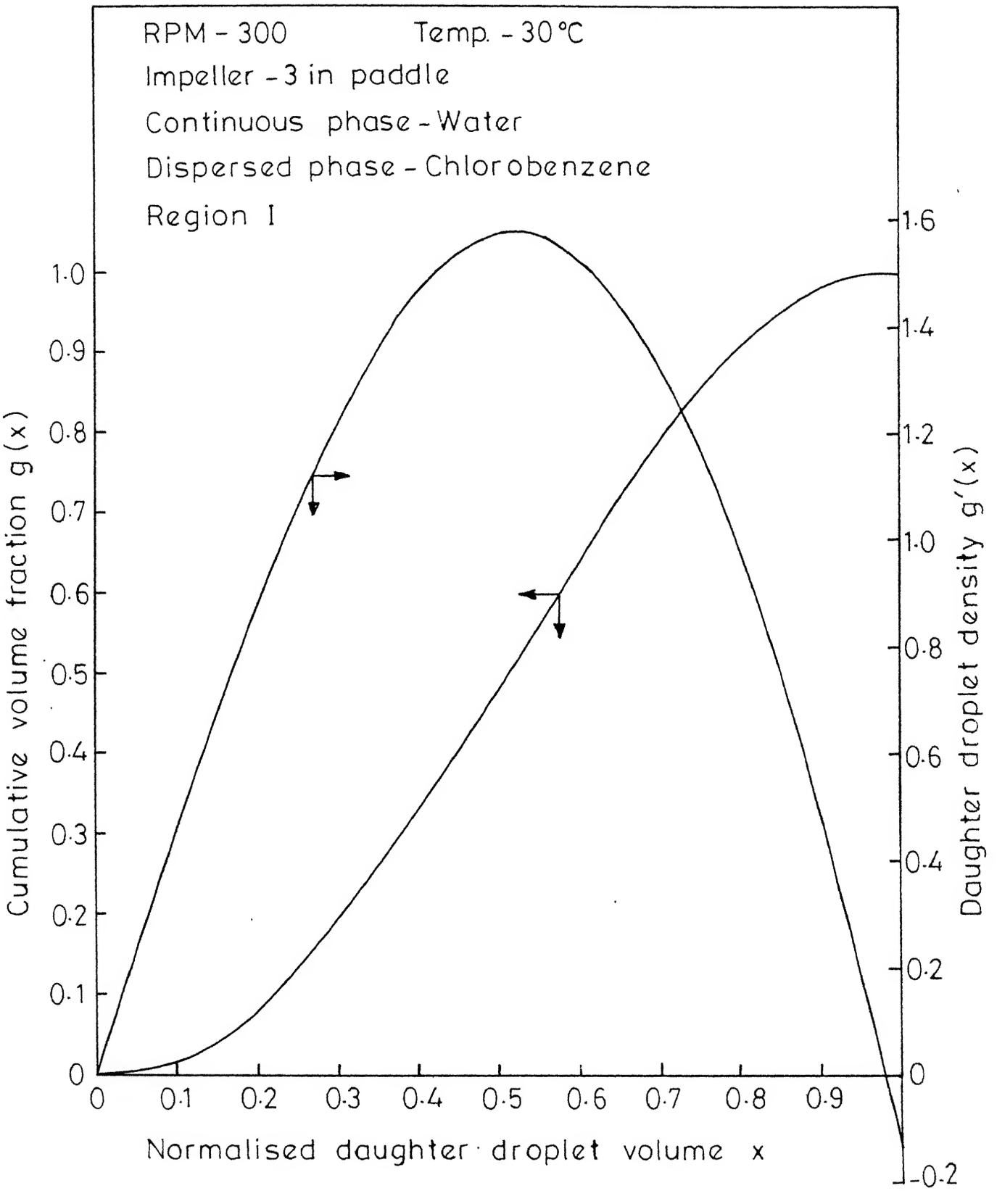

Fig. 6·41 - Plots of estimated daughter droplet distribution and density.

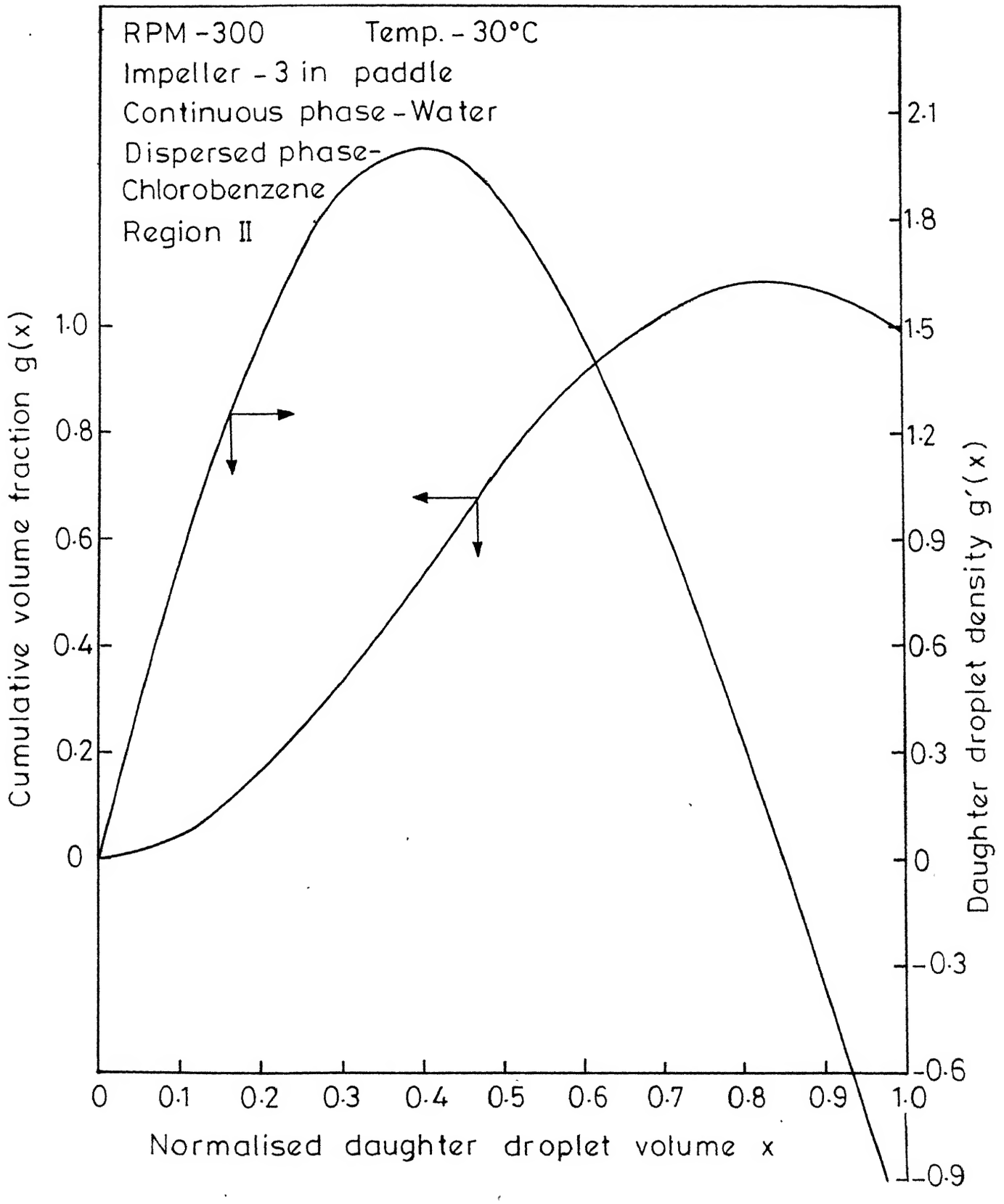

Fig. 6-42 - Plots of estimated daughter droplet distribution and density.

TABLE 6.12: MEAN AND STANDARD DEVIATION OF DAUGHTER DROPLET DENSITY g'(x)

System	Agitator speed, RPM	Impeller dia. in.	Region	Mean	Standard deviation
Water-CCl_4+i-Octane (50-50 per cent)	480	3	I	0.7657	0.2715
			II	0.7656	0.2748
Water-CCl_4+i-Octane (50-50 per cent)	420	3	I	0.7517	0.2865
			II	0.7340	0.3085
Water-CCl_4+i-Octane (50-50 per cent)	300	3	I	0.7966	0.2289
			II	0.8085	0.2090
Water-Anisole+CCl_4 (80-20 per cent)	300	3	I	0.7907	0.2396
			II	0.7143	0.3250
Water-Chlorobenzene	300	3	I	0.7496	0.1493
			II	0.6775	0.3538
Water-CCl_4+i-Octane (50-50 per cent)	480	2	I	0.8058	0.2133
			II	0.8059	0.2133

TABLE 6.13: MEAN AND STANDARD DEVIATION OF THE ESTIMATED DAUGHTER DROPLET DENSITY

System	Agitator speed, RPM	Impeller dia., in.	Region	Mean	Standard deviation
Water-CCl_4+i-Octane (50-50 per cent)	480	3	I	0.5383	0.2216
			II	0.5330	0.2211
Water-CCl_4+i-Octane (50-50 per cent)	420	3	I	0.5064	0.2157
			II	0.4681	0.2020
Water-CCl_4+i-Octane (50-50 per cent)	300	3	I	0.5963	0.2201
			II	0.6213	0.2145
Water-Anisole+CCl_4 (80-20 per cent)	300	3	I	0.5842	0.2217
			II	0.4325	0.1814
Water-chlorobenzene	300	3	I	0.5044	0.2153
			II	0.3621	0.0991
Water-CCl_4+i-Octane (50-50 per cent)	480	2	I	0.6147	0.2164
			II	0.6159	0.2161

droplet volume of the estimated g(x) is found to be lower than the mean daughter droplet volume computed from the moments of g(x). Moreover, the estimated daughter droplet density became negative for large daughter droplet volumes when the standard deviation computed from the moments of g(x) is high. The estimated daughter droplet distribution and density were found to be particularly bad in case of water chlorobenzene system for region II. It can also be observed that the value of estimated daughter droplet density at normalised daughter droplet volume of 1.0 was found to be a large positive value in all cases where the standard deviation computed from the moments of g(x) was small. In view of these, it may be necessary to include more number of terms in the orthogonal polynomial expansion for accurate estimation of function Kg(x). As stated earlier, such an attempt was desisted because of large errors involved in the calculation of higher moments. Therefore, the estimated daughter droplet distributions are only qualitative estimations.

The following inferences could therefore be made from the experimental results:

(i) The assumption of 'similar breakage' is valid.

(ii) The breakage mechanism seems to be the same for all the systems and experimental conditions.

(iii) The normalised daughter droplet density is more or less same for all the cases.

(iv) The daughter droplet density is broad.

6.4.4 Variation of the Rate Constant K with $\bar{\varepsilon}$ and σ:

The functional dependence of the rate constant K in the 'power law' approximation Kv^n of the transitional breakage probability on the physical properties of the system and the experimental conditions is given by,

$$K \alpha v_s^{-n} \alpha N^{\frac{18n}{5}} L^{\frac{12n}{5}} \rho^{\frac{9n}{5}} \sigma^{\frac{-9n}{5}}$$

Figure 6.43 shows a log-log plot of the rate constant K versus the agitator speed for water - CCl_4+i-Octane (50-50 per cent) system for region I. Since the value of the exponent n for region I was around 1.0, the functional dependence of the rate constant K on the agitator speed N is according to the model,

$$K \alpha N^{18/5}.$$

From Figure 6.42 it can be seen that the computed values of K fall on a straight line of slope 3.38. Hence, the functional dependence of the computed values of K on the agitator speed N for region I agrees fairly well with the model. For region II, the value of the exponent n for water-CCl_4 +i-octane (50-50 per cent) system at the agitator speeds of 300 RPM and 420 RPM were around 1.5 and at the agitator speed of 480 RPM the exponent was around 2.0. Therefore, the comparison of the rate constant K could be made

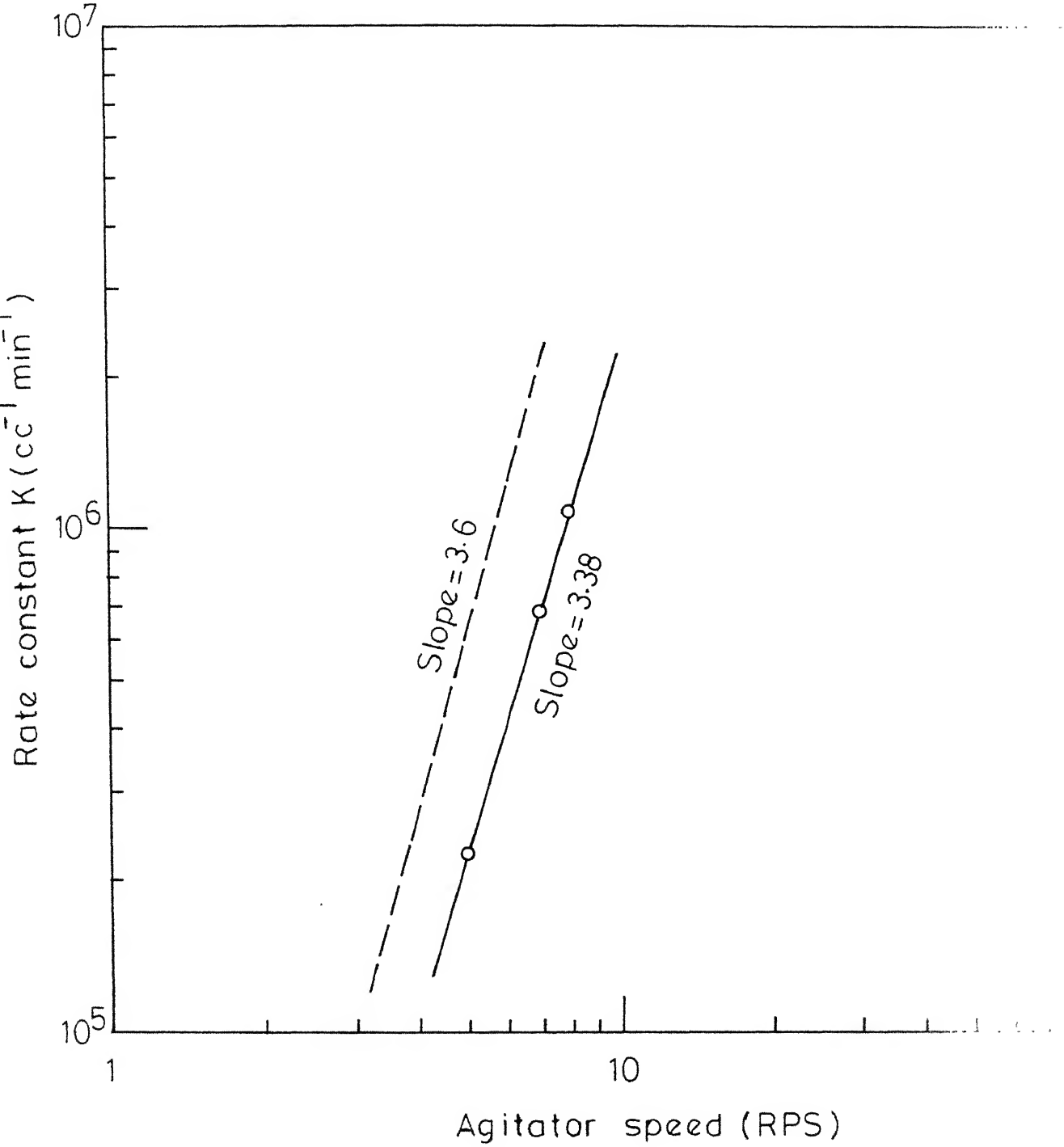

Fig.6.43 - Plot of rate constant K versus agitator speed for region I.

only for the computed values for the agitator speeds of 300 RPM and 420 RPM. Figure 6.44 gives the plot of K versus N for these two agitator speeds. If the average value of the exponent is taken to be 1.5,

$$K \alpha N^{5.4}$$

From Figure 6.44 it can be seen that the agreement between the computed values of K and the model is not bad considering the fact that there was appreciable variation in the value of the exponent.

Figure 6.45 gives the plot of computed rate constant K versus the interfacial tension σ for region I at the agitator speed of 300 RPM. Comparison could be made only for water-CCl_4+i-octane (50-50 per cent) and water-Anisole + CCl_4(80-20 per cent) systems for reasons stated earlier. As the value of the exponent n in both the cases were around 1.0, the functional dependence of K on σ is given by,

$$K \alpha \sigma^{-9/5}.$$

The computed values compare very well with the model as can be seen from Figure 6.45. Since the value of the exponent n for region II was around 1.8 in case of water-Anisole + CCl_4 (80-20 per cent) and water-chlorobenzene systems, the functional dependence of K on σ according to the model is $K \alpha \sigma^{-3.24}$. The values of the computed rate constants K are more or less same in both the cases as can be seen from Table 6.10.

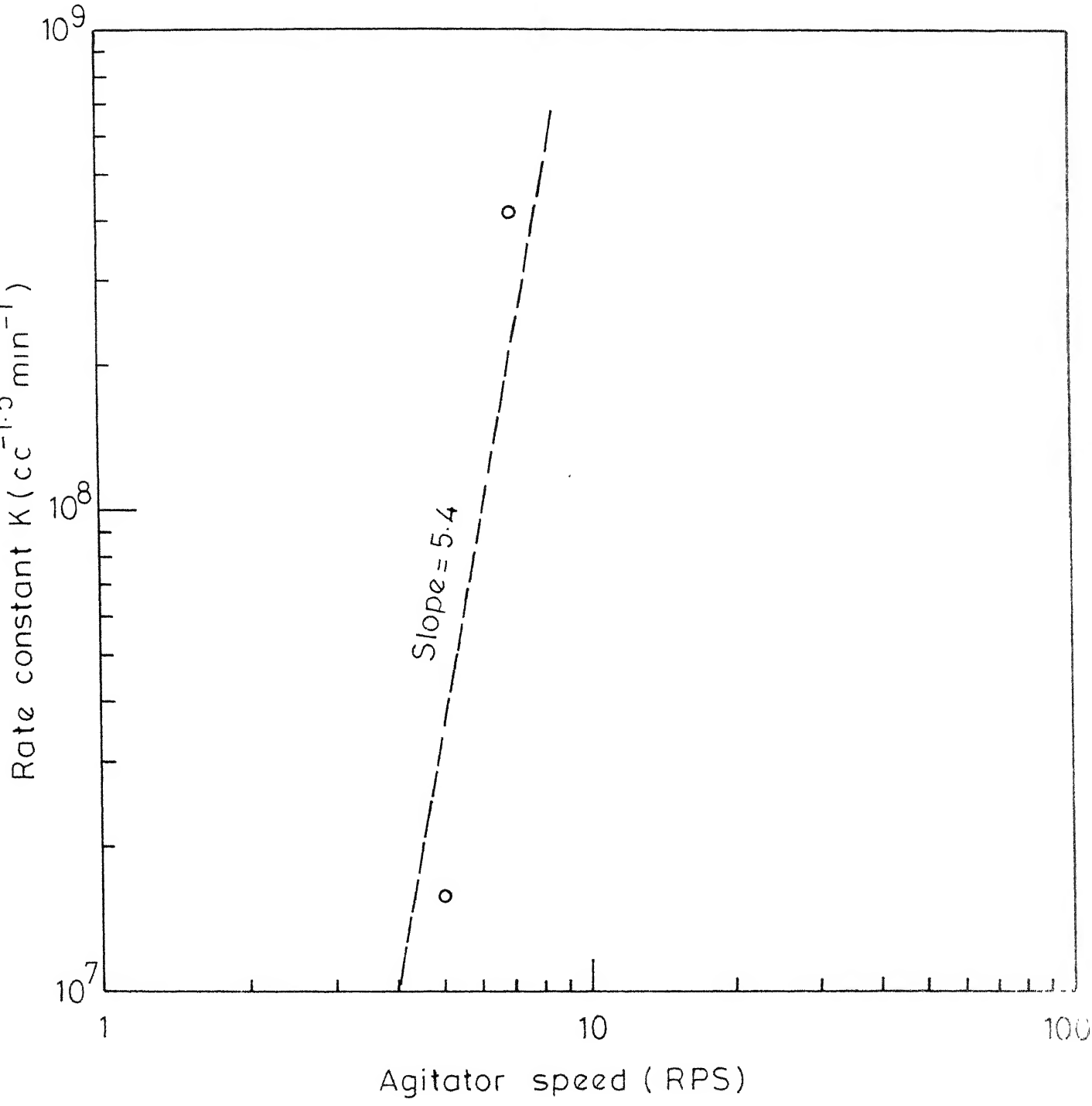

Fig. 6 44 - Plot of rate constant K versus agitator speed for region II

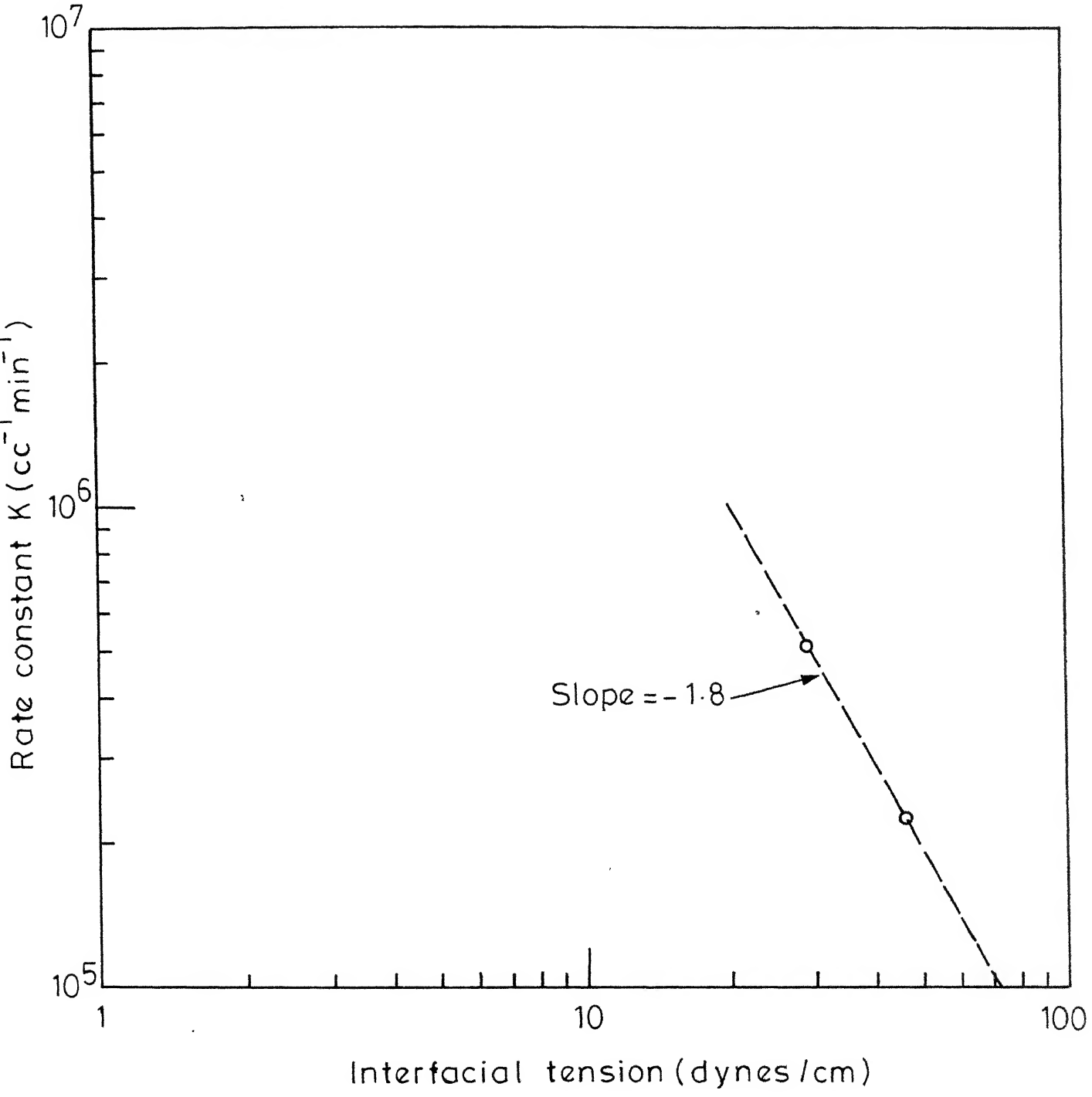

Fig. 6·45 - Plot of rate constant K versus interfacial tension for region I.

Hence, the agreement between the model and the computed values of K is very poor. This may be attributed to the peculiar behaviour of water-chlorobenzene system for which the region corresponding to the exponent value 1.0 could not be identified at small stirring times.

6.5 EQUILIBRIUM DROP VOLUME DISTRIBUTION:

Equilibrium drop volume distributions were measured for water-CCl_4+i-octane (50-50 per cent) system at the agitator speeds of 420 and 300 RPM with 3 inch diameter paddle impeller and at the agitator speed of 480 RPM with 3 inch diameter as well as 2 inch diameter paddle impellers. Measurements of equilibrium drop volume distributions were also made at the agitator speed of 300 RPM for water-Anisole + CCl_4 (80-20 per cent) system and water-chlorobenzene system. Figures 6.46 through 6.51 give the plot of equilibrium drop volume density $f_v(d/\bar{d}_{32})$ versus non-dimensionalized drop size $d/\bar{d}_{32}$.

6.5.1 Prediction of the Equilibrium Drop Volume Distribution from the Kinetic Model:

Solution of the population balance equation using the asymptotic expansion of the proposed transitional breakage probability under the assumption of constant coalescence frequency and binary uniform breakage yielded the equilibrium drop volume density.

$$f_n(\xi) = \frac{1}{\sqrt{2\pi}\,\sigma} \exp\left[-\frac{(\xi-1)^2}{2\sigma^2}\right] \qquad (3.2.19)$$

where $\xi = \frac{d}{d^*}$, $\sigma = \frac{3}{25(\alpha B-1)}$, and d^* is the diameter for which the density exhibits maximum.

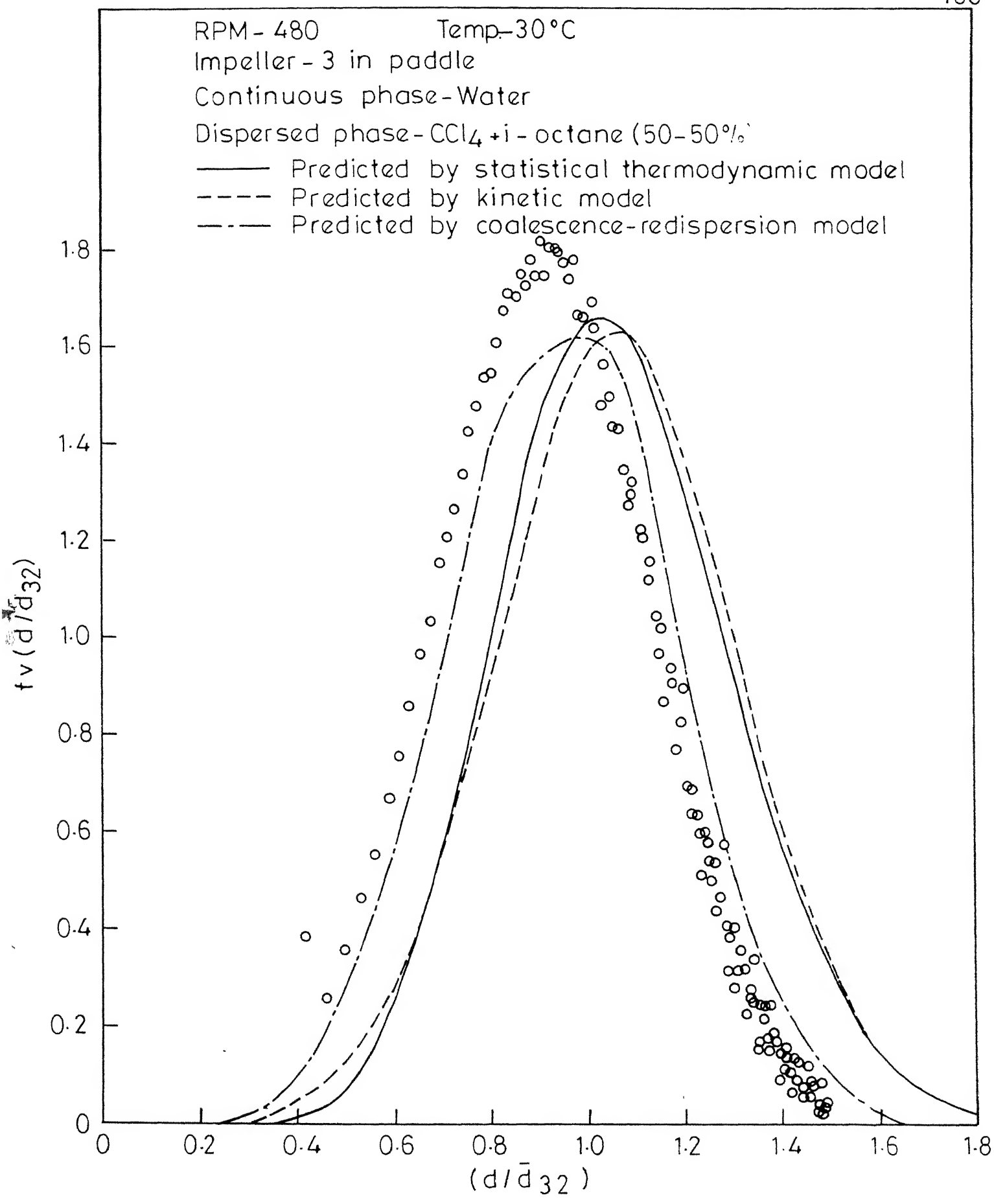

Fig.6.46 - Plot of equilibrium drop volume density $f_v(d/\bar{d}_{32})$ vs. $(d/\bar{d}_{32})$.

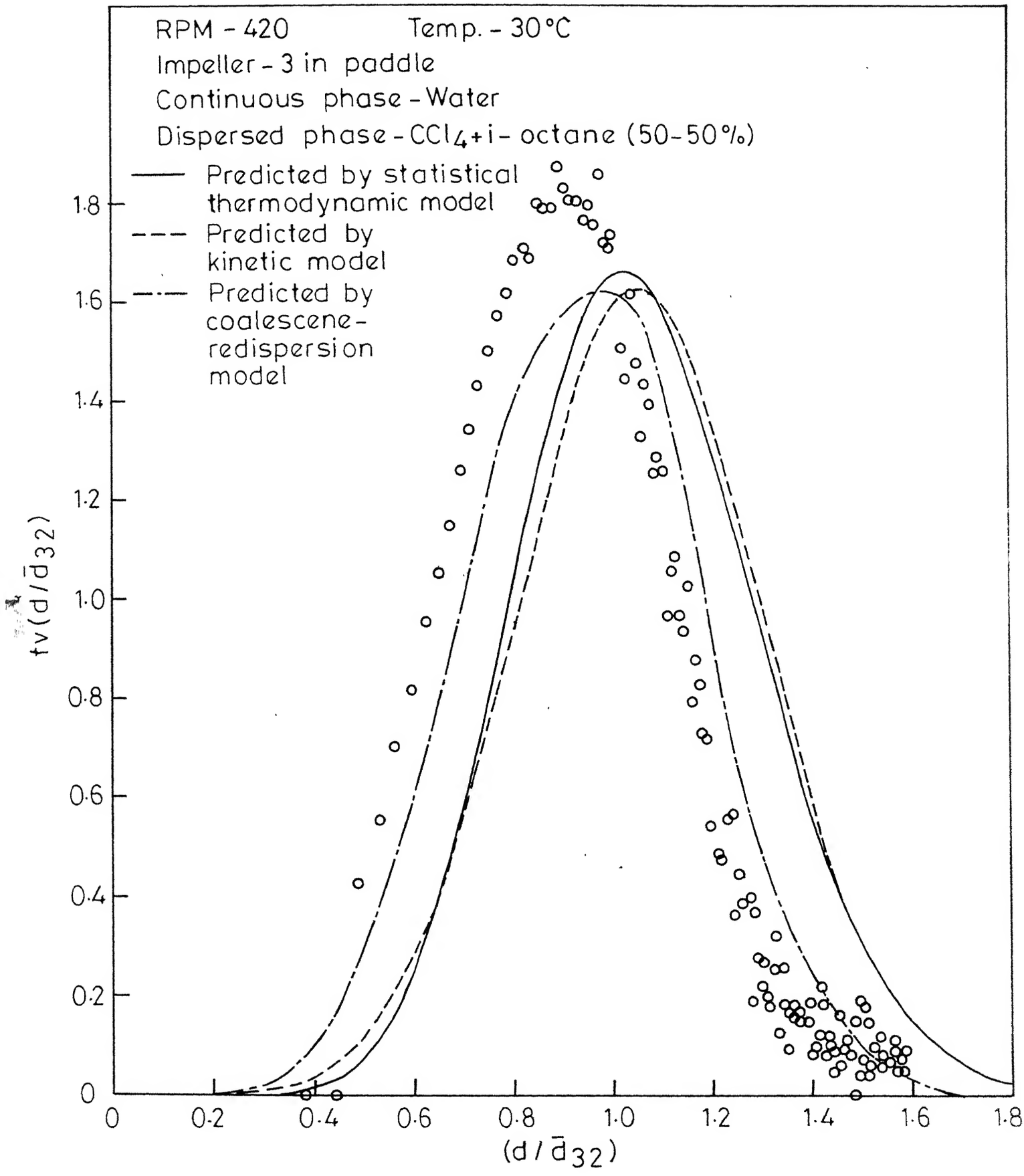

Fig. 6.47 - Plot of equilibrium drop volume density $fv(d/\bar{d}_{32})$ vs. $(d/\bar{d}_{32})$.

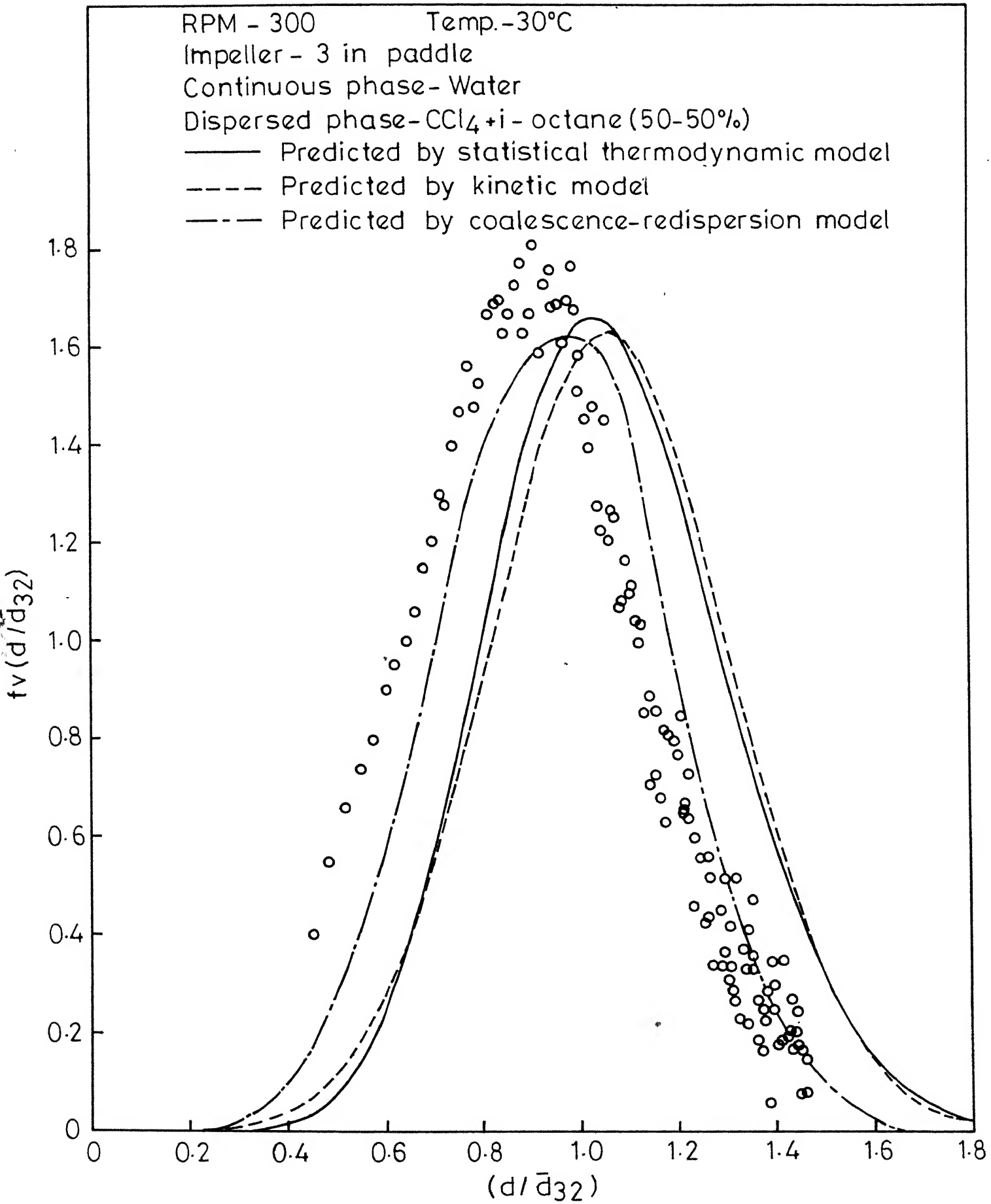

Fig. 6.48 - Plot of equilibrium drop volume density $f_v(d/\bar{d}_{32})$ vs. $(d/\bar{d}_{32})$.

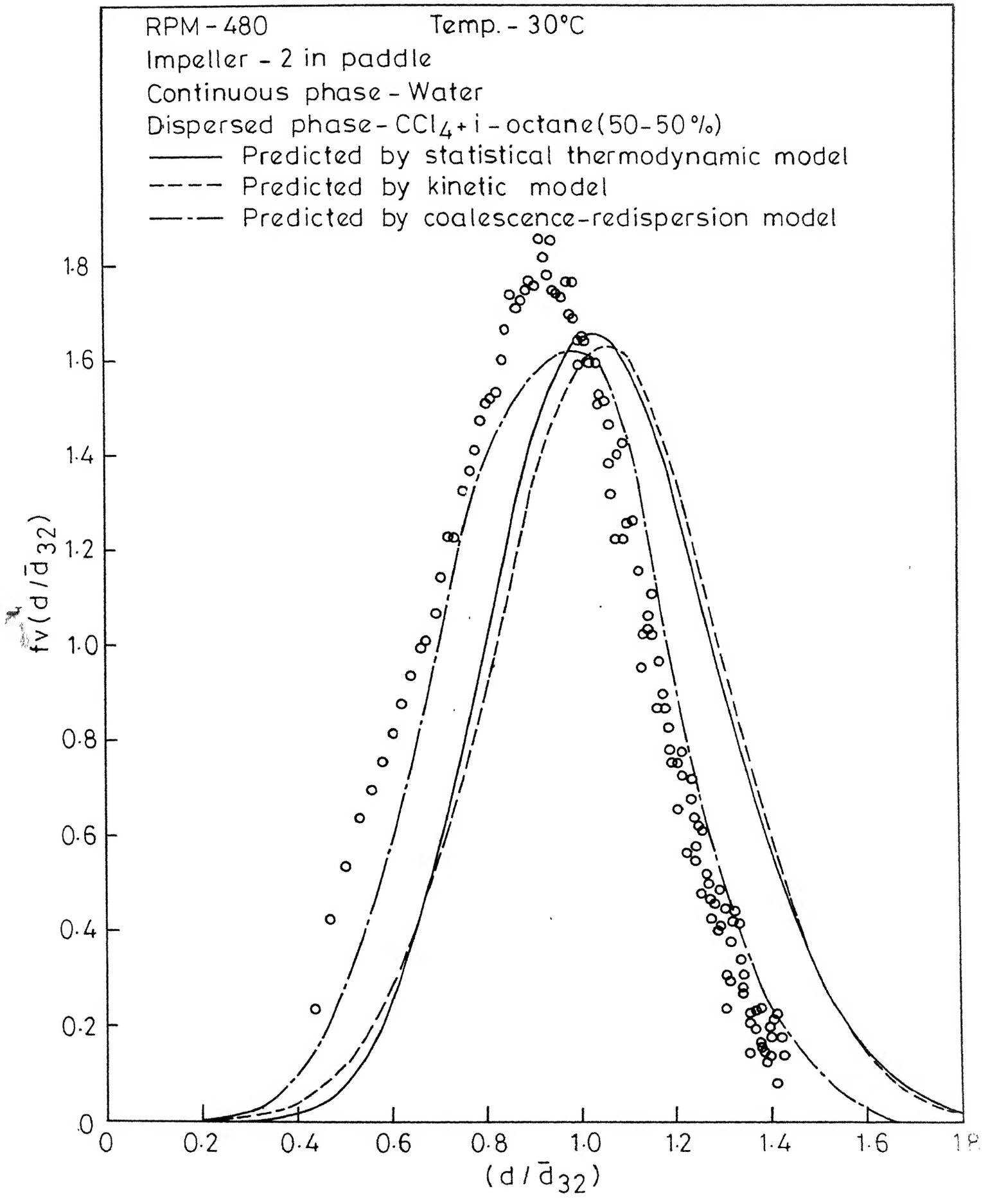

Fig. 6.49 - Plot of equilibrium drop volume density $f_v(d/\bar{d}_{32})$

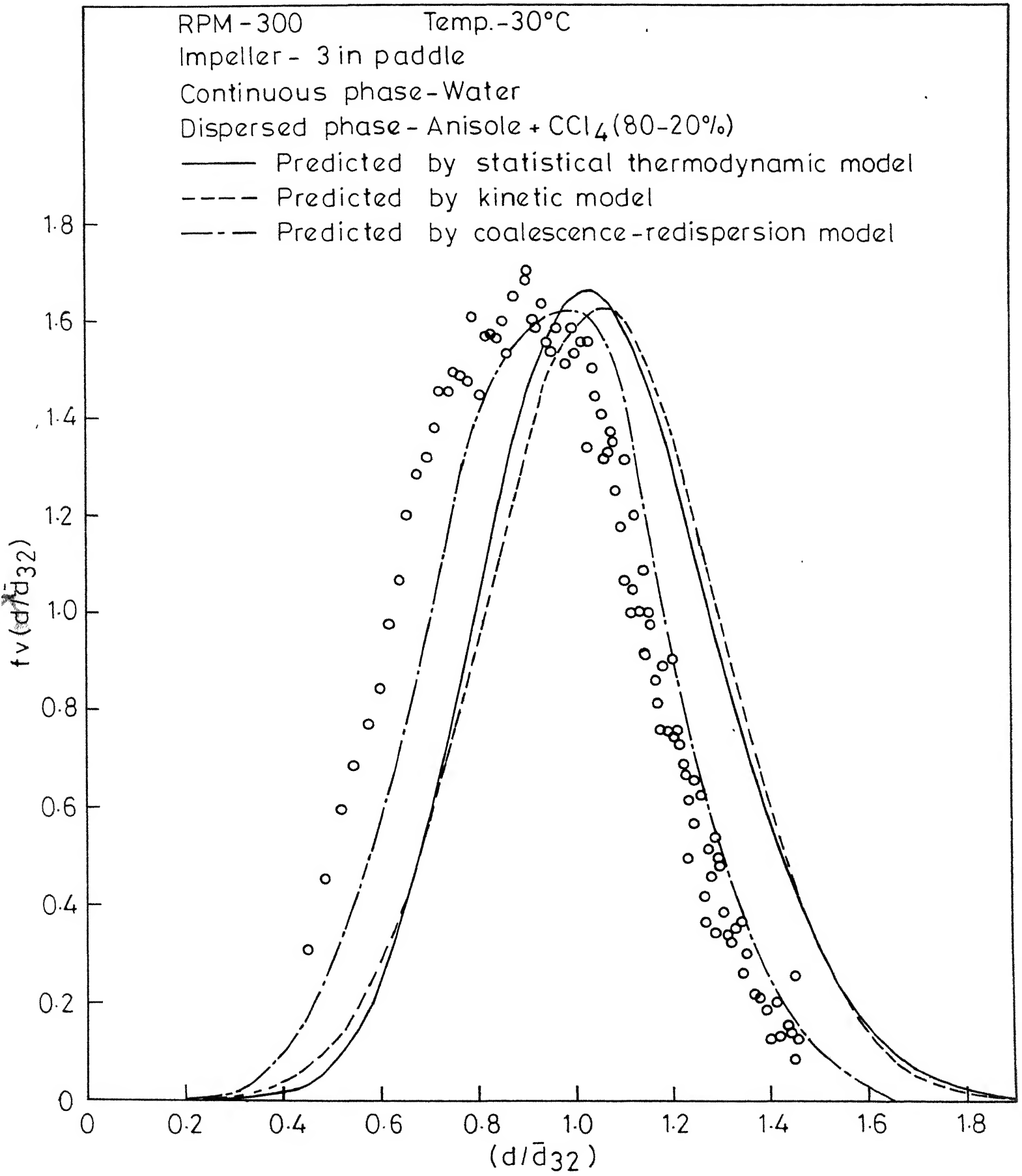

Fig. 6.50 - Plot of equilibrium drop volume density $f_v(d/\bar{d}_{32})$ vs. $(d/\bar{d}_{32})$

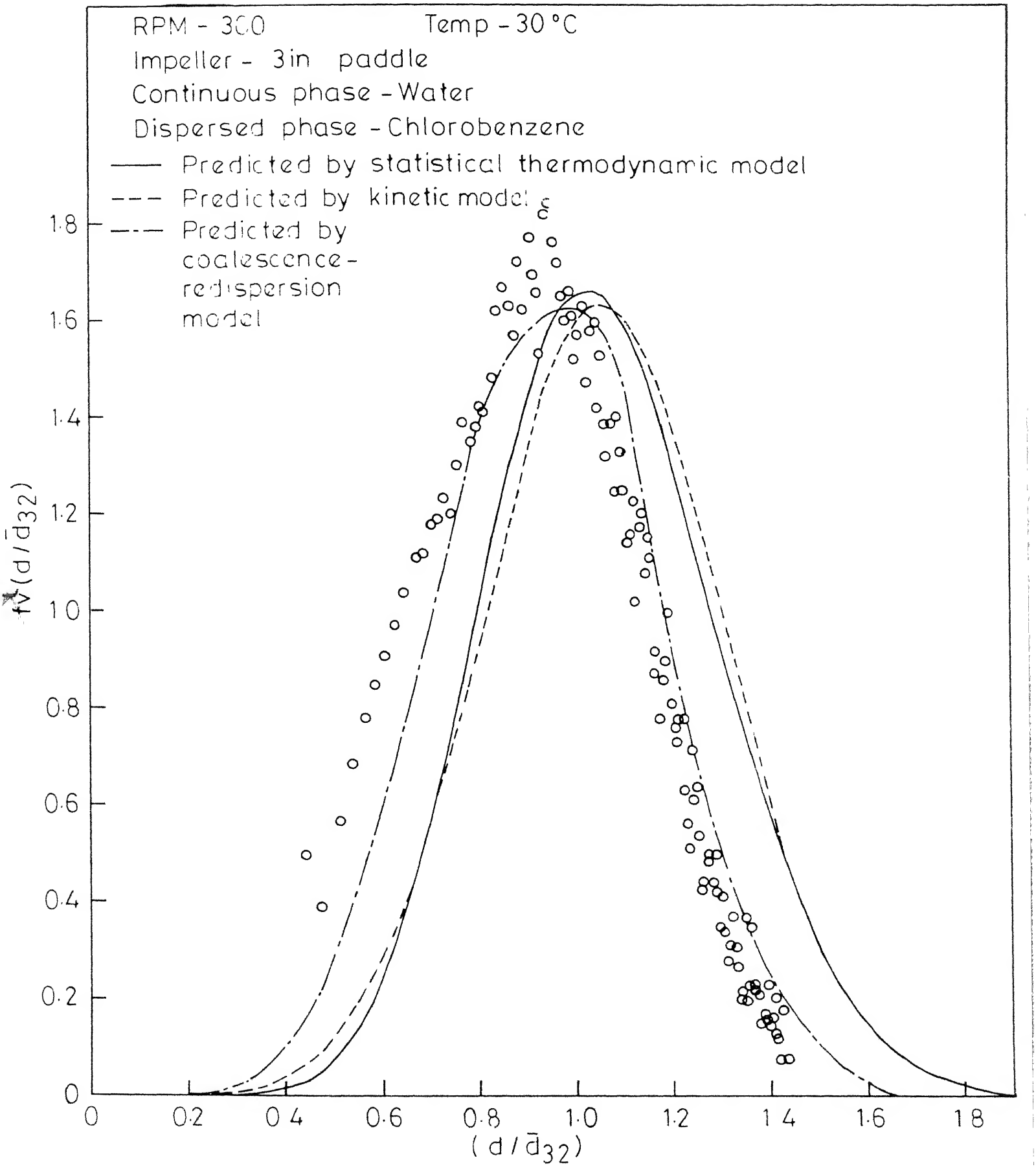

Fig 6 51 - Plot of equilibrium drop volume density fv (d / $\bar{d}_{32}$) vs. (d / $\bar{d}_{32}$).

Quantitative comparison of the derived distribution with the experimental data is possible only if the value of α is known. α is defined as

$$\alpha = \left(\frac{d^*}{d_s}\right)^{-5/3} \qquad (3.2.12)$$

From equation (3.1.10), we get

$$\left(\frac{d_s}{L}\right) = C_4 \, N_{We}^{-0.6} \qquad (3.1.10)$$

From the correlations of Chen and Middleman [30] for the sauter mean drop diameter $\bar{d}_{32}$ in batch agitated dispersion,

$$\left(\frac{d_{32}}{L}\right) = 0.053 \, N_{We}^{-0.6} \qquad (6.5.1)$$

i.e. $$\frac{\bar{d}_{32}}{d_s} = C_5 \text{ a constant.}$$

It was observed by Chen and Middleman [30] that the equilibrium density exhibits a maximum at $\frac{d}{\bar{d}_{32}} = 1.06$.

i.e. $$d^* = 1.06 \, \bar{d}_{32} \qquad (6.5.2)$$

Therefore, $$\left(\frac{d^*}{d_s}\right) = 1.06 \, C_5 \qquad (6.5.3)$$

Now, the transitional breakage probability $\Gamma(v)$ predicted by the model is given by

$$\Gamma(v) = \lambda \, \text{erfc} \left[\left(2(2^{1/3}-1)\right)^{1/3} 6^{2/3} \left(\frac{\sigma}{\rho}\right)^{1/2} \left(\frac{\pi}{6}\right)^{1/9} v^{-5/18}/2 \, \bar{\varepsilon}^{1/3} \right] \qquad (3.6)$$

Introducing the factor 0.2 in the argument of the complimentary error function,

$$\Gamma(v) = \lambda \operatorname{erfc}\left[0.2\left(2(2^{1/3}-1)\,\pi^{1/3}\,6^{2/3}\,\frac{\sigma}{\rho}\right)^{1/2} \left(\frac{\pi}{6}\right)^{1/9} v^{-5/18}/2\;\bar{\varepsilon}^{\,1/3}\right]$$

i.e. $$\Gamma(d) = \lambda \operatorname{erfc}\left[0.2\left(2(2^{1/3}-1)\,\pi^{1/3}\,6^{2/3}\,\frac{\sigma}{\rho}\right)^{1/2} \left(\frac{\pi}{6}\right)^{-1/6} d^{-5/6}/2\;\bar{\varepsilon}^{\,1/3}\right]$$

The maximum stable drop diameter d_s can now be defined as,

$$\frac{0.2\sqrt{a}\,\left(\frac{\pi}{6}\right)^{-1/6} d_s^{-5/6}}{2\,\bar{\varepsilon}^{\,1/3}} = 3.5 \qquad (6.5.4)$$

where $a = 2(2^{1/3}-1)\,\pi^{1/3}\,6^{2/3}\,\frac{\sigma}{\rho}$

i.e. $$d_s^{-5/3} = \frac{24.4}{(0.2)^2(2^{1/3}-1)6}\,\frac{\bar{\varepsilon}^{\,2/3}\,\rho}{\sigma} \qquad (6.5.5)$$

Since the empirical correlation of Chen and Middleman [30] would be used for the evaluation of $\left(\frac{d}{d_s}^*\right)$, the maximum stable drop diameter d_s should be calculated for the vessel geometry and impeller used by Chen and Middleman [30].

Power input for a baffled stirred vessel with turbine impeller [15,16] is given by

$$Pg_c = 6.3\,N^3L^5.$$

$\bar{\varepsilon} = \frac{Pg_c}{\frac{\pi}{4}T^2H} = 1.27\,N^3L^2$ for T=H and $\frac{L}{T} = 0.54$, the dimensional ratios being the same as those used by Chen and Middleman[30]. Using this relation for $\bar{\varepsilon}$, we get,

$$\left(\frac{d_s}{L}\right) = 0.0253\,N_{We}^{-0.6} \qquad (6.5.6)$$

Therefore, $\frac{d_{32}}{d_s} = 2.095$ or $\frac{d^*}{d_s} = 2.22$

i.e. $\alpha = 0.264$

As $B = 12.25$, $\sigma^2 = \frac{3}{25(\alpha B-1)} = 0.05351$ (6.5.7)

and $\sigma = 0.2313$ (6.5.8)

Therefore the equilibrium drop volume density in terms of $(d/\bar{d}_{32})$ is given by

$$f_v\left(\frac{d}{d_{32}}\right) = \frac{\bar{d}_{32}}{d^*} \frac{1}{\sqrt{2\pi}\cdot 0.2313} \exp\left[-\frac{\left\{\frac{1}{1.06}\frac{d}{\bar{d}_{32}} - 1\right\}^2}{0.10702}\right]$$

$$= \frac{1}{\sqrt{2\pi}\,(0.2313)(1.06)} \exp\left[-\frac{\left\{\frac{1}{1.06}\frac{d}{\bar{d}_{32}} - 1\right\}^2}{0.10702}\right] \quad (6.5.9)$$

6.5.2 Comparison of the Drop Volume Density Predicted by the Kinetic and Statistical Thermodynamic Models:

The equilibrium drop volume density predicted by the kinetic model as given by equation (6.5.9) is plotted in Figures 6.46 through 6.54. The equilibrium drop volume density predicted by the statistical thermodynamic model is also shown in Figures 6.46 through 6.54 for comparison. It can be seen that the equilibrium drop volume density predicted by these models agree very well with each other. It is very interesting to note that the equilibrium drop volume density arrived at through two entirely different approaches predict

more or less the same density. This could be viewed as vindication of both the models.

6.5.3 Comparison of the Predicted Equilibrium Drop Volume Density with the Experimental Data:

Figures 6.46 through 6.54 compare the experimental data with the predicted equilibrium drop volume density. The equilibrium drop volume density predicted by the coalescence - redispersion model [47] is also shown in Figures 6.46 through 6.54 for comparison. From Figures 6.46 through 6.51 it can be seen that the experimental drop volume density agrees fairly well with gaussian approximation. However, there is a shift of the experimental data towards small non-dimensionalized droplet sizes $d/\bar{d}_{32}$ compared to all the three models though the agreement with coalescence-redispersion model seems to be better. In Figures 6.46 through 6.51 the experimental drop volume density exhibits a maximum at around $d/\bar{d}_{32}=0.9$ in all the cases. This is in disagreement with the experimental observation of Chen and Middleman[30] who observed a maximum at $d/\bar{d}_{32} = 1.06$. The maximum value of the density in Figures 6.46 through 6.51 is around 1.8 in all the cases. Figure 6.52 compares the three models with the experimental data of Chen and Middleman [30]. The kinetic and statistical thermodynamic models agree well with the experimental data. Figure 6.53 compares the three models with the experimental data of Brown and Pit [36]. The agreement of

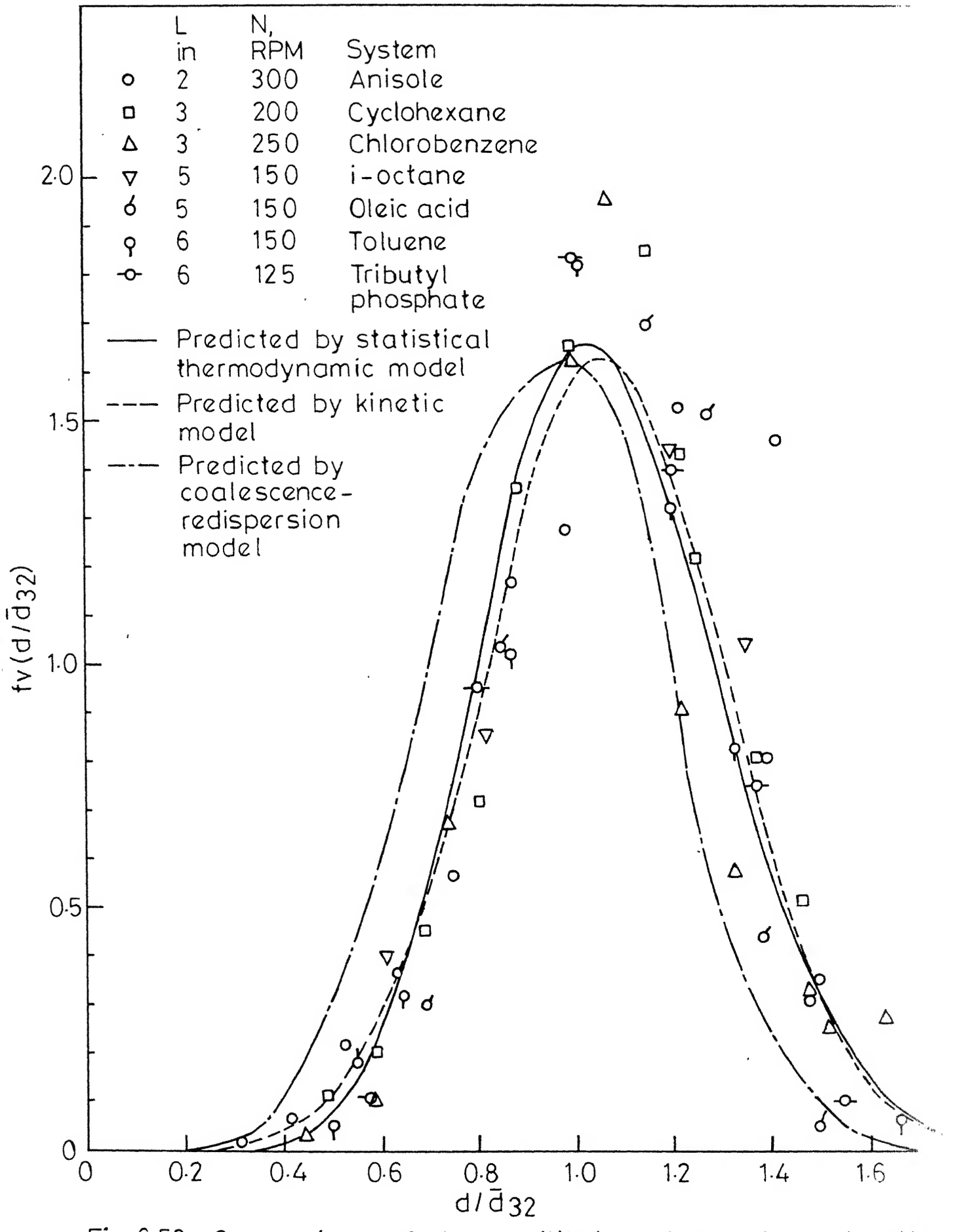

Fig.6.52 - Comparison of the equilibrium drop volume densit predicted by the present models with the data of Chen.H.T. and Middleman S.

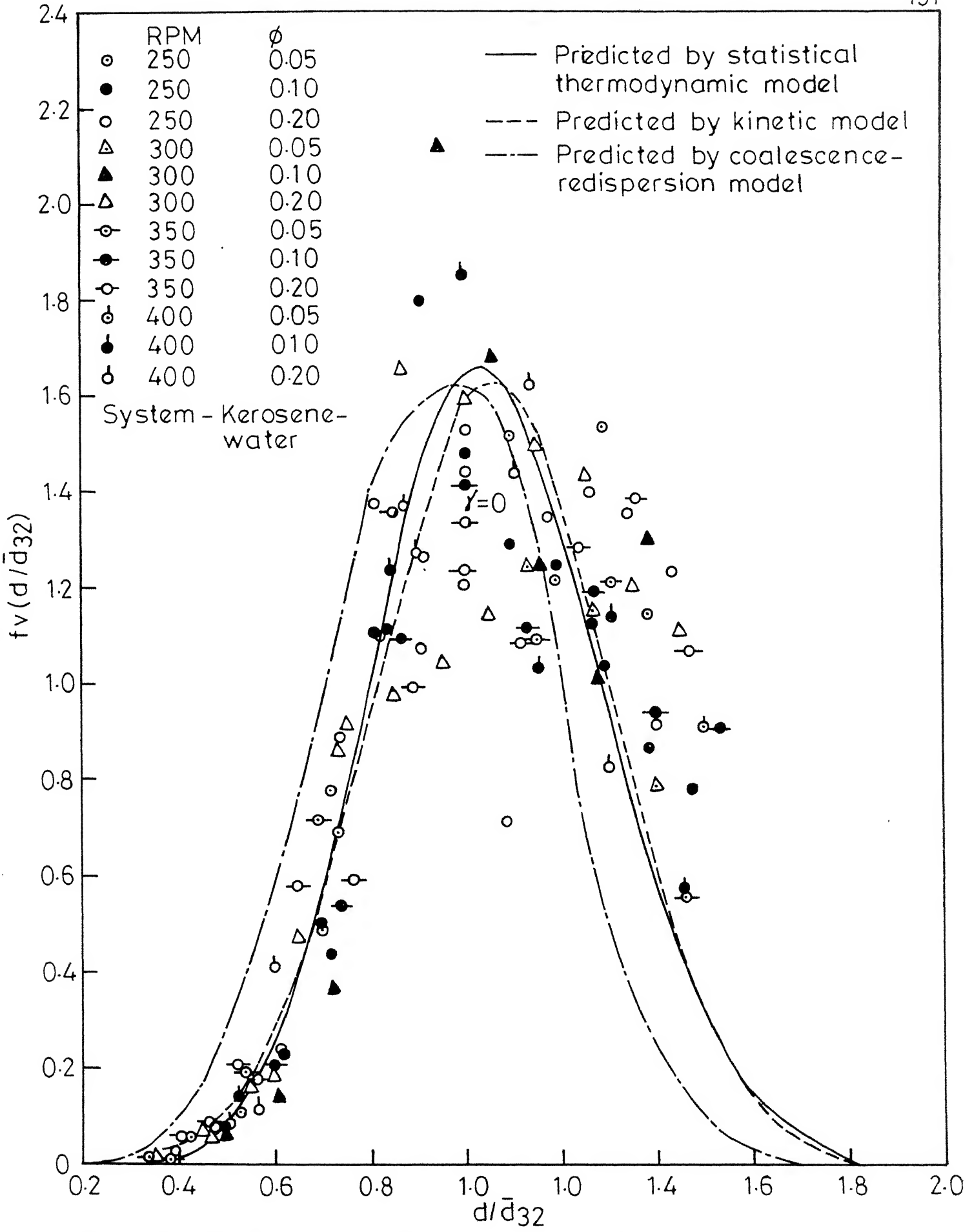

Fig.6·53 - Comparison of the equilibrium drop volume density predicted by the present models with the data

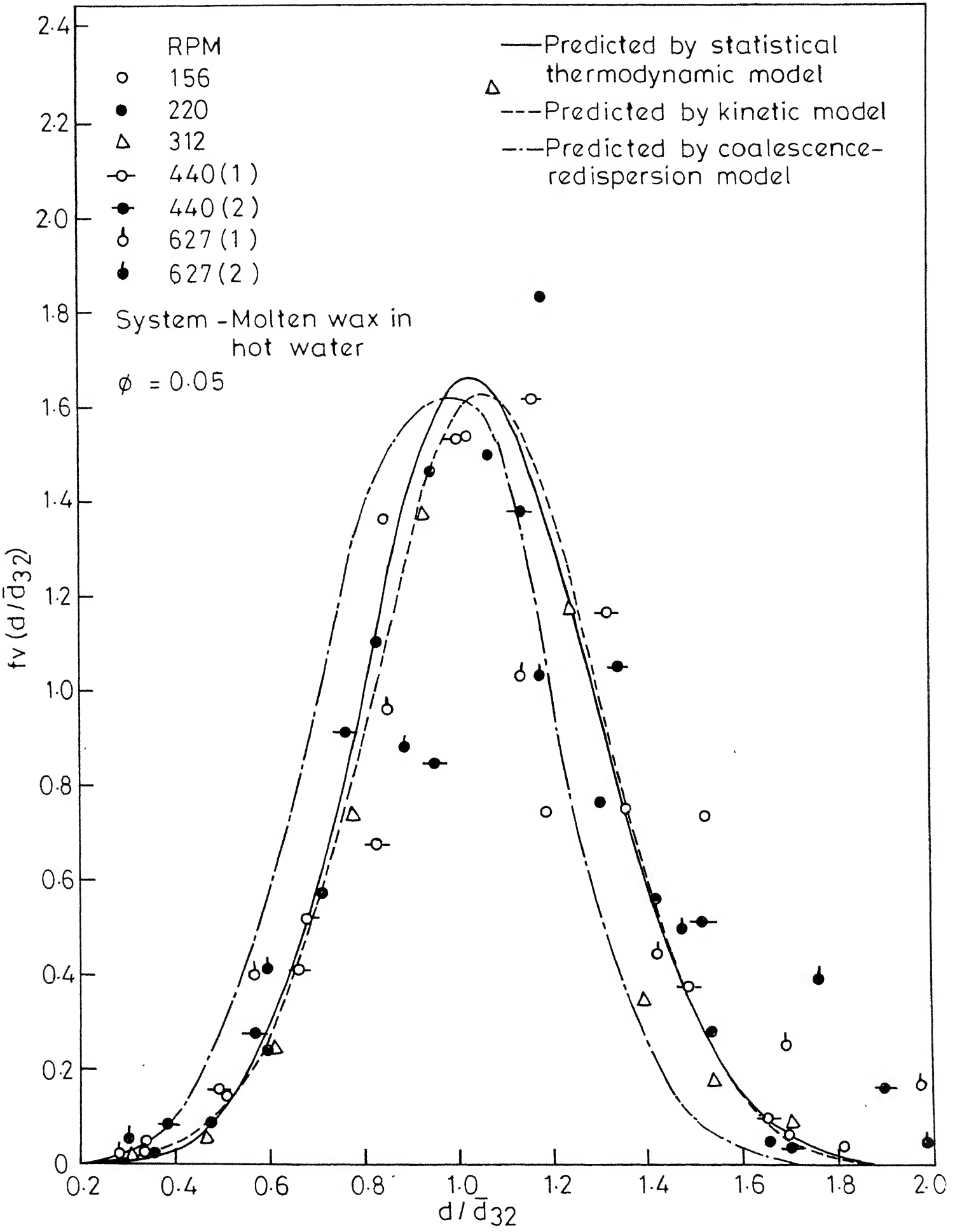

Fig.6·54 - Comparison of the equilibrium drop volume density predicted by the present models with the data of Shinnar.

the kinetic and statistical thermodynamic models with the experimental data is good only for small sizes i.e. $d/\bar{d}_{32} < 0.8$. This is because of a lot of scatter for large drop sizes i.e. for $d/\bar{d}_{32} > 0.8$. The scatter can be attributed to the experimental errors inherent in the experimental technique viz. photomicrography. Photomicrography directly gives the number density with respect to the drop diameter. Conversion of number density to volume density magnifies errors in the drop size measurement especially for large drop sizes as the conversion involves the evaluation of the third moment of the number density. In fact, only Brown and Pit [ ] have observed a bimodel equilibrium volume density for agitated lean liquid-liquid dispersions. This could also be due to the experimental errors. Figures 6.54 compares the three models with the experimental data of Shinnar [33]. The agreement between the kinetic and statistical thermodynamic models and the experimental data seems to be good except for the agitator speed of 627 RPM. From Figures 6.52 through 6.54 it can be observed that the coalescence-redispersion model does not agree with the experimental data of Chen and Middleman [30], Brown and Pit [36] and Shinnar [33]. Hence, it is found that there is a discrepancy between the present experimental observations of equilibrium drop volume density and the experimental data of Chen and Middleman [30], Brown and Pit [36] and Shinnar [33].

The validity of this correlation for the present experimental data is verified. Figures 6.55 and 6.56 show plots of $\bar{d}_{32}$ versus the agitator speed N and $\bar{d}_{32}$ versus the interfacial tension σ. Dotted straight lines of slopes -1.2 and 0.6 are shown in Figures 6.55 and 6.56 respectively for comparison of the correlation with the present experimental data. The sauter mean drop diameter $\bar{d}_{32}$ obtained from the present experimental data exhibits the functional dependence $\bar{d}_{32} \propto N^{-0.95}$ and $\bar{d}_{32} \propto \sigma^{0.64}$ as can be seen from Figures 6.55 and 6.56. Though the values of $\bar{d}_{32}$ obtained from the present work would have been higher due to experimental errors, the functional dependence of $\bar{d}_{32}$ on N and σ agreed fairly well with the correlation of Chen and Middleman [30]. This is probably the reason for the consistency of the experimental equilibrium drop volume density $f_v(d/\bar{d}_{32})$ in terms of non-dimensionalized drop size $d/\bar{d}_{32}$.

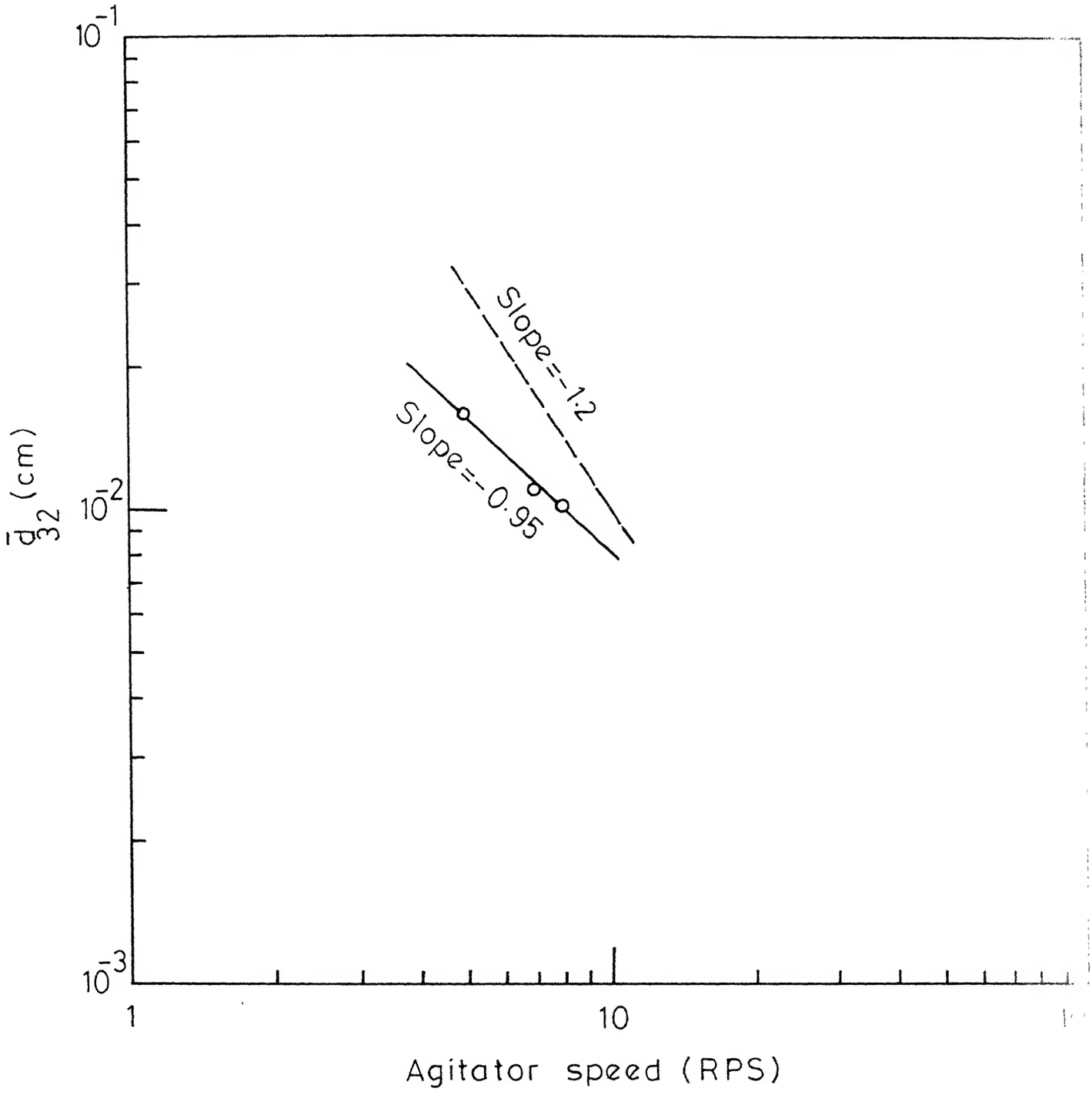

Fig. 6.55 - Plot of $\bar{d}_{32}$ versus agitator speed.

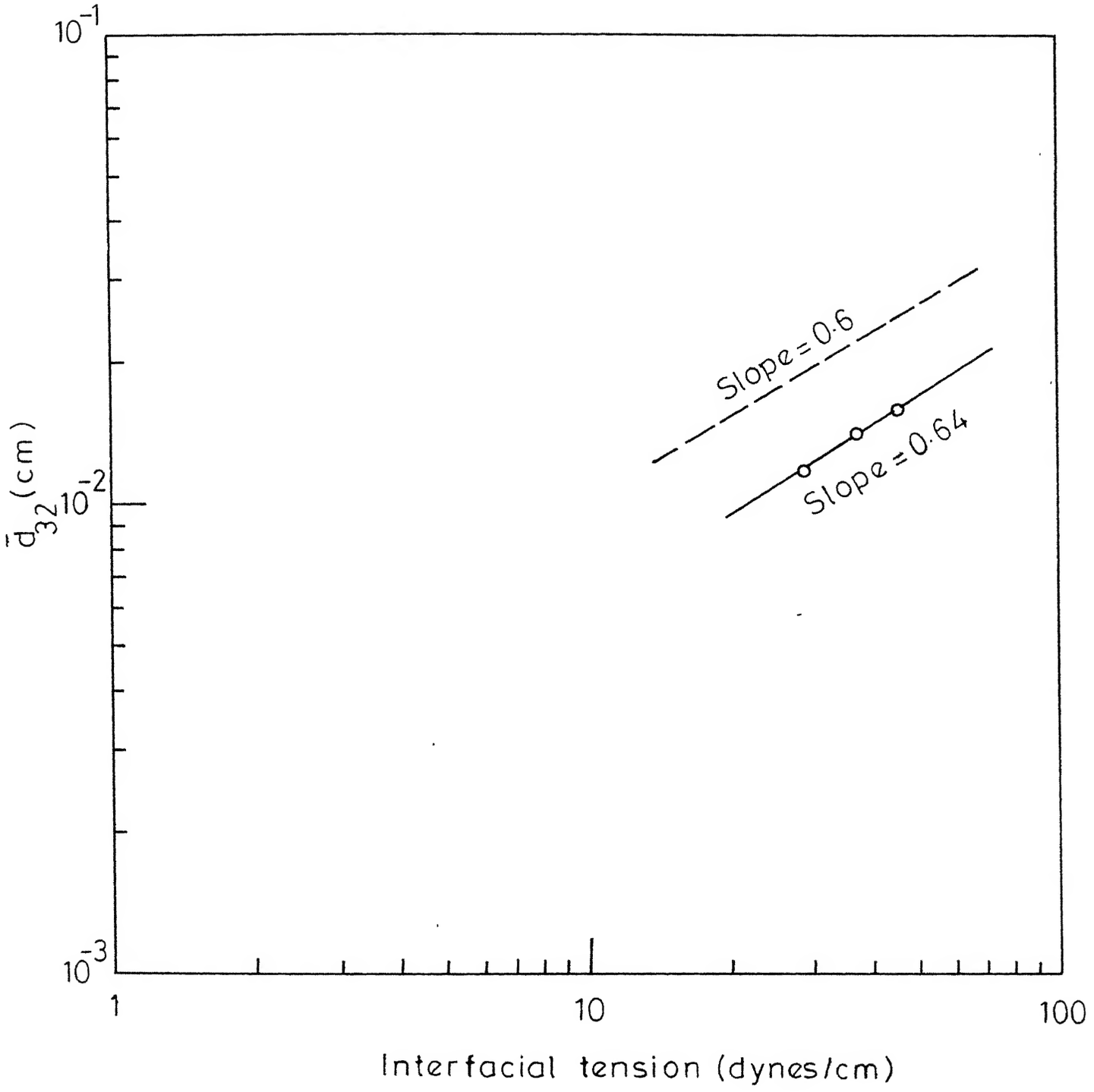

Fig. 6.56 - Plot of $\bar{d}_{32}$ versus interfacial tension.

CHAPTER 7

CONCLUSIONS AND RECOMMENDATIONS

An attempt has been made to study drop breakage in agitated lean liquid-liquid dispersions. Drop breakage in agitated lean liquid-liquid dispersions is random and hence is represented by related probabilities, namely, the transitional breakage probability and the daughter droplet distribution.

A model for transitional breakage probability of droplets in agitated lean liquid-liquid dispersion was proposed based on the mechanism of breakage of droplets due to their oscillations resulting from relative velocity fluctuations. The oscillating droplet was modelled as an undamped simple harmonic oscillator. The restoring action of the droplet due to the interfacial tension was represented by the restoring action of the spring of the simple harmonic oscillator. Fragmentation of the droplet was assumed to occur if the turbulent motion provides the minimum increase in the interfacial energy required for breakup. The velocity and pressure fluctuations occurring on the surface of a droplet were thought of as due to turbulent eddies 'striking' the surface of the droplet. It was postulated that the number of eddies arriving on the surface of the droplet is a poisson process. The probability density of relative velocity between

two points in an agitated vessel was assumed to be gaussian in the derivation of the transitional breakage probability. A universal transitional breakage probability in terms of non-dimensionalized drop diameter was derived for all dispersed phases whose density and viscosity are almost the same as that of the continuous phase. The maximum stable drop diameter derived from the model showed a dependence of $N_{We}^{-0.6}$. It was shown that the proposed transitional breakage probability could be approximated by a series of 'power law' models Kv^n with different exponents for different drop volume regions and that the value of the exponent increased with decrease in droplet volume. A functional relation for the rate constant K in the power law approximation Kv^n of the transitional breakage probability was derived in terms of the parameters and physical properties of the system. A universal non-dimensional drop volume distribution for agitated lean liquid-liquid dispersions was derived by analytical solution of the population balance equation simplified by order of magnitude estimates under the assumptions of constant coalescence frequency and uniform binary breakage. Interestingly enough, this analytical solution yielded a gaussian non-dimensionalized equilibrium drop volume density as suggested by Chen and Middleman [30].

The prediction of equilibrium drop size distribution by solution of population balance equation necessitates the

knowledge of breakage and coalescence. Even for lean dispersions, where the interaction between droplets is negligible, it is necessary to take coalescence into account which makes the population balance equation non-linear. Hence it becomes necessary to make simplifying assumptions for the population balance equation to be amenable to solution. Prediction of equilibrium drop size distribution from a statistical thermodynamic viewpoint overcomes this drawback as it considers only the total energy of the system i.e. the kinetic, potential and interfacial energies of droplets. A statistical thermodynamic model for equilibrium drop size distribution was proposed. As the interaction between droplets is negligible for a lean liquid-liquid dispersion, the system was assumed to consist of independent droplets. A canonical ensemble of droplets was considered in the derivation of equilibrium drop size distribution. The energy of a droplet was split into: (i) Kinetic energy of pulsating convective motion, (ii) Kinetic and potential energies of oscillation and (iii) Potential energy of a droplet at its spherical equilibrium shape. The energy of oscillation was calculated by viewing the oscillation of a droplet as forced oscillation of an incompressible sphere due to random periodic disturbing pressure acting at two diametrically opposite points on the surface of the sphere. Potential and kinetic energies of oscillation were represented in terms of a deformation

coordinate η and its conjugate momentum p_η. Potential energy of a droplet at its spherical equilibrium position was taken as the work done in transferring the dispersed phase reversibly from a bath of dispersed phase liquid at the same temperature, pressure and chemical potential as that of the continuous phase into the continuous phase in the form of a spherical droplet. A partition function for a droplet was derived. A droplet was found to have 6 degrees of freedom. Equilibrium drop size distribution was predicted from the partition function of a droplet. A universal non-dimensionalized drop volume density was derived in terms of dimensionless drop diameter $d/\bar{d}_{32}$.

Drop volume distributions in a batch agitated lean liquid-liquid dispersion eventually approach an asymptotic distribution in the similarity variable $(1+Kt)v^n$ if (i) the transitional breakage probability $\Gamma(v)$ follows a 'power law' Kv^n and (ii) the breakage is 'similar', i.e. the daughter droplet size distribution depends only on the ratio of the daughter and parent droplet volumes [4,53]. The existence of such a similarity transformation was made use of to verify the model for transitional breakage probability and also to obtain the exponent n, the rate constant K and the daughter droplet distribution from the transients of drop volume distribution in a batch agitated lean liquid-liquid dispersion.

Drop volume distribution measurements were made in a jacketted glass vessel agitated by a 6 blade paddle impeller. Measurements were made at the dispersed phase volume fraction of 0.1 per cent in order to minimise drop coalescence. Microencapsulation technique was employed to freeze the system at the time of measurement. This technique encapsulates the droplets with a thin nylon film formed as a result of an interfacial polycondensation reaction. The volume distribution of droplets was measured by means of electronic size analysis (Coulter Counter). Special probe assemblies consisting of platinum electrodes with aperture of 2 mm and 0.8 mm diameter were used to monitor the droplets. The pulse signals from the probe were processed and fed to a Multichannel analyser to give number count of droplets for different droplet volumes. This yielded the volume distribution of droplets.

Transients of drop volume distribution in agitated lean liquid-liquid dispersions were measured for water-CCl_4 + i-Octane (50-50 per cent) system at three different agitator speeds of 480, 420 and 300 RPM with 3 inch diameter paddle impeller and at the agitator speed of 480 RPM with 2 inch diameter paddle impeller. Transients of drop volume distribution were also measured at the agitator speed of 300 RPM with 3 inch diameter paddle impeller for water-Anisole + CCl_4 (80-20 per cent) and water-chlorobenzene systems. Experimental

results showed that the transitional breakage probability could be approximated by a 'power law' of varying exponents. Three distinct regions of exponents 1.0, 1.5 and 2.0 could be identified. The value of the exponents obtained from the experimental data agreed fairly well with the values of 1.08, 1.42 and 2.12 obtained from the approximation of the predicted transitional breakage probability by a series of 'power law' models of varying exponents. The intermediate value of around 1.8 obtained for the exponent for water-chlorobenzene and water-Anisole + CCl_4 (80-20 per cent) systems in region II is believed to be due to overlapping of two regions.

As the transitional breakage probability $\Gamma(v)$ could be approximated by a series of 'power law' models with different values of exponent for different droplet volume range and for each of these regions $Kv^n \cdot t$ is the similarity transformation which would collapse all the drop volume distributions in that region into a single curve, one would expect that a transformation $\Gamma(v) \cdot t$ would collapse all the drop volume distributions at all times into a single curve irrespective of their region if the model for transitional breakage probability is indeed valid. However, the computations of $\Gamma(v)$ as predicted by the model yielded very large values of maximum stable drop volume v_s. Therefore a factor of 0.2 was introduced in the arguement of the

complementary error function in order to match the variation of the proposed transitional breakage probability with droplet volume in the range of drop volumes encountered with experimentally observed variation. It is believed that the introduction of this factor is necessary to account for the important inhomogeneities in the flow field of an agitated vessel. The transformation

$$\text{erfc}\left[\left\{2(2^{1/3}-1)\,\pi^{1/3}\,6^{2/3}\,\frac{\sigma}{\rho}\right\}^{1/2}\left(\frac{\pi}{6}\right)^{1/9}\nu^{-5/18}\varepsilon^{-1/3}\right]\cdot t$$

seems to collapse all the drop volume distributions more or less into a single curve thus vindicating the model for the transitional breakage probability.

The drop volume distributions in a region were transformed using a modified similarity transformation $(\frac{v}{\bar{v}})\cdot t^{1/n}$, $\bar{v}$ and n being an average drop volume and the exponent of 'power law' approximation of transitional breakage probability for that region respectively. The similarity transformation $(\frac{v}{\bar{v}})t^{1/n}$ collapses all the drop volume densities in a region into a single curve thus vindicating the assumption of 'similar breakage' made in the derivation of the similarity transformation. Hence the moments of the function Kg(x) were computed from the moments of the modified drop volume density f $\{(\frac{v}{\bar{v}})\cdot t^{1/n}\}$. The function Kg(x) was then estimated from its moments through orthonormal polynomial expansion with the weighting function $(3x^2-2x^3)$. The rate constant K of 'power law' approximation

Kv^n of the transitional breakage probability was then estimated from Kg(x). The estimation of the daughter droplet size distribution g(x) was found to be only qualitative which is believed to be due to the inclusion of insufficient number of terms in the orthonormal polynomial expansion. Inclusion of more terms in the polynomial expansion was desisted due to the inaccuracies involved in the evaluation of higher moments of modified drop volume density $f\{(\frac{v}{\bar{v}}).t^{1/n}\}$. The estimated daughter droplet distribution g(x) indicated that (i) the breakage mechanism seems to be the same for all systems and experimental conditions (ii) the normalised daughter droplet density is more or less same for all the cases and (iii) the daughter droplet density is broad. The functional dependence of the estimated rate constant K with respect to the agitator speed and interfacial tension agrees well with the model.

Equilibrium drop volume distributions were measured for water-CCl_4+i-Octane (50-50 per cent) system at the agitator speeds of 420 and 300 RPM with 3 inch diameter paddle impeller and at the agitator speed of 480 RPM with 3 inch as well as 2 inch diameter paddle impellers. Measurements of equilibrium drop volume distributions were also made at the agitator speed of 300 RPM with 3 inch diameter paddle impeller for water-Anisole + CCl_4 (80-20 per cent) and water-chlorobenzene systems. The measured non-dimensionalized

equilibrium drop volume density $f_V(d/\bar{d}_{32})$ was compared with the density predicted by (i) Kinetic model (ii) statistical thermodynamic model and (iii) Coalescence-redispersion model. The non-dimensionalized equilibrium drop volume density $f_V(d/\bar{d}_{32})$ predicted by the kinetic and statistical thermodynamic models agree very well with each other. It is very interesting to note that the equilibrium drop volume distribution arrived at through two entirely different approaches predict more or less the same density. This could be viewed as vindication of both the models. The experimental non-dimensionalized drop volume density $f_V(d/\bar{d}_{32})$ agreed fairly well with the gaussian approximation. However, there is a shift in the experimental drop volume density towards smaller dimensionless drop diameter $(d/\bar{d}_{32})$ when compared with the kinetic and statistical thermodynamic models and the agreement with the coalescence-redispersion model seems to be better. Comparison of the non-dimensionaliz equilibrium drop volume density predicted by these models with the experimental data of Chen and Middleman [30], Brown and Pit [36] and Shinnar [33] showed that the experimental data agreed fairly well with the kinetic and statistical thermodynamic models and that the coalescence-redispersion model did not agree with the experimental data. Hence it was found that there is a discrepancy between the present experimental data of equilibrium drop volume density and the

experimental data of Chen and Middleman [30], Brown and Pit[36] and Shinnar [33]. The reason for this discrepency could be the loss of count of very small voltage pulses corresponding to droplets of very small volumes due to poor signal to noise ratio for these droplets. The variation of the measured sauter mean drop diameter $\bar{d}_{32}$ with agitator speed and interfacial tension agreed fairly well with the correlation of Chen and Middleman [30].

The experimental verification of the model for transitional breakage probability and the inferrence of daughter droplet distribution attempted in the present work is limited to agitated lean liquid-liquid dispersions with paddle impeller and a few dispersed phases. It is necessary to conduct similar experiments for more number of systems and different types of impellers in order to establish the validity of the present model for transitional breakage probability more firmly. Since the hydrodynamic characteristics of the flow field in a continuous well-stirred vessel is more or less same as that in a batch well stirred vessel, it is believed that the present model for the transitional breakage probability should also hold good for continuous systems. Ramkrishna [4] has shown the method of prediction of steady state drop volume distribution in a continuous agitated lean liquid-liquid dispersion with the knowledge of transitional breakage

probability, daughter droplet distribution and inlet drop size distribution. It may be necessary to make measurements of steady state drop volume distribution in a continuous agitated lean liquid-liquid dispersion with known inlet drop size distribution in order to verify the validity of the present model for transitional breakage probability in continuous systems. The final objective of the study of drop breakage in agitated lean liquid-liquid dispersions is to predict rate processes in liquid-liquid dispersions by taking the simultaneity of heat and/or mass transfer and droplet phenomena into account. The present model for transitional breakage probability, if found satisfactory for continuous agitated lean liquid-liquid dispersions, could be used to predict the mass transfer rate of a solute from the dispersed phase into the continuous phase [1], in a continuous agitated lean liquid-liquid dispersion. Experiments could be conducted to simulate a stage of a continuous multi-change extractor and the steady state mass transfer rates could be measured and compared with the theoretical predictions.

REFERENCES

1. Shah, B.H. and Ramkrishna, D., Chem. Eng. Sci., 1973, 28, 389.
2. Ramkrishna, D., Paper presented at 71st National Meeting of the American Institute of Chemical Engineers, February 1972 at Dallas, Texas, U.S.A.
3. Valentes, K.J., Bilous, O. and Amundson, N.R., Ind. Eng. Chem. Fund., 1966, 5, 271.
4. Ramkrishna, D., Chem. Eng. Sci., 1974, 29, 987.
5. Giffen, E., and Muraszew, A., 'The Atomisation of Liquid Fuels', Chapman and Hall Ltd., London (1953).
6. Clayton, W., 'The Theory of Emulsions and Their Technical Treatment', 5th edition, J.A. Churchil, Ltd., London (1954).
7. Squire, H.B., British Journal of Appl. Phys., 1953,4,167.
8. Hinze, J.O., A.I.Ch.E.J., 1955, 1, 289.
9. Taylor, G.I., Proc. Roy. Soc., 1934, A146, 501.
10. Tomotika, Proc. Roy. Soc., 1935, A150, 322.
11. Rumscheidt, F.D. and Mason, S.G., J.Colloid Sci., 1961, 16, 238.
12. Holland, F.A. and Chapman, F.S., 'Liquid Mixing and Processing in Stirred Tanks', Chapman and Hall Ltd., London (1966).
13. Hyman, D., 'Mixing and Agitation', 'Advances in Chemical Engg.', Vol.3, p.120.
14. Nagata, S., Yamamoto, K., Hashimoto, K. and Naruse, Y., Mem. Fac. Eng. Kyoto, 1959, 21, 260.

15. Rushton, J.H., Costich, E.W., and Everett, H.J., Chem. Eng. Progr., 1950, 46, 395.

16. Rushton, J.H., Costich, E.W., and Everett. H.J., ibid, 1950, 46, 467.

17. Holmes, D.B., Voncken, R.M., and Dekker, J.A., Chem. Eng. Sci., 1964, 19, 201.

18. Cutter, L.A., A.I.Ch.E.J., 1966, 12, 35.

19. Schwartzberg, H.G. and Treybal, R.E., Ind. Eng. Chem. Fund., 1968, 7, 1.

20. Kim, W.J. and Manning, F.S., A.I.Ch.E.J., 1964, 10,747.

21. Mujumdar, A.S., Huang, B., Wolf, D., Weber, M.E. and Doughlas, W.J.M., Can. J. Chem.Eng., 1970, 48, 475.

22. Komasawa, I., Kuboi, R. and Otake, T., Chem. Eng. Sci., 1974, 29, 641.

23. Ananda Rao, M. and Broadkey, R.S., Chem.Eng. Sci., 1972, 27, 137.

24. Günkel, A.A. and Weber, M.E., A.I.Ch.E.J., 1975, 21, 931.

25. Chao, S.H., Amarnath, P.H., and Becker, H.A., Paper presented at the 21st Canadian Chemical Engg. Conference, Montreal, Canada, (Oct.1971).

26. Gal-Or, B., Klinzing, G.E. and Tavlarides, L.L., Ind. Eng. Chem., 1969, 61, 21.

27. Tavlarides, L.L., Coulaloglou, C.A., Zeitlin, M.A., Klinzing, G.E. and Gal-Or, B., Ind. Eng.Chem., 1970,62,6.

28. Shinnar, R. and Church, J.M., Ind. Eng. Chem., 1960, 52, 253.

29. Levich, V., 'Physicochemical Hydrodynamics', Prentice-Hall Inc., (1962).

30. Chen, H.T., and Middleman, S., A.I.Ch.E.J., 1967,13, 989.

31. Vermuellen, Theodore, Williams, G.M. and Langlois, G.E., Chem. Eng. Progr., 1955, 51, 85F.

32. Calderbank, P.H., Trans. Inst. Chem. Engs., 1958, 36, 43.

33. Shinnar, R., J. Fluid Mech., 1961, 10, 259.

34. Sprow, F.B., Chem.Eng. Sci., 1967, 22, 435.

35. Rodger, W.A., Trice, V.G. and Rushton, J.H., Chem. Eng. Progr., 1956, 52, 515.

36. Brown, D.E. and Pitt, K., Chem.Eng. Sci., 1972,27, 577.

37. Sprow, F.B., A.I.Ch.E.J., 1967, 13, 995.

38. Vandervoen, J.H., M.S. Thesis, University of California(1960).

39. Mlynek, Y. and Resnick, W., A.I.Ch.E.J., 1972, 18, 122.

40. Park, J.Y. and Blair, L.M., Chem.Eng. Sci., 1975, 30, 1057.

41. Schindler, H.D. and Treybal, R.E., A.I.Ch.E.J., 1968,14,790.

42. Coulaloglou, C.A. and Tavlarides, L.L., A.I.Ch.E.J., 1976, 22, 289.

43. Hulbert, H.M. and Katz, S.L., Chem. Eng. Sci., 1964, 19, 555.

44. Curl, R.L., A.I.Ch.E.J., 1963, 9, 175.

45. Baynes, C.A., and Laurence, R.L., Ind. Eng. Chem. Fund., 1969, 8, 71.

46. Valentes, K.J. and Amundson, N.R., Ind. Eng. Chem. Fund., 1966, 5, 533.

47. Bajpai, R.K., Ramkrishna, D. and Prokop, A., Chem. Eng. Sci., 1976, 31, 913.

48. Steidl, H., Collection, Czech. Chemical Communication, 1968, 33, 2191.

49. Collins, S.B. and Knudson, J.G., A.I.Ch.E.J., 1970,16, 1072.

50. Zeitlin, M.A. and Tavlarides, L.L., Can. Jour. Chem. Eng., 1972, 50, 207.

51. Swift, D.L. and Friedlander, S.K., J.Colloid Sci., 1964, 19, 621.

52. Kapur, P.C., Chem. Eng. Sci., 1970, 25, 899.

53. Fillipov, A.F.; Theory of Prob. and Applic., 1961, 6, 275.

54. Madden, A.J. and McCoy, B.J., Chem. Eng. Sci., 1969, 24, 416.

55. Coulaloglou, C.A. and Tavlarides, L.L., Chem. Eng. Sci., 1977, 32, 1289.

56. Batchelor, G.K., Proc. Camb. Phil. Soc., 1951, 47, 359.

57. Erickson, L.E., Fan, L.T., Shah, P.S. and Chen, M.S.K., Biotech. Bioeng., 1970, 12, 713.

58. Khinchin, A.I., 'Mathematical Foundations of Statistical Mechanics', Dover Publications, Inc., N.Y. 1949.

59. Landau and Lifshitz, 'Fluid Mechanics', Course of Theoretical Physics, Volume 6, Pergamon Press, p 239.

60. Berg, R.H., 'Electronic Size Analysis of Sub-Sieve Particles by Flowing Through a Small Liquid Resistor', Symposium on Particle Size Measurement, Sixty-First Annual Meeting Papers ASTM Special Technical Publication No.234, p.245.

61. Allen, T., 'Particle Size Measurement', Chapman and Hall Ltd., The Macmillen Co., N.Y. (1959).

62. Fernandes, J.B. and Sharma, M.M., Chem.Eng. Sci., 1967, 22, 1267.

63. Mack, D.E. and Kroll, A.E., Chem.Eng. Prog., 1948, 44, 189.

64. Morgan, P. and Kwolek, S.L., J. Poly.Sci., 1959, 40, 289.

APPENDIX I

ORDER OF MAGNITUDE ESTIMATES OF THE POPULATION BALANCE EQUATION

For an equilibrium distribution narrow around the maximum stable drop diameter d_s, we can divide the distribution into three zones as shown in Figure I.1.

Zone I: Zone of droplets of small volume, $\xi << 1$.

Zone II: Zone, where most of the distribution is concentrated, $\xi \sim 1$.

Zone III: Zone of droplets of large volume $\xi >> 1$.

For Zone I the population balance equation at equilibrium in non-dimensionalized volume is

$$0 = 2 \int_x^\infty \gamma(x') \frac{F(x')}{x'^2} dx' - \mu \frac{F(x)}{x} \int_0^\infty \frac{F(x')}{x'} dx' \quad (I.1)$$

as i) droplets do not break in Zone I, ii) production of droplets in Zone I due to coalescence of smaller drops is negligible. Differentiating (I.1) w.r.t. x

$$0 = -2 \gamma(x) \frac{F(x)}{x^2} - \mu \kappa \frac{d}{dx} \left[\frac{F(x)}{x}\right]$$

For $x \varepsilon I$, $\gamma(x) = 0$ so that $\frac{d}{dx} \left[\frac{F(x)}{x}\right] = 0$ and we write

$$F(x) = nv^* x$$

where n = Number of droplets in Zone I per unit interval of non-dimensionalized drop volume x.

Thus

$$f(\xi) = 3 nv^* \xi^5 \quad (I.2)$$

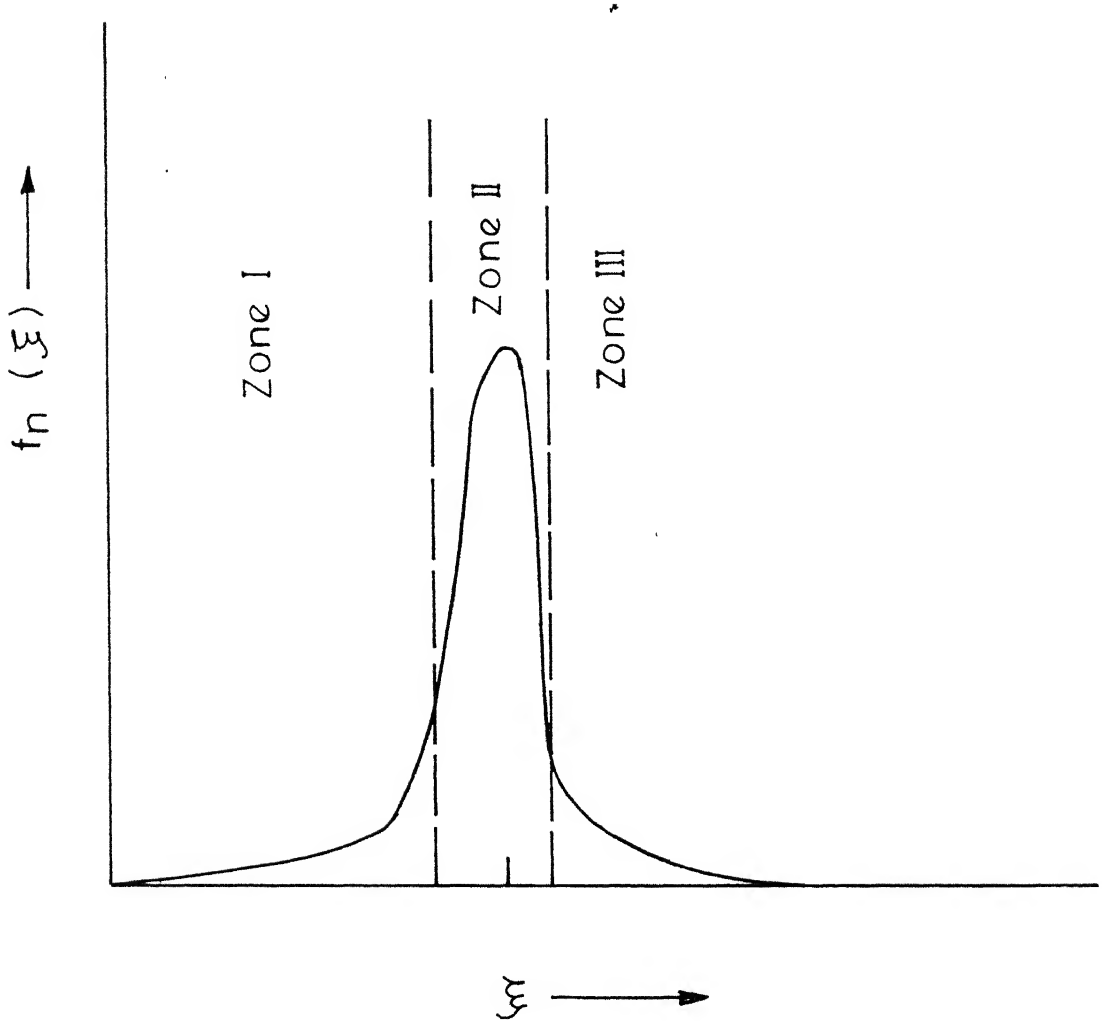

Fig. I.1 - Different zones of equilibrium drop volume density.

From (I.1) we have

$$0 = 2\int_{\xi}^{\infty} \gamma(\xi') \frac{f(\xi')}{\xi'^{6}} d\xi' - \frac{\mu f(\xi)}{3\xi^{5}} \int_{0}^{\infty} \frac{f(\xi')}{\xi'^{3}} d\xi'$$

so that dividing by dispersed phase fraction V

$$\int_{\xi}^{\infty} \gamma(\xi') \frac{f_n(\xi')}{\xi'^{6}} \cdot d\xi' \sim \frac{\mu}{2} \frac{f(\xi)}{3\xi^{5}} \int_{0}^{\infty} \frac{f_n(\xi')}{\xi'^{3}} d\xi' \qquad (I.3)$$

$$\xi \varepsilon I$$

Since $f_n(\xi)$ is concentrated around $\xi=1$, taking the order of magnitude of terms in (I.3)

$$\gamma(\xi) \sim \frac{\mu}{2} nv^* \qquad \text{where } \xi \varepsilon \text{ I or II}$$

or

$$\mu \sim \frac{2\gamma(\xi)}{nv^*} = \frac{2\gamma(\xi)x'}{nv^* x'} \qquad x' \varepsilon I \qquad (I.4)$$

Since nv^*x' is the volume of drops in unit non-dimensionalized volume interval around $x' = \xi'^3$ we may write from (I.4)

$$\mu \sim \frac{2\gamma(\xi)\, x'}{\Delta V} \qquad x' < 1,\ \Delta \ll 1$$

or equivalently $\mu \gg \gamma(\xi)$.

Since $\gamma(\xi) = A \exp\left[-B\,\xi^{-5/3}\right]$ it can easily be seen that for $\xi \varepsilon$ II

$$\gamma'(\xi) \sim \frac{5B}{3} \gamma(\xi) \sim 20\, \gamma(\xi) \qquad (I.5)$$

Now $$f_n'(\xi) \sim \frac{1}{|\xi - 1|} \qquad (I.6)$$

and

$$\int_{0}^{\infty} \frac{f_n(\xi')}{\xi'^{3}} d\xi' = \frac{K}{V} \sim 1 \qquad (I.7)$$

For Zone II, the population balance equation is given by Eq.(3.2.7), which on division by V^2 yields

$$0 = \underbrace{\frac{\gamma(\xi) f_n(\xi)}{V\xi}}_{I} - \underbrace{\frac{1}{V}\gamma'(\xi)\, f_n(\xi)}_{II} - \underbrace{\frac{\gamma(\xi) f_n'(\xi)}{V}}_{III}$$

$$+ \frac{\mu}{2}\,\frac{\xi^5}{V}\underbrace{\int_0^{\xi} \frac{f(\xi')}{\xi'^3}\,\frac{d}{d\zeta}\left[\frac{f_n(\zeta)}{\zeta^5}\right] d\xi'}_{IV} - \underbrace{\frac{\mu\kappa}{V} f_n'(\xi)}_{V} +$$

$$+ \underbrace{\frac{5\,\mu\kappa}{V}\,\frac{f_n(\xi)}{\xi}}_{VI} \qquad (I.8)$$

We now consider the coalescence integral for $\xi \in II$

$$I = \int_0^{\xi} \frac{f(\xi')}{\xi'^3}\,\frac{d}{d\zeta}\left[\frac{f_n(\zeta)}{\zeta^5}\right] d\xi'$$

The contribution to this integral can come from any one of the following cases:

(i) $\xi' \in I$, $\zeta \in II$; (ii) $\xi' \in II$, $\zeta \in I$; (iii) $\xi' \in I$, $\zeta \in I$.

If we denote the corresponding values of I by $I_{(i)}$, $I_{(ii)}$, and $I_{(iii)}$, then from (I.2) we have

$$\frac{d}{d\zeta}\left[\frac{f_n(\zeta)}{\zeta^5}\right] = 0$$

which implies that $I_{(ii)} = I_{(iii)} = 0$ so that $I = I_{(i)}$.

or

$$I = \int_0^{\xi} 3nv^*\xi'^2\,\frac{d}{d\zeta}\left[\frac{f_n(\zeta)}{\zeta^5}\right] d\xi', \quad \xi' \in I, \quad \zeta \in II$$

Considering the order of magnitude of different terms in (I.8) it can be shown that

$$I \sim \frac{\gamma(\xi)}{V}; \quad II \quad \frac{20\gamma(\xi)}{V}; \quad III \sim \frac{\gamma(\xi)}{V} \frac{1}{|\xi-1|}$$

$$IV \sim \frac{2\gamma(\xi)}{V} \frac{\xi'^3}{|\xi-1|}; \quad V \sim \frac{2\gamma(\xi)\kappa\xi'^3}{\Delta V^2 |\xi-1|}; \quad VI \sim \frac{5\gamma(\xi)\kappa\xi'^3}{\Delta V^2}$$

where $\xi = 1$, $\xi' \ll 1$, $\Delta \ll 1$, and $\Delta \ll \xi'^3$. From these estimates it is clear that the coalescence integral IV is of a smaller order of magnitude than the other terms in (I.8).

APPENDIX II

CALIBRATION OF THE PROBES

Ten samples of narrow distribution of spherical glass particles in the size range of 50 to 800 microns were used for the calibration of the probes. Average particle volume of a sample was measured through microscopic counting. A slide of the sample was prepared and the number counts of particles of different sizes were measured by viewing the sample through microscope. The average particle volume of the sample was calculated from the measured number density.

It was necessary to calibrate the Multichannel analyser prior to the calibration of the probes in order to get the relationship between the channel number and the pulse amplitude. Voltage pulses of variable amplitude were fed from ORTEC precision pulse generator to the MCA. The pulses had a very small rise time and hence were acceptable to the MCA. Since the voltage pulses from the precision pulse generator were of the same amplitude, the pulses were logged in one particular channel corresponding to the pulse amplitude. Figure II.1 shows the plot of channel number versus pulse amplitude. The relationship is linear as can be seen from Figure II.1. By least square fit the equation of the straight line is

$$y = 18.82\ x - 0.7775 \qquad \text{(II.1)}$$

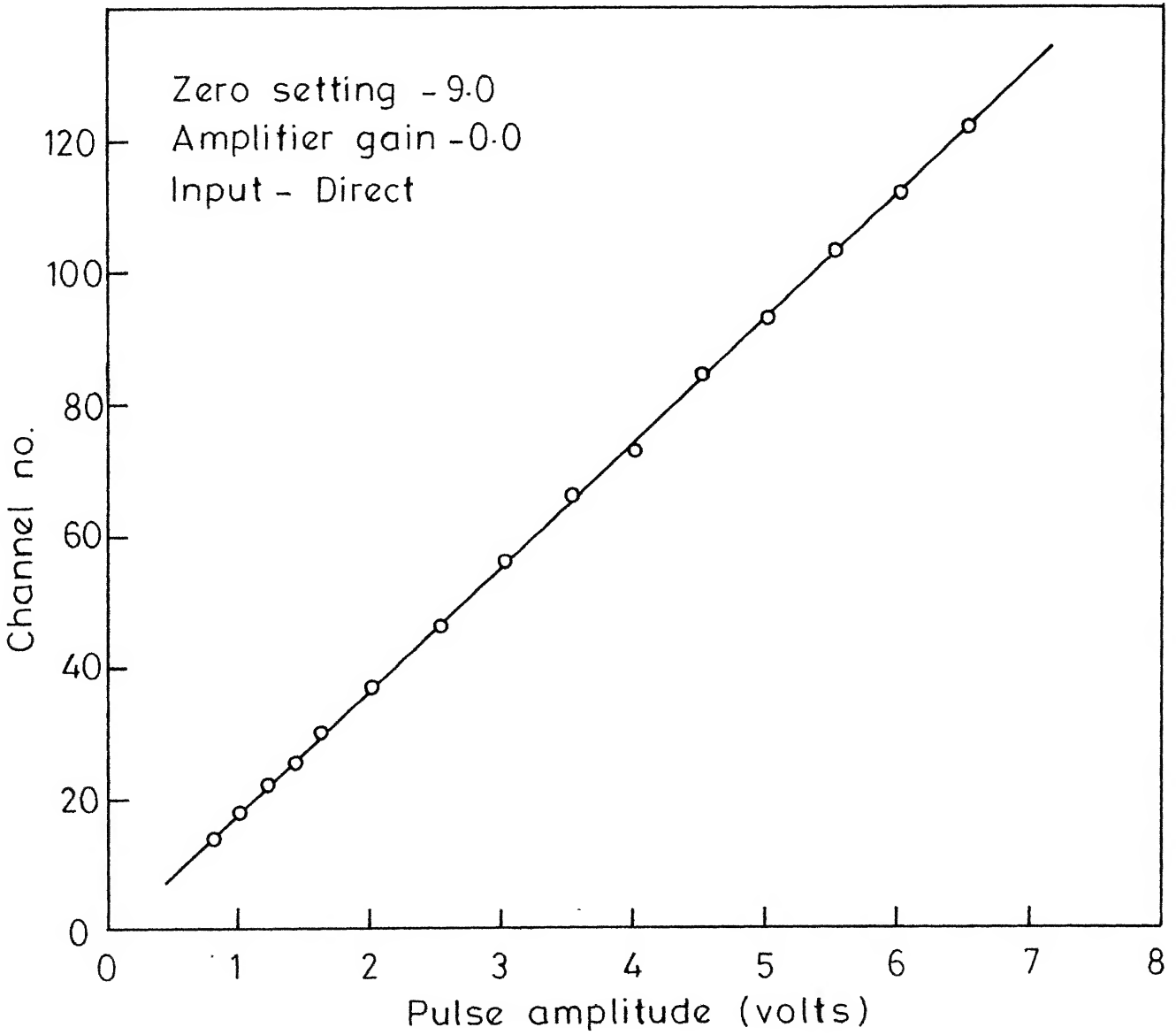

Fig. II.1 - Calibration curve for MCA.

where y = channel number

and x = pulse amplitude in volts

In equation (II.1) the intercept-0.7775 refers to the channel number corresponding to a pulse of zero volts.

A sample of narrow distribution of spherical glass particles was suspended in a conducting medium of NaCl solution. The probe to be calibrated was immersed in the suspension. The probe was filled with the conducting medium by withdrawing NaCl solution into the probe through the application of vacuum. Current and gain settings were adjusted. The electrophoresis power supply was put on to apply 60 volts D.C. between the electrodes. Now, a sample of the suspension was withdrawn through the aperture by slowly opening the stopcock connected to the vacuum pump. The amplitude of the amplified voltage pulses were observed in the oscilloscope. If the pulses were not in the proper range, current and gain settings were readjusted to get voltage pulses in the proper range. The output from the pulse shaper was logged in the MCA and the spectrum of the sample was taken. The average channel number of the spectrum was calculated from the printout of the MCA. Since the sample was a narrow distribution of glass particles, the average channel number should correspond to the average particle volume of the sample. Since the pulses from the probe were amplified prior to the analysis by the MCA,

comparison of the channel numbers for samples of different average particle volumes could be done only if the amplification factor is maintained constant. Hence the average channel number of the spectrum was converted to a base value corresponding to a current of 1 mA and the amplifier gain of 100. The same procedure was repeated for different samples at the same NaCl concentration to get a set of readings at a particular resistivity of the medium. In all the readings, the D.C. voltage across the electrodes at the reference current of 1 mA was measured. Since the resistivity of the medium was maintained constant for a set of readings, D.C. voltage also was constant. In effect, the D.C. voltage across the electrodes at the reference current of 1 mA corresponds to the resistivity of the medium. In all the observations, it was ensured that the average particle size of the sample did not exceed 40 per cent of the aperture diameter of the probe in order to avoid deviations from linear volumetric response. Since -0.7775 was the intercept in the calibration curve for the MCA, the set of average channel number and the corresponding average particle volume was fitted to a straight line

$$y = mx - 0.7775$$

where y = Average channel number

and x = Average particle volume

From equation (5.2.1), we see that the amplitude of the pulse from the probe is proportional to the resistivity of the medium if the resistivity of the particle is very much higher than that of the medium. Therefore the same set of observations were made at different NaCl concentrations to obtain the effect of the resistivity of the medium. Since the D.C. voltage across the electrodes corresponds to the resistivity of the medium, one would expect the slope m to be a linear function of the D.C. voltage. Figures II.2 and II.3 give the plots of average channel number versus particle volume for probes I and II for different D.C. voltages. The insets in Figures II.2 and II.3 give the plot of the slope versus the D.C. voltage.

The relationship between the channel number and particle volume obtained through least square fit for both the probes are given by,

Probe I of aperture diameter 2 mm:

$$y + 0.7775 = (0.02345\ V + 1.3041)\ x \qquad \text{(II.2)}$$

Probe II of aperture diameter 0.8 mm:

$$y + 0.7775 = (0.16925\ V + 15.8227)\ x \qquad \text{(II.3)}$$

where y = Channel number

x = Particle volume (CC x 10^6)

V = D.C. voltage (volts)

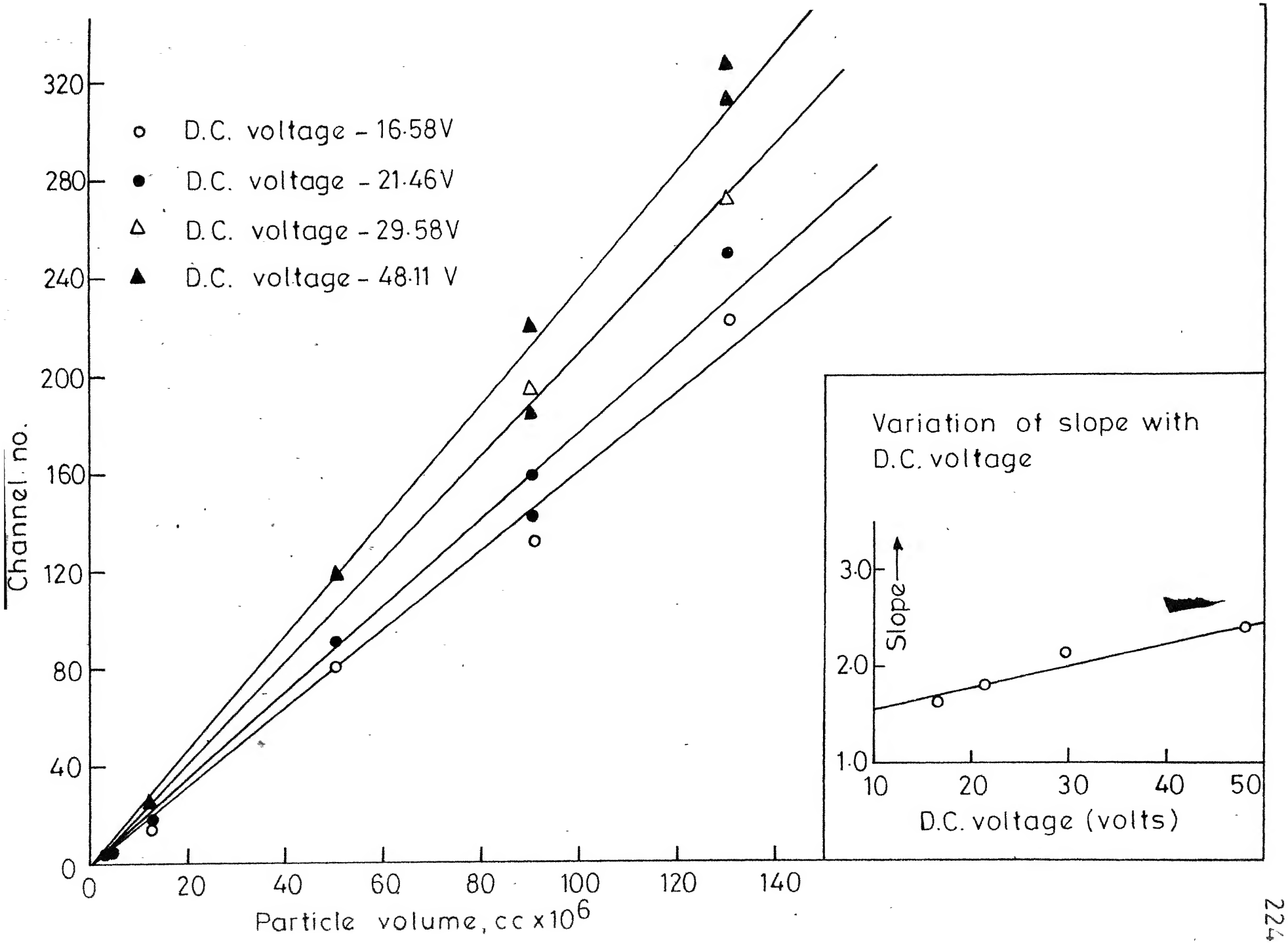

Fig II 2 - Calibration curve for probe I

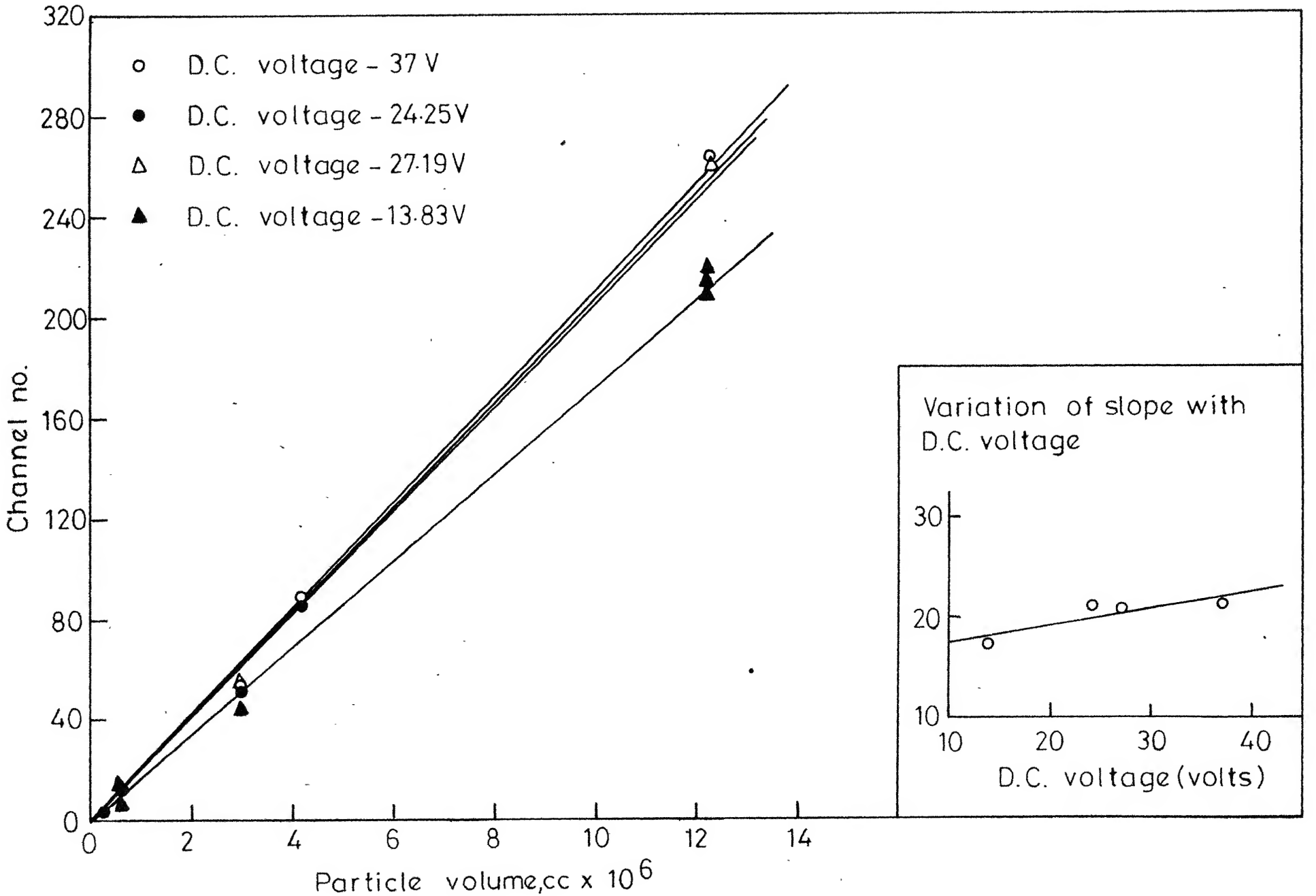

Fig. II. 3 - Calibration curve for probe II.

Since this relationship is obtained for the reference current of 1 mA, amplifier gain of 100 and unit attenuation, the relationship for other current, gain and attenuator settings could be obtained by multiplying this relationship by the ratio of amplification factor and the reference amplification factor.

APPENDIX III

ENCAPSULATION TECHNIQUE

The encapsulation technique makes use of a polycondensation reaction between a diacid chloride and a diamine. P. Morgan and S.L. Kwolek [64] showed that when the solution of a diacid chloride is brought in contact with an aqueous diamine solution, high polymer forms in a fraction of a second near the interface. The reaction rates were found to be very high and the main reaction was found to be considerably faster than any important side reaction at the polymerisation site.

The chemistry of interfacial polycondensation reaction was found to be simple [64]. Any diacid chloride and a diamine are believed to react by S_N2(nucleophilic) mechanism to form a protonated amide from which a proton is rapidly eliminated in the presence of more base. The proton acceptor is presumably an amine group on a diamine molecule or the end of an oligomer chain. Water also could act as a proton carrier.

$$Cl - \overset{O}{\overset{\|}{C}} - (CH_2)_8 - \overset{O}{\overset{\|}{C}} - Cl + H_2N(CH_2)_6NH_2 \xrightarrow{k_2}$$

$$\left[Cl\overset{O}{\overset{\|}{C}}(CH_2)_8\overset{O}{\overset{\|}{C}}-\overset{H}{\overset{|}{N}}(CH_2)_6NH_2\right] \xrightarrow[k_{H^+}]{\text{Diamine}}$$

(Cl on the carbonyl carbon; H on the nitrogen)

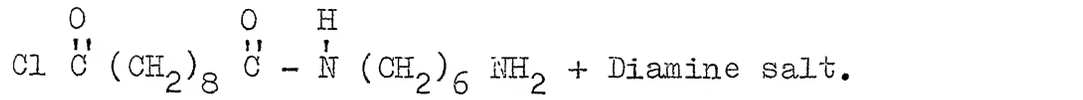

In the presence of a base (NaOH), the reaction occurs as follows:

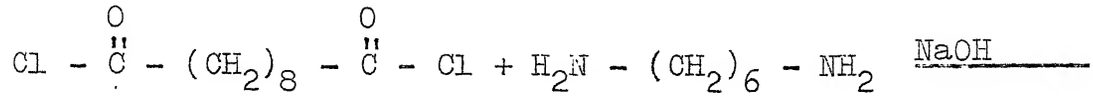

Sebacoyl chloride Hexamethylene diamine

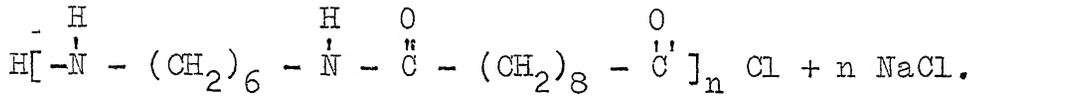

Nylon 6-10.

It was found that the thickness of the polymer varies with the solvent, concentrations and reaction times. In my case, for very short reaction times, the thickness varies from 0.1 micron to a few microns.

Madden and McCoy [54] used sebacoyl chloride and hexamethylene diamine for encapsulation of CCl_4 droplets in water. They observed that the hydrolysis of sebacoyl chloride does take place to some extent influencing the drop size distribution. They also observed that hydrolysis results in the shift of the drop size distribution towards larger size. They suggested that diacid chlorides of higher molecular weight should be used to minimise the bad effects of hydrolysis. Mylnek and Resnick [39] used terephthalic acid chloride and piperazine for encapsulating drops of CCl_4, i-octane mixture in water. In the present work, terephthalic acid chloride and piperazine were used for encapsulation. In the presence of a base (NaOH), the reaction occurs as follows,

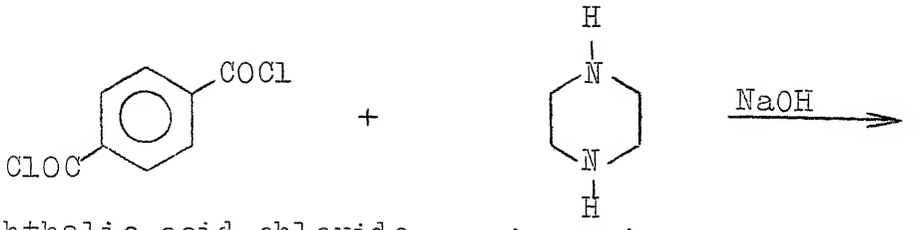

Terephthalic acid chloride piperazine

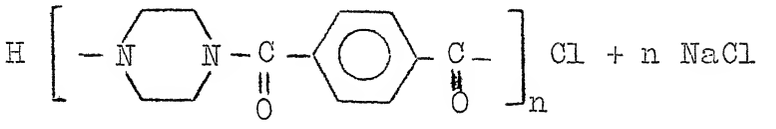

Nylon

The concentration of terephthalic acid chloride in CCl_4 was 1 per cent by weight. A mixture of equal volumes of aqueous solutions of piperazine (2 gms/litre) and NaOH solution (1.3N) gave diamine solution of required concentration. At the time of encapsulation, 50 cc of this diamine solution was added to the continuous phase.